

https://dspace.org/

Application of 3D seismic analysis techniques to evaluate ore resources on Kloof, South Deeps and Driefontein gold mines, Witwatersrand Basin, South Africa.

Manzi, Musa Siphiwe Doctor

2014-03-07
http://hdl.handle.net10539/14073

Downloaded from a DSpace repository. https://dspace.org/

Application of 3D seismic analysis techniques to evaluate ore resources on Kloof, South Deeps and Driefontein gold mines, Witwatersrand Basin, South Africa.

By

Musa Siphiwe Doctor Manzi

A thesis submitted to the

Faculty of Science, University of the Witwatersrand

in fulfilment of the requirements for the degree of

Doctor of Philosophy

School of Geosciences

University of the Witwatersrand



Johannesburg, 2013

DECLARATION

I declare that this thesis is my own, unaided work. It is being submitted for the Degree of Doctor of Philosophy at the University of the Witwatersrand, Johannesburg. It has not been submitted before for any degree or examination in any other University.

_____

Musa Siphiwe Doctor Manzi

_____day of_____20_____in_____

ABSTRACT

This thesis presents the application of the state-of-the-art processing, interpretation and modeling to the 3D reflection seismic data that were acquired between 1988 and 2003 across the West Rand and West Wits line goldfields of the Archean Witwatersrand Basin. The re-processing of the old 3D seismic data using new imaging techniques, such as 3D Kirchhoff prestack time migration (KPSTM), has led to better imaging of the ore body, structures (faults and dikes), and steeply dipping stratigraphy.

Detailed interpretations of the highly auriferous Ventersdorp Contact Reef (VCR) using advanced complex seismic trace and horizon - based seismic attributes, have led to discoveries of ore blocks (~ 1 km long and ~ 250 m wide) that are bound by multi-fault segments of the first-order scale Bank and West Rand faults, leading to an increase of the resource portfolio and potentially, the quantity of the reserves. In particular, the edge detection attributes have resolved faults with throws as small as 10 m and complex structural architectures such as intersecting and cross-cutting faults, and fault bifurcations which are difficult to detect using conventional techniques (e.g., amplitude, dip and azimuth). Potential conduits, such as faults and dikes for migration of water and methane into underground workings were also mapped using edge detection attributes. These results have the potential to play into safe mine planning.

The interpretation of the merged 3D seismic datasets, integrated with underground maps, boreholes, absolute and relative geochronological data, has added to our understanding of the gross structural architecture and Neoarchaean tectonic evolution of the goldfields. On a first-order scale (400 m - 2.5 km) the data resolved: (1) the northerly-trending disharmonic Libanon Anticline with a wavelength of 8 km and amplitude of 2 km, which was formed during deformation in the Umzawami Event (ca 2.73 Ga); and (2) the north-northeast trending, west-dipping (65°–70°W) listric West Rand and Bank faults, which were formed during a major extensional event, herein termed the Hlukana-Platberg Event (2.70-2.64). On a second-order scale (25 m - 400 m) the datasets resolved: (1) the Tandeka and Jabulani thrusts 1.5 km below the West Rand and Bank faults in the depth interval of 6-8 km; and (2) a series of drag synclines and rollover anticlines in the immediate footwall and hangingwall of the West Rand and Bank faults.

Further to this, the seismic sections across the goldfields provided evidence that the first- and second-order scale faults, thrust and folds were dissected, eroded and overlain by the Transvaal Supergroup above an angular unconformity. The oldest approximate age for the Transvaal Supergroup is given as 2.58 Ga, thus constraining the age of the faults, thrust and folds to the Neoarchaean or pre-2.58 Ga.

DEDICATION

To my late mom, Jabu Manzi, for her consistent encouragement.

To my adoptive parents, Rosalind and Edward Thomas, for their unequaled love, support and godly example to me.

PREFACE

I consider myself very fortunate to have been given the opportunity to undertake a PhD research project on the Archean Witwatersrand Basin in South Africa, which is the world's largest gold deposit. As a result, this research has provided insight into the most controversial academic research debates regarding the origin of gold and tectonic evolution of the Witwatersrand Basin. It has also provided the gold mines from West Rand and West Wits Line goldfields with a world-class structural model of the ore body for mine planning and designs.

I have been intrigued by research involving a combination of physics, mathematics and geology ever since my undergraduate years and now during my PhD studies at the University of Witwatersrand Johannesburg. Working with Prof Hearne and Dr Vittoria Pischedda as an assistant researcher for three years in the physics research laboratories, including the High Pressure, Mossbauer and Laser laboratories, provided me an opportunity to explore and appreciate the beauty of mineral physics. Secondly, assisting Dr Susan Webb during my third year BSc with many geophysical projects on the Bushveld Complex, introduced me to the application of physics principles in Earth Science – a crucial route that moved me from Physics to the Geosciences department. I thank her that I am a geophysicist today.

It was through my BSc honours project entitled; *"Phase Weighted Stacking– noise reduction and detection of weak, but coherent seismic signals"*, as supervised by Prof Gordon Copper, that I was introduced to seismic research. However, it was during my MSc studies that I was introduced to, and fell in love with the topic of *"Application of 3D seismic reflection in the Witwatersrand Basin for mine planning and designs"* as supervised by Professors Kim Hein and Raymond Durrheim.

My research studies, like many other research projects, never followed the initially proposed pathway. Originally, this work was restricted to an MSc study involving the interpretation of the seismic data, but the MSc opened opportunities to address several issues including the strato-tectonic evolution of the Witwatersrand Basin, the ingress of water into the mines, influx of flammable methane gas into the mining levels, and the discovery of new ore resources in the complex faulted areas. These opportunities consequently motivated the conversion of the MSc to PhD candidature. This doctoral thesis makes a step towards addressing and solving some of these problems.

ACKNOWLEDGEMENTS

Many people have played a pivotal role in assisting me during my PhD journey. I would like to wholeheartedly thank my principal supervisor, Professor Kim Hein, and second supervisor, Professor Raymond Durrheim for their patience, guidance and great deal of faith in me throughout my young scientific career. I am very blessed to have worked with them; it would not have been possible to complete this doctoral thesis without their unequivocal support throughout. Kim and Ray not only were my supervisors but also played a critical parenting role in my life. They were always available when I had questions. I had a privilege to learn from their enormous skill and experience in the mining industry, not to mention their unsurpassed knowledge of structural geology and exploration geophysics, respectively. They took care of my personal needs (mainly finances) to help me focus on my research, and ensured that I published many research papers and finished my thesis on time. My long lasting discussions with them, accompanied by good cups of coffee, constructive arguments and social meetings were highly appreciated.

The good advice, support and friendship of Gold Fields Ltd representative, Nick King, was invaluable in providing me with the geological and geophysical data, mine models and company reports. This thesis would not have been possible without his help, for which I am extremely grateful. I would also like to acknowledge the financial support of Gold Fields Ltd and its entire staff, particularly Billy Mills. It was particularly kind of them to allow me to visit the mines, which helped improved my understanding of geology.

I would also like to acknowledge Prof Gordon Cooper, Dr Susan Webb and Dr Lindsay Linzer, for their technical support during my PhD study. I am also indebted to Prof George Smith (University of Cape Town, Department of Geological Sciences), Rodney Segage, Saheed Kenku and Samir Elamri (all from Schlumberger, Cape Town) who gave me a chance to use world-class software packages for seismic processing and interpretations. I am grateful to Mark Gibson, project manager for 2003 3D seismic project, Dr Mark Muller, and Jeanne-Claire Trickett for sharing their seismic interpretation skills and for answering Kingdom Suite questions.

Above all, I would like to thank my nieces, Joy and Hope, for their love, understanding and support throughout my career.

Without the love and support of Nonhlanhla, Elizabeth and Sibongile, the emotional toil of completing this work while parenting my nieces would have been unbearably onerous. The decision to pursue a PhD in geophysics was supported by my loving adoptive parents.

I would also like to acknowledge the financial, academic and support of the University of Witwatersrand Johannesburg. The library and computer facilities of the university have been indispensable. I particularly thank the School of Geosciences for their support and assistance during my PhD studies, especially the Head of School, Prof Roger Gibson. I participated and benefited a lot

from the School's Weekly Geotalks, which helped me shape my geological background. I had the opportunity to present at several local symposia and conferences, and in several cases won prizes for my research.

Of course, I thank all my friends and colleagues (some of whom happen to be geologists) for their scientific and social contributions including, Dr Vittoria Pischedda, Grant Bybee, Prof Lew Ashwal, Slindile Wela, Trishya Owen-Smith, Prof Tamiru Abiye, Oleg Brovko, Dr Jeremie Lehmann, Dr Loronzo Milani, Anika Solanki, Stefanie Weise, Nqobile Mzobe and all that I have forgotten. Family and friends are greatly thanked for their support during the course of this study and the memorial times spent together.

Last but by far not least, I thank my incredible, wonderful partner, Ntokozo Buthelezi. Her love and support kept me on the right track towards the end of my PhD. Thank you.

CONTENTS

Declaration ii

Abstract iii

Dedication iv

Preface v

Acknowledgements vi

List of appendices ix

List of figures x

1. Introduction 1

1.1 Motivation and objectives 1

1.2 Thesis structure 2

1.3 Authorship statement 3

1.4 Presentations, abstracts and reports 6

2. The 3D reflection seismic method 8

2.1 Background 8

2.2 Acquisition 8

2.3 Processing 10

2.3.1 Velocity model 10

2.3.2 Migration 13

2.3.3 Migration algorithms 13

2.3.4 Time and depth migration 17

2.3.5 Poststack migration 17

2.3.6 Prestack migration 18

2.4 Interpretation 18

2.4.1 Traditional 3D seismic interpretation 19

2.4.2 Autotracking and manual picking 19

2.4.3 Faults and their impacts on mining 20

2.4.4 Detection of faults 21

2.4.5 Data conditioning 22

2.4.6 Mean and median filters 22

2.4.7 Bi-harmonic filter 23

2.5 Horizon-based seismic attributes 25

2.5.1 Amplitude 25

2.5.2 Dip magnitude and dip-azimuth 25

2.5.3 Edge detection attribute 25

2.6 Complex trace attribute analysis 27
2.7 Modeling 28
2.7.1 Fault-horizon projection 28
2.7.2 Non-Uniform Rational B-spline 28
2.8 References 31

3. Summary of scientific contributions 36

4. Application of 3D seismic techniques to evaluate ore resources in the West Wits Line goldfield and portions of the West Rand goldfield, South Africa 44

5. 3D edge detection seismic attributes used to map potential conduits for water and methane in deep gold mines in the Witwatersrand Basin, South Africa 53

6. Neoarchaean tectonic history of the Witwatersrand Basin and Ventersdorp Supergroup: New constraints from high-resolution 3D seismic reflection data 68

7. A review of reflection seismic investigations in three major metallogenic regions: The Kevitsa Ni–Cu–PGE district (Finland), Witwatersrand goldfields (South Africa), and the Bathurst Mining Camp (Canada) 80

8. Seismic attribute analysis to enhance detection of thin gold-bearing reefs: South Deep Gold mine, Witwatersrand Basin, South Africa 99

9. The Ventersdorp Contact Reef (VCR) model in the Kloof Gold Mine (South Africa) as derived from 3D seismics, geological mapping and exploration borehole datasets 143

10. 3D modeling of the ore body structural complexities: KDC East Gold Mine, South Africa 180

11. Conclusions 184

Appendix A: Pseudotachylite in the south boundary fault at the Cooke Shaft, Witwatersrand Basin South Africa 186

Appendix B: Evidence for Neoarchaean extensional faults in the Vredefort Dome, South Africa 198

List of Figures

Figure 2.1: Schematic reflection raypaths over a horizontal interface across which there is a contrast in impedance, Z ($Z_2 > Z_1$ or $Z_2 < Z_1$). 8

Figure 2.2: Seismic section (amplitude display) across the Western Ultra Deep Levels mines showing the imaging of a reflective contact between metamorphosed basalts of the Klipriviersberg Group and the quartzites of the Central Rand Group. 8

Figure 2.3: Seismic survey geometry. (a) Recording of a single source for a horizontal layer, (b) Common midpoint (CMP) gather for a horizontal layer, (c) Recording of a single source for a dipping layer, (d) Common midpoint gather for a dipping layer. If a horizontally-layered model is considered, rays in a CMP gather are reflected from the same depth point under different angles. By assuming a source and receiver location to coincide during the acquisition, a CMP gather may contain a zero-offset ray that originates from source-receiver pair at the CMP location (b). If a dipping reflector is considered, a CMP gather has rays reflected from different points on a reflector (d). 11

Figure 2.4: Depth converted time migrated sections using finite difference migration algorithm. (a) Unsmoothed velocity field provides a much stretched seismic horizons and distorted structures (possibly under-migrations). This shows a huge depth mis-tie between the VCR and BLR horizons and borehole control. (b) Smoothed velocity field provides stable seismic horizons and structures. These results show a very good depth tie between the VCR and BLR horizons and boreholes. 12

Figure 2.5: Depth-converted (amplitude display) seismic sections from 1994 Leeudoorn data. (a) The 3D poststack finite difference depth migrated (PSDM) section. (b) The 3D prestack Kirchhoff time migrated (PSTM) section. Note that PSTM shows better resolution relative to the poststack depth migration that was originally applied to the same data set, shown in (a). 16

Figure 2.6: Depth-converted (amplitude display) seismic sections from 1994 Leeudoorn data. (a) The 3D poststack depth migrated (PSDM) section. (b) The PSTM section. The PSTM provides better imaging of the dipping reflectors. 16

Figure 2.7: Detailed depth structure map of the Venterdorp Contact Reef (VCR) derived from conventional picking across survey areas, showing faults' polygons of all strikes and dips. 20

Figure 2.8: (a) Seismic section (amplitude display) across Kloof Gold Mine. (b) Manual picked and autotracked seismic horizon data points. (c) Smoothed horizon by bi-harmonic smoothing operator. 24

Figure 2.9: VCR edge attribute map of the VCR overlain with water and methane data in Kloof Gold Mine. Structures such as Danies Fault and Shaft 4 Fault show good correlation with water and methane data (color bar is given in %). 26

Figure 2.10: (a) Modelled fault surfaces and fault pillars (changed dip of faults from vertical) using NURBS. (b) Modelled fault surfaces, showing fault intersections. (c) Horizon modeling around the fault zones. (d) Projection of fault pillars into horizon breaks (faults). 29

Figure 2.11: Integrated structural ore body modeling workflow. Inst.: Instantaneous. Steps listed above complement each other, yet they are applied at different stages during interpretation and modeling of the ore body. 31

1. INTRODUCTION

1.1 Motivation and objectives

"If we can't mine safely, we won't mine at all", Nick Holland (CEO of Gold Fields Limited)

The geologically complex Archean Witwatersrand Basin of South Africa has produced more than 40% of the world's gold ever mined. With gold reserves in decline at relatively shallow depths (~ 500 m), most gold mining currently takes place at depths between 3.0 and 4.2 km below surface. At these depths, the mapping and delineation of subsurface structures such as dikes and major faults is difficult using conventional techniques (e.g., gravity, magnetic, borehole data, 2D reflection seismics, surface and underground geological mapping). The increase in mining depth, the complex geometry of the gold-bearing horizons, and inherent structural complexity of the Witwatersrand Basin, to state only a few, make it difficult to place shafts and support infrastructure, or to operate the mines safely. This means that there are an increasing number of technical challenges in the exploration for, and the extraction of new resources.

The 3D seismic reflection technique had its origin in the exploration for oil and gas in the 1960s, where it was used to locate oil and gas reservoirs. Over the past 20 years, the technique has been used worldwide for mine planning, design, and risk reduction in deep mines.

In the late 1980s, the 3D seismic reflection technique became the core geophysical tool for Witwatersrand gold mines, being used to delineate gold-bearing reefs, faults, dikes and folds. Although 3D seismics was deemed costly, its application made the prediction of hazards along drilling trajectory possible. It facilitated optimum planning of drilling targets while mitigating risks.

The first 3D seismic survey in the Witwatersrand Basin was shot in 1988 over South Deep gold mine lease area. Since then, it has been applied across parts of the Witwatersrand goldfield to great effect. Recent developments in a multitude of processing, interpretation and structural modeling techniques have motivated the re-processing and interpretation of the old 3D seismic datasets.

In this research project, several state-of-the-art processing, interpretation and modeling techniques were applied to the 3D reflection seismic data that were acquired between 1988 and 2003 across the West Rand and West Wits Line goldfields in the Witwatersrand Basin, covering mines and exploration leases of AngloGold Ashanti (Mponeng, Western Ultra Deep Levels), Gold Fields (South Deeps), and Sibanye Gold (Kloof-Driefontein Complex-KDC). The surveys were merged to obtain a single unique seismic volume (40 km east-west × 16 km north-south × 11 km depth) for interpretation. This research has broad impacts in several ways:

- The re-processing of the old data using advanced imaging techniques provided better characterization of gold-bearing horizons and resolution of complex arrangements of faults and dikes.

- The merging of the 3D seismic surveys provided a seamless data cube, which made it possible to image the regional first-order (kilometers to tens of kilometers) and second-order scale (meters to hundreds of meters) strato-structural architecture of the Witwatersrand Basin in 3D. From this it was possible to establish the relative chronology of faults and dikes that lead to a full evaluation of the strato-tectonic evolution of the Witwatersrand Basin. The relative chronologies also provided some limited constraints on ore genesis models.
- Important to mine safety, the re-interpretation of the old data using the latest interpretation techniques (e.g., seismic attribute analysis) enabled the detection of dikes and faults with throws as small as 10 m, which can have direct impact on mine planning decisions.
- Through the correlation of faults and dikes with known intersections of water and flammable gas (e.g., methane), it was possible to determine which faults and dikes transmitted water and methane to underground mine workings. Thus this research also indirectly addressed mine safety issues.

1.2 Thesis structure

This thesis is divided into eleven chapters. The introduction (Chapter 1) highlights the motivation and objectives of the study. Chapter 2 provides an overview of the theory and application of 3D seismic reflection method to the exploration of mineral deposits. The acquisition, processing and interpretation aspects of the 3D seismic reflection data are summarized. In addition, the old and new imaging, interpretation and modeling algorithms are compared, and assessment is made of their shortcomings, relative merits and applicability. Chapter 3 is a summary of the scientific contributions. Chapters 4-10 contain papers that have been published, or accepted for publication, and Chapter 11 presents the conclusions of the research.

The main findings (Chapters 4-10) of the research may be divided into four themes:

Theme 1: Comparison between new 3D seismic processing algorithms and older algorithms in the imaging of the gold-bearing reefs and complex structures in the West Wits Line and South Deep goldfields of the Witwatersrand Basin.

The new 3D seismic imaging algorithms, such as 3D Kirchhoff prestack time migration (KPSTM), have considerable advantages over conventional algorithms (e.g., 3D finite difference poststack time migration) in the imaging of the gold-bearing reefs and complex structures. Furthermore, the advantage that new horizon-based seismic attributes, such as dip, azimuth and edge detection attributes, have over conventional interpretation methods (e.g., manual, autotracking) in the discovery of the new economic ore body blocks and delineation of complex structural architectures (faults and dikes) was demonstrated. Additionally, the inter-relationship between the activity of faults and the distribution of the gold-bearing reefs is examined (Chapter 4). The application of edge

detection seismic attribute is discussed as a technique for optimum imaging of faults and dikes that are more likely to act as potential conduits for the transmission of water and methane gas, to underground mine workings (Chapter 5).

Theme 2: Demonstration of how the re-processed and merged 3D seismic datasets, correlated with absolute and relative geochronology, borehole, and underground mapping datasets, can characterize gold-bearing horizons and establish a chronology of Neoarchean tectonic events leading to the establishment of a full strato-structural history for the Witwatersrand Basin (Chapter 6).

The timing of fault activity and dike intrusions constrain ore genesis models for the Witwatersrand Basin (Chapter 7), and are crucial for mine planning and safety, and potentially enhance financial evaluation of the gold resources. They also potentially play a critical role in constraining the tectonic evolution of the pseudotachylite-bearing faults in the West Rand goldfield (Appendix A).

Theme 3: Demonstration of how the extraction of complex trace seismic attributes from the seismic cube can enhance detection of thin gold-bearing reefs with thickness below the tuning thickness, the application of these attributes is thus a powerful tool in the exploration of reefs (Chapter 8). The results have implication for mining production, and improve the understanding of the behavior of seismic wavelets within a wedge-shaped package of quartzite and gold-bearing conglomerate reefs that invariably exhibit low impedance contrasts.

Theme 4: Demonstration of how the integration of 3D seismics with geological mapping and exploration borehole datasets can assist in the development of a robust ore resource model for the Witwatersrand Basin.

Fault statistics derived from the integrated 3D seismics and underground mapping data are used to: (1) delineate fault architectures and their distribution in the Kloof gold mine lease area, and (2) predict fault spacing and offset of the gold-bearing VCR (Chapter 9-10). The fault statistical analysis was included to define likely zones of difficult mining conditions around faults and dikes, such as fault geometry, distribution, and ore body compartments.

To ensure robust ore body modeling, sophisticated modeling algorithms derived from Non-Uniform Rational B-Splines (NURBS) were incorporated to handle complex structural architectures such as cross-cutting faults and multiple fault bifurcations. The simultaneous integration of a variety of datasets provided a means to overcome seismic resolution limits, and led to a reliable geological ore body model that could be used for future mine planning and designs.

1.3 Authorship statement

Gold Fields Limited representatives (too many to mention) and supervisors (Kim A.A. Hein and Raymond J. Durrheim) were responsible for setting the project objectives and its concepts. The overview of the candidate's contribution to each paper is summarized below. The candidate was the first author of Chapters 1-6, 8-10 and 11; the third and fourth author for Chapter 7 and Appendix A,

respectively. Professor Kim A.A. Hein supervision was of the geology (e.g., review on the absolute and relative geochronological data), and structural components. Professor Raymond J. Durrheim's supervision was mainly on the geophysical component.

Chapter 4: *Manzi, M.S.D., Gibson, M.A.S., Hein, K.A.A., King, N., Durrheim, R.J., 2012a. Application of 3D seismic techniques to evaluate ore resources in the West Wits line goldfield and portions of the West Rand goldfield, South Africa. Geophysics 77, WC163–WC171, doi:10.1190/GEO2012-0133.1.*

The candidate was responsible for the re-processing of the 1994 Leeudoorn 3D seismic data datasets, and interpretation of the entire merged 3D seismic reflection data that covers the West Wits Line goldfield and some portion of the West Rand goldfields. Other co-authors: M.A.S. Gibson, the manager for the acquisition of 2003 Kloof-South Deep seismic project, contributed with the reviewing of the manuscript and providing guidance with the acquisition and field processing parameters. Nick King, the representative of Gold Fields Limited, provided the geological mapping, and surface and underground borehole information.

Chapter 5: *Manzi, M.S.D., Durrheim, R.J., Hein, K.A.A., King, N., 2012b. 3D edge detection seismic attributes used to map potential conduits for water and methane in deep gold mines in the Witwatersrand basin, South Africa. Geophysics 77, WC133–WC147, doi: 10.1190/GEO2012-0135.1.*

This popular article was selected by the Society of Exploration Geophysicists as the *Best Geophysics Paper* in 2012. The candidate was responsible for the re-picking of the new velocity fields for prestack time migration and subsequent time-to-depth conversion, and interpretation of the entire merged 3D seismic reflection data. Other co-author: Nick King provided the water and methane datasets (in x, y, z) intercepted underground, and geological models from KDC East Gold Mine (Kloof Gold Mine).

Chapter 6: *Manzi, M.S.D., Hein, K.A.A., King, N., Durrheim, R.J., 2013. Neoarchaean tectonic history of the Witwatersrand Basin and Ventersdorp Supergroup: New constraints from high resolution 3D seismic reflection data. Tectonophysics 590, 94-105, doi: 10.1016/j.tecto.2013.01.014.*

The candidate was responsible for seismic interpretation of the data with strato-tectonics interpretations being led by Kim Hein. The co-authors engaged in discussions and performed manuscript review.

Chapter 7: *Alireza Malehmir, Emilia Koivisto, Musa Manzi, Saeid Cheraghi, Raymond J. Durrheim, Gilles Bellefleur, Chris Wijns, Kim A.A. Hein, Nick King., in press. A review of reflection seismic investigations in three major metallogenic regions: The Kevitsa Ni–Cu–PGE district (Finland), Witwatersrand goldfields (South Africa), and the Bathurst Mining Camp (Canada).Ore Geology Reviews. http://dx.doi.org/10.1016/j.oregeorev.2013.01.003.*

The candidate was only responsible for seismic and structural interpretation of the data that covers the Witwatersrand Basin and the writing of that section, and also performed the overall review of the manuscript. Other authors: Alireza Malehmir, the first author, was responsible for the setting of the manuscript outline and its conception, seismic analysis of the Finland region and the overall review of the manuscript. Emilia Koivisto and Gilles Bellefleur were responsible for the Finland and Canada seismic interpretation, and writing of those sections. Others engaged in discussions and performed manuscript review.

Chapter 8: *Musa S.D. Manzi, Kim A.A. Hein, Raymond J. Durrheim, and Nick King, accepted, Seismic attribute analysis to enhance detection of thin gold-bearing reefs: South Deep Gold mine, Witwatersrand Basin, South Africa, Journal of Applied Geophysics.*

The candidate was responsible for the interpretation of the 3D seismic data. Nick King provided the geomodels from South Deep Gold Mine.

Chapter 9: *Musa S.D. Manzi, Kim A.A. Hein, Raymond J. Durrheim, and Nick King, accepted, The Ventersdorp Contact Reef (VCR) model in the Kloof Gold Mine (South Africa) as derived from 3D seismics, geological mapping and exploration borehole datasets. International Journal of Rock Mechanics and Mining Sciences.*

The candidate was responsible for data interpretation, fault statistical analysis and data integration. Nick King provided the geomodels from Kloof Gold Mine.

<u>Supplementary Peer Reviewed Abstract:</u>

Chapter 10: *Musa M.S. Manzi, Kim A.A. Hein, and Raymond J. Durrheim, 2013, 3D modeling of the ore body structural complexities: KDC East Gold Mine, South Africa. 12th Society for Geology Applied to Mineral Deposits, Biennial Meeting, mineral deposit research for a high-tech world, 12–15th August 2013, Uppsala, Sweden, p. 85-88.*

The candidate was responsible for data interpretation, fault statistical analysis and data integration. Nick King provided the geomodels from Kloof Gold Mine.

Supplementary manuscript:

Appendix A: *P.W. Mambane, K.A.A. Hein, S.G. Twemlow, M.S.D. Manzi, 2011. Pseudotachylites in the South Boundary Fault at the Cooke Shaft, Witwatersrand basin, South Africa. South African Journal of Geology, 114, 109-120.*

The candidate's contribution to this manuscript was minor. The candidate was responsible for the interpretation of the seismic section.

Appendix B: *Sello Mashabela, Kim A.A. Hein, Roger L. Gibson, Musa S. Manzi, 2013. Evidence for Neoarchaean extensional faults in the Vredefort Dome, South Africa. Geophysical Research Abstracts. EGU General Assembly, 15, 3923.*

The candidate's contribution to this abstract was minor. The candidate was responsible for the interpretation of the seismic section.

1.4 Presentations, abstracts (peer-reviewed) and reports:

During the course of this research, quarterly company reports where submitted to Gold Fields Limited. The research was also presented at several symposia, conferences, and departmental geo-talks, and in several cases has won prizes. These include:

- Manzi, M., Hein, K.A.A., Durrheim, R.J. 2013. 3D modeling of the ore body structural complexities: KDC East Gold Mine, South Africa. 12th SGA Biennial Meeting, Mineral deposit research for a high-tech world, 12–15th August 2013, Uppsala, Sweden.
- Manzi, M., Hein, K.A.A., Durrheim, R.J. 2013. 3D Reflection seismic investigations of the structure and tectonics of the Witwatersrand Basin. 8th Annual AfricaArray Workshop, 15-18 January 2013.
- Manzi, M., Hein, K.A.A., Durrheim, R. J., Cooper, G.J. 2012. Through the looking glass of 3D seismic techniques in deep underground gold mines, Witwatersrand Basin, Showcase Day, University of the Witwatersrand Johannesburg, 17 October 2012.
- Manzi, M., Hein, K.A.A., Durrheim, R.J. 2012. 3D seismic technique used to map potential conduits for water and methane in deep gold mines of South Africa. University of the Witwatersrand Johannesburg, Cross-Faculty Symposium, 19 October 2012 (Prize winner for poster presentation).
- Manzi, M., Hein, K.A.A., Durrheim, R. J., Cooper, G.J. State-of-art in seismic processing and interpretation, South Africa, Geotalk, April 2012.

- Manzi, M., Hein, K.A.A., Durrheim, R. J., Cooper, G.J. 3D seismic attributes for fault detection, Witwatersrand basin, South Africa, Geosynthesis (Cape Town), August 2011.
- Manzi, M., Hein, K.A.A., Durrheim, R. J., Cooper, G.J. Interpretation of 3D seismic data from deep gold mines in the Witwatersrand Basin, South Africa, Geotalk, University of Witwatersrand, April 2011.
- Manzi, M., Hein, K.A.A., Durrheim, R. J., Cooper, G.J. Nothing as expensive as 3D seismic data that cannot be interpreted, AfricaArray, 2010. University of Witwatersrand, November 2011.
- Manzi, M., Hein, K.A.A., Durrheim, R. J. Cooper, G.J. Interpretation of 3D seismic data from deep gold mines in the Witwatersrand Basin, South Africa, AfricaArray, University of Witwatersrand, April 2011.
- Manzi, M., Hein, K.A.A., Durrheim, R. J. Cooper, G.J. Nothing as expensive as 3D seismic data that cannot be interpreted, Geotalk, University of Witwatersrand, 2010. University of Witwatersrand, March 2010.
- Manzi, M., Hein, K.A.A., Durrheim, R.J. 2010. Seismic and Structural interpretation using 3D Reflection Seismic Data from West Rand and Carletonville Goldfields, Witwatersrand Basin. University of Cape Town, August 2011.

2. THE 3D REFLECTION SEISMIC METHOD

"In practical seismic imaging, we don't throw older technology away when new processes take over." (French, 1990).

2.1 Background

Over the past 20 years, the application of the 3D seismic technique has been advantageous to deep mineral mining, because it provided high-resolution imaging of the geometry of the seismic horizons (Pretorius et al., 1994; Milkereit et al., 1996, 2000; Pretorius et al., 2000; Trickett et al., 2004; Malehmir et al., 2012). The technology fast became a key tool for deep exploration and mine planning in the geologically and structurally complex Witwatersrand Basin, being implemented to image gold-bearing reefs (conglomerate units) at great depths (Gibson et al., 2000; Salisbury et al., 2003).

2.2 Acquisition

The reflection seismic technique uses energy sources (e.g., Vibroseis systems) to inject seismic waves into the Earth's subsurface. The waves may be reflected by lithological and structural boundaries such as unconformities, conformities and faults. The reflected wave is measured by the arrays of receivers (geophones) at the surface. The reflected signal results from the abrupt changes in the elastic properties of rocks. The most important parameter that influences the strength of the reflection is the contrast in acoustic impedance (product of the seismic velocity and density) (Figure 2.1). Major changes in this parameter within rocks usually produce strong reflections that allow the subsurface geology to be interpreted. The ability of the boundary to generate a strong reflection is described by reflection coefficient, which describes the amplitude of a reflected wave relative to an incident wave. For an interface to be detected by the reflection seismic method it should reflect at least 6% of incident energy (Salisbury et al., 2003). A good example of a strong and continuous seismic reflector is shown in Figure 2.2 and Chapters 4-6, where the auriferous Ventersdorp Contact Reef (VCR) is well imaged due to a major acoustic impedance contrast between metamorphosed basalts of the Klipriviersberg Group (~6400 m/s velocity and ~2.90 g/cm^3 density) and quartzite units at the top of the Central Rand Group (~5700 m/s velocity and 2.67 g/cm^3 density).

The reflection from an interface is generated from a finite area on the reflector surface defined by first Fresnel Zone, which is the subsurface area where the reflected energy arrives at the surface within the time interval equal to half the dominant period (Yilmaz, 2001). Since the seismic energy is transmitted through the Earth as a wave, rather than a narrow beam, there is always uncertainty about the exact position of an imaged structure. The area of uncertainty is known as the Fresnel Zone

sampling and the size of the Fresnel depends on the dominant seismic wavelength and depth (Yilmaz, 1987; 2001).

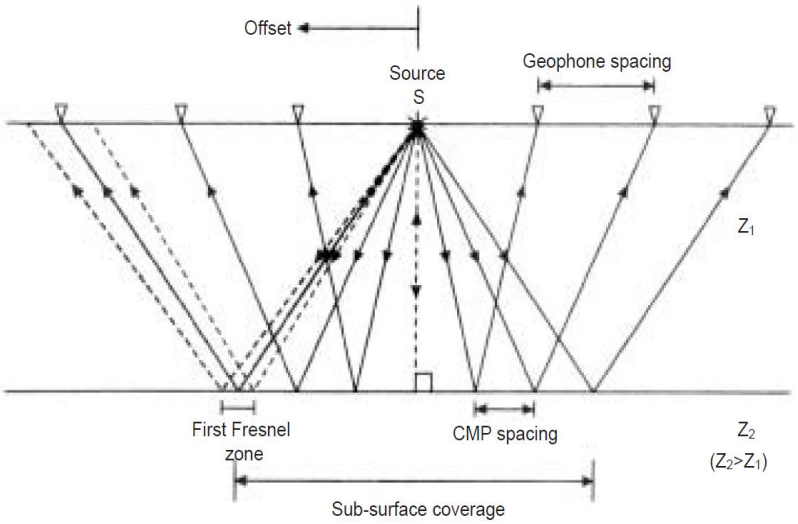


Figure 2.1: *Schematic reflection raypaths over a horizontal interface across which there is a contrast in impedance,* Z *(*$Z_2 > Z_1$ *or* $Z_2 < Z_1$*) (after Trickett et al., 2004).*

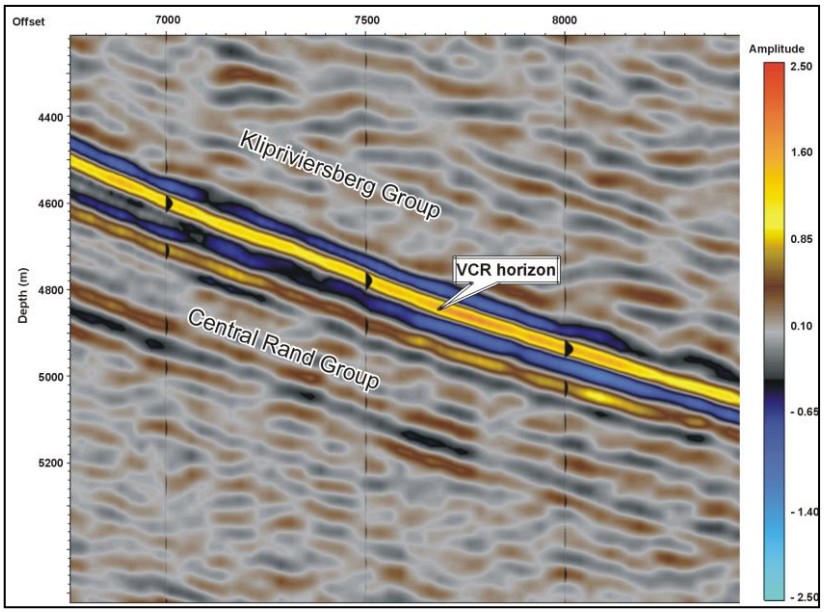


Figure 2.2: *Seismic section (amplitude display) across the Driefontein gold mine showing the imaging of a reflective contact between metamorphosed basalts of the Klipriviersberg Group and the quartzites of the Central Rand Group, which coincides with the Ventersdorp Contact Reef (VCR) horizon.*

In addition, the optimum imaging of the dimension and geometry of the target deposit, and its complex offsets (fault/dikes) depends on the seismic resolution limit (which is the ability to distinguish closely spaced reflection events as separate events both vertically and horizontally). The seismic resolution limit is defined by the dominant seismic wavelength, which in turn depends on the

seismic velocity of the rocks and the dominant frequency of the seismic pulse. Conventionally, the top and bottom of the target (or reefs) cannot be resolved if its thickness is less that the tuning thickness (i.e., a quarter of the dominant seismic wavelength), and the lateral extent of the geological feature cannot be discerned if it is narrower than the width of the first Fresnel zone. However, advanced interpretation techniques, such as seismic trace and horizon-based attribute analysis and fault statistical analysis enable greater resolution to be achieved, although the resolvability will depend on the combination of diffractions and geometric attributes (e.g., strike, dip, and azimuth), not solely on the seismic amplitude (Milkereit et al., 2000; White et al., 2012).

Other acquisition parameters such as the bin dimension, fold-of-coverage, and source and receiver geometry can also affect the quality of imaged subsurface structures. These parameters are, in turn, dependent on the seismic design limitations such as site conditions, topography, accessibility, man-made noise, and the properties of the surface layer. In addition, seismic design parameters depend on the geology (depth and geometry of the ore body), the logistic requirements and cost of the survey. Consequently, the quality of seismic interpretation and structural modeling rely strongly on satisfactory processing. Thus, the seismic design, acquisition and processing techniques are normally chosen to achieve a high interpretation quality. Importantly, a seismic workflow from the design-to-structural modeling should not be segregated, but be treated as a single integrated system. A detailed discussion of the seismic design and the acquisition parameters can be found in Chapter 4.

2.3 Processing

The main objective of 3D seismic data processing is to suppress incoherent noise, enhance the reflected wave signal, move (or migrate) seismic reflections to their true positions in time and space, and thus produce the best possible image of the subsurface. This section highlights only those processing steps that are relevant to this doctoral thesis, mainly velocity analysis and migration techniques. Other processing parameters are summarized in Table 2 of Chapter 5.

2.3.1 Velocity model

Obtaining high-resolution and 'focused' images of the subsurface structure, especially in tectonically complex areas such as the Witwatersrand Basin, requires a good approximation of the Earth's velocity. The velocity model is derived from selected common midpoint (CMP) gathers, which are groups of seismograms that have the same midpoint between a source (s) and receiver (g) (Figure 2.1). The velocity field is then used for normal moveout (NMO) correction of CMP gathers (flattening of reflection hyperbolas), CMP stacking (improving S/N ratio), and migration (increasing lateral resolution), and time-to-depth domain conversion of the data (Mayne, 1962; Sheriff and Geldart, 1995; Yilmaz, 2001). NMO is a process whereby non-zero offset data are converted to zero-offset data, while CMP stacking is a process whereby the CMP gathers are summed after NMO-

correction to produce a single stacked trace, thus attenuating the random noise and increasing the S/N ratio (Yilmaz, 2001).

A good approximation of the velocity model enables flattening of the hyperbolic events and provides the best possible result when the seismic reflections are stacked. The approximation of a hyperbolic travel-time curve is defined by Yilmaz (2001) as:

$$t^2(h,V) = t_0^2 + \frac{4h^2}{V^2}, \tag{2.1}$$

where t is the two-way travel time, V is the velocity of the layer, t_0 is the two-way travel time at zero-offset, and h is the half-offset (distance between the receiver and a source), which is defined by $(s+g)/2$, where s and g is a source and a receiver, respectively (see Figures 2.1 a-d for the reflection seismic survey geometry). The velocity model is one of the most important parts of the data processing as it affects all succeeding steps.

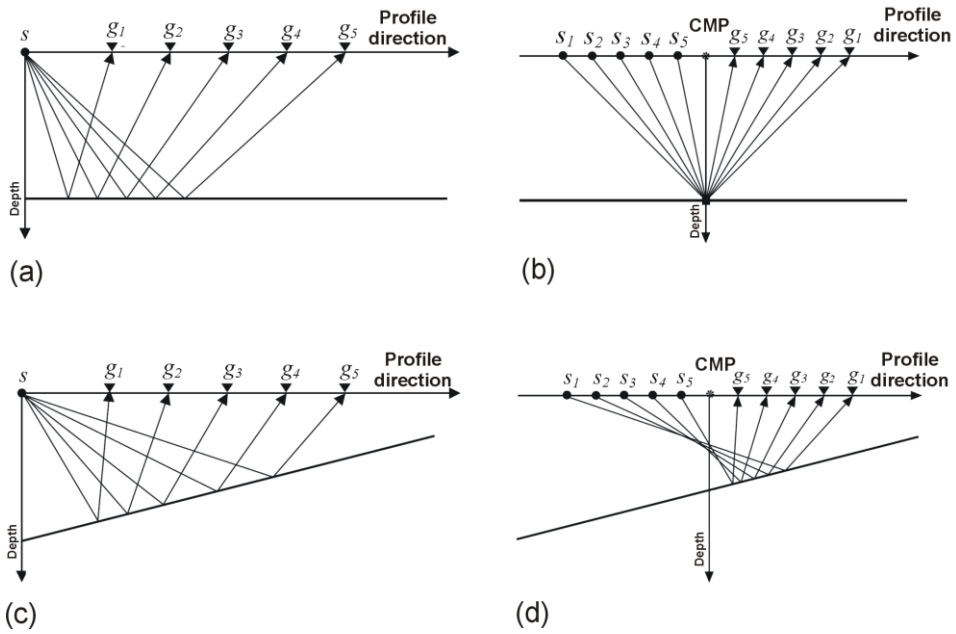


***Figure 2.3**: Seismic survey geometry. (a) Recording of a single source for a horizontal layer, (b) Common midpoint (CMP) gather for a horizontal layer, (c) Recording of a single source for a dipping layer, (d) Common midpoint gather for a dipping layer. If a horizontally-layered model is considered, rays in a CMP gather are reflected from the same depth point under different angles.*

A traditionally applied method (which was also implemented in Chapter 4 and 5) for velocity analysis in structural complex areas, characterized by large lateral and vertical velocity variations, is the Constant Velocity Stacks (CVS) (Yilmaz, 1979; 2001). This approach involves stacking of the CMP gathers with a range of constant velocities and consequent estimation of the stacking velocity (from constant velocity stacks) by picking the velocity that provides the best lateral continuity of the

reflection event (Mayne, 1962; Yilmaz, 2001). The hyperbolic approximation formula for stacking velocity as derived from Equation 2.1 is given by:

$$t^2(h,V_{stk}) = t_{0\,stk}^2 + \frac{4h^2}{V_{stk}^{\;2}}, \tag{2.2}$$

where V_{stk} is the stacking velocity that provides the best fit hyperbola. Although the stacking velocity model works perfectly for horizontally-layered reflective interfaces, it does not work as well for steeply dipping events due to reflection point dispersal (Yilmaz, 2001). Errors due to steeply dipping events on stacking velocities are conventionally reduced by dip moveout (DMO) processing (Judson et al., 1978; Yilmaz, 1979; Hale, 1984). Other factors that affect velocity analysis include S/N ratio, statics (near surface velocity anomalies), the depth and moveout of the reflector, and the number of seismic traces. A comparison between a good and bad approximation of the velocity field is shown in Figure 2.4 (see also Figure 4 of Chapter 5), where the Ventersdorp Contact Reef and Black Reef horizons are distorted and under-migrated due to a wrong velocity model used prior to stacking. Obviously, neglecting these factors may be detrimental to the seismic imaging of the subsurface, since the stacking velocity is conventionally used as the initial guess for migration velocities and consequent migration (mainly poststack).

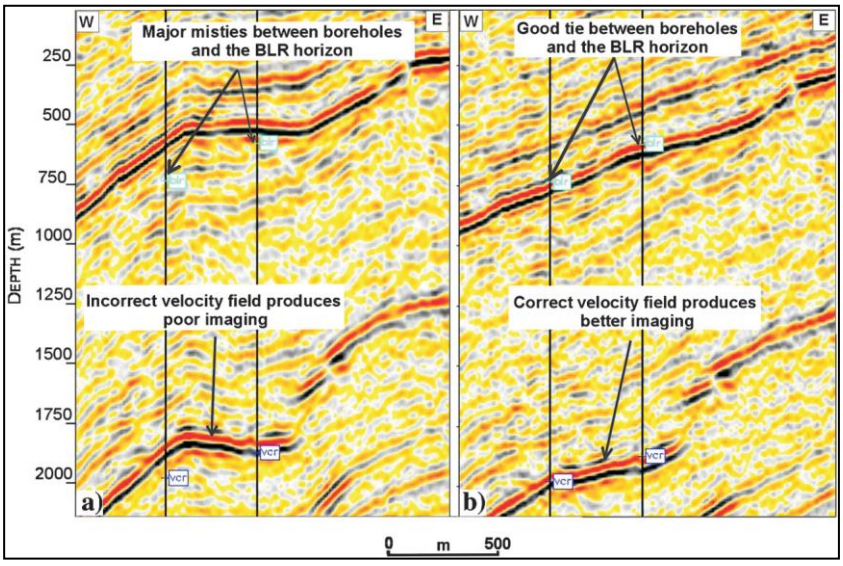


Figure 2.4: *Depth converted time migrated sections using finite difference migration algorithm. (a) Unsmoothed velocity field produces stretched seismic horizons and distorted structures (possibly under-migrations), and shows a large depth mis-tie between the VCR and BLR horizons and borehole control. (b) Smoothed velocity field provides stable seismic horizons and structures, and a very good depth tie between the VCR and BLR horizons and boreholes.*

2.3.2 Migration principles

The time image obtained from the propagation of elastic waves through the Earth does not correctly represent the true image of structures within the Earth. For example, dipping reflectors are incorrectly positioned on the CMP stacked seismic section. Migration, a wave-equation-based tool, is therefore used to undo the wave-propagation effects and provide a true image of the Earth. Migration increases the spatial resolution of the seismic image by (1) migrating dipping reflections to their true locations, (2) shortening dipping reflections, (3) moving reflections up-dip, and (4) collapsing diffractions (Yilmaz, 1979; Yilmaz et al., 2001). Today, a variety of migration techniques are implemented in software packages for imaging complex structures or steeply dipping stratigraphy. These migration techniques are applied either in time or depth domain, pre-or post-stack. This study has focused on the prestack time migration (PSTM) using the Kirchhoff wave-equation method and poststack depth migration (PSDM) using the finite-difference wave-equation method.

2.3.3 Migration algorithms

Migration algorithms are traditionally categorized into three types, (1) Kirchhoff migration (algorithm based on integral methods), (2) Finite-difference migration (algorithm based on differential method) (3) Frequency-wavenumber migration (algorithms implemented in the F-K domain). A comprehensive review of these algorithms and their technical details is given by Chun and Jacewitz (1978), Claerbout (1985), Gardner (1986), Yilmaz (1987; 2001), and Whitmore et al. (1988).

Prior to the introduction of Kirchhoff migration method (c.f., Chapters 4-5), the finite-difference method was the most used algorithm in seismic imaging. Finite-difference (FD) migration is a recursive, wave-equation based method that employs the wavefield downward continuation principle through the application of a FD approximation to the space-time wave equation (Hale, 1991b; Chang and McMechan, 1994). In general terms, the FD method may be conceptualized as a process where the receivers are moved deeper into the Earth in incremental steps each time computing the wave field that would be recorded.

The major advantage of FD migration is that it handles lateral velocity variations in complex areas (Chang and McMechan, 1994; Yilmaz, 2001). Major disadvantages of this method include its inability to handle steep dips and dispersion of waves along reflectors with steep dips (Etgen and Nichols, 1999; Yilmaz, 2001). In addition, the method has been considered expensive as it is computationally time consuming, and is thus prohibitive for implementation in the imaging of large 3D subsurface structures. One major reason for extra computation is that the finite-difference migration includes the aperture (output traces) for all depths, even if there was no energy present at those trace locations (Yilmaz, 2001). As a result, this has made the finite-difference method economically uncompetitive compared to other migration methods.

The Kirchhoff migration method, on the other hand, is relatively cheaper than finite-difference migration and has been effectively used in the oil and gas industry for velocity analysis, time and

depth imaging. It has only rarely been applied to the hardrock environments. This method is non-recursive and uses the Kirchhoff equation (integral form) of the wave equation (Yilmaz, 2001). The wave equation implemented in the Kirchhoff migration has been defined by Gazdag (1978) as:

$$u(r,t) = \frac{1}{2\pi}\int dt_0 \int \frac{dA_0 \cos\beta}{r}\left[\left(\frac{1}{V}\right)u'(r_0,t_0) + \left(\frac{1}{r}\right)u(r_0,t_0)\right] \tag{2.3}$$

where $t_0 = t - (r/V)$ (which is the travel time at zero-offset), A_0 is the amplitude of the wave at the source (zero-offset), V is the interval velocity, β is the angle dependence of amplitude, r and r_0 is the distance travelled by the wave and distance of the wave at the source, respectively.

The algorithm is based on Huygens principle, which states that every point on a wavefront represents a secondary source that generates seismic waves in a forward direction. These secondary sources are regarded as point apertures, which generate seismic waves, or diffraction hyperbola that are dependent on the angle of propagation (Bleistein, 1987; Yilmaz, 1987; 2001).

In the Kirchhoff migration, each diffraction hyperbola is collapsed to its apex (or origin). The algorithm then sums up all data values along a diffraction that is centered on each point on the output migrated section (Yilmaz, 2001). The major advantages of the Kirchhoff migration over other methods (e.g., diffraction summation), as highlighted in Equation 2.3, are its ability to compensate for amplitude variations due to spherical divergence or spreading factor ($1/r$), obliquity ($\cos\beta$), and wavelet shaping factors (distortions of amplitude and phase during wavefront propagation) before summing. The depth Kirchhoff migrated (KM) image of the subsurface is represented by Duquet et al. (2000) and Yilmaz (2001) as:

$$KM(x_0,z_0) = \sum_{[data\ within\ aperture]} scale\ \ factor \times phase\ \ factor\ \ (input\ \ section(x - x_0, t_0)) \tag{2.4}$$

where the *aperture* is defined as the range of summation, (x_0, z_0) is the zero-offset position of the image. The second term in Equation 2.3 has been dropped, because it is proportional to $(1/r^2)$. Furthermore, contrary to the FD method, the technique handles lateral velocity variations in structurally complex areas, steep dips up to 90° and beyond much more accurately than other migration techniques (e.g. finite difference algorithm) (Li and Lynn, 1991; Yilmaz, 2001). The dips beyond 90° may represent overturned structures such as anticlines and synclines. Although arguments for seismic imaging using the Kirchhoff migration versus finite-difference migration remains the subject of debate amongst geophysicists, there is increasing evidence that the Kirchhoff migration is a superior imaging technique, especially in structurally complex areas (Yilmaz, 2001).

An example of the power of Kirchhoff migration over the finite difference method is shown in Figures 2.5 and 2.6 (also discussed in Chapter 4), where the technique plays a key role in imaging the intersection of faults and horizons, and steeply dipping stratigraphy. This technique has become the basis for many poststack and prestack migrations, and is extremely flexible for different types of acquisition geometries (Bleistein, 1987; Bancroft, 1995). Clearly, a method that can efficiently improve subsurface images, such as that in Figures 2.5 and 2.6, is extremely useful. Improved modeling of the velocity field for finite-difference migration, which also tends to provide better imaging of horizon continuity and faults, may be an exception (Chapter 5, see Figure 4). In any case, the implication is that the smoother the velocities used for finite-difference migration, the greater its accuracy, and the more time consuming and expensive it may be.

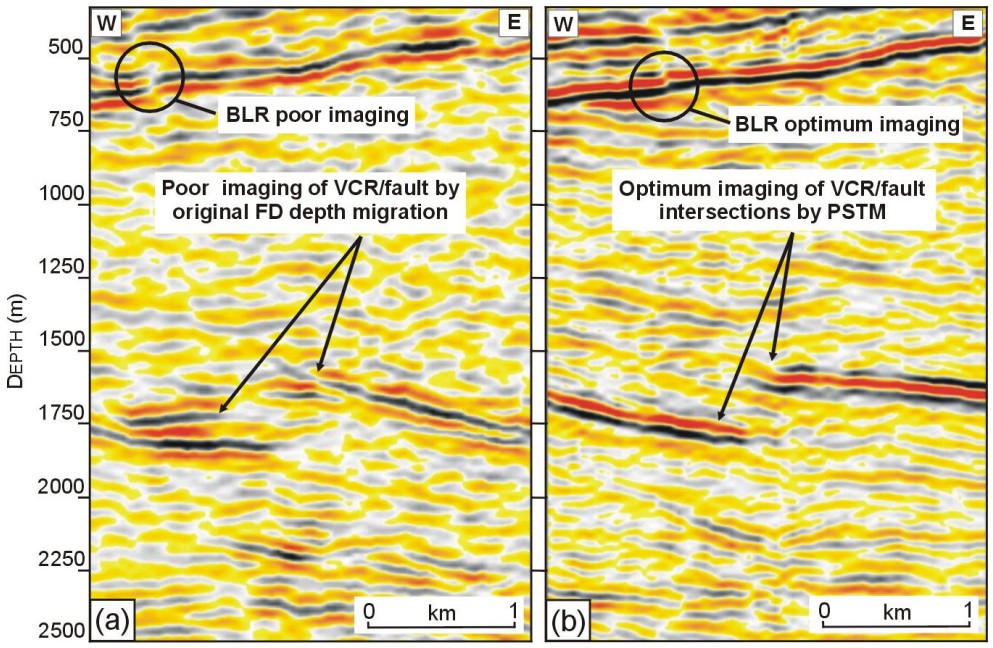


Figure 2.5: *Depth-converted (amplitude display) seismic sections from 1994 Leeudoorn data. (a) The 3D poststack finite difference depth migrated (PostSDM) section. (b) The 3D prestack Kirchhoff time migrated (PreSTM) section. Note that PSTM shows better resolution relative to the poststack depth migration that was originally applied to the same data set, shown in (a).*

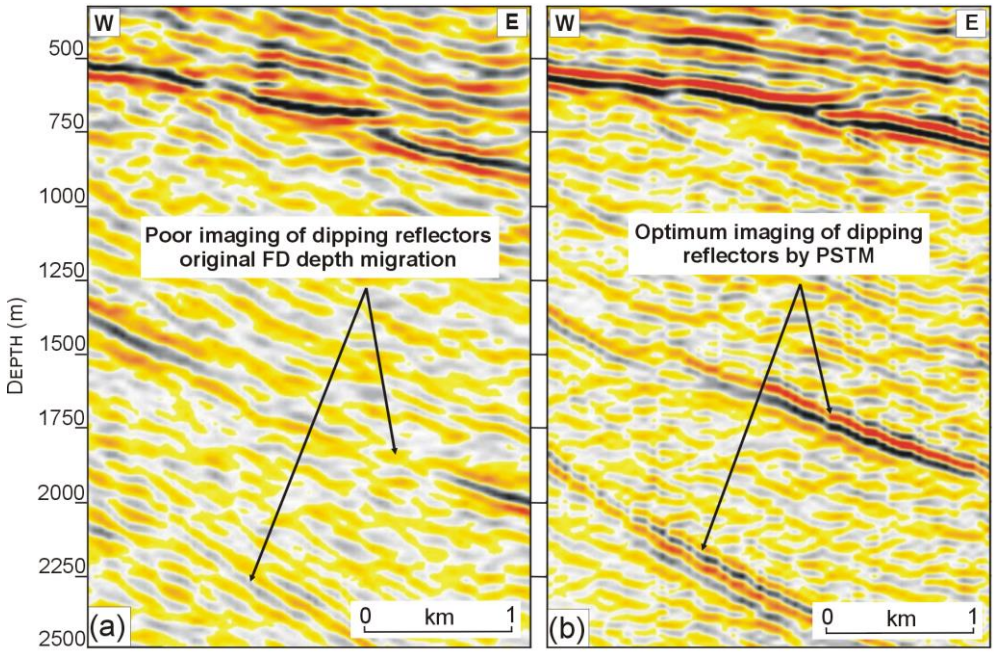


Figure 2.6: *Depth-converted (amplitude display) seismic sections from 1994 Leeudoorn data. (a) The 3D poststack depth migrated (PostSDM) section. (b) The PreSTM section. The PreSTM provides better imaging of the dipping reflectors.*

2.3.4 Time and depth migration

Generally, migration in the time domain treats the imaging velocity field (e.g., stacking velocity) as the root mean square (rms) velocity field and collapses the hyperbolic diffractions to their origin (apexes) in time (Bishop et al., 1985; Yilmaz, 2001). This assumption about the velocity field produces errors in the final time migrated section. Migration in depth domain, in contrast, assumes an interval velocity field (which is the subsurface Earth model) and estimates the shape of diffractions by wavefront modeling. In addition, depth migration can be used prior to data stacking to estimate the velocity field. Unlike routine estimation of the velocities for time migration, estimating interval velocities for depth migration is one of the major problems in the processing workflow (Leslie and Lawton, 1998).

To date, mineral, oil and gas industries are still plagued by persistent depth discrepancies between seismic models and geological information such as underground mapping and boreholes drilled into structurally complex areas. Publications in Chapters 4-5 address the issue of major mis-ties between seismic data and geological information due to inaccurate velocity fields used for depth migration, and consequent time-to-depth conversion. Chapter 9, in contrast, tackles this problem by using heuristic methods to minimize such mis-ties both vertically and horizontally. Given a correct velocity field, depth migration ought to be superior to time migration in accurately positioning subsurface structural images. Moreover, the incorporation of physically meaningful velocity fields in depth migration provides a quality check that is not possible with time migration.

However, time migrated data is preferred far more than depth migrated data. The reason for this is that the interpretation requires the data in the time domain (although the Earth is represented in the depth domain) because seismic attributes only work with time and frequency, not depth and wavelength (Chapter 8).

2.3.5 Poststack migration

Conventionally, after the application of processing steps such as scaling, deconvolution, statics and velocity analysis, the application of dip-moveout (DMO) corrections and CMP stacking to the data, the final stacked section is migrated to provide a structural image for interpretation (Etgen, 1998; Yilmaz, 2001). As indicated by its name, the depth migration after stack is referred to as poststack migration or poststack depth migration (PSDM). This conventional method assumes the zero-offset of the stacked section. It does not produce correct images of reflectors in geologically complex areas that are characterized by strong lateral velocity variations (e.g., Witwatersrand Basin). In such areas, the migration after stacking of the data produces puzzling (e.g., smearing, pinch-outs and diffractions with steeply dipping tails crossing flat events) and distorted stacked images (Hill, 2001). The reason for this is that in complex areas the reflection moveout may not be parabolic, and therefore cannot be represented by hyperbolic traveltime equation (Equation 2.1). In order to correct

for the shortcomings in poststack migration, the NMO and stacking steps are eliminated and the migration on the CMP gathers is applied, that is, prestack migration.

2.3.6 Prestack migration

In the prestack time migration, the Kirchhoff wave-equation algorithm is often an algorithm of choice in complex structural environments. The technique has proven to focus diffractions better and move dipping events to their true positions in each common-offset section (Biondi and Palacharla, 1996). In addition, the technique (in time domain) is also useful in refining and estimating the RMS velocity model, which yields much better results because the energies in the migration gathers are at the correct migrated positions (Biondi and Vaillant, 2000). Thus prestack time migration is very sensitive to the approximation of the velocity field used for migration.

Based on a vast amount of research over the last decade (Biondi and Vaillant, 2000; Yilmaz, 2001) the preference of poststack migration over prestack migration may have the following effects on the final migrated sections, and thus result in the wrong interpretation: (1) synclines and anticlines may become broader and narrower, respectively, (2) horizons may move up dip, and (3) the crest of the anticline and low point of the syncline may not move. Chapters 4 and 5 address these problems, where the re-processing of the old data by Kirchhoff prestack time migration (KPSTM) tremendously improves the imaging of faults, horizons, synclines and anticlines compared to finite-difference poststack depth migration initially applied to the data. Chapter 4 also shows that although prestack time migration technique might continue to reduce exploration risk, stability and efficiency of the well-established methods, in particular poststack migration, can still be useful in mining areas that are characterized by less complex velocity variations. Thus, these techniques should not be discarded.

2.4 Interpretation

"There is nothing as expensive as a 3D seismic data that cannot be interpreted", Albert (2004).

As previously stated, the quality of the seismic interpretation is dependent on the accuracy of 3D seismic migration techniques used during processing. Although the processing steps undertaken for Gold Fields Limited 3D seismic data offered great advantages for accurate interpretation, the conventional interpretation techniques did not allow for exploitation of the data to its full potential. For example, subtle or sub-seismic geological features (i.e., features below the seismic resolution limit) could not be recognized on a migrated seismic section. However, sophisticated seismic attribute analysis, implemented in the new advance interpretation software packages, can be used to enhance the detection of these features in the data.

2.4.1 Traditional 3D seismic interpretation

The traditional seismic interpretation work flow begins with the picking and tracking of outstandingly clear, strong and laterally consistent seismic horizons, or mapping of prominent first-order scale faults (see Section 2.1.3.2.2 and Chapter 6 for the scaling of faults) of the area at a wide line spacing (e.g., on a 1 km grid) of the vertical migrated seismic sections.

Seismic horizons are defined as surfaces, or reflectors that the seismic interpreter selects for picking based on their lateral continuity and strong seismic amplitudes. These horizons may represent stratigraphic boundaries, unconformities, or the top and bottom of the auriferous reefs. The amplitude-based interpretation is the first pass indication of the likely imaging ability of any horizon and fault that is present in the data. The amplitude display shows the changes in seismic acoustic impedance and thus helps to identify changes in lithological characteristics in the data. These seismic horizons and faults are first picked along the seismic sections, both inline and crossline, and depth slices. On seismic sections, the horizons are picked either as a peak or trough depending on the data polarity.

The borehole information, synthetic seismograms and Vertical Seismic Profile (VSP) data can assist the initial stage of picking by improving the understanding of expected polarity of seismic horizons (Chapter 5, see Figure 5). In the absence of borehole controls, a reasonable guess based on experience can be made.

2.4.2 Autotracking and manual picking

The European (or Australian) standard was used for this seismic interpretation. The European standard defines a black peak as a positive amplitude event (decrease in acoustic impedance), while a white trough corresponds to a negative event (increase in acoustic impedance) (Brown, 1996; 2001). Thus, the seismic pick would correspond to the crest of the waveform, which in turn corresponds with the peak of the seismic amplitude. Seismic horizons are then picked manually or automatically (autotracking) through software packages and the picking capability is dependent on the quality of the data or faulting.

The objective of autotracking is to speed up the picking process and ensure that the peak amplitude is correctly picked along the horizon. However, in areas characterized by complex faulting, low S/N ratio, and changes in the data polarity, autotracking may fail at some points on the horizons. As a result, manual picking is done at close line spacing or on every single line to facilitate detailed structural interpretation.

The next step in the interpretation process is to generate structural contour maps for each horizon. The maps incorporate fault polygon systems, which are the arrays of picked first- to third-order scale faults that are arranged into polygonal network (Figure 2.7). The latest development in interpretation software packages and workstations has maximized the interpretability and 3D

visualization of huge data. The interpretation procedures are described and discussed in details in Chapters 4-6.

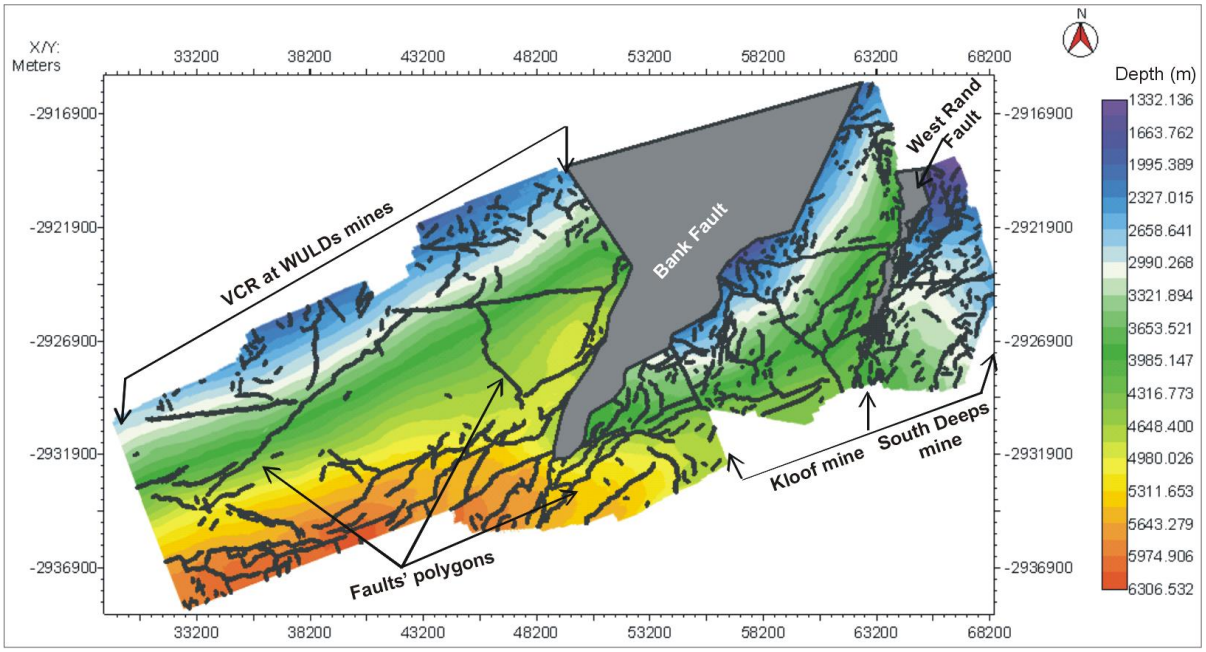


Figure 2.7: *Detailed depth structure map of the Venterdorp Contact Reef (VCR) derived from conventional picking across survey areas, showing faults polygons of all strikes and dips.*

2.4.3 Faults and their impacts on mining

Faults are any breaks that produce displacements of the strata. Faults and dikes play a critical role in the ore body behavior. Faults have a number of effects, almost always undesirable, on underground gold mining. These effects include: (1) physical displacement of gold-bearing reefs that may make the reefs impractical to mine, (2) reducing the stability of the mining hangingwall in underground workings, and (3) they may act as conduits for ingress of water and flammable gas into underground workings. Faults have their origin and evolution in a range of processes such as compression and extension. It is important to effectively recognize faults in the seismic data and determine their orientation and amount of vertical displacement (throw). This type of information can assist in (1) the unraveling the fault generation mechanisms and timing, (2) mitigating the risk of falls of ground or rockbursts ahead of mining.

Faults can exhibit complex structural architectures such as multi-fault segments that bound ore body blocks, multiple bifurcations from a single plane to form a branched fault array, and late faults that crosscut and offset fault systems. These features have significant impact on mine development. Failing to identify fault (and dike) arrays is risky in terms of mine planning and design.

Unfortunately, even with a state-of-art processing, structural architectures such as thin dikes, near-vertical faults, and faults with offset as low as 5 m cannot be resolved on the migrated seismic sections because they fall below the quarter dominant wavelength of seismic resolution limit. These discontinuities may show only minor changes in the seismic waveform that are not easily resolved

using conventional interpretation. They might, however, be resolved in interpreted horizons using horizon-based seismic attribute analysis (e.g., dip magnitude, dip-azimuth).

2.4.4 Detection of faults

The resolution of fault imaging is primarily a function of the dominant frequency and the S/N ratio of the field data. The Earth is a low pass filter, so high frequencies are attenuated, and thus the dominant seismic wavelength increases with depth, resulting in poor detection of subtle geological features at great depth. A widely accepted vertical seismic resolution limit rule for fault detection is defined as $\lambda/8$ for data with high S/N, but practically it is defined as $\lambda/4$ in which $\lambda = v/f$, where λ is the seismic wavelength, v the mean velocity and f the dominant frequency (Chopra et al., 2006; Zeng, 2009). By using a one-quarter dominant wavelength of the seismic resolution limit (where v = 6500 m/s and f = 65 Hz), faults were divided into three main categories:

(1) The *first-order scale* structures, which refer to faults with a throw of 400 m to 2.5 km.

(2) The *second-order scale* structures, which refer to faults with a throw of less than 400 m, but greater than conventional one-quarter wavelength, or 25 m.

(3) The *third-order scale* structures, which refer to faults with a throw of less than one-quarter of a wavelength.

The first and second-order scale faults are relatively easy to identify and pick. These faults, particularly first-order scale faults, play a major role in constraining the gross strato-structural evolution and tectonic history of the Witwatersrand Basin. Publications in Chapters 4-7 address this issue. Third-order scale faults cannot be visualized conventionally (on seismic cross-section), but can only be detected through computation of seismic attributes. Chapters 5-6 examine the importance of detecting third-order scale faults in terms of mining and mine safety. In addition, Chapter 7 considers fault activity with respect to fluid transmission in order to constrain the ore genetic models.

Seismic attributes have played an integral part in improving the quality and efficiency of fault detection in 3D seismic interpretations (Barnes, 1991; Taner, 2001; Chopra et al., 2006; Chopra and Marfurt, 2007). If well understood and computed, these tools can significantly improve the conventional interpretation processes such as automatic horizon tracking and manual picking. The biggest challenge in the application of seismic attributes is their sensitivity to noise (both coherent and incoherent). In this study, a new fault-detection approach that enhances seismic interpretation is introduced. This can be categorized into three main steps:

(1) Data conditioning through smoothing operators such as median, mean, or a combination of the two, and the bi-harmonic filtering operator.

(2) Computation of horizon-seismic attributes such as amplitude, dip-magnitude, dip-azimuth and edge detection.

(3) Re-picking of the seismic horizons and faults using complex trace attribute displays.

2.4.5. Data conditioning

Both manual picking and autotracking are sensitive to signal variations resulting from low S/N ratio and structural complexity of the area. This implies that the autotracking technique is only good for rapid mapping of faults in the data with high S/N ratio. The post-horizon/fault picking smoothing filters (mean, median and bi-harmonic smoothing operators) are computed and assigned to the interpreted horizons to suppress any fluctuation, coherent or incoherent noise that is introduced during autotracking and manual picking (Figure 2.8 a, b). These smoothing filters are also used to discriminate between phase distortion effects and energy focusing mechanisms in a high S/N dataset.

2.4.6 Mean and median filters

The arithmetic mean and median filters are nonlinear smoothing operators (low pass filters). These filters have been applied in many studies, both in one and two dimensions (Davies, 1992). The arithmetic mean filter (moving average) tends to smooth the high frequency background noise and computes the average of the amplitudes at the sample positions within a specific window (Gupta, 2011). In other words,

$$f(x,y) = \frac{1}{lk} \sum_{(s,t)\in S_{xy}} g(s,t) \tag{2.5}$$

where S_{xy} is the set of data points in the horizon image $g(s,t)$ within a chosen window size $l \times k$. On the other hand, the median filter replaces the amplitude of the central sample in the horizon with the median of the gray levels in the neighborhood of that sample. It is given by:

$$f(x,y) = \underset{(s,t)\in S_{xy}}{median}\{g(s,t)\} \tag{2.6}$$

These filters smooth the isolated horizon noise, and enhance long-wavelength structures (faults and dikes) while suppressing short wavelength structures as a result of blurring. In addition, they provide maximum resolution for the identification and location of faults. They also eliminate errors that result from false complex fault geometries created by conventional picking around faults, and thus minimize unrealistic horizon and fault interpretation. These filters have the ability to enhance subtle laterally continuous events by effectively de-noising horizon images even when characterized by low S/N (Basir et al., 2013). The key to reducing a processing time and successful implementation of these filters is to choose a small and fixed window size.

Unfortunately, the arithmetic mean and median filters tend to smooth both the noise and edges, and severely smear and distort the edges by shifting their positions. This may have serious implications in the final horizon model. This problem is solved by applying a bi-harmonic operator to a horizon filtered by the median plus mean operators. The process tends to remove the effect of smoothing over the edges.

2.4.7 Bi-harmonic filter

A bi-harmonic operator has been used in many applications including elasticity, fluid mechanics and biomedical fields (Li and Zhu, 2009; Shi et al., 2012). A bi-harmonic smoothing operator function is elliptic and is an approximation to the 4th order derivative of the image. It is computed from the Laplacian operator (edge detector); that is, it is the square of the Laplacian equation (Aronszajn et al., 1983):

$$\Delta^2 u(x, y, z) = 0 \tag{2.7}$$

where $\Delta = \partial^2/\partial x^2 + \partial^2/\partial y^2 + \partial/\partial z^2$ represents the Laplacian operator in 3D, u represents the interpreted horizon with pixel intensity values (x, y, z). The operator can be described as the sum of the 4th derivatives for the inlines and crosslines in the seismic data. This operator highlights areas where the data changes with depth. That is, it detects and sharpens edges such as the faults as well as highlighting areas that are difficult to pick due to low S/N, geological and structural complexity. Thus the operator filters out isolated noise and separates gross structural configurations (long wavelength) from faults and dikes (short wavelength).

The advantage of applying this filter is that no smoothing takes place if a fault is detected. Thereby filtering suppresses random noise and enhances the continuity of events while preserving acuity of the edges (faults) (Figure 2.8c). This explains the superiority of the bi-harmonic operator over mean and median filters. However, a bi-harmonic operator needs slightly more computation time than mean and median filter. More importantly, care must be taken not to introduce noise into the data during application since the bi-harmonic smoothing filter is a higher-order derivative operator. If not applied carefully, this can significantly affect the fault geometry and horizon stability. Nevertheless, the final horizon surface smoothed by this operator is considered well-conditioned for seismic attribute analysis.

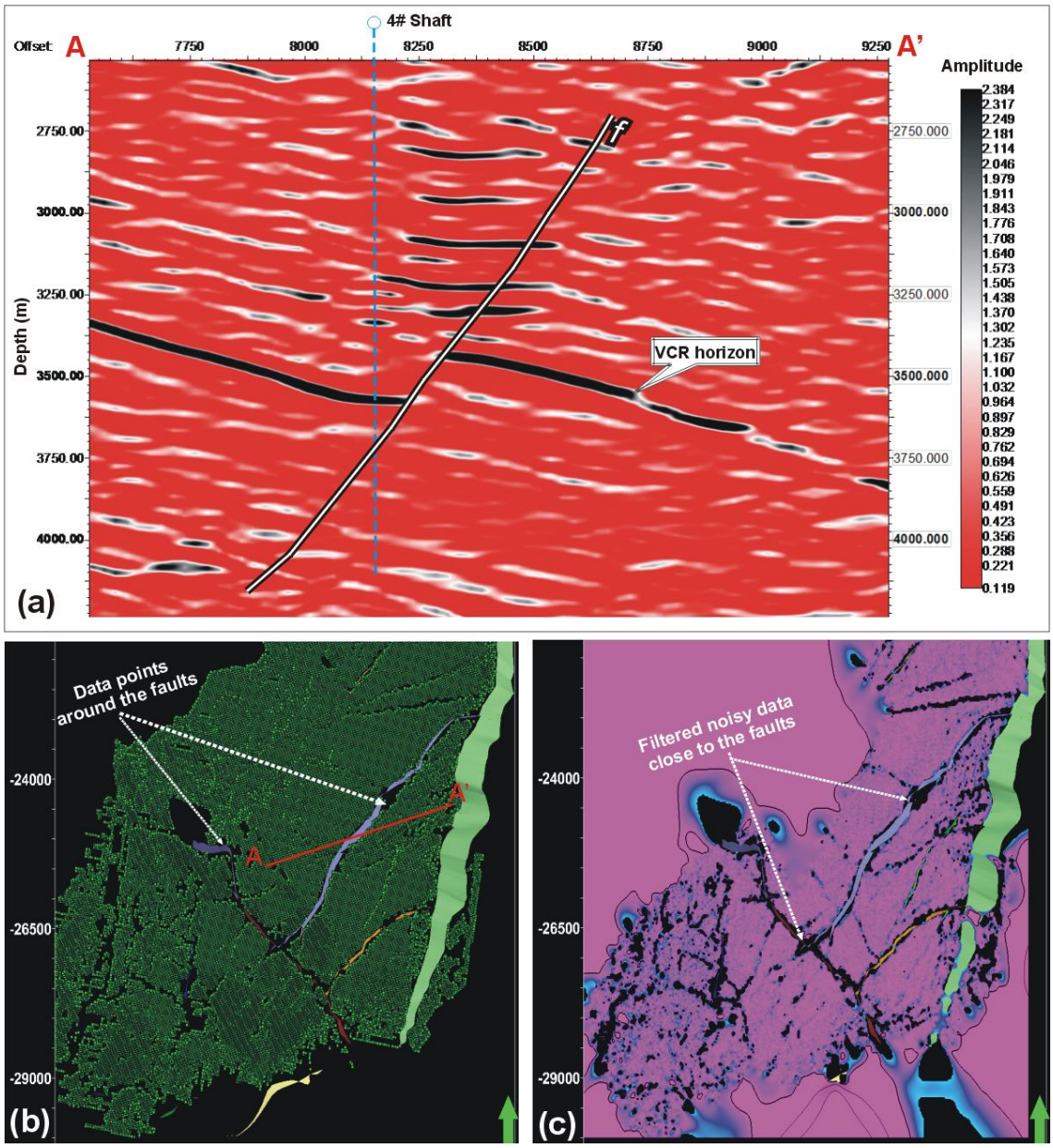


Figure 2.8: *(a) Seismic section (amplitude display) across Kloof Gold Mine. (b) Manually picked and autotracked seismic horizon data points. (c) Smoothed horizon by bi-harmonic smoothing operator.*

2.5 Horizon-based seismic attributes

"Seismic attributes are all the information obtained from seismic data, either by direct measurements or by logical or experience based reasoning", Taner (2001).

2.5.1 Amplitude

This attribute measures the reflected energy within a given window, and thus eliminates the undesirable phase effects observed when picking amplitudes directly. Although the amplitude attribute adequately defines the general structural architecture of an area, information derived from horizon-based attributes, such as dip-magnitude, dip-azimuth and edge detection reveal subtle information and structural complexities (Marfurt, 2006).

2.5.2 Dip-magnitude and dip-azimuth

Dip-magnitude and dip-azimuth, introduced by Rijks and Jauffred (1991), have been found to be very useful in the detection of third-order scale faults. Rijks and Jauffred (op cit.) simply defined dip and dip-azimuth as the magnitude (or amount of inclination of a horizon) and the direction of the time gradient computed at each sample trace of the interpreted horizon grid, respectively. In simple mathematical form,

$$Dip = \sqrt{(dt/dx)^2 + (dt/dy)^2} \tag{2.8}$$

$$Dip - azimuth = \arctan\left(\frac{(dt/dx)}{(dt/dy)}\right) \tag{2.9}$$

where dt/dx and dt/dy are the dip in the x and y direction, respectively. Dip and dip-azimuth, like many seismic attributes, have their own mapping limitations. Firstly, the dip attribute can only detect a fault when its dip angle is noticeably different from that of the horizon. Conversely, a dip-azimuth can only detect a fault whose dip direction is distinctly opposite to that of the layers (Chapter 4, see Figure 9). To overcome the problem of differences in detectability between dip and dip-azimuth in this study, the edge detection attribute was used.

2.5.3 Edge detection attribute

The edge detection attribute is basically a combination of dip and azimuth variations that are normalized to the local noise of the picked horizon grid. This attribute, when displayed in suitable color bars, can highlight subtle faults and complex fault architectures such fault connectivity, fault continuity, multiple fault bifurcations and crosscutting relationship between fault systems. Such small details and complexity can easily be missed by dip, dip-azimuth and conventional interpretations of the seismic vertical sections (Chapter 4, see Figure 9). One of the most spectacular examples of the power of edge detection over conventional interpretations is discussed in Chapter 5 where the

technique identified a range of subtle faults and dikes that were propagated between Black Reef and VCR reflectors. This technique indicated that sub-vertical faults that were active after deposition of the Black Reef at approximately 2.58 Ga, are connected with the aquifers in dolomitic rocks above the Black Reef Formation, and are most likely to allow fluid and methane to flow into the underground workings below (i.e., into the VCR level). The fault-reef connectivity, timing of fault activity and dike intrusions would not have been mapped without the implementation of this attribute (Chapter 5-6).

Furthermore, the mapping and projection of dikes into the reef horizons, integrated with geochemical information, can be used to test the ore genetic models, particularly the notion of basin-scale fluid movement caused by later tectonic or thermal events (Chapter 7).

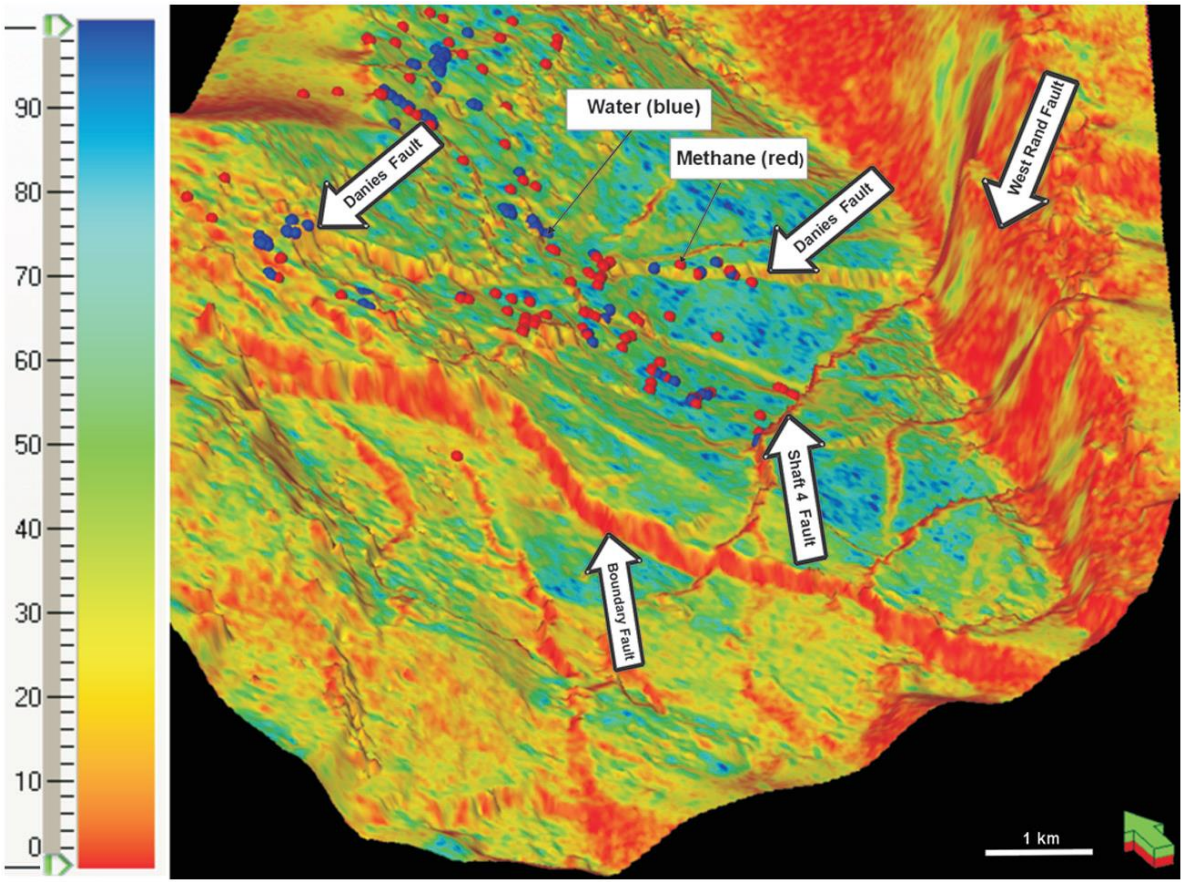


Figure 2.9: *VCR edge attribute map of the VCR overlain with water and methane data in Kloof gold mine. Structures such as Danies Fault and Shaft 4 Fault show good correlation with water and methane data (color bar is given in %).*

2.6 Complex trace attribute analysis

"About 3 to 5 boreholes in faulted areas associated with mine development would obviously not have been drilled if the 3D seismic data was available prior to drilling", Exploration manager at South Deep Gold Mine, South Africa.

Sometimes the reefs that are being mined are thinner than the tuning thickness (typically quarter of the dominant seismic wavelength), which is the thickness where the seismic wavelets interfere constructively (Chapter 8). These reefs have complex geometries and are often bounded by low acoustic impedance layers. Thus they cannot be recognized by simple seismic mapping of horizons or by looking for amplitude anomalies. So, conventional horizon picking and tracking on seismic traces with interfering wavelets will not suffice because some wavelets will show as 'doublets'. These reefs, however, can be typically resolved through computation of complex or instantaneous seismic attributes, particularly the amplitude-independent complex attributes (e.g., instantaneous phase and paraphase). The paraphase is similar to instantaneous phase, but with the predictable background removed. These attributes define the continuity of thin and weak seismic events.

Complex trace analysis is commonly used in engineering fields such signal processing and analysis (Gabor, 1946; Bracewell, 1965; Oppenheim and Schafer, 1975). A complex seismic trace is defined by the real trace component and an imaginary trace component part (which is the Hilbert transform of the real component). Instantaneous attributes are typically extracted along seismic traces to resolve information that is hidden in the migrated seismic sections (Barnes, 1991; Taner, 2001; Chopra et al., 2006; Chopra and Marfurt, 2007). These attributes can help to detect subtle variations in thin layering and also highlight instability in the phase wavelet. In addition, they bring out the subtle information, facilitating the shape and continuity of thin reefs. These attributes are integrated with borehole data during interpretation to ground truth the data and constrain seismic phase shifts in seismic attribute displays.

The problem of resolving thin bed, wavelets doublets and interference is well known in the oil and gas industry where attempts to resolve the top and bottom of thin reservoirs has proved challenging (Widess, 1973; Chopra et al., 2006; Purnomo and Harith, 2010). Chapter 8 highlights that it is not enough to simply rely on the amplitude response as a direct indicator of a thin reef, especially when confined in the complex geological geometries such as the auriferous clastic package at the South Deep gold mine. Generally, data conditioning using poststack noise reduction techniques (e.g., Automatic Gain Control) are used to significantly improve the performance of seismic complex attribute displays.

In summary, these tools have proven to be powerful in assisting conventional picking and tracking of thin horizons in seismic sections characterized by low amplitudes, complex faulting and

low S/N ratio. If these are ignored during interpretation, they could result in some boreholes being drilled in the faulted areas resulting in high cost and risks.

2.7 Modeling

Modeling of structurally complex ore bodies typically involves: (1) 3D seismic imaging, (2) picking of horizons, (3) data conditioning using image processing filters, (4) detection of faults by attribute analysis, (5) fault-horizon projection, (6) integration of seismic data with borehole and underground mapping data, and (7) fault statistical analysis.

Using advanced modeling software packages and algorithms it is now possible to generate a high quality 3D structural framework model (fault-horizon projection) which can cope with structurally complex architectures, such as multiple fault bifurcations, intersecting and cross-cutting faults. In particular, integration of a wide range of datasets helps to reduce the risk and increase the reliability of the final ore body model (Chapters 9-10).

2.7.1 Fault-horizon projection

The ‘fault sticks’ (3D fault and dike surfaces), detected by the edge detection attributes are modified through their ‘pillars’ (edges of fault sticks) and projected into the horizon. The application of edge detection attributes ultimately allows the tying of mis-positioned manually and auto-tracked fault sticks to their appropriate positions. However, modeling or movement of fault sticks with conventional modeling techniques creates 3D horizon-fault curve geometries that are jagged, since these techniques cannot model curving, intersecting and cross-cutting faults. This is because these techniques are derived from explicit equations, and thus only allow for linear interpolations between fault sticks (i.e., faults can only move along specific degrees and planes). To overcome these false curve geometries, ‘NON-Uniform Rational B-spline (NURBS)’ is used to allow the 3D interpolation between faults and horizons.

2.7.2 Non-Uniform Rational B-spline

The NON-Uniform Rational B-spline (NURBS) is a class of parametric curve representations. Since its development in the 1950s, NURBS has been commonly used in computer-aided designs, engineering and currently in 3D modeling software packages (De Boor, 1972; Watt and Watt, 1992). The technique provides great flexibility in adjusting complex structural architectures during modeling. It allows multi degrees of movement through fault pillars during interpolation (Figure 2.10). NURBS is defined as the generalized non-rational B-splines, which are designed from rational Bézier curves (Cox, 1972). The B-spline curve is defined by Foley (1994) as:

$$C(u) = \sum_{i=0}^{n} N_{i,p} P_i \qquad a \le u \le b \tag{2.8}$$

where P_i are the geometric coefficients, or control points (fault pillars), u is real number and subset of break points (which join the fault segments together) in the knot vector of the fault polygon. $N_{i,p}(u)$ are the p-degree B-spline basis functions (rational functions) defined from non-periodic and non-uniform knot vector (which is a set of break points in the fault polygons) (De Boor, 1972; Foley, 1994). In its simplest form, the NURBS curve can be described from B-splines using rational basis functions as:

$$C(u) = \frac{\sum_{i=0}^{n} N_{i,p}(u) w_i P_i}{\sum_{i=0}^{n} N_{i,p}(u) w_i} \qquad a \le u \le b \tag{2.8}$$

where w_i are the weights which control the fault pillars (P_i), i.e., if the weight is varied fault pillars would attract or repulse the curve more (Peigl, 1991; Rogers, 1991).

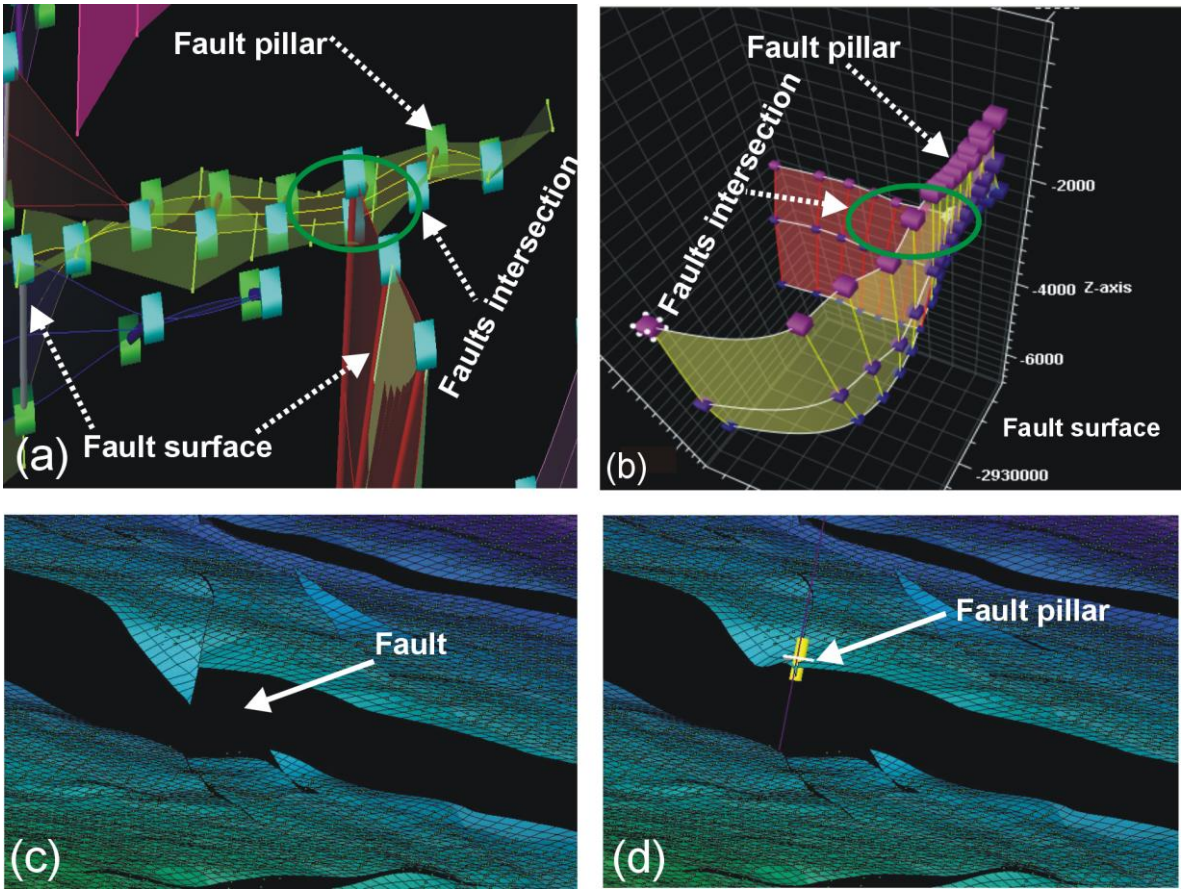


Figure 2.10: *(a) Modelled fault surfaces and fault pillars (changed dip of faults from vertical) using NURBS. (b) Modelled fault surfaces, showing fault intersections. (c) Horizon modeling around the fault zones. (d) Projection of fault pillars into horizon breaks (faults).*

In summary, the NURBS is a suitable way to model a 3D ore body, or any object composed of complex curves and surfaces. Modeling of the ore body using NURBS depends on the types of fault geometries to be incorporated and projected in the model. For example, some ore bodies are characterized by thrust faults and reverse faults geometries with varying degrees of reactivation, which cannot be seen on seismic sections. Incorporating these types of faults in the model is a challenge because although constraints on simple normal faults are well understood, the characteristic of thrust and reverse faults is not well understood and therefore cannot be easily incorporated in a model (Chapters 6-7).

In Chapter 7 (see Figure 2), extension architectures on a horizon-fault model are derived from a series of 3D structural restorations, which were performed to access the general geometric evolution through time. The contribution in Chapter 9 evaluates and bridges a gap between seismic processing (Chapters 4-6), seismic and structural interpretation (Chapters 6-8), and introduces structural modeling using a variety modeling techniques to construct the ore body geological model.

Finally, Figure 2.11 presents a workflow for integrated structural ore body modeling (e.g., 3D seismic, geological mapping and borehole data). In addition, the model workflow incorporates the statistical analysis of fault parameters such as fault distribution patterns, position, continuity, strike, dip, dip direction, pitch and hade, fault length, compartmentalization and fault throw. The computation of fault statistics is discussed in Chapters 9-10.

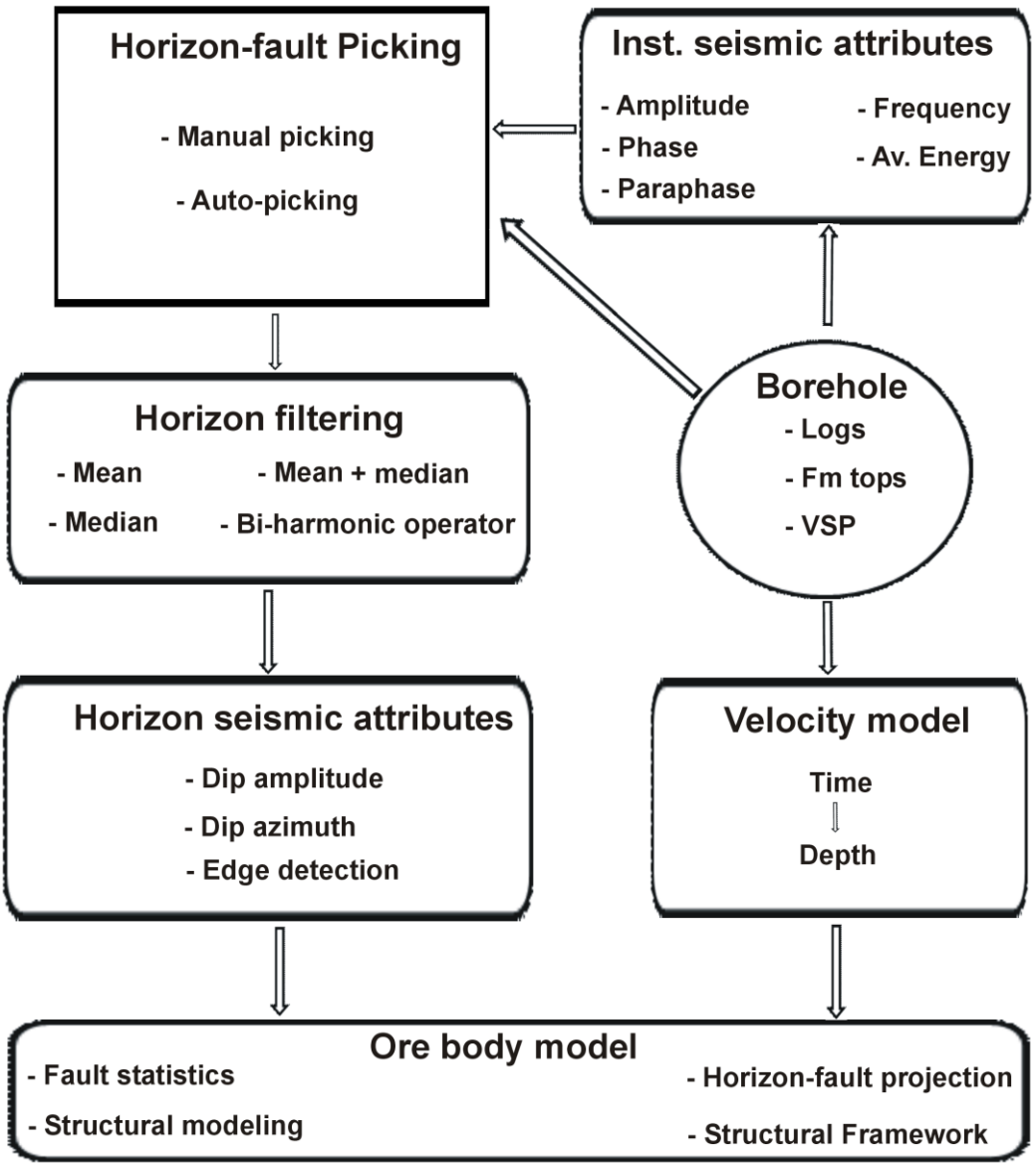


Figure 2.11: *Integrated structural ore body modeling workflow. Inst.: Instantaneous. Steps listed above complement each other, yet they are applied at different stages during interpretation and modeling of the ore body.*

2.8 References

Aronszajn, N., T. M., Greese, and L. J., Lipkin, 1983, Polyharmonic functions, Clarendon Press, Oxford University, New York.

Bancroft, J., 1995, A practical understanding of migration and dip moveout: Lecture Note, Department of Geology and Geophysics, the University of Calgary.

Barnes, A. E., 1991, Instantaneous frequency and amplitude at the envelope peak of a constant phase wavelet: Geophysics, **56**, 1058-1060.

Basir, H. M., A., Javaherian, and M.T., Yaraki, 2013, Multi-attribute ant-tracking and neural network for fault detection: a case study of an Iranian oilfield: Journal of Geophysics and Engineering, **10**, 1-10. doi:10.1088/1742-2132/10/1/015009.

Biondi, B., and G. Palacharla, 1996, 3D prestack migration of common-azimuth data: Geophysics, **61**, 1822-1832.

Biondi, B., and L., Vaillant, 2000, 3D wave-equation prestack imaging under salt: 70th Annual International meeting, Society of Exploration Geophysicists, Expanded Abstracts, 906-909.

Bishop, T., K. Bube, R. Cutler, R. Langan, P. Love, J. Resnick, R. Shuey, D. Spindler, and H. Wyld, 1985, Tomographic determination of velocity and depth in laterally varying media: Geophysics, **50**, 903-923.

Bleistein, N., 1987, On the imaging of reflectors in the Earth: Geophysics, **52**, 931-942.

Bracewell, R. N., 1965, The Fourier transform and its applications. New York: McGraw-Hill, 1965 pp.

Brown, A. R., 1996, Seismic attributes and their classification: The Leading Edge, **10**, 1090.

Brown, A. R., 2001, Understanding seismic attributes: Geophysics**, 66**, 47-48.

Chang, W., and G. A. McMechan, 1994, 3D elastic prestack, reverse-time depth migration: Geophysics, **59**, 597-610.

Chopra, S., J. P. Castagna, and O. Portniaguine, 2006, Seismic resolution and thin-bed reflectivity inversion: Canadian Society of Exploration Geophysicists Recorder, **31**, 19-25.

Chopra, S. and K. J. Marfurt, 2007, Seismic attributes for prospect identification and reservoir characterization: Society of Exploration Geophysicists, Geophysical Developments Series 11, Tulsa, OK, 464 pp.

Chopra, S. and K. J. Marfurt, 2008, Emerging and future trends in seismic attributes. The Leading Edge, **27**, 298-318.

Chun, J., and C. Jacewitz, 1978, A fast multi-velocity function frequency domain migration: Presented at the 48th Annual International meeting, Society of Exploration Geophysicists.

Claerbout, J. F., 1985, Imaging the Earth's interior, Blackwell Scientific Publications. Oxford, London, Edinburgh, 399 pp.

Cox, M. G., 1972, The numerical evaluation of b-splines. Journal Institute Mathematics Applications, **10**, 134–149.

Davies, E. R., 1992, The relative effects of median and mean filters on noisy signals: Journal of Modern Optics, **39**, 103-113.

De Boor, C., 1972, On calculating with b-splines. Journal of Approximation Theory, **6**, 50–62.

Duquet B., K. Marfurt, and J. Dellinger 2000, Kirchhoff modeling, inversion for reflectivity, and subsurface illumination: Geophysics, **65**, 1195-1209.

Etgen, J. T., 1998, V (z) F-K prestack migration of common-offset common-azimuth data volumes, part 1: Theory: 68th Annual International Meeting, Society of Exploration Geophysicists, Expanded Abstracts, 1835-1838.

Etgen, J., and D. Nichols, 1999, Application of the Li correction to explicit depth extrapolation methods: 69th Annual International meeting, Society of Exploration Geophysicists, Expanded Abstracts, 1366-1369.

Foley J. D., 1994, Introduction to Computer Graphics, Addision-Wesley, 746 pp.

Gabor, D., 1946, Theory of communication: Journal of the Institute of Electrical Engineers, **93**, 429 457.

Gardner, G. H. F., S. Y. Wang, N. D. Pan, and Z. Zhang, 1986, Dip moveout and prestack imaging: 18th Offshore Technical Conference, **2**, 75-84.

Gazdag, J., 1978, Wave equation migration with phase-shift method: Geophysics, **43**, 1342-1351.

Gibson, M. A. S., S. J. Jolley, and A. C. Barnicoat, 2000, Interpretation of the Western Ultra Deep Levels 3D seismic survey: The Leading Edge, **19**, 730–735, doi: 10.1190/1.1438704.

Gumerov, N. A., R. Duraiswami, 2006, Fast multipole method for the biharmonic equation in three dimensions: Journal of Computational Physics, **215**, 363–383.

Gupta, G., 2011, Algorithm for image processing using improved median filter and comparison of mean, median and improved median filter: International Journal of Soft Computing and Engineering , **1**, 2231-2307.

Hale, D., 1984, Dip-moveout by Fourier transform: Geophysics, **49**, 741-757.

Hale, D., 1991b, 3D depth migration by McClellan transformations: Geophysics, **56**, 1778-1785.

Hill, N. R., 2001, Prestack Gaussian-beam depth migration: Geophysics, **66**, 1240-1250.

Judson, D. R., P. S. Schultz, and J. W. C. Sherwood, 1978, Equalizing the stacking velocities of dipping events via Devilish: Presented at the 48th Annual International meeting, Society of Exploration Geophysicists, San Francisco.

Leslie, J. M., and D. C. Lawton, 1998, Depth migration of anisotropic physical model data: Geo-Triad 1998 Abstracts, 77-78.

Li, X., and J. Zhu, 2009, A Galerkin boundary node method for biharmonic problems, Engineering Analysis with Boundary Elements, **33**, 858–865.

Li, Z., and W. Lynn, 1991, Enhancements to prestack frequency-wavenumber (f-k) migration: Geophysics, **56**, 27-40.

Malehmir, A., H. Thunehed, and A. Tryggvason, 2009, The Palaeoproterozoic Kristineberg mining area, northern Sweden: results from integrated 3D geophysical and geologic modeling, and implications for targeting ore deposits: Geophysics, **74**, B9–B22. doi: 10.1190/1.3008053.

Malehmir, A., R. Durrheim, G. Bellefleur, M. Urosevic, C. Juhlin, D. White, B. Milkereit, and G. Campbell, 2012. Seismic methods in mineral exploration and mine planning: a general

overview of past and present case histories and a look into the future: Geophysics, **77**, WC173–WC190. doi:10.1190/GEO2012-0028.1.

Marfurt, K. J., 2006, Robust estimates of 3D reflector dip and azimuth: Geophysics, **71,** 29–40.

Mayne, W. H., 1962, Common reflection point horizontal data stacking techniques. Geophysics, **27**, 927–938. doi:10.1190/1.1439118.

Milkereit, B., D.W. Eaton, J. Wu, G., Perron, M. H., Salisbury, and E., Berrer, 1996, Seismic imaging of massive sulphide deposits: part II. Reflection seismic profiling. Economic Geology, **91**, 829–834.

Milkereit, B., E. K. Berrer, A. R. King, A. H. Watts, B. Roberts, and E. Adam, 2000, Development of 3D seismic exploration technology for deep nickel–copper deposits - a case history from the Sudbury Basin, Canada: Geophysics, **65**, 1890–1899.

Oppenheim, A. V., and R. W. Schafer, 1975, Digital signal processing: Englewood Cliffs, New Jersey, Prentice Hall.

Peigl, L., 1991, On NURBS: A survey: Institute of Electrical and Electronic Engineering Computer Graphics and Applications, **11**, 55 - 71.

Pretorius, C. C., W. H. Steenkamp, and R. G. Smith, 1994, Developments in data acquisition, processing, and interpretation over ten years of south vibroseismic surveying in South Africa: Proceedings of the 15th CMMI Congress, South African Institute of Mining and Metallurgy, **3**, 249–258.

Pretorius, C. C., W.F. Trewick, A. Fourie, and C. Irons, 2000, Application of 3D seismics to mine planning at Vaal Reefs gold mine, number 10 shaft, Republic of South Africa: Geophysics, **65**, 1862-1870.

Purnomo, E. W., and Z. Z. T. Harith, 2010, Combination of minimum-maximum (m-m) attribute and zero-intens-difference (z-i-d) attribute for estimating seismically thin-bed thickness: ITB Journal of Engineering Science, **43**, 78-100.

Rijks, E. J. H., and J. C. E. M. Jauffred, 1991, Attribute extraction: An important application in any detailed 3D interpretation study: The Leading Edge, **10**, 11–19.

Rogers, D. F., and R. A. Earnshaw, 1991, State of the art in Computer Graphics - visualization and modeling, Springer-Verlag, New York, 225 – 269.

Salisbury, M. H., G. W. Harvey, and L. Mathews, 2003, The acoustic properties of ores and host rocks in hardrock terranes, in: D.W. Eaton, B. Milkereit, and M.H. Salisbury, eds., Hardrock Seismic Exploration, Geophysical Developments **10**: Society of Exploration Geophysicists, 9-19.

Sheriff, R. E., and L. P. Geldart, 1995, Exploration Seismology, 2nd edition. Cambridge University Press, 592 pp.

Shi, Z., Y., Cao, Q. Chen, 2012, Solving 2D and 3D poisson equations and biharmonic equations by the Haar wavelet method: Applied Mathematical Modeling, **36**, 5143-5161.

Shurtleff, R. N., 1984, A prestack f-k procedure for prestack migration and migration velocity analysis: Presented at the 46th Meeting, European Association of Exploration Geophysicists.

Stevenson, F., R. M. A. Higgs, and R. J. Durrheim, 2003, Seismic imaging of precious and base-metal deposits in South Africa, in D. W. Eaton, B. Milkereit, and M. H. Salisbury, eds., Hardrock seismic exploration, Geophysical Developments **10**: Society of Exploration Geophysicists, 141–156.

Taner, M. T., 2001, Seismic Attributes, Canadian Society of Exploration Geophysicists Recorder, 48-56.

Trickett, J. C., W. A. Duweke, and S. Kock, 2004, Three-dimensional reflection seismic: Worth its weight in platinum: International Platinum Conference, South African Institute of Mining and Metallurgy, 257–264.

Watt A., and M. Watt, 1992, Advanced animation and rendering techniques, Association for Computing Machinery press, Addison-Wesley, New York, 455 pp.

White, D. J., D. Secord, and M. Malinowski, 2012, 3D seismic imaging in the Flin Flon VMS mining camp: part I - seismic results. Geophysics, **77**, WC47–WC58.

Whitmore, N. D., S. H. Gray, and A. Gersztenkorn, 1988, Two-dimensional poststack depth migration: a survey of methods: First Break, **6**, 189-197.

Widess, M. B., 1973, How thin is thin bed? Geophysics, **38**, 1176-1180.

Yilmaz, Ö., 1979, Pre-stack partial migration: Society of Exploration Geophysicists, PhD thesis, Stanford University.

Yilmaz, Ö., 1987, Seismic data processing: Society of Exploration Geophysicists, Tulsa Oklahoma, 526 pp.

Yilmaz, Ö., 2001, Seismic data analysis - Processing, inversion, and interpretation of seismic data. Society of Exploration Geophysicists, Tulsa, Oklahoma, 2027 pp.

Yilmaz, Ö., I. Tanir, and C. Cregory, 2001, A unified 3D seismic work flow: Geophysics, **66**, 1699-1713, doi: 10.1190/1.1487112.

Zeng, H., 2009, How thin is a thin bed? An alternative perspective: The Leading Edge, **28**, 1192-1197.

3. SUMMARY OF SCIENTIFIC CONTRIBUTIONS

In this section the novel contributions to knowledge made by this study are highlighted.

The publication entitled *"Application of 3D seismic techniques to evaluate ore resources in the West Wits line goldfield and portions of the West Rand goldfield, South Africa. Geophysics 77, WC163–WC171, doi:10.1190/GEO2012-0133.1."* (Chapter 4) bridges the gap between old exploration technology that only allowed for the delineation of gold bearing horizons and offsets (faults) at shallow depth of ~ 0.5 km, and new technology that provides high-resolution 3D images of the subsurface structures at great depths of ~ 4.5 km.

The new interpretation techniques have proven to be effective in enhancing faults and dikes which offset the gold-bearing horizons with throws below seismic resolution limit. However, as evidenced in the 1994 Leeudoorn old data, the overall performance of these techniques is highly dependent on the signal-to-ratio (S/N) of the data, which in turn depends mainly on the velocity field and migration techniques. In order to maximize the resolution of the data, we re-processed the 1994 Leeudoorn data by migrating the data before stacking using the advanced Kirchhoff migration algorithm in time domain, i.e., Kirchhoff prestack time migration (KPSTM). The Kirchhoff migration technique was implemented for the first time in the Witwatersrand Basin. As evidenced in many petroleum studies, this technique has proven successful in improving the quality of the data by imaging steeply dipping horizons and subtle geologic structures in mining areas characterized by major lateral velocity variations, compared to conventional poststack depth migration (PSDM) using the finite difference migration (FD) algorithm.

To test whether the improvement in imaging was due to Kirchhoff prestack migration, or the revised interpreted velocity field picked during re-processing, both the old and newly picked velocity model was tested in the Kirchhoff time migration workflow. It was concluded that high-definition of structures were mainly due to the combination of the new velocity field and Kirchhoff migration technique. In addition, the poor imaging of the reefs, stratigraphy and faults in the 1994 Leeudoorn data is mainly attributed to inaccurate velocity fields used for finite depth migration, rather than the poststack depth migration as such. Based on these results, the following PSTM workflow in areas characterized by highly dipping stratigraphy and complex faulting was proposed:

(1) Produce the PSTM gathers at velocity locations using the interpreted velocity model.

(2) Pick the first iteration of PSTM velocities.

(3) Migrate the total volume with the first iteration velocities.

(4) Pick second-pass PSTM velocities from gathers migrated with first iteration velocities.

(5) Re-stack the PSTM gathers with second pass velocities.

(6) Depth convert the data using interval velocities derived from borehole information and PSTM data.

More importantly, for the first time in the Kloof gold mine, a 250 m wide and 1 km long block of the Ventersdorp Contact Reef (VCR) was identified using 3D seismics, and this block is bounded by the multi-fault segments of the West Rand Fault (WRF) Zone. Discoveries of this nature are crucial for the ore resource calculation and financial evaluation of the VCR ore body, and life-of-mining planning.

Attribute analysis, such as dip amplitude, dip-azimuth and edge detection on the horizon data, has enhanced the detection of subtle features that have a direct impact on mine production and stope development. The edge detection attribute, in particular, has shown its superiority over dip and dip-azimuth by further enhancing the detection of intersecting, cross-cutting, and multi-bifurcating faults, which are impossible to visualize in seismic sections using traditional interpretation.

It was concluded that the new imaging techniques and the application of 3D seismic attributes have assisted in the discovery and evaluation of resources, and the reduction of structural risks in strategic mine planning. This could not have been achieved through conventional processing and interpretation techniques that are widely employed by the mining industry.

The award-winning publication entitled *"3D edge detection seismic attributes used to map potential conduits for water and methane in deep gold mines in the Witwatersrand basin, South Africa. Geophysics 77, WC133–WC147, doi: 10.1190/GEO2012-0135.1.*" (Chapter 5) investigates the mechanisms by which water and methane gas is transported to underground workings using 3D seismics.

This study was motivated by the deaths and injuries to mine workers from ingress of water and influx of methane gas to underground workings. Methane tends to migrate from high to low pressure zones, either as a gas or dissolved in ground water. Possible sources of the Witwatersrand methane include the mantle (brought up by granitic intrusions and syenite dikes), kerogen derived from ancient algal mats, or coal seems found in the Karoo sediments above the Transvaal Supergroup. The coal seams of the Karoo Supergroup, in particular, are probably the main source of methane into the gold mines from Witwatersrand goldfields.

The edge detection attribute computed for both the Black Reef (BLR), which is the base of the Transvaal Supergroup, and the Ventersdorp Contact Reef (VCR), which is the base of the Ventersdorp Supergroup, has identified a number of structures (faults/dikes) that connect the BLR and VCR horizons. They may have intersected dolomitic aquifers above the BLR and transported water and methane to underground workings (VCR level) but this needed further investigation. These faults could not be tracked conventionally on the seismic sections, implying that they have throws less than one-quarter of the dominant wavelength (~20-25 m).

These subtle faults are interpreted to have undergone reactivation during the post-BLR deformation event, and some structures are interpreted to represent dikes that were emplaced after the

deposition of the Black Reef Formation. They include dykes of the Bushveld Complex, Pilanesburg, Karoo and post-Karoo Supergroup. To test which structures are associated with water and methane, water-methane intersection data from Kloof gold mine were superimposed on the VCR edge detection map. It was observed that more than 60% of the structures (mostly those that dip ~60° and sub-vertical) had good correlation and connection with water and methane intersections. However, it was difficult to determine:

(1) Which faults and dikes intersect dolomitic aquifers above the BLR.

(2) Which of the aquifers may have once been charged by methane derived from coal seams, if at all.

(3) Which of the faults and dikes, if they show good correlation with water, are prone to fluid transmission.

These questions require further investigation. Further to this, although the sources of methane have not been confidently identified, it was shown that methane, along with water, can ingress along structures that are seismically imaged. It was suggested that methane derived from the coal seams of the Karoo sediments might have entered groundwater aquifers in dolomite within Transvaal Supergroup prior to Karoo Supergroup erosion.

Finally, regardless of the source of methane, these findings can be used to assess and mitigate the risks posed by inrushes of fissure water and the ignition of flammable gases as mining proceeds to greater depths, or prior to opening and extending a mine.

The publication entitled *"Neoarchaean tectonic history of the Witwatersrand Basin and Ventersdorp Supergroup: New constraints from high resolution 3D seismic reflection data. Tectonophysics 590, 94-105, doi: 10.1016/j.tecto.2013.01.014.*" (Chapter 6) tests and constrains several episodes of deformation (e.g., positive and negative inversion) in the Witwatersrand Basin. This research further synthesizes a new Neoarchean evolution for first-order scale structures in terms of deformation sequence and relation to current models.

To do this, the re-processed and merged high-resolution 3D seismic data that were acquired between 1994 and 2003, covering the West Wits Line (Western Ultra-deep Levels (WUDLs), Kloof–Driefontein Complex (KDC)) and West Rand (South Deep) goldfields were interpreted. The merged 3D coverage amounts to ~ 7040 km^3 with the dominant frequency of 65 Hz and mean velocity of 6500 m/s, providing a vertical resolution limit of 25 m (typical one-quarter dominant wavelength).

To investigate the geometric evolution of first-order scale structures, depositional and erosional patterns, three main steps were taken:

(1) Mine blocks (i.e., WUDLs, KDC West and East, South Deep), were treated individually by interpreting 2D lines across them.

(2) A regional 3D fault-horizon model was built.

(3) Various restorations were performed to allow 3D visualization of the structural history through time.

(4) The vertical displacements (throw) on extensional first-order faults using seismic sections orthogonal to fault strike on the Ventersdorp Contact Reef (VCR) horizon were measured.

Seismic sections provide new information regarding the geometry of the first-order scale faults, the West Rand Fault (1.6–2.0 km normal throw; 600 m sinistral offset) and Bank Fault (2.0–2.5 km normal throw; 800 m sinistral offset). These form a rift-like like system of listric faults that trend north-northeast and dip steeply (65°–70°) to the west.

Neoarchean extensional faulting was observed for the West Rand Fault (WRF) and Bank Fault (BF) in many seismic profiles. For example, the seismic sections showed that these faults displace the stratigraphy from the top of Ventersdorp Supergroup (ca. 2.720–2.630 Ga) through Central Rand Group (ca. 2.902–2.849 Ma) and down to the West Rand Group (ca. 2.985–2.902 Ga), and form a décollement horizon in the West Rand shale units. These first-order scale faults and their associated drag synclines and anticline, as seen on reflective seismic horizons, is attributed to the massive Platberg-Hlukana age extension event (2.70–2.64 Ga). More importantly, this study supports some previous studies by Dankert and Hein (2010) that the WRF and BF do not breach the base of the Black Reef Formation of the Paleoproterozoic Transvaal Basin (ca. 2.58–2.20 Ga), thus constraining extension to between 2.714 Ga and 2.588 Ga. Our tectonic model also supports studies by Hall (1996) who pointed out that the Venterspost sediments, Ventersdorp Contact Reef and overlying metabasalts of the Klipriviersberg Group are contemporaneous with the earliest Ventersdorp volcanism.

In contrast, the research does not support arguments presented by Coward et al. (1995) that the BF displaces the Transvaal Basin by at least 200 m in the study area. Faults with throws of ~ 200 m fall into the category of second-order scale structures, so it would have been readily easy to identify displacement of 200 m on the seismic section. That was not the case. Additionally, although a number of faults and dikes were identified through attribute analysis that are associated with post-Transvaal Basin deposition, their displacements are only in order of meters to tens of meters, and are not related to WRF and BF formation.

This study also confirms that the majority of tectonically- or fault-induced pseudotachylite veins (which are attributed to the activity of the West Rand Fault zone and Panvlakte Fault) in the West Rand goldfield were formed pre- 2.58 Ga, that is, before the deposition of the lower Transvaal Basin. Hence the West Rand and Panvlakte fault segments do not cross-cut and displace the base of the basin i.e., Black Reef (BLR) Formation (Appendix A, see Figure 4). These findings question studies by Killick and Roering (1990) which correlate pre-2.58 Ga faults-induced friction-induced pseudotachylites with 2.02 Vredefort Dome impact-induced pseudotachylites.

Furthermore, the merging of the data made it possible to identify, for the first time, the first-order scale northerly-trending, upright, tight to open Libanon Anticline (8 km wavelength and 2 km amplitude) and its parasitic second-order scale folds and reverse faults (such as Tandeka and Jabulani

thrusts). These are interpreted to have formed prior to fold-thrust development during the compressional deformation, Umzawami Event (ca 2.73 Ga), which terminated the deposition of the Central Rand Group sediments at the end of Asazi Event (ca. 2.90 Ga).

The tectonic evolution model proposed in this study is supported by absolute and relative U–Pb geochronological age data, borehole and underground mapping datasets. In particular, the merging and availability of the historical 3D seismic datasets has enabled us to investigate new first-order scale structures at the *'data merge boundary'* for the first time.

The publication entitled *"A review of reflection seismic investigations in three major metallogenic regions: The Kevitsa Ni–Cu–PGE district (Finland),* **Witwatersrand goldfields (South Africa),** *and the Bathurst Mining Camp (Canada), in press, Ore Geology Reviews. http://dx.doi.org/10.1016/j.oregeorev.2013.01.003."*(Chapter 7, section 4) analyses the inter-relationship between the timing of faults activity, dike intrusion and gold-bearing distribution to provide 3D seismic constraints that might help to resolve the controversy regarding the source of gold in the Witwatersrand Basin. The three competing genetic models include unmodified placer, modified placer occurring at peak-metamorphism and an early, pre-metamorphic hydrothermal model.

To constrain the age limits of the structures, both the Ventersdorp Contact Reef and Black Reef gold-bearing horizons were interpreted. The Black Reef, in particular, was interpreted using advanced attribute analysis to constrain ages of the structures relative to the deposition of the Transvaal Supergroup. The timing of fault activity has a number of potential effects on the origin of gold. For example, 3D seismic imaging and interpretation of growth faults and syn-sedimentary faults (like those seen in the Kloof gold mine) may be used to test the placer model. Faults that were active during the deposition of the VCR could affect gold distribution, while structures that were only active prior to VCR deposition should have no control on gold distribution.

Additionally, post-Black Reef dikes that were mapped and projected at Black Reef level through attribute analysis, as evidenced in South Deep, Kloof and Driefontein gold mines, may have acted as barriers that prevented laterally continuous flow of the gold-bearing fluids.

To test the possible transmission of fluid through faults, the seismically imaged faults were correlated with known water and gas intersection data. The correlation between seismically imaged faults and dikes with water and methane intersection data (see Chapters 5 and 6) shows that water and methane mostly occur along second- to third-order scale structures that were active after the deposition of base of the Transvaal Basin.

On the first-order-scale, it is clear that the West Rand and Bank faults and their associated second-order scale listric and growth faults were formed prior to deposition of the Black Reef, meaning that they probably had no control on the distribution of the Black Reef facies.

In the absence of gold grade data, this structural analysis could not resolve the debate, but rather sought to demonstrate that 3D seismic can provide valuable information that can be used to test the ore genetic models.

The publication entitled *"Seismic attribute analysis to enhance detection of thin gold-bearing reefs: South Deep Gold mine, Witwatersrand Basin, South Africa, accepted, Journal of Applied Geophysics."* (Chapter 8) shows the state-of-the-art in seismic interpretation of the thin gold-bearing reefs using complex trace attribute displays.

Previous publications (Chapters 4-7) have presented structural results that are based solely on the seismic amplitude attribute response of the top of the Ventersdorp Contact Reef (VCR) and Black Reef (BLR) horizons. In the South Deep gold mine, it was difficult to identify, to consistently pick, and to track the Elsburg Conglomerate reef (EC, ~ 20 m thick conglomerate unit) using conventional amplitude displays. The difficulty in picking the EC reef was due to its highly variable amplitude reflection character and its geometry at the base of a complex Elsburg Reef clastic wedge package (UER). A decrease in acoustic impedance or interference, in particular, due to wide variation of quartzite and conglomerates units within the UER package, made an individual reef unresolvable by conventional amplitude-based interpretation.

To enhance the mapping of the EC reef and its subcrop position against the VCR (which is critical for EC resource evaluation and mine planning at South Deep gold mine), a combination of seismic instantaneous attributes and volumetric attributes were extracted from the seismic volume. The instantaneous attributes, mainly phase-derived ones, have enhanced the detection of the EC reef and its continuity. These attributes (mainly paraphase) emphasize the optimum imaging of a number of subtle faults on the migrated seismic sections that offset the EC reef, which do not show up clearly on conventional amplitude displays and other amplitude-dependent seismic attributes.

On the other hand, color coded instantaneous attributes coupled with isopach analysis and volumetric attributes (e.g., root mean square amplitude and zero-crossing) have enabled the detection and location of the interference position as coinciding with the EC subcrop position. The EC reef depth position shows a very good correlation with the borehole controls. The depth discrepancies between the logged positions of the EC reef and boreholes throughout the mining area fall within the positional accuracy of the seismic survey of ± 25 m vertical resolution (considering the seismic bin size of 25 m).

This study further revealed that the detectability of the thin reef is dependent on many factors such as its geometry, impedance contrast of the materials above and below, complexity of the adjacent layers, and the quality of the 3D seismic data. The study also showed that the amplitude-independent instantaneous attribute analysis (e.g., phase and paraphase) can aid in improving our understanding of the character of thin reefs. It can mitigate drilling risks and increase the value of the 3D seismic data, especially in areas with low acoustic impedance contrasts and complex reef geometries. These

findings can be factored in the current mine geological model, thus improving the evaluation of the EC reef in the South Deep gold mine.

The publication entitled *"The Ventersdorp Contact Reef (VCR) model in the Kloof Gold Mine (South Africa) as derived from 3D seismics, geological mapping and exploration borehole datasets, accepted, International Journal of Rock Mechanics and Mining Sciences.*" (Chapter 9) warns us against throwing older technologies away when new ones take over, and shows the power of integrating 3D seismic data with borehole and underground geological mapping data.

This study integrated 3D seismic data with information about faults and dikes that were mapped both in underground workings and from underground exploration holes. And that would have been used to develop a mine ore body model. By doing so, the 3D seismic imaging limitations, such as the vertical resolution limit (one-quarter of the dominant wavelength ~25 m) and horizontal resolution limit (dominant wavelength ~100 m) were overcome.

It was shown that regardless of the quality of the data, state-of-art processing (Chapter 4) and interpretation techniques (Chapter 6), there remained structures (faults and dikes) that offset the ore body that could not resolved. These structures can have a significant impact on mine development. By combining seismic and underground mapping data, it was possible to (1) assess structures that were under-sampled by seismics, and (2) better define fault architectures and likely zones of difficult mining ground conditions around faults and dikes.

The fault statistical analysis (such as fault spacing or compartment size, patterns, continuity, fault offset or throw, fault heave, strike, dip, dip direction, fault length, pitch and hade) derived from these data sets improved the understanding of the complex fault architecture (e.g., intersecting faults, cross-cutting and multi-bifurcations of faults) in Kloof gold mine. The *compartment maps*, in particular, computed for stoped-out and development areas identified small fault-bounded compartments (0-50 m fault spacing) that were not predicted by 3D seismic data. The zones with closed-spaced faults (0-50 m fault compartment) were interpreted as zones that may increase risks during mining. Clearly, this confirms that seismics fails to detect fault-bounded compartments falling below the seismic dominant wavelength of 100 m.

Furthermore, *fault throw analysis* showed that the majority of seismically-imaged faults exhibit throws ranging from 16-30 m, while underground mapped faults exhibit throws in range of 6-8 m. At the fault intersection points on the integrated datasets, a complex series of minor faults with all orientations exhibit throws of less than 4-6 m. Thus the underground mapping and seismic data complement each.

Using surface and underground borehole control, a heuristic approach was developed to minimize the depth discrepancies that occur between seismically-derived horizon and borehole controls. The lateral positioning of structures in the seismic horizon was further corrected by tying seismic data and infrastructures such as shafts. The root mean-square high amplitudes of isolated

bodies coincided with stopes and shafts; however the seismic anomalies were offset from the expected positions by 200 m to the west and approximately 40 m to the north. This discrepancy is interpreted to be, in part, related to the velocity field used during time-to-depth conversion of the data.

In summary, a Ventersdorp Contact Reef (VCR) ore body model was derived using a unique workflow. To incorporate complex structural architectures and ensure the robustness of the fault-horizon model, the advanced Non-Uniform Rational B-splines (NURBS) modeling techniques was used.

GEOPHYSICS, VOL. 77, NO. 5 (SEPTEMBER-OCTOBER 2012); P. WC163–WC171, 11 FIGS.
10.1190/GEO2012-0133.1

Application of 3D seismic techniques to evaluate ore resources in the West Wits Line goldfield and portions of the West Rand goldfield, South Africa

Musa S. D. Manzi[1], Mark A. S. Gibson[2], Kim A. A. Hein[1], Nick King[3], and Raymond J. Durrheim[4]

ABSTRACT

As expensive as 3D seismic reflection surveys are, their high cost is justified by improved imaging of certain ore horizons in some of the Witwatersrand basin gold mines. The merged historical 3D seismic reflection data acquired for Kloof and South Deep mines forms an integral part of their Ventersdorp Contact Reef mine planning and development programme. The recent advances in 3D seismic technology have motivated the reprocessing and reinterpretation of the old data sets using the latest algorithms, therefore significantly increasing the signal-to-noise ratio of the data. In particular, the prestack time migration technique has provided better stratigraphic and structural imaging in complex faulted areas, such as the Witwatersrand basin, relative to older poststack migration methods. Interpretation tools such as seismic attributes have been used to identify a number of subtle geologic structures that have direct impact on ore resource evaluation. Other improvements include more accurate mapping of the depths, dip, and strike of the key seismic horizons and auriferous reefs, yielding a better understanding of the interrelationship between fault activity and reef distribution, and the relative chronology of tectonic events. The 3D seismic data, when integrated with underground mapping and borehole data, provide better imaging and modeling of critical major fault systems and zones of reef loss. Many faults resolve as multifault segments that bound unmined blocks leading to the discovery and delineation of resources in faulted areas of the mines.

INTRODUCTION

In the early 1980s, the planning of new mines and extension of existing mines relied mostly on geologic models that were based on a combination of gravity, aeromagnetic, and borehole data (Durrheim, 1986; Stevenson et al., 2003). Although magnetic and gravity techniques are effective in the delineation of subsurface structures such as dikes and major faults (Weder, 1994; Trickett et al., 2004), they are unable to map the structure of deeply buried strata in detail (Pretorius et al., 1994; Stevenson et al., 2003), which is critical for the very deep gold mines of the Witwatersrand Basin. Furthermore, they cannot resolve gold-bearing reefs and fault geometries with the accuracy required for optimal mine planning (Stevenson et al., 2003; Trickett et al., 2004). Although borehole data provide accurate geologic information, this information is restricted to the vicinity of the borehole (Trickett et al., 2004).

Since the late 1980s, the Witwatersrand gold mines have made use of 3D seismic reflection surveys to facilitate reliable mine planning and design. In 2003, Gold Fields Ltd. conducted a high-resolution 3D seismic reflection survey (the Kloof-South Deep survey), targeting the down-dip portion of the auriferous Ventersdorp Contact Reef (VCR) in the Kloof and South Deep gold mines, which are located west and east of the West Rand Fault, respectively (Figure 1). The Kloof gold mine is a large, shallow to ultradeep level mine with workings accessed through five shaft systems. The mine exploits various gold reefs (mainly VCR) at depths

Manuscript received by the Editor 16 April 2012; published online 6 September 2012.
[1]University of the Witwatersrand, School of Geosciences, Johannesburg, Republic of South Africa. E-mail: musa.manzi@students.wits.ac.za; kim.ncube-hein@wits.ac.za.
[2]High Power Exploration, Johannesburg, Republic of South Africa. E-mail: mark.g@ipulse.fr.
[3]Gold Fields Limited, South Deep Gold Mine, Johannesburg, Republic of South Africa. E-mail: nick.king@goldfields.co.za.
[4]University of the Witwatersrand, School of Geosciences, Johannesburg, Republic of South Africa and CSIR Center for Mining Innovation, Johannesburg, Republic of South Africa. E-mail: raymond.durrheim@wits.ac.za.
© 2012 Society of Exploration Geophysicists. All rights reserved.

Downloaded 10 Sep 2012 to 146.141.1.82. Redistribution subject to SEG license or copyright; see Terms of Use at http://segdl.org/

between 2000 and 3350 m below the surface. The South Deep gold mine is an intermediate to ultradeep level mine comprising two shaft systems. It exploits VCR and Upper Elsburg reefs at depths between 2000 and 3500 m below the surface. The primary objective of the survey was to image the VCR orebody to the northwest and southeast of the West Rand Fault over the depth range of 2000 to 4500 m. The true seismic volume extends to approximately 9 km deep, with an east–west extent of 40 km and north–south extent of 16 km (i.e., 5760 km^3). The secondary objective was to image the cutoff of the VCR on the downthrown and upthrown blocks of the West Rand Fault to assist resource evaluation and mine planning.

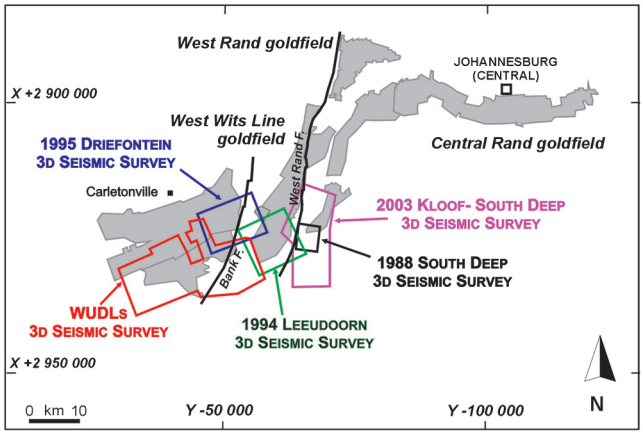


Figure 1. Location of the Witwatersrand basin historical 3D seismic reflection survey areas (after Gibson et al., 2000).

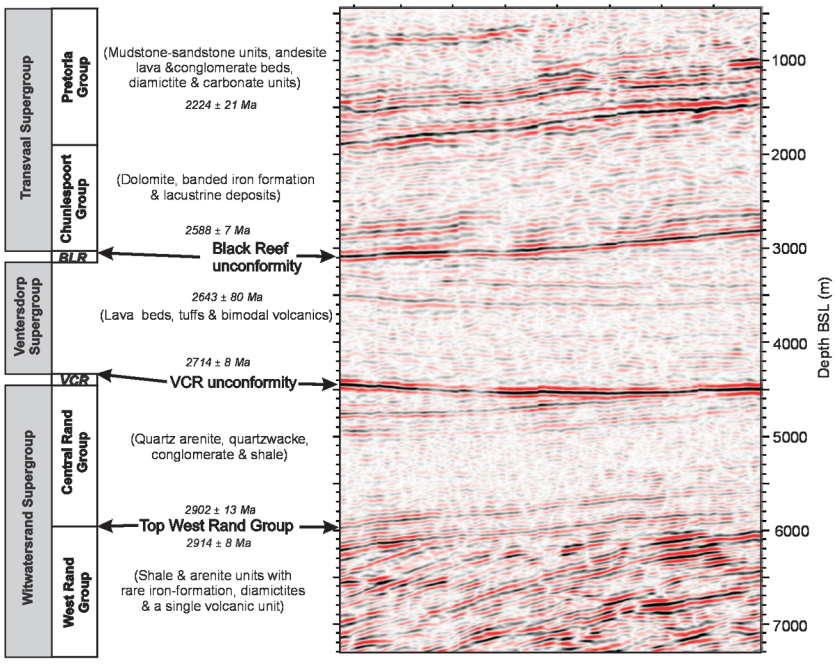


Figure 2. Generalized stratigraphy of the West Wits Line goldfield, derived from the depth-converted PSTM seismic section. Geochronological data and geology after Dankert and Hein (2010).

Recently, the application of 3D seismic imaging has brought precision to drilling boreholes in geologically complex areas (De Wet and Hall, 1994; Trickett et al., 2004). In this study, we present the detailed interpretation of five merged historical 3D seismic reflection surveys from gold mines on the West Wits Line and West Rand. We also show how the new migration algorithms and improvement in interpretation techniques can maximize the high-resolution image of ore horizons and structures, thus improving mine planning and design and reducing mining risks.

The 2003 Kloof-South Deep survey was designed to overlap with the 1988 South Deep survey, the first 3D seismic survey conducted in South Africa, and the 1994 Leeudoorn 3D seismic survey. The three surveys were merged and processed as a single entity of final depth-converted prestack time migrated (PSTM) seismic volume to produce a single seismic cube. To improve the resolution of the old data, the 1994 Leeudoorn data set was reprocessed using the latest processing algorithms. Following the successful interpretation of the data, the single seismic cube was merged (postmigration) with the Western Ultra Deep Levels (WUDLs) survey, which was acquired in 1995 and covers the Driefontein gold mine to the west of the Bank Fault (Figure 1). The Driefontein gold mine comprises eight shaft systems. It exploits various gold-bearing reefs, mainly VCR and Carbon Leader Reef (CLR) that occur at depths between 600 and 3300 m below the surface. The WUDLs survey also covers the Mponeng, Savuka, and Tautona gold mines. The Mponeng Mine is one of the deepest and richest gold mines in the world, exploiting VCR at depths between 2400 and 3900 m below the surface, whereas the Savuka and Tautona gold mines exploit mainly CLR at depths up to 3450 m.

These data sets were incorporated into one continuous volume and used to study the regional structural setting, including major and minor structures. The overall aims were to investigate (1) the application of the PSTM technique in structural enhancement, (2) the geometry of faults and their impact on mining, and (3) the use of attribute analysis to map structures that cannot be resolved through conventional interpretation.

GEOLOGIC SETTING AND MINEABLE REEFS

The famous Archean Witwatersrand basin is the largest gold province in the world (Phillips and Law, 2000; McCarthy, 2006). In the past century, it has produced about 40% of the world's mined gold and is estimated to still contain 30% of the world's known gold reserves (Stanistreet and McCarthy, 1991). Its exploration and exploitation has produced a huge geologic and geophysical database.

A generalized lithostratigraphic column of the Witwatersrand basin is summarized in Figure 2. The Witwatersrand Supergroup overlies the Dominion Group unconformably and comprises lower and upper successions, namely the West Rand and Central Rand Groups (Dankert and Hein, 2010). The Dominion Group is not shown on Figure 2 because it is beneath our zone of interest.

Downloaded 10 Sep 2012 to 146.141.1.82. Redistribution subject to SEG license or copyright; see Terms of Use at http://segdl.org/

The West Rand Group unconformably overlies the Dominion Group with clastic and largely marine sediments (ca. 2985–2902 Ma; Kositcin and Krapež, 2004; U-Pb detrital zircon SHRIMP). Unconformably overlying the West Rand Group are the quartzite, conglomerate, and shale units of the Central Rand Group (ca. 2902–2849 Ma; Kositcin and Krapež, 2004; U-Pb detrital zircon SHRIMP). The Central Rand Group contains most of the auriferous reefs mined throughout the basin, including the Elsberg, Kloof, Libanon, and Kimberley reefs of the Johannesburg Subgroup, and the Bird, Carbon Leader, North Leader, and Middelvlei reefs of the Turffontein Subgroup (De Kock, 1964). The upper part of the Central Rand Group is unconformably overlain by the VCR of the Venterspost Formation (ca. 2729 ± 19 Ma; Kositcin and Krapež, 2004; U-Pb detrital zircon SHRIMP). The VCR represents an erosional surface that was formed at the end of deposition of the Central Rand Group (McCarthy, 2006).

Above the VCR is the late-Archean Ventersdorp Supergroup (ca. 2.72–2.63 Ga), which comprises ultramafic and mafic lavas of the Klipriviersberg Group (ca. 2709 ± 8 Ma), and metasedimentary rocks and bimodal volcanics of the Platberg Group (Van der Westhuizen et al., 1991). The Pniel Group (Phillips and Law, 2000; Jolley et al., 2004) overlies the Platberg Group and Klipriviersberg Group (cf., Dankert and Hein, 2010).

Unconformably overlying the Ventersdorp Supergroup is the relatively thin Black Reef Formation (BLR), which occurs at the base of the Transvaal Supergroup (ca. 2588 ± 6 Ma; Krapež, 1985; Vos, 1975; Jolly et al., 2004). The Transvaal Supergroup comprises lower and upper successions, namely the Chuniespoort and Pretoria Groups. The dolomites, quartzites, and shales of the Chuniespoort Group were deposited in a stable marine environment, interspersed with lava flows in the upper portion of the stratigraphy (Gibson et al., 2000; McCarthy, 2006).

SEISMIC DATA AND PROCESSING

The merged 2003 Kloof-South Deep, 1988 South Deep, and 1994 Leeudoorn 3D seismic data sets were passed through the same standard workflow, including field preprocessing and full processing. Field processing, which provides brute stacks with elevation corrections, was done to evaluate the quality of the data, estimate the signal-to-noise ratio (S/N), and detect and remove bad and noisy traces. Full processing improved the S/N through various prestack operations such as trace editing, gain recovery, linear noise removal, surface-consistent "spiking" deconvolution, zero phase spectral whitening, trace balancing, velocity picking, and a 35% stretch mute. Appropriate static and phase corrections were calculated and applied prestack before merging the two data sets. A 90° phase shift and −8 ms bulk time shift was applied to the Leeudoorn data to correct for relative phase and time shifts observed between the Kloof-South Deep and Leeudoorn data sets. These two data sets were then successfully merged into one seamless data cube. No evidence of the data merge was identified in the data volume during subsequent analysis and processing.

Subsequent processing steps on the merged cube included the application of refraction statics, normal move-out correction, 3D Kirchhoff dip move-out correction, stacking, final datum shift to 1500 m above sea level, 3D finite difference depth migration, velocity analysis, and prestack time migration (PSTM) using the 3D Kirchhoff algorithm. Finally, depth conversion was carried out using interval velocities derived from surface borehole intersections and PSTM picks of the VCR and BLR. The PSTM depth-domain volume was shifted 330 m to correspond with the 1995 WUDLs datum of 1830 m above the sea level. The WUDLs and the Kloof-South Deep data sets were then merged to produce a single cube. However, the splice between the WUDLs-Driefontein and Kloof-South Deep data is obvious as the 1995 WUDLs-Driefontein data has a lower S/N than the 2003 Kloof-South Deep data.

All seismic data sets contain noise. This noise could result from acquisition, processing artifacts, or random sources. The relatively poor quality of the 1994 Leeudoorn and 1995 WUDLs-Driefontein data sets resulted from the combination of old acquisition systems and processing algorithms. The 1994 Leeudoorn data was reprocessed using PSTM in an attempt to improve the data quality. PSTM is a process by which each trace is migrated before stacking the common offset gathers, and is a relatively advanced migration technique commonly used in the petroleum industry (Yilmaz et al., 2001; Cameron et al., 2008). Prior to the Kloof-South Deep survey, PSTM had not been applied to Witwatersrand Basin data. The technique, generally known to be useful in defining stratigraphic and structural discontinuities in areas characterized by complex faulting and moderate lateral velocity variations, was deemed appropriate for application to the Witwatersrand basin. The application of 3D prestack Kirchhoff time migration to 1994 Leeudoorn data improved imaging of the VCR, faults, and stratigraphy when compared to the older poststack finite difference depth migration technique originally applied to the same data (Figures 3a–3d)

Although PSTM improved the S/N, it should be noted that the northern part of the survey area, accounting for about 5%–8% of the total planned subsurface imaging area, remained poorly imaged due to dolomite outcrops (Figure 4). The deterioration of the seismic data quality over dolomite is a well-known problem (cf., Wright et al., 2000; Šumanovac and Weisser, 2001) not only in South Africa, but elsewhere in the world. The deterioration is the result of scattering of the seismic energy due to karst weathering. It is very unlikely that imaging of the VCR and structures will ever be achieved in this area.

SEISMIC INTERPRETATION METHOD

The interpretation of seismic data was carried out using various advanced seismic interpretation software packages. These packages provide a true 3D modeling and visualization environment, allowing complex geologic modeling of seismic interpretation data, as well as enhanced visualization of faults and horizons.

The seismic reflectors, faults, and other discontinuities were manually picked from trace to trace along inline, crossline, and depth slices. The reliability with which seismic reflectors are picked is a combination of the S/N and structural complexity. Therefore, in structurally complex areas of the study and those zones of data with poor S/N, careful picking of reflections and faults was required before they could be confidently assigned as robust picks in the final geologic model. To map the major structures, seismic sections were initially interpreted at a relatively wide line spacing; for example, every fifth crossline and inline of the seismic volume. Once a wide grid of picks was completed, infill picks were made at a close line spacing, facilitating a detailed structural interpretation. To make sure that subtle faults were not missed during the picking process, every single seismic line was interpreted. Finally, the seismically

Downloaded 10 Sep 2012 to 146.141.1.82. Redistribution subject to SEG license or copyright; see Terms of Use at http://segdl.org/

defined VCR and associated faults were integrated with borehole information to create a robust geologic model of the VCR orebody.

Interpretations of the auriferous VCR and BLR were of particular interest in this study, because the reefs are economically important. The VCR unconformity is a major economic horizon of interest in the Witwatersrand Basin and it forms an important marker across the study area. The depth of the VCR unconformity in the study area is between 2000 and 4500 m below the surface. The VCR is typically less than 2 m thick and is not directly imaged seismically. It occurs at a major and laterally extensive acoustic impedance contrast between high-velocity, dense andesitic lavas of the Klipriviersberg Group and the underlying relatively low-velocity, less-dense quartzite units of the Central Rand Group; i.e., it is the reflective interface that is imaged. Based on interval velocities, the VCR was picked as a peak because of the decrease of seismic velocity from the overlying Ventersdorp Group lavas (approximately 6400 m/s) to the underlying Central Rand quartzite units (approximately 5750 m/s). The interpretation of the VCR surface constrained pre-, syn-, and post-Central Rand Group age structures with a view to developing an understanding of the prevailing tectonic environment.

The quartzites and conglomerates of the BLR produce a prominent and laterally extensive acoustic impedance contrast between the overlying dolomites of the Chuniespoort Group of the Transvaal Supergroup and the underlying lower-velocity, less dense Ventersdorp lavas. This acoustic impedance contrast gives rise to a strong reflection. The BLR was mapped to constrain the ages of structures relative to the deposition of the metasedimentary sequences of the Transvaal Supergroup.

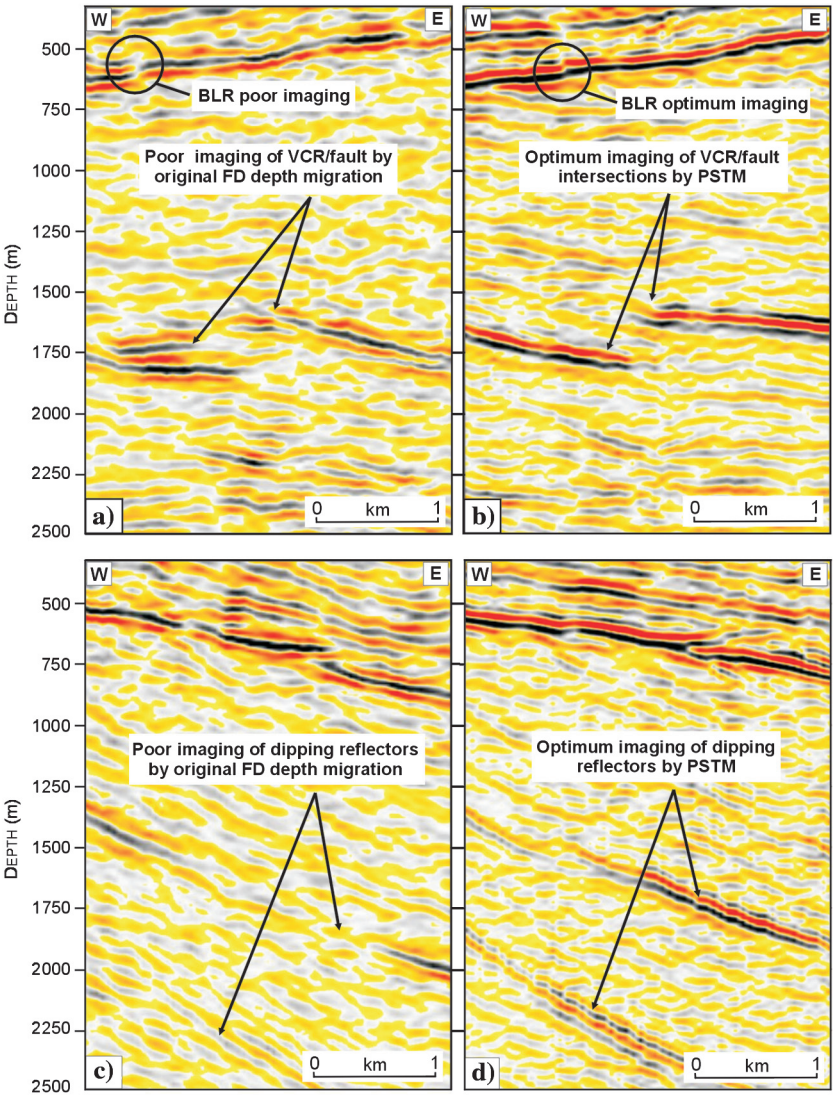


Figure 3. Depth-converted (amplitude display) seismic sections from 1994 Leeudoorn data. (a) The 3D poststack finite difference depth migrated (PSDM) section. (b) The 3D prestack Kirchhoff time migrated (PSTM) section. Note that PSTM shows better resolution relative to the poststack depth migration that was originally applied to the same data set, shown in (a). (c) The 3D poststack depth migrated (PSDM) section. (d) The PSTM section. The PSTM provides better imaging of the dipping reflectors.

SEISMIC RESOLUTION LIMITS AND SEISMIC ATTRIBUTES

The seismic energy is transmitted through the earth as a wave, rather than a narrow beam. Therefore, there is always uncertainty about the exact position of an imaged feature. This uncertainty is often described in terms of the Fresnel Zone. Aspects of the seismic design that were appropriate for assessing the resolution at primary target depths (e.g., VCR at 2000–4500 m) include the dominant frequency (65 Hz), interval velocity (6500 m/s), and dominant wavelength (100 m). Fresnel zone radii of 320 and 475 m were obtained for VCR target depths of 2000 and 4500 m, respectively. A bin size of 25 m was used for stacking, yielding a fold of 32.

Faults with throws that are much less than the dominant seismic wavelength are often difficult to see in the seismic migrated section. Seismic attribute analysis was used to enhance subtle features. Seismic attributes such as dip, azimuth, and edge detection were computed for each horizon to assist the identification of minor faults. The dip and azimuth are the horizon-based seismic attributes most commonly used to enhance structural interpretation (Dalley et al., 1989; Rijks and Jauffred, 1991). The dip and azimuth are, respectively, the magnitude and direction of the gradient vector, which are computed at each grid of the interpreted horizon (Rijks and Jauffred, 1991). The edge detection attributes are a combination of dip and azimuth variations that are normalized to local noise of the interpreted horizon. These attributes are very effective in enhancing structural continuity and detecting crosscutting or conjugate relationships of faults.

RESULTS

At the regional scale, the VCR exhibits a variable strike and dip across the study area as a result of folding, warping, and faulting. The VCR is crosscut by two first-order scale structures, namely, the West Rand and Bank faults, as well

Downloaded 10 Sep 2012 to 146.141.1.82. Redistribution subject to SEG license or copyright; see Terms of Use at http://segdl.org/

as a variety of second and third-order faults. The West Rand and Bank faults generally trend north-northeast and dip to the west (Figures 5 and 6). These faults are listric in form; dipping relatively steeply (65°–70°) at a depth of 1.5 km below the surface, and less steeply (40°) at depths of approximately 3.0–3.5 km below the surface. At greater depths, where the faults intersect the top of the West Rand Group, the dip decreases to 5°–10° before shallowing out within the upper shale units to form a décollement horizon. The West Rand and Bank faults have maximum normal throws of 1.5 and 2.0 km, respectively, and maximum sinistral offsets of 600 and 800 m, respectively (Figures 5 and 6). However, displacement is variable along the strike and dip of the faults, and should be taken into account in mine planning.

Importantly, the West Rand Fault resolves as two sympathetic fault segments that wedge an approximately 100 m wide and 1.0 km long discrete VCR block (Figure 5). The identification of this new VCR block enhances resource calculation and financial valuation of the VCR and life-of-mine planning. The identification

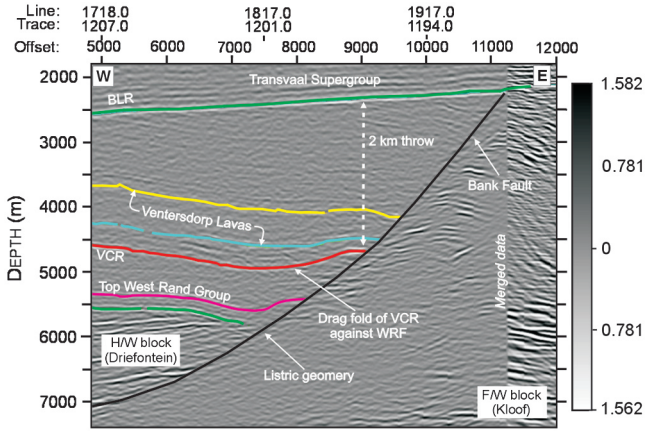


Figure 6. Seismic section (amplitude display) across the Bank Fault with a throw of 2 km showing the listric (concave-up) nature of the fault.

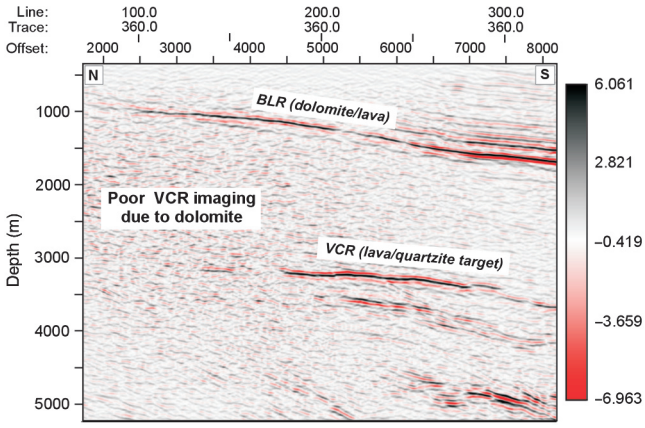


Figure 4. North–south depth–converted PSTM section (amplitude display) clearly showing poor VCR imaging over dolomite outcrop area.

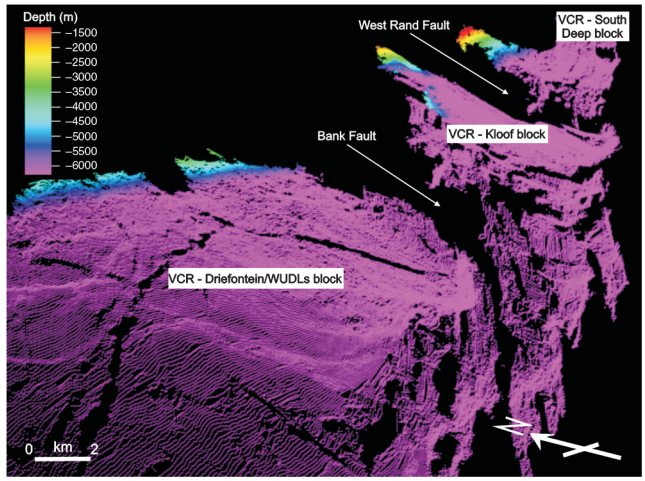


Figure 7. The 3D regional seismic VCR orebody model, with the West Rand Fault and Bank Fault showing similar geometry. The west–east dimension of the image is 28 km.

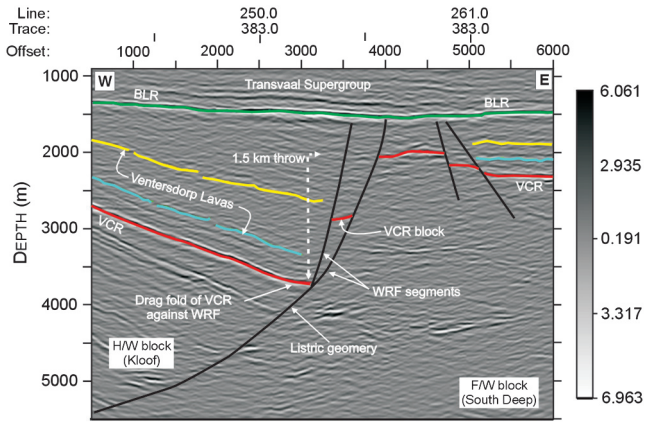


Figure 5. Seismic section (amplitude display) across the West Rand Fault with a throw of 1.5 km in the north of study area, showing sympathetic faults bounding a VCR block in the fault zone.

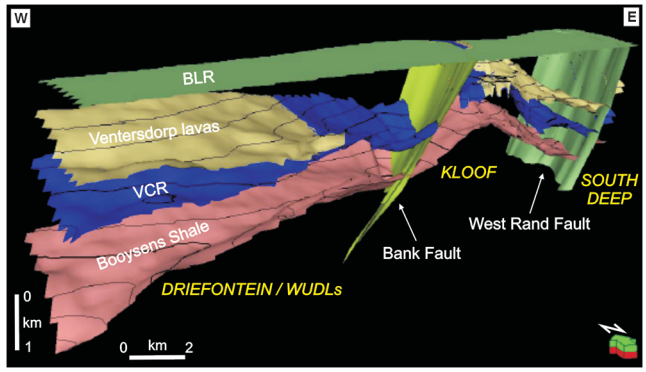


Figure 8. The 3D regional model constructed from reflectors of the BLR, Ventersdorp lavas, VCR, and Booysens Shale.

Downloaded 10 Sep 2012 to 146.141.1.82. Redistribution subject to SEG license or copyright; see Terms of Use at http://segdl.org/

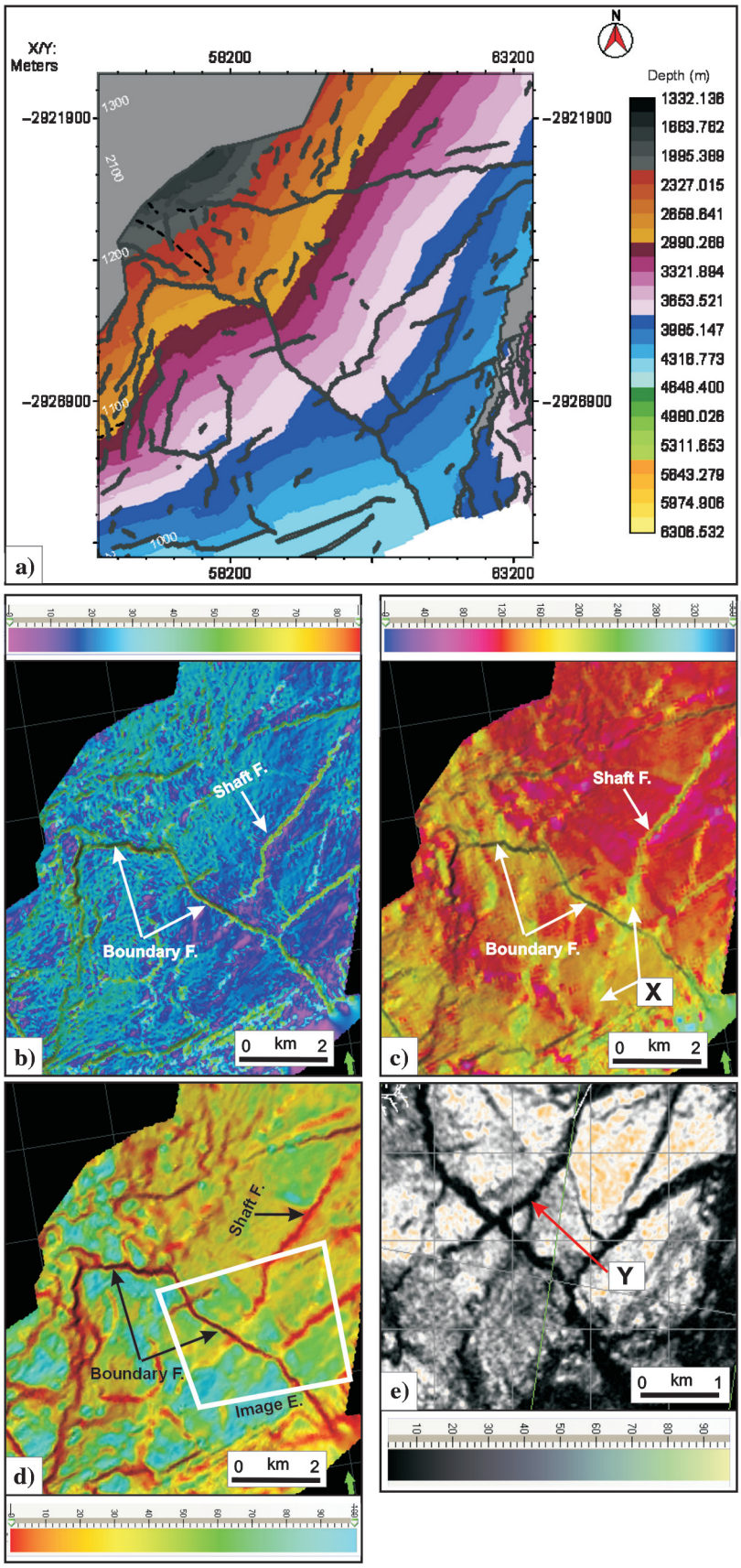


Figure 9. Seismic attributes computed for the VCR horizon at Kloof gold mine. (a) The VCR depth-structure map. (b) Dip attribute display (color bar is given in degrees). (c) Azimuth attribute display, showing the continuation of the shaft fault at position X (color bar is in degrees). (d and e) Color-coded edge attribute displays, clearly showing the crosscutting relationship between the shaft fault and boundary fault (color bar is given in percentages). The SF is seen in image E trending northeasterly; it bifurcates close to the BF (at position Y), and continues on the southwest side of the fault.

Downloaded 10 Sep 2012 to 146.141.1.82. Redistribution subject to SEG license or copyright; see Terms of Use at http://segdl.org/

of the fault-bounded wedge is important for mine planning and safety.

Additionally, several upthrown blocks on the eastern side of the West Rand Fault (Figure 5) that are accessible for mining were also revealed by this study, with considerable gain-of-ground. Thus resource and financial valuation are further enhanced.

In contrast to these discoveries, imaging of the West Rand and Bank faults also indicated they are subtended by clusters of secondary and tertiary faults in their fault damage zones. This is likely to translate into poor ground conditions locally and a loss-of-ground. Clearly, understanding the distribution of the structures is important for (1) predicting face advance rates close to and in fault zones, and (2) wall rock stability around fault zones in terms of fall-of-ground and microseismicity.

Furthermore, the 3D seismic model of the VCR ore horizon (Figure 7) and pre-BLR stratigraphy showed that the West Rand and Bank faults have similar geometries (c.f., Figures 5, 6, 7, and 8); and may have been active at the same time. Importantly, the BLR is not crosscut by major faults in the model, whereas the underlying reflectors are crosscut by faults at all scales. This concurs with studies by Coward et al. (1995), Gibson et al. (2000), Dankert and Hein (2010), and Mambane et al. (2011) which concluded that the West Rand and Bank faults were only active prior to the deposition of the BLR because they do not breach the base of the Transvaal Supergroup. The corollary is that they were excised during a period of significant erosion at the end of deposition of the Pniel Group; i.e., pre-2.58 Ga (cf., Krapež, 1985).

The seismic attributes were able to image faults that are not resolvable using conventional interpretation methods (Figure 9a). The dip and azimuth attributes computed for VCR ore horizon at Kloof survey area successfully imaged smaller faults in the survey area. Comparison of the azimuth and dip attribute maps show that the azimuth attribute map provides a better enhancement of faults relative to dip attribute map (Figure 9b and 9c). For example, the relationship between the northeast-trending Shaft Fault (SF) and northwest-trending Boundary Fault (BF) is well imaged in the azimuth attribute map, but not in the dip attribute map. It is clear that the BF is crosscut by the SF, and is thus older than the SF. This was not known prior to this study. Furthermore, edge detection maps reveal some fault architectures that are not detectable by either conventional picking, the dip, or the azimuth attributes. The SF bifurcates to form a south-southwestern trending branch and a southwest trending branch (Figure 9d and 9e). These structural relationships are difficult to see in seismic sections, and would not have been identified without the application of these attributes. Future mine development plans will need to be updated to take the new structural parameters into account.

Seismic attributes have identified a large number of smaller faults with variable throws that intersect the VCR, some with offsets as small as 15 m or less that would not have been detected through normal picking. Ignorance of these faults could significantly impede mine development, and their heaves (in the case of normal offset) could translate into loss-of-ground and a decrease in the volume of the mineable orebody. However, the attributes failed to identify faults at the edges of the survey where the data were of poor quality. The poor quality of data was an unavoidable effect of the low fold and poor performance of migration near the survey boundaries. It was clear that taking conventionally interpreted ore horizons as true geologic forms leads to a poor model and could increase risk.

The seismic attributes also enhanced 3D accuracy in the positioning of faults that were incorrectly positioned using conventional picking. For example, some of the conventionally picked faults that showed no correlation with VCR topographic breaks were moved to their correct position (Figure 10a and 10b).

The final result of this research has been the development of a regional stratostructural model of the VCR defined from conventional and attribute analysis (Figure 11). The model displays

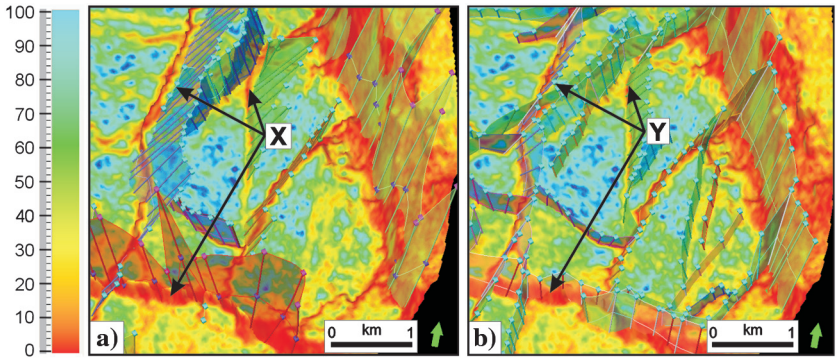


Figure 10. The VCR edge attribute map (color bar is given in percentages). (a) There is a mis-tie between the conventionally picked fault surfaces and the VCR topographic breaks. The position of mis-ties between the VCR breaks and faults is indicated (X). (b) The good tie between fault surfaces and VCR topographic breaks after repositioning of the faults. The positions of good ties between the VCR breaks and faults after modeling is indicated (Y).

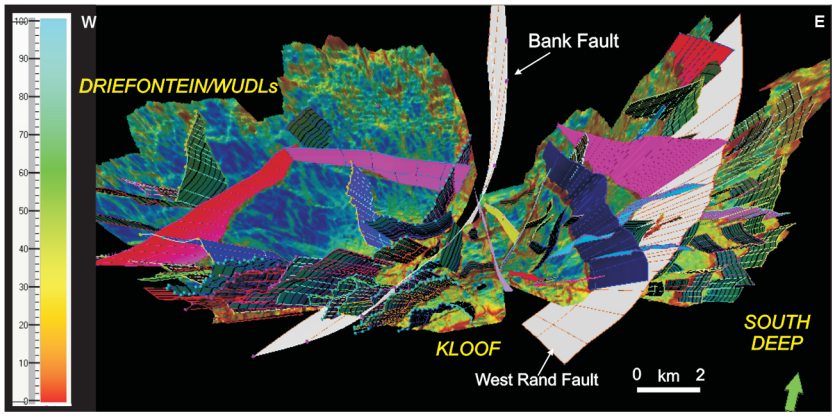


Figure 11. The 3D regional model defined from edge detection attribute analysis constructed from regional VCR pick of the merged surveys (color bar is given in percentages). The model incorporates the major West Rand Fault and Bank Fault, as well as a suite of subtle structures.

Downloaded 10 Sep 2012 to 146.141.1.82. Redistribution subject to SEG license or copyright; see Terms of Use at http://segdl.org/

VCR paleotopography, fault geometries (i.e., dip angles, strike, and dip directions), dikes, and continuity of structures across the mines in the study areas. This model can now be factored into future mine development strategies for better placement of shafts and improved life-of-mine planning; i.e., the high degree of structural resolution afforded by this interpretation will guide future exploration drilling activities and enable the layout of tunnels and stopes to be optimized.

DISCUSSION

With the exception of the unavoidable poor quality of the data in the north of the surveyed area due to outcropping dolomites, the overall quality of the data of the merged 3D seismic reflection surveys was good, providing high-resolution imaging of faults. Further field trials could be conducted in the future to determine parameters that may improve the data in these areas. Parameter testing on a small 2D trial line could investigate (1) increased fold-of-coverage, (2) vibrator force, and (3) an increase in the source effort with longer sweeps.

It is now clear that several structures are laterally continuous across the study area. This understanding could not have been achieved without merging the data sets. The improved acquisition parameters on the 2003 Kloof-South Deep survey, mainly the increased offset, lead to better imaging of the VCR and West Rand Group of reflectors.

Reprocessing of the 1994 Leeudoorn data using PSTM delivered improved VCR and structural imaging; however, the final data are not as good as that of the 2003 Kloof-South Deep surveys. The modeling of first-order structures and their associated second and third-order faults has been possible. The attributes analysis has achieved its objective in reducing structural risk in strategic mine planning. Several structures interpreted by previous workers in noisy areas were found not to exist, whereas many new structures were identified. A structural model incorporating the VCR and faults has been generated for merged data sets, with faults of ~25 m throw being seen, and faults of ~10 m throw being imaged with relative confidence using attribute analysis. The results can be incorporated into geologic plans for each of the mine shafts covered by the surveys.

CONCLUSION

The 3D seismic reflection technique may be deemed very costly. However, its application in the Witwatersrand basin has, over the years, been recognized as a core geophysical method that mitigates the risks associated with the deep mining and drilling of deep costly surface exploration boreholes into faulted areas. The attribute analysis has provided the mines with an improved ability to validate structures, model faults, and their fault loss zones, with throws ranging from 2.5 km, to less than 25 m. By merging the 2003 Kloof-South Deep survey (which incorporated the reprocessed 1994 Leeudoorn survey), and the 1995 WUDLs survey (which incorporated the 1995 Driefontein survey), an extensive and contiguous 3D seismic model of the VCR and BLR has been generated. This model, coupled with the constraining surface borehole data and VCR paleogeomorphological model, will provide Gold Fields Mining Ltd. with a world-class resource model. The seismic model serves as the basis for accurate mine designs and project scheduling.

ACKNOWLEDGMENTS

Gold Fields Mining Ltd. is acknowledged for funding this project and providing permission to publish the results. We wish to thank Schlumberger for providing the Petrel® interpretation software, Rock Deformation Research (RDR), Compagnie Générale de Géophysique (CGG), G. Smith, J. Trickett, L. Lindzay, and M. Muller for their major contribution in this study. Finally, we are also grateful to the SEG associate editors and three anonymous reviewers for their constructive comments and valuable suggestions.

REFERENCES

Cameron, M., S. Fomel, and J. Sethian, 2008, Time-to-depth conversion and seismic velocity estimation using time-migration velocity: Geophysics, **73**, no. 5, VE205–VE210, doi: 10.1190/1.12967501.

Coward, M. P., R. M. Spencer, and C. E. Spencer, 1995, Development of the Witwatersrand Basin, South Africa, *in* M. P. Coward, and A. C. Ries, eds., Early precambrian processes: Geological Society, Special Publications 95, 243–269.

Dalley, R. M., E. C. A. Gevers, G. M. Stampfli, D. J. Davies, C. N. Gastaldi, P. A. Ruijtenberg, and G. J. O. Vermeer, 1989, Dip and azimuth displays for 3D seismic interpretation: First Break, **7**, 86–95.

Dankert, B. T., and K. A. A. Hein, 2010, Evaluating the structural character and tectonic history of the Witwatersrand Basin: Precambrian Research, **177**, 1–22, doi: 10.1016/j.precamres.2009.10.007.

De Kock, M., 1964, The geology and economic significance of the West Wits Line, *in* S. H. Haughton, eds., The geology of some ore deposits in Southern Africa: Geological Society of South Africa, 323–386.

De Wet, J. A. J., and D. A. Hall, 1994, Interpretation of the Oryx 3D seismic survey: Proceedings of the XVth CMMI Congress, South African Institute of Mining and Metallurgy, **3**, 259–270.

Durrheim, R. J., 1986, Recent reflection seismic developments in the Witwatersrand basin, *in* M. Barazangi, and L. Brown, eds., Reflection seismology, a global perspective: American Geophysical Union, Geodynamics Series 13, 77–83.

Gibson, M. A. S., S. J. Jolley, and A. C. Barnicoat, 2000, Interpretation of the Western Ultra Deep Levels 3D seismic survey: The Leading Edge, **19**, 730–735, doi: 10.1190/1.1438704.

Jolley, S. J., S. R. Freeman, A. C. Barnicoat, G. M. Phillips, R. J. Knipe, A. Pather, N. P. C. Fox, D. Strydom, M. T. G. Birch, I. H. C. Henderson, and T. W. Rowland, 2004, Structural controls on Witwatersrand Gold mineralization: Journal of Structural Geology, **26**, 1067–1086, doi: 10.1016/j.jsg.2003.11.011.

Kositcin, N., and B. Krapež, 2004, SHRIMP U-Pb detrital zircon geochronology of the late Archean Witwatersrand Basin, relation between zircon provenance age spectra and basin evolution: Precambrian Research, **129**, 141–168, doi: 10.1016/j.precamres.2003.10.011.

Krapež, B., 1985, The Ventersdorp Contact placer: A gold-pyrite placer of stream and debris-flow origins from the Archaean Witwatersrand Basin of South Africa: Sedimentology, **32**, 223–234, doi: 10.1111/sed.1985.32.issue-2.

Mambane, P. W., K. A. A. Hein, S. G. Twemlow, and M. S. D. Manzi, 2011, Pseudotachylite in the south boundary fault at the Cooke Shaft, Witwatersrand Basin, South Africa: South African Journal of Geology, **114**, 109–120.

McCarthy, T. S., 2006, The Witwatersrand supergroup, *in* M. R. Johnson, C. R. Anhaeusser, and R. J. Thomas, eds., The geology of South Africa: Geological Society of South Africa, Johannesburg/Council for Geosciences, 155–186.

Phillips, G. N., and J. D. Law, 2000, Witwatersrand gold fields: Geology, genesis and exploration, *in* S. G. Hagemann, and P. E. Brown, eds., Gold 2000: Reviews in economic geology, Society for Economic Geology, **13**, 439–500.

Pretorius, C. C., W. H. Steenkamp, and R. G. Smith, 1994, Developments in data acquisition, processing, and interpretation over ten years of south vibroseismic surveying in South Africa: Proceedings of the XVth CMMI Congress, South African Institute of Mining and Metallurgy, **3**, 249–258.

Rijks, E. J. H., and J. C. E. M. Jauffred, 1991, Attribute extraction: An important application in any detailed 3D interpretation study: The Leading Edge, **10**, 11–19.

Stanistreet, I. G., and T. S. McCarthy, 1991, Changing tectonosedimentary: Scenarios relevant to the development of the Late Archaean Witwatersrand Basin: Journal of African Earth Sciences, **13**, 65–81.

Stevenson, F., R. M. A. Higgs, and R. J. Durrheim, 2003, Seismic imaging of precious and base-metal deposits in South Africa, *in* D. W. Eaton, B.

Downloaded 10 Sep 2012 to 146.141.1.82. Redistribution subject to SEG license or copyright; see Terms of Use at http://segdl.org/

Milkereit, and M. H. Salisbury, eds., Hardrock seismic exploration: SEG Geophysical developments, 141–156.
Šumanovac, F., and M. Weisser, 2001, Evaluation of resistivity and seismic methods for hydrogeological mapping karst terrains: Journal of Applied Geophysics, **47**, 13–28, doi: 10.1016/S0926-9851(01)00044-1.
Trickett, J. C., W. A. Duweke, and S. Kock, 2004, Three-dimensional reflection seismic: Worth its weight in platinum: International Platinum Conference, South African Institute of Mining and Metallurgy, 257–264.
Van Der Westhuizen, W. A., H. De Bruiyn, and P. G. Meintjes, 1991, The Ventersdorp supergroup: An overview: Journal of African Earth Sciences, **13**, 83–105.
Vos, R. G., 1975, An alluvial plain and lacustrine model for Precambrian, Witwatersrand Deposits of South Africa: Journal of Sedimentary Petrology, **45**, 480–493.
Weder, E. E. W., 1994, Structure of the area south of the central rand gold mines as derived from a gravity and vibroseis surveys: Proceedings of the XVth CMMI Congress, South African Institute of Mining and metallurgy, 271–281.
Wright, C., E. J. Walls, and D. de J. Carneiro, 2000, The seismic velocity in the vicinity of a mine tunnel at Thabazimbi, South Africa: Journal of Applied Geophysics, **44**, 369–382, doi: 10.1016/S0926-9851(00)00014-8.
Yilmaz, O., I. Tanir, and C. Cregory, 2001, A unified 3D seismic work flow: Geophysics, **66**, 1699–1713, doi: 10.1190/1.1487112.

Downloaded 10 Sep 2012 to 146.141.1.82. Redistribution subject to SEG license or copyright; see Terms of Use at http://segdl.org/

GEOPHYSICS, VOL. 77, NO. 5 (SEPTEMBER-OCTOBER 2012); P. WC133–WC147, 17 FIGS., 2 TABLES.
10.1190/GEO2012-0135.1

3D edge detection seismic attributes used to map potential conduits for water and methane in deep gold mines in the Witwatersrand basin, South Africa

Musa S. D. Manzi[1], Raymond J. Durrheim[2], Kim A. A. Hein[1], and Nick King[3]

ABSTRACT

Inrushes of ground water and the ignition of flammable gases pose risks to workers in deep South African gold mines. Large volumes of water may be stored in solution cavities in dolomitic rocks that overlie the Black Reef (BLR) Formation, while there are several possible sources for methane, namely, coal seams, kerogen found in some gold ore bodies, or methane introduced by igneous intrusions. Potential conduits that may transport water and methane to underground workings were mapped using 3D reflection seismic data. Edge detection attributes successfully identified many faults, some with displacements as small as 10 m. Faults that displace the Ventersdorp Contact Reef (VCR) and the BLR horizons were of special interest, as known occurrences of fissure water and methane in underground workings show a good correlation with faults that were imaged on the VCR and BLR horizons. Because there are uncertainties in determining the linkage of faults with aquifers and methane sources, it is considered prudent to assume that all structures that displace the VCR and BLR horizons are potential conduits.

INTRODUCTION

The deep gold mines of South Africa employ labor-intensive mining methods with as many as 5000 miners working in a single shaft. The miners face various hazards, including rock falls, rockbursts associated with mining-induced seismic events, moving trains transporting ore and waste rock, handling of explosives, inrushes of water, and flammable gases (Adams et al., 2007). In this paper, we discuss the use of 3D seismics to address the risks posed by flooding and flammable gases. Mining engineers have devised many ways to minimize the risks associated with water inrush and methane ignition. However, the mechanism whereby methane and water is transported to mine workings is not well understood.

The 3D seismic reflection technique was first implemented to image oil and gas reservoirs in the 1960s (Pretorius et al., 1994; Salisbury et al., 2003). Over the past 20 years, 3D seismics has been used worldwide for mine planning, design, and risk reduction in the deep metal mines (Milkereit et al., 1996, 2000; Pretorius et al., 2000; Trickett et al., 2004; Malehmir and Bellefleur, 2009; Malehmir et al., 2012). Recently, the technique has played an increasingly important role in the exploration of the Witwatersrand basin in South Africa, being used to delineate major gold-bearing horizons for mine planning and production purposes (Pretorius et al., 2003; Salisbury et al., 2003; Stevenson et al., 2003; Manzi et al., 2012). Although 3D seismic surveys are expensive relative to linear 2D surveys, they give full representations of the subsurface. Therefore, 3D seismic surveys offer great advantage for processing and interpretation of the seismic data.

Since the late 1980s, global developments in the acquisition, processing, and interpretation of 3D seismic data have made the technique increasingly effective to the point that it has become fundamental and a well-established method in the development of the seismic and structural models.

In this study, we use high-resolution 3D seismic data acquired in the West Rand and West Wits Line (Carletonville) gold fields (Figure 1) to investigate the role that faults might play in transporting water and methane to mine workings. To achieve this goal, we use 3D horizon-related edge detection attribute analysis to better define fault architectures that often are difficult to resolve in

Manuscript received by the Editor 18 April 2012; published online 6 September 2012.
[1]University of the Witwatersrand, School of Geosciences, Johannesburg, Republic of South Africa. E-mail: Musa.Manzi@students.wits.ac.za; kim.ncube-hein@wits.ac.za.
[2]University of the Witwatersrand, School of Geosciences, Johannesburg, Republic of South Africa; and CSIR Centre for Mining Innovation, Johannesburg, Republic of South Africa. E-mail: Raymond.Durrheim@wits.ac.za; RDurrhei@csir.co.za.
[3]South Deep Gold Mine, Gold Fields Limited, Johannesburg, Republic of South Africa. E-mail: nick.king@goldfields.co.za.
© 2012 Society of Exploration Geophysicists. All rights reserved.

Downloaded 10 Sep 2012 to 146.141.1.82. Redistribution subject to SEG license or copyright; see Terms of Use at http://segdl.org/

seismic sections. Horizon attributes, such as dip and dip azimuth, were introduced by Dalley et al. (1989) and Rijks and Jauffred (1991).

Recent improvements in mapping techniques implemented in the interpretation software, such as edge detection attributes, has allowed optimum imaging of subtle faults (throw less than ~15 m). This study is, to our knowledge, the first to use edge detection seismic attributes to study the relationships between faults and sources of water and methane in the Witwatersrand basin. The application of these techniques has led to a robust definition of subtle faults that has direct impact on mine planning decisions.

RISKS POSED BY FLOODING AND FLAMMABLE GASES

In the West Rand and West Wits Line gold fields of the Witwatersrand basin, gold-bearing strata are overlain by the Malmani Dolomite sequence that measures up to a kilometer in thickness (Figure 2a and 2b). The dolomite potentially is charged with large volumes of groundwater in fissures and solution cavities. The sequence is intruded by vertical dikes that are impervious to water and divide the aquifer into several compartments. To mitigate the risk of water inrushes when sinking a shaft or developing a tunnel, test boreholes are drilled into the surrounding rock mass. If any water is encountered, the holes are sealed.

The control of water is more difficult during stoping operations as the hangingwall may sag with development of fractures that cannot be easily sealed.

Until 1968, the flow of water into the stopes at many mines was accepted as inevitable. Water emerging from fissures was channeled into drains, pumped to the surface, and transported away from the mine area by means of canals. On 26 October 1968, a massive inrush of water occurred at No. 4 Shaft of West Driefontein mine, overwhelming the capacity of the pumps (Cousens and Garrett, 1969). The flow continued for 23 days before it was stemmed. All 1400 miners in the area of No. 4 shaft were safely evacuated, but production at the mine, at that time the world's biggest gold producer, was severely affected.

Following the West Driefontein disaster, a new strategy was implemented to mitigate the risk of water inrushes from overlying dolomite compartments. The compartments were dewatered by sustained pumping, and the water disposed of in such a way that it could not find its way back into an aquifer (Ngcobo, 2006). Although the dewatering strategy certainly was effective, it triggered sinkholes and was costly to sustain. Much of the ore in Witwatersrand gold mines has been extracted, and production in many mines has decreased or ceased. Consequently, the pumping of ground water has slowed or stopped. The water level is rising in some compartments, raising concerns about the integrity of water-barrier pillars that protect adjacent operating mines.

Furthermore, many of the gold mines are classified as "fiery" as they are prone to the influx of flammable gases, principally methane. The ignition of these gases have led to several disasters, including at Mponeng mine in the West Wits Line gold field on 29 July 1999, causing 19 deaths and two injuries (Motaung, 2000), and at Beatrix mine in the Free State gold field on 15 May 2000 and 8 May 2001, causing seven and 13 deaths, respectively (Kritzinger, 2001). Also, on 11 November 1999, a 16-m-long cavity was formed following a normal development blast at a depth of 2800 m in the Moab Khutsong mine in the Klerksdorp gold field (Ortlepp, 2001).

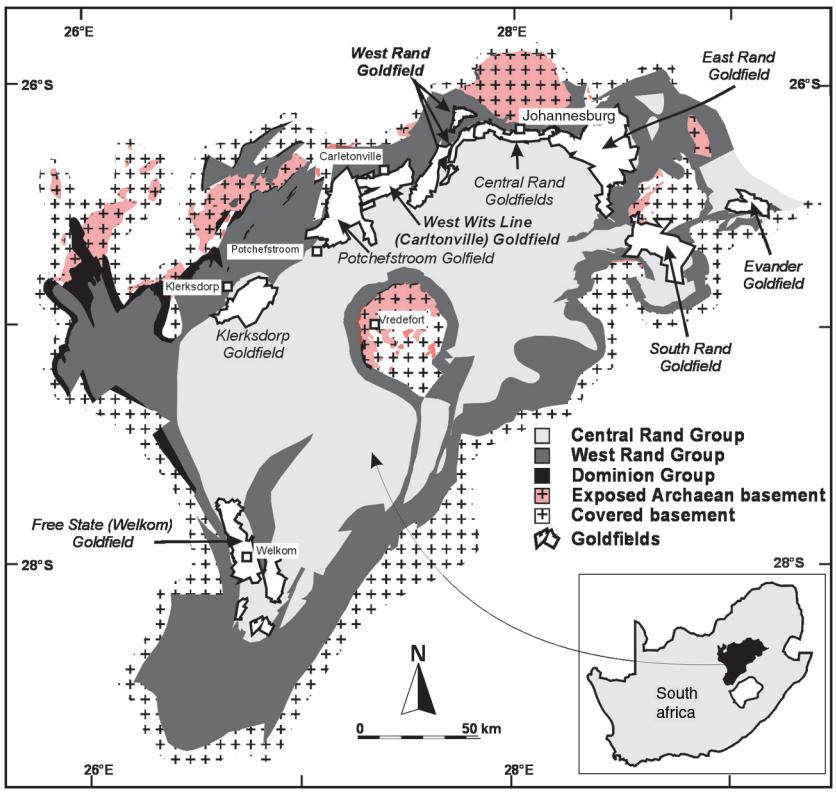


Figure 1. The location map of the West Rand and West Wits Line (Carletonville) gold fields of the Witwatersrand basin in South Africa (after Dankert and Hein, 2010).

Downloaded 10 Sep 2012 to 146.141.1.82. Redistribution subject to SEG license or copyright; see Terms of Use at http://segdl.org/

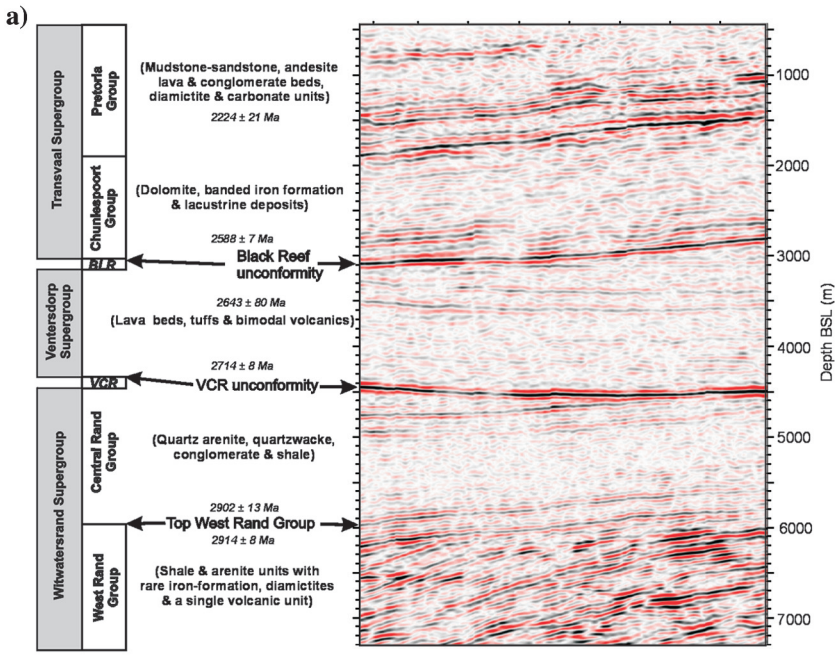
It was interpreted to be the result of an outburst of highly compressed gas. Fortunately, no ignition occurred, although sampling of the return air from the tunnel showed a high concentration of flammable gas, and a strong smell of sulphurated hydrogen was detected.

The origin and transportation of the combustible gases found in the Archean quartzite and conglomerate units of the Witwatersrand basin has been investigated by several workers and reviewed by Cook (1998). Possible sources include primordial methane transported from the mantle by granitic intrusions and syenite dikes; kerogen, interpreted to be derived from ancient algal mats that are sometimes found together with gold, notably in an ore body known as the Carbon Leader Reef; or coal seams found in much younger Karoo strata. The Karoo Supergroup overlies much of the Witwatersrand basin, and its coal seams are regarded as the main source of methane into the Witwatersrand basin gold mines, especially in the Free State gold field (Spencer and Walter, 2000).

The methane migrates from the source to mine workings through faults and fractures, either as a gas or dissolved in ground water. The pressure decreases when a void is reached and the gas exsolves into the atmosphere. Permeability is confined to joints and faults as the host rocks are not porous. Major faults can provide conduits for water ingress because the roughness of the fault walls permits the presence of a network of small cavities that can be water-bearing (Bekker, 1986). Many dikes have major fault planes at their contact margins that can act as conduits.

GEOLOGIC SETTING

The gold-bearing conglomerates (or reefs) of the Archean Witwatersrand Supergroup, which crop out near present day Johannesburg, were discovered in 1886. The West Rand and West Wits Line goldfields, located on the northern rim of the Witwatersrand basin about 40 and 60 km southwest of Johannesburg, are concealed by younger overlying strata. The gold fields were discovered in the



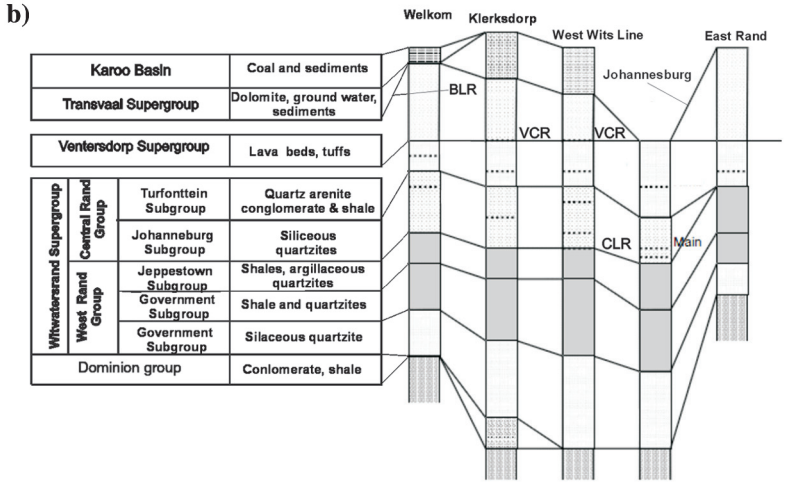


Figure 2. (a) Generalized stratigraphy of the West Wits Line gold field, derived from depth converted prestack time migrated (PSTM) seismic section. Geochronological data and geology provided by Dankert and Hein (2010). (b) Generalized stratigraphic column of the Witwatersrand basin showing important gold-bearing horizons or reefs within the Central Rand Group. The West Wits Line and West Rand gold fields are overlain by the dolomitic aquifers of the Transvaal Supergroup. Karoo sediments and coals have been eroded in these gold fields (Cook, 1998).

Downloaded 10 Sep 2012 to 146.141.1.82. Redistribution subject to SEG license or copyright; see Terms of Use at http://segdl.org/

1930s through drilling that was guided by magnetic and gravity surveys. The geology and structural setting of the Witwatersrand basin is documented by many authors, including Coward et al. (1995), Gibson et al. (2000), Jolley et al. (2004), Beach and Smith (2007), and Dankert and Hein (2010). In summary, the Witwatersrand Supergroup unconformably overlies the Dominion Group. The Supergroup is subdivided into the (lower) West Rand and (upper) Central Rand groups (McCarthy, 2006; Dankert and Hein, 2010) (Figure 2a and 2b). Unconformably overlying the Central Rand Group is the Ventersdorp Supergroup, with the Ventersdorp Contact Reef (VCR) of the Venterspost Formation. The Ventersdorp Supergroup consists of the volcanic Klipriviersberg Group, the predominantly metasedimentary Platberg Group, and the Pniel Group (Coward et al., 1995; Jolley et al., 2004). Unconformably overlying the Ventersdorp Supergroup is the relatively thin Black Reef Formation (BLR), which is the basal lithostratigraphic unit of the Transvaal Supergroup. This Supergroup is divided into the Chuniespoort Group and the Pretoria Group. Considerable volumes of groundwater are stored within the dolomitic aquifers of the Malmani Subgroup of the Chuniespoort Group (McCarthy, 2006; Mambane et al., 2011) (Figure 2a and 2b).

This study focuses on Driefontein, Kloof and South Deep gold mines (owned by Gold Fields Ltd.) and Mponeng, Tautona, and Savuka gold mines (owned by AngloGold Ashanti), and their down-dip extensions (Figure 3a). The southern portion of the Kloof mining areaformerly was known as the Leeudoorn mine (Figure 3a). The down-dip extension of Mponeng, Savuka, Tautona, and Driefontein was known as Western Ultra Deep Levels (WUDLs).

The West Wits Line and West Rand goldfields are separated by the Bank Fault (Figure 3a). The Driefontein mine is situated west of the Bank Fault, and is one of the largest mines in the West Wits Line goldfield. The most important ore body at Driefontein mine is the Carbon Leader Reef, which constitutes about 75% of the ore reserve, with the VCR providing about 20%. The Kloof mine lies to the east of the Bank Fault (Figure 3a); three reefs are exploited,

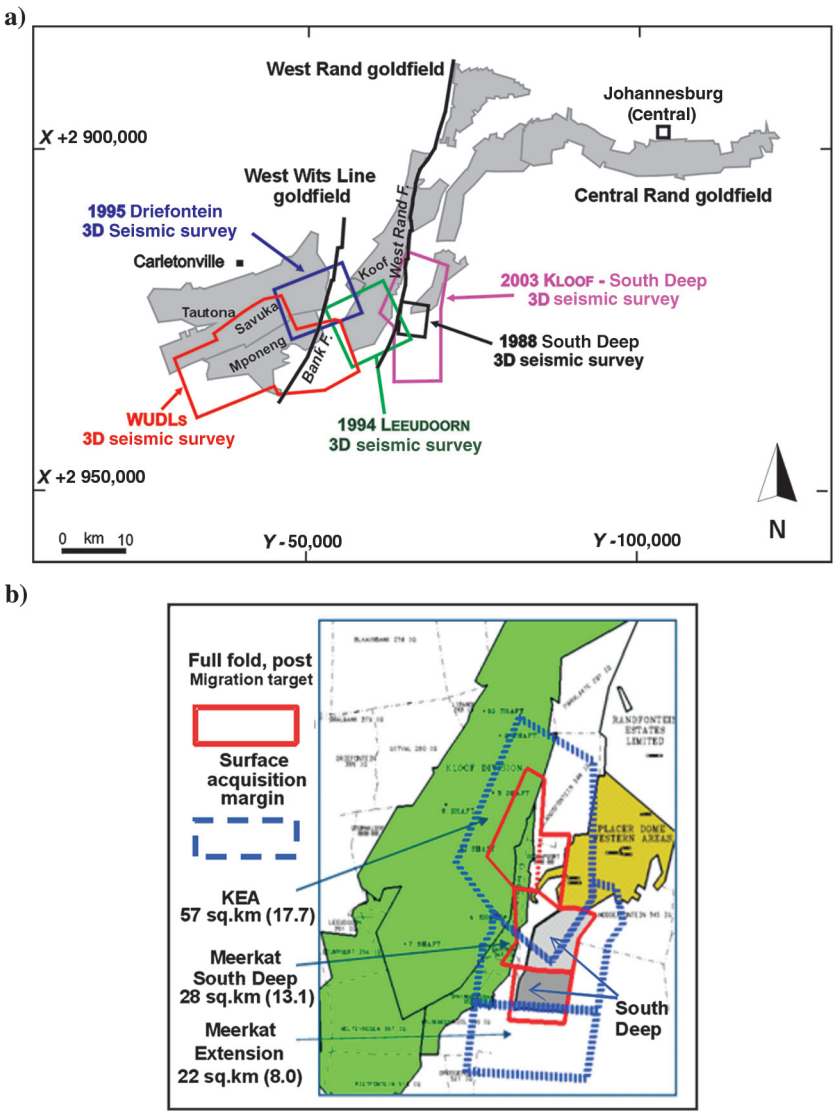


Figure 3. (a) The location of historical surveys for Kloof, South Deep, Driefontein, and WUDLs (after Manzi et al., 2012). (b) KEA and Meerkat (South Deep) seismic survey acquisition margin and targeted areas.

Downloaded 10 Sep 2012 to 146.141.1.82. Redistribution subject to SEG license or copyright; see Terms of Use at http://segdl.org/

although the VCR is by far the largest contributor, representing 88% of the ore reserve. The South Deep mine is situated to the east of Kloof mine and the West Rand Fault (Figure 3a and 3b). With some 78.2 million ounces of resources and 29.3 million ounces of reserves, South Deep is the largest undeveloped gold ore body in the world. The bulk of the ore is found in the Upper Elsburg Reefs, although some VCR also is present.

Two prominent seismic reflectors were used to map the geologic structure in this study, namely the bottom contact of the BLR which lies at the base of the Transvaal Supergroup, and the bottom contact of the Ventersdorp Supergroup lavas, which marks the position of the VCR ore body.

DESIGN, ACQUISITION, AND PROCESSING OF THE 3D SEISMIC SURVEY

The seismic data covering the extensions of the Kloof and South Deep mines were acquired in 2003. The primary goal of the seismic survey was to image the VCR ore body. Stratigraphic dips of 15°–35° were anticipated west of the West Rand Fault and 10°–20° to the east of the West Rand Fault. The VCR consists of conglomerates with varying clast sizes in a quartzite matrix. The VCR rarely exceeds 1.5 m in thickness and is too thin to be directly detected by surface reflection seismics. Instead, it is the boundary between the lavas of the overlying Ventersdorp Supergroup and the quartzite units of the Central Rand Group that is imaged because the quartzite units have a lower density and seismic velocity. A secondary goal was to image the base of the BLR, which lies some 1500 m above the VCR at depths of 200–1500 m. The BLR Formation is a thin quartzite separating the Ventersdorp lavas below from the dolomites of the Chuniespoort Group. The dolomites have higher density and seismic velocity; therefore, it is the Ventersdorp-Chuniespoort contact that gives rise to a strong seismic reflection.

The survey consisted of 4155 shot points recorded over an area of approximately 96 km^2 covering the Kloof Extension Area (KEA), Meerkat (South Deep Mine), and Meerkat Extension areas (Figure 3b). The acquisition parameters are summarized in Table 1. To avoid any reduction in data quality owing to poor source and receiver coupling, scattering of energy, attenuation of high frequencies, or potentially poor static solutions, no shots or receivers were located on rock dumps and slimes dams located on the Kloof and South Deep mines. The placement of compensation shots was monitored carefully to ensure that the fold of coverage was maintained and that the minimum offsets within each bin remained acceptable. The compensation shot strategy only was feasible because the target depth is in excess of about 3000 m beneath the obstacles. Although a detailed description of the survey design is beyond the scope of this paper, the following points merit mention as they are relevant to the resolution of the survey.

- A 25×25 m^2 bin size was chosen to avoid spatial aliasing up to a stratigraphic dip of 35° (the maximum dip observed at Kloof mine), based on interval velocity of 6500 m/s and a maximum frequency of 100 Hz (the upper limit of the sweep used in the survey).
- A maximum shot-receiver offset of 3325 m was chosen to provide fullfold coverage over the range of VCR target depths between 3000 and 4200 m. A greater maximum offset would run the risk of producing data recorded at less than full fold at the shallower target range.
- The nominal fold of coverage was 36 to the west of the West Rand Fault, and 30 to the east of the fault. This represents a significant increase in fold compared with all previous deep Witwatersrand basin 3D seismic surveys, which were

Table 1. Field acquisition parameters for 2003 3D Kloof-South Deep seismic surveys.

Recorded by	CGG	Crew 303,32,44
Instrumentation	System	Sercel 408
	Geophones	10 Hz
	Data media	3490 Cartridge
	Data format	SEGD IEEE Demultiplexed
	Record length	6 s
	Sample interval	2 ms
	System polarity	SEG standard
Parameters	Bin dimensions	25×25 m
	Survey pattern	Orthogonal
	Live patch asymmetrical	12 lines × 108 1296 channels
	Live patch symmetrical	12 lines × 90 1080 channels
	Asymmetrical split	1–45 ∗ 46–108 Ch 108 to the east
	Symmetrical split	1–45 ∗ 46–90
	Shot line separation	450 m
	Shot line direction	9.51°
	Shot line angle to receiver line	90°
	Shot point separation	50 m
	Total number of shot points	4155
	Receiver line separation	400 m
	Receiver line direction	99.51°
	Receiver point separation	50 m
	Total number of receiver points	4957
	Array	Linear, 12 phones/string
	Array length	Variable 36–85 m — bunched, length based on topography
Source	Vibroseis	
	Pattern	4 Vibs inline 45-m array
	Sweep	16 s 12–96 Hz
		4 sweeps/V_P

Downloaded 10 Sep 2012 to 146.141.1.82. Redistribution subject to SEG license or copyright; see Terms of Use at http://segdl.org/

Table 2. Processing parameters for 2003 3D Kloof-South Deep and 1994 Leeudoorn seismic data sets.

Processing route	Parameters
Data reformat	From SEGD to Promax internal format
Trace editing	Air-blast attenuation applied
Geometry application	Source, receiver, offsets, etc., assigned to each trace
Gain recovery: spherical divergence correction	$1/(TV \wedge 2)$, where V = 5500 m/s
Surface consistent spiking deconvolution	Operator design window at 0 m offset: 100–2500 ms, operator length: 120 ms, white noise stabilization: 1%
Zero-phase spectral whitening	Eight frequency windows, 500-ms sliding window
3D refraction statics correction	Surface layer V0 = 1200 m/s (constant), seismic datum elevation: 1500 m a.m.s.l
Statics application	Smooth processing datum
First-pass interactive velocity analysis	Every 600 m in crossline and inline directions
First-pass surface consistent residual statics	Maximum power autostatics, 300-ms time gate around flattened horizons
Interim stack: Leeudoorn and Kloof-South Deep	Data sets stacked separately, 35% stretch mute and 500-ms AGC applied
Prestack phase rotation and time-shift to match Leeudoorn and Kloof data sets	Leeudoorn data: time shift of −8 ms and 90° phase shift
Prestack merge of Kloof-South Deep and Leeudoorn data sets	Refraction statics calculated on the merged data and tied to upholes
Second-pass interactive velocity analysis	Every 600 m in crossline and inline directions
Second-pass surface consistent residual statics application	Maximum power autostatics, 300-ms time gate around flattened horizons
CDP trim statics	Nonsurface consistent CDP statics
DMO velocity analysis	Full 3D Kirchoff DMO using 50-m inline and crossline distance
Prestack time migration (PSTM) flow	
First-pass PSTM velocity analysis	DMO velocities removed and PSTM velocities picked
PSTM	Full 3D Kirchoff using velocity model from smoothed first pass PSTM velocities
Second-pass PSTM velocity analysis	Second pass PSTM velocities picked
NMO correction	Second pass PSTM velocities applied
Stack	
Band-pass frequency filter	Time varient Ormsby zero-phase filter, 0–1400 ms: 15/20 – 80/90 Hz
Depth conversion	Using interval velocities derived from borehole data and BLR and VCR time horizons
WUDLS data merge	Kloof-South Deep data depth shifted to 1830 m a.m.s.l datum and regridded to match WUDLs orientation

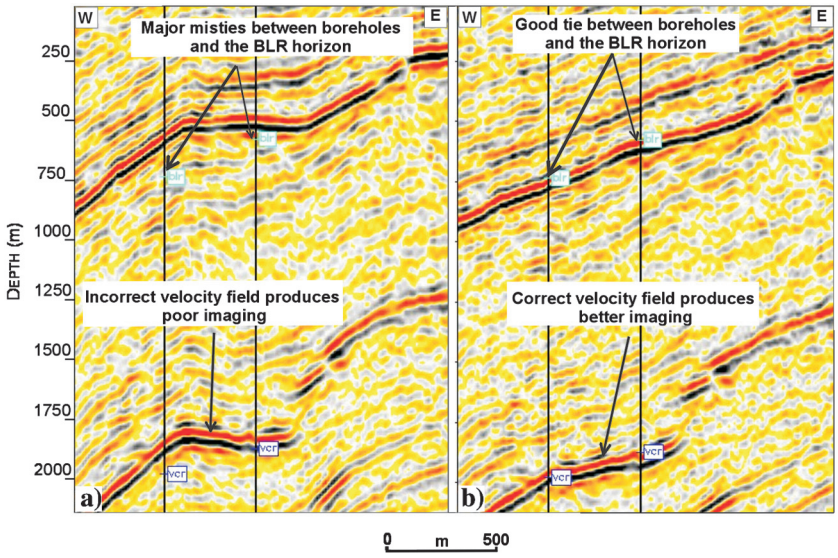


Figure 4. Depth converted time migrated sections using finite difference migration algorithm. (a) Unsmoothed velocity field provides a very stretched seismic horizons and distorted structures (possibly undermigrations). This shows a huge depth mis-tie between the VCR and BLR horizons and borehole control. (b) Smoothed velocity field provides stable seismic horizons and structures. These results show a very good depth tie between the VCR and BLR horizons and boreholes.

Downloaded 10 Sep 2012 to 146.141.1.82. Redistribution subject to SEG license or copyright; see Terms of Use at http://segdl.org/

typically 20 fold. This fold was recorded with no increase in costs relative to earlier surveys due to the ability of the instrumentation to deal with larger numbers of receivers.

- The migration aperture varied depending on target depth and dip. The dip migration aperture (margin) was designed so that it could provide fullfold coverage of the subsurface target area after migration. The diffraction migration aperture of 1125 m (at 4200 m VCR target depth with 15° dip) was chosen to provide 75% of diffraction energy at all predicted major fault cutoffs of the VCR.

The processing parameters for Kloof, South Deep, and Leeudoorn data sets are summarized in Table 2. The table does not list the DMO to depth migration (finite-difference poststack method) tests initially applied to the data sets. The more detailed data processing and merging steps undertaken are described in Manzi et al. (2012). The following summary highlights important processing steps that are relevant to this paper, mainly velocity analysis. The 2003 Kloof-South Deep prestack data were merged with the reprocessed 1994 Leeudoorn data that covers the southern portion of Kloof mine (Figure 3a and 3b). The Leeudoorn survey consisted of 5739 shots recorded over an area of 70 km^2. The 1994 Leeudoorn and 2003 Kloof-South Deep data sets were processed individually through to residual statics to allow comparison of the two data sets. Appropriate static and phase corrections were calculated and applied before prestack merging of the two data sets (Table 2). The merged data set covers an area of 147 km^2 with 9894 shot points.

Prestack processing included radial filtering to remove ground roll, Wiener-Levinson deconvolution and zero-phase spectral

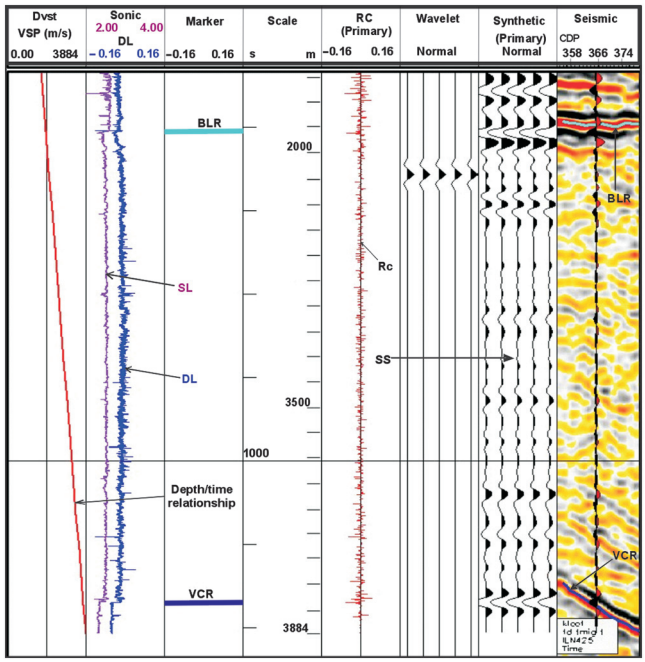


Figure 5. Seismic data and the synthetic seismogram derived from sonic and density log for the borehole, showing a good correlation with the BLR and VCR horizons. DL: Density log; Rc: Reflection coefficients; SL: Sonic log; SS: Synthetic seismogram; BLR: Black Reef; VCR: Ventersdorp Contact Reef.

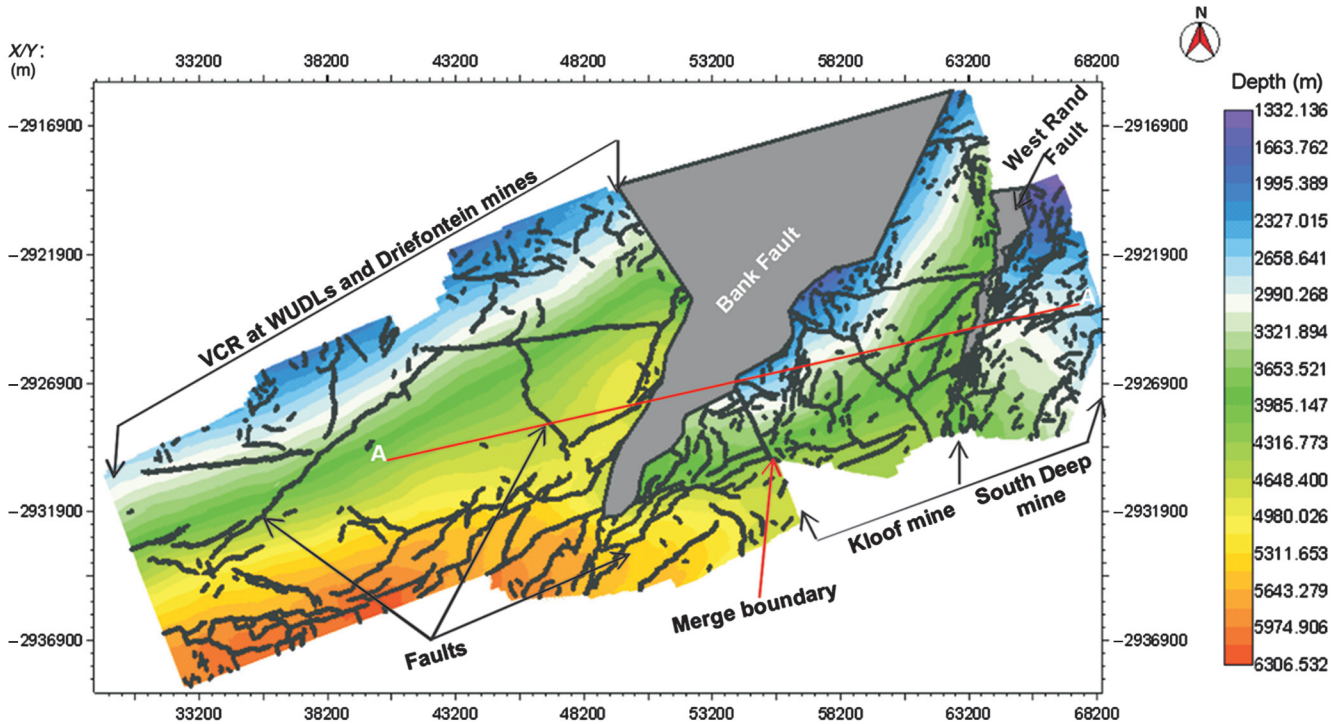


Figure 6. Detailed depth structure map of the Venterdorp Contact Reef (VCR) derived from conventional picking across survey areas, showing faults of all strikes and dips.

Downloaded 10 Sep 2012 to 146.141.1.82. Redistribution subject to SEG license or copyright; see Terms of Use at http://segdl.org/

whitening to improve resolution, the application of residual statics and velocity analysis. Time migration was performed using the finite difference algorithm. The BLR and VCR time horizons were picked, using borehole logs for control. A three-layer interval velocity model was derived. The layers are:

- datum to BLR (yielding the interval velocity for the Transvaal Supergroup rocks)
- BLR to VCR (interval velocity of Klipriviersberg lavas)
- below VCR to Booysens Shale (using stacking velocity due to no borehole control)

The velocity field used for the 3D finite-difference partial prestack time migration (PSTM) and for depth conversion had short wavelength velocity variations due to irregular borehole spacing and very densely spaced underground boreholes. This resulted in

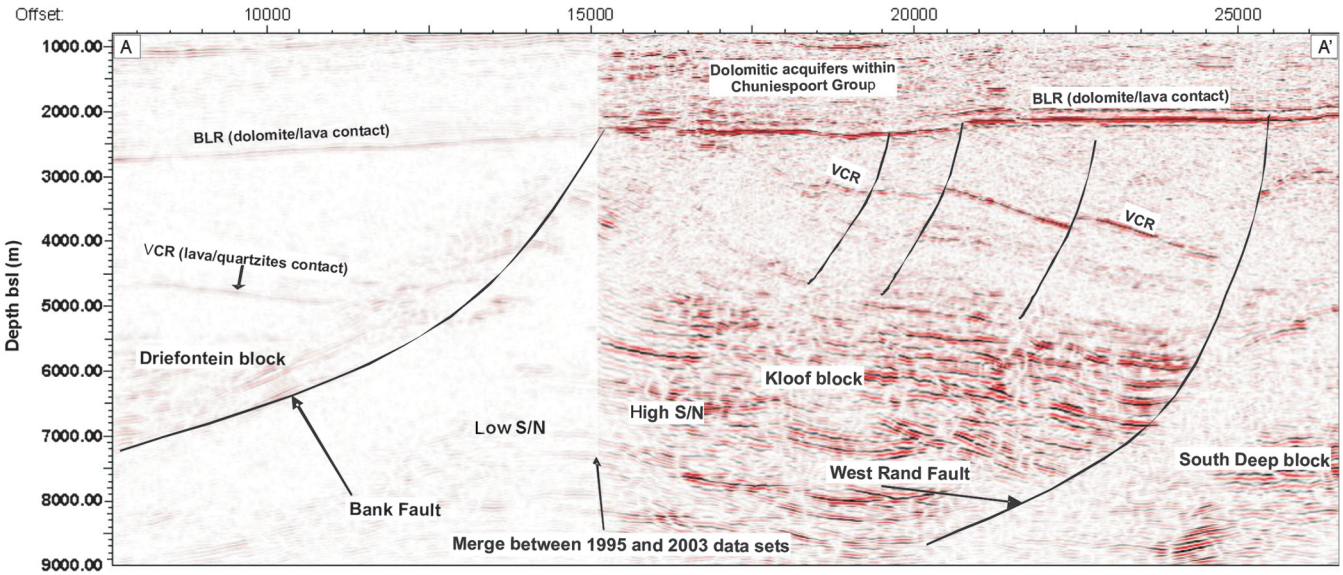
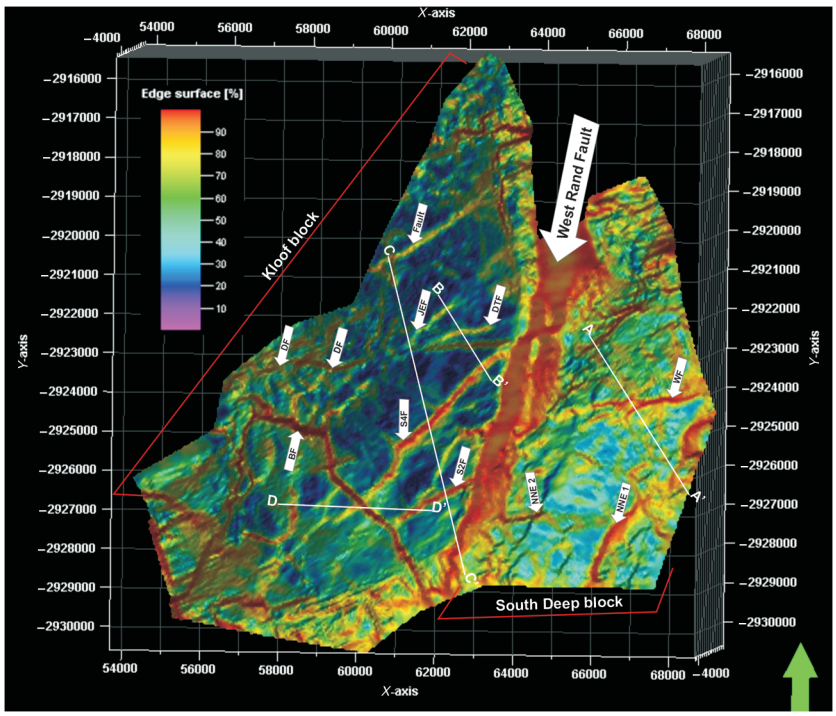


Figure 7. North–northeast regional crossline seismic section (line AA′ in Figure 6) through WUDLs, Driefontein, Kloof, and South Deep surveys. The West Rand and Bank Faults do not breach the BLR. The merge boundary between WUDLs, Driefontein, and Kloof-South Deep surveys is identifiable in the seismic section.

Figure 8. Three-dimensional visualization of the VCR edge detection attributes through Kloof and South Deep surveys. Map shows optimum imaging of structures at this horizon. The West Rand Fault (WRF) is the major structure separating Kloof and South Deep gold mines. DF: Danies Fault; DTF: Danies Twin Fault; JEF: Jocks Extension Fault; BF: Boundary Fault; S2F: Shaft 2 Fault, S4F: Shaft 4 Fault, WF: Wrench Fault, NNE 1: North-northeast 1, NNE 2: North-northeast 2.



Downloaded 10 Sep 2012 to 146.141.1.82. Redistribution subject to SEG license or copyright; see Terms of Use at http://segdl.org/

a poor migration quality, with a stretched seismic section (possibly owing to undermigration) and mis-ties between the picked horizons and borehole control (Figure 4a). The velocity field derived from boreholes was then gridded in 600-m cells, the same spacing as was used for velocity analysis. The smoothed interval velocities improved the migration quality, yielding a better tie between the picked horizons and borehole control (Figure 4b). These velocities were calibrated against the vertical seismic profile (VSP) result shown in Figure 5, which was recorded over the depth range 3100–3420 m at 5-m intervals. The purpose of the VSP was to characterize the seismic signature of stratigraphic horizons imaged by the seismic data. The borehole logging provided control for synthetic modeling and lithological discrimination.

A second pass of interactive velocity analysis was performed at 600-m intervals in crossline and inline directions and used for a migration and depth conversion (Table 2). Finally, the Kloof-South Deep and Leeudoorn PSTM data cube was merged with the WUDLs survey acquired by AngloGold Ashanti in 1995. It is important to note that the WUDLs data were never reprocessed; therefore, the data have a relatively poor signal-to-noise ratio (S/N) compared with the 2003 Kloof-South Deep data.

INTERPRETATION AND ATTRIBUTE ANALYSIS

The topography of the reflectors marking the base of the BLR and the base of the Ventersdorp Supergroup were mapped in detail to resolve fault zones that could provide water conduits from aquifers above the BLR to VCR workings. The reflectors were prominent across the seismic volume and correlated well with synthetic seismograms computed from selected VSP data.

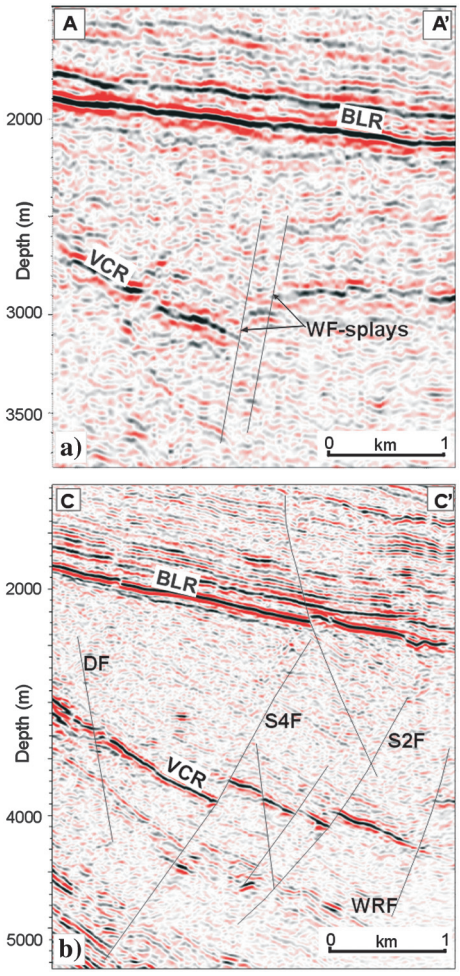


Figure 9. (a) North–northwest seismic section across the South Deep mine (line AA′ in Figure 8) showing the Wrench Fault (WF) splays. (b) North–northwest seismic section across the Kloof mine (line CC′ in Figure 8) showing the Danies Fault (DF), Shaft 4 Fault (S4F), Shaft 2 Fault (S2F) and the West Rand Fault (WRF). These faults do not crosscut the BLR on the migrated sections.

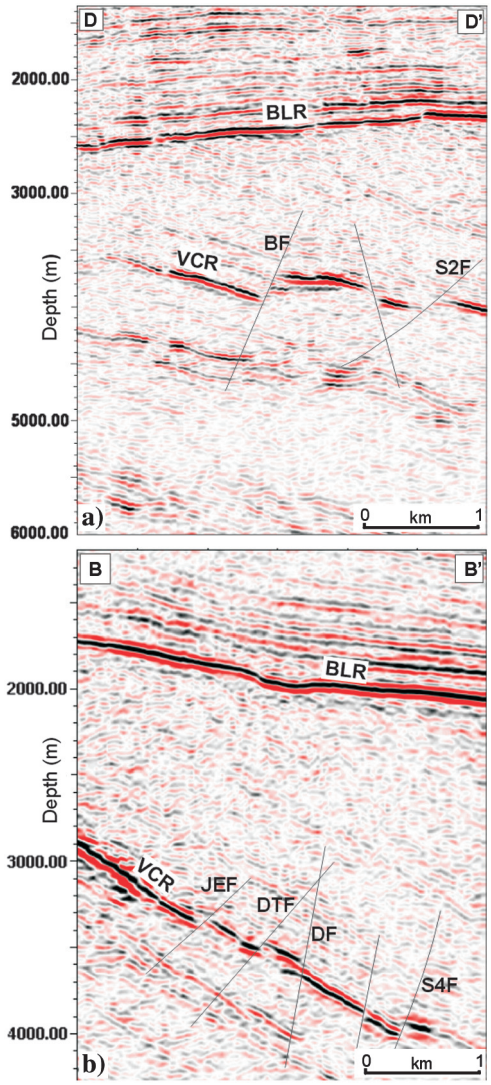


Figure 10. (a) West–east seismic section across the Kloof mine (line DD′ in Figure 8) showing a Boundary Fault (BF) and Shaft 2 Fault (S2F). (b) North–northwest seismic section (line BB′ in Figure 8) showing Jocks Extension Fault (JEF), Danies Twin Fault (DTF), Danies Fault (DF) and Shaft 4 Fault (S4F). Note that none of these faults crosscut the BLR.

Downloaded 10 Sep 2012 to 146.141.1.82. Redistribution subject to SEG license or copyright; see Terms of Use at http://segdl.org/

The horizons and faults were manually picked on every seismic line of the depth-converted PSTM data because this was found to image faults better than auto-track picking. Even so, the smallest fault that could be manually picked on a migrated section had a throw of about one-quarter of the dominant wavelength, or about 25 m for this data set. Seismic attribute analysis was used to enhance the structural resolution further.

Attribute analysis is applied in most seismic interpretation projects where high resolution is required. We used the edge detection tools developed by Rock Deformation Research (2004) implemented in the Petrel software. The edge-detection algorithms combine dip and azimuth variations, normalized to the local noise surface, which overcomes the difference in detectability between the dip and dip azimuth attributes identified by Rijks and Jauffred (1991). Application of these edge detection techniques has contributed immensely to high-resolution imaging of structures such as faults, dikes, and fractures for the petroleum industry (Rock Deformation Research, 2004), in some cases yielding an order of magnitude increase in the number of structures imaged. The techniques also improve the lateral resolution of the fault traces, which aids in characterizing fault continuity and connectivity.

RESULTS

Fault mapping

The BLR and VCR reflectors are well developed throughout the area covered by the interpretation, and line-by-line manual picking provided a very robust interpretation of the VCR and BLR horizons. Numerous faults of many orientations were clearly mapped on the VCR depth structure map (Figure 6). The major West Rand and Bank Faults displace the VCR horizon by several kilometers. However, no displacement of the BLR is discernable on a seismic section (Figure 7), and thus, these faults do not appear to link aquifers in the dolomites above the BLR with the VCR stopes. However, a displacement less than the resolution limit (about 25 m) cannot be excluded. Edge detection attributes were computed for the VCR and BLR horizons to investigate possible subtle faults that appear at both elevation levels. The most prominent features revealed by edge attribute analysis of the VCR horizon in Kloof and South Deep mines, are shown on Figure 8. They include:

- West Rand Fault (WRF), a major north–northeast-trending listric fault (maximum throw ~2 km) that dips 65°–70° to the west
- Danies Fault (DF), an east-trending normal fault antithetic to the WRF that dips steeply 75°–80° to the south
- Danies Twin Fault (DTF), an east-trending normal fault synthetic antithetic to the WRF that dips steeply (76°) to the north
- Boundary Fault (BF), a north–northwest-trending normal fault antithetic to the WRF that dips steeply (70°–80°) to the southwest
- Two north–northeast-trending normal faults synthetic to the WRF, locally termed the Shaft 2 Fault (S2F) and Shaft 4 Fault (S4F), that dip moderately (50°–55°) to the west
- Wrench Fault (WF), an east-trending "dextral" strike-slip fault that separates the South Deep mine into two distinct blocks
- North–northeast-trending features synthetic to the WRF, termed NNE 1 and NNE 2, that dip 70°–80° to the west

The seismic sections in Figures 9 and 10 show structures that have displaced the VCR horizon but not the BLR. Figure 11 presents the 3D model of the VCR edge detection attribute together with the structures that are interpreted to have displaced the VCR but not the BLR. These faults were derived from the manually picked faults and remodeled to correlate with the VCR topographic breaks revealed by edge detection attributes.

The structural interpretation derived from edge detection attributes for the BLR and VCR horizons over the entire mining areas is shown in Figures 12 and 13. The edge detection attributes reveal more than 60% of structures (faults and dikes) that have propagated

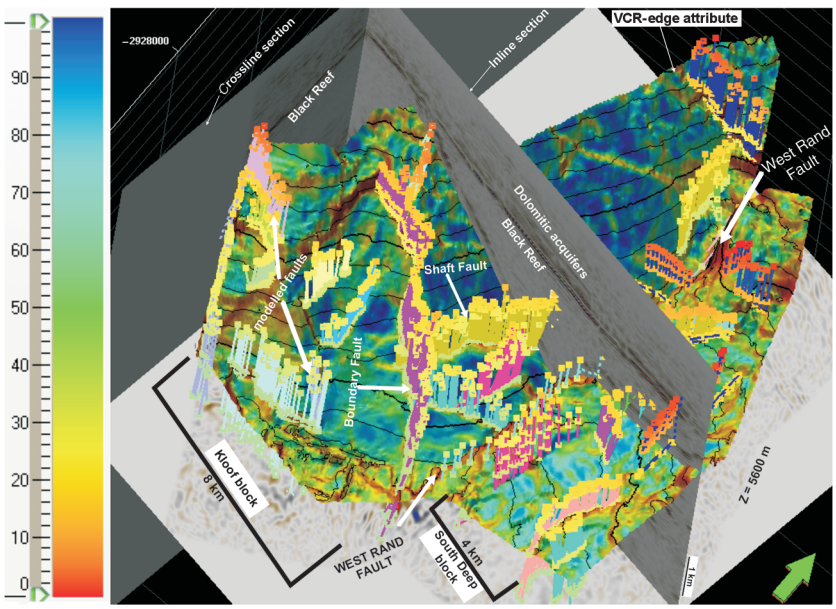


Figure 11. Three-dimensional visualization (view from southwest) of combined 3D VCR edge detection surface and modeled faults (color bar for edge detection attribute is given in%). These faults do not offset the BLR on seismic sections.

Downloaded 10 Sep 2012 to 146.141.1.82. Redistribution subject to SEG license or copyright; see Terms of Use at http://segdl.org/

between VCR and BLR horizons (Figure 14). These include Danies Fault, Danies Twin Fault, Boundary Fault, and Shaft 4 and Shaft 2 faults in Kloof Gold Mine. In Driefontein Mine, the structures that have propagated between VCR and BLR include:

- North–northeast-trending faults adjacent to Bank Fault. These faults are situated in a structurally complex area at the down-dip edge of the survey area. The S/N is low, and thus, there is some uncertainty in their position.
- K1 and K2. The variability in their continuity on the BLR horizon could be due to variations in fault throw or oversmoothing of the BLR horizon prior to the computation of the edge attributes.
- K3, a subvertical normal fault located at the central part of the mine block. The positioning of this fault in the BLR is not precise, i.e., it is shifted slightly to the west when compared with its position in the VCR level. This mispositioning could be due to the combination of the mispicking in the seismic sections and velocity model used for migration and time-to-depth conversion.
- K4, north–northwest-trending fault in the far western part of the mine

This suggests that these faults have throws below the level required to see them on the BLR level on the seismic sections. The continuity of the several structures seen on the VCR and BLR horizons varies along the length of the structures. This could be due to variations in the throw along the fault plane. The positions and dips of Danies Fault, Boundary Fault, and Shaft Faults have been confirmed by underground mapping, whereas other seismically mapped features do not coincide with any geologically mapped structures. Importantly, most of these structures lie in areas that have not yet been mined and most of these faults have displacements below the one-quarter wavelength threshold required to pick them on a conventional seismic section. Although the area has been quite extensively drilled to map the down-dip extension of the ore bodies, the spacing between boreholes is typically greater than 1.0 km, and it is not possible to determine from borehole data alone whether differences in reef elevation of a few tens of meters between boreholes is due to faulting or folding.

Some of the faults mapped on the VCR and BLR horizons could not be tracked between the horizons on the migrated seismic sections, owing to the large vertical separation between these

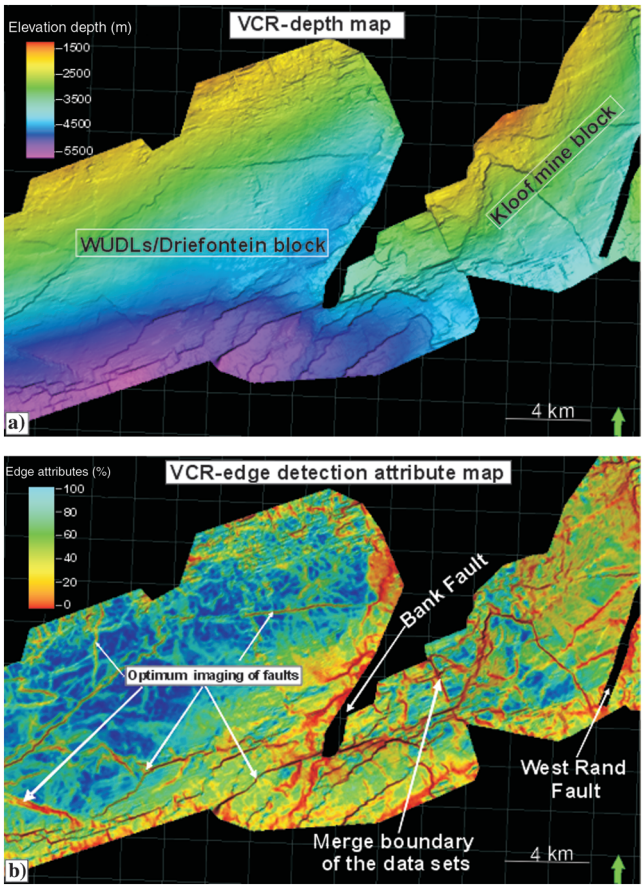


Figure 12. VCR maps showing imaging of faults before and after the computation of edge detection attributes. (a) VCR depth map (gridded) showing imaging of faults through conventional interpretation. (b) VCR edge attribute map showing high-resolution imaging of the faults, mostly with throws as small as 10 m.

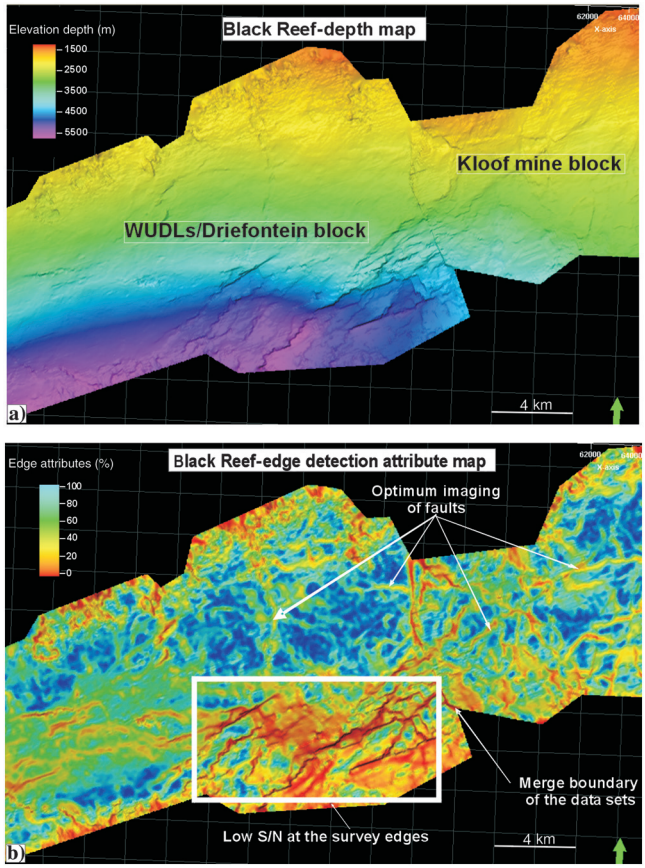


Figure 13. BLR maps showing imaging of faults before and after the computation of edge detection attributes. (a) Regional BLR depth map showing structures defined from the conventional interpretation. (b) Regional BLR edge attribute map showing high-resolution imaging of minor faults. Multicolored strips represent the subtle discrete or sharp edges on the horizon, which can be associated to low throw faults. Note the merged boundary of the data that shows up as a fault.

Downloaded 10 Sep 2012 to 146.141.1.82. Redistribution subject to SEG license or copyright; see Terms of Use at http://segdl.org/

two horizons, poor reflectivity of markers within the Ventersdorp lavas between the two horizons, and the large range in dip angles of faults. Therefore, the linkage of displacements on the VCR and BLR levels sometimes was uncertain. However, there are many fault traces that can be confidently projected from the VCR to the BLR horizons. These may represent faults that were reactivated during the post-BLR deformation event described by Coward et al. (1995), Gibson et al. (2000), and Dankert and Hein (2010). According to D'Agostino et al. (1998) and Jackson et al. (2006), many structures in extensional basins are reactivated during later deformational events. Some structures are probably related to dikes that were emplaced after deposition of the Transvaal Basin including Bushveld, Pilanesberg, Karoo, and post-Karoo age dikes (Vermaakt and Chunnett, 1994; Coward et al., 1995; Cook, 1998; Robb and Robb, 1998).

Relationship between faults and occurrences of fissure water and gas

A study of the relationship between the geologic structures and the occurrence of methane and groundwater was carried out at Kloof Gold Mine. The known occurrences of methane and water on the VCR horizon are shown together with the faults modeled by the Rock Deformation Research (2004) and faults interpreted from this study using edge detection attributes in Figure 15. The S/N in the northwestern portion of the Kloof survey area is low, owing to the presence of mining excavations. This reduced the confidence with which we were able to map and interpret the faults (Figure 15). Superposition of the fault map on the water and methane data suggests that structures that dip ~60° (e.g., Shaft 2 Fault and Shaft 4 Fault) or subvertically (e.g., Danies Fault) are most likely to contain water or gas.

The superposition of the VCR edge detection attribute on the water and methane data from Kloof Gold Mine shows that the Shaft 4 Fault (S4F) and Danies Fault (DF), which intersect BLR, have a good correlation with water and methane intersections (Figure 16). Water and methane often occur at several locations on a structure. The high interconnectivity and crosscutting relationship between faults (e.g., Boundary fault and Shaft 4 Fault), as shown on edge attribute maps, implies that any structure could have connectivity to aquifers above the BLR and provide a conduit for water or methane to the VCR mining horizon. These results provide high confidence that the structures that are associated with water and methane transport can be imaged by the seismic method. However, it is difficult to determine which faults and dikes intersect aquifers above the BLR and which of these aquifers may have once been charged by methane derived from coal seams. Furthermore, the ability to image the structures also is dependent on the original S/N of the manually picked horizons. A conservative approach is probably best at this stage, and to assume that any of

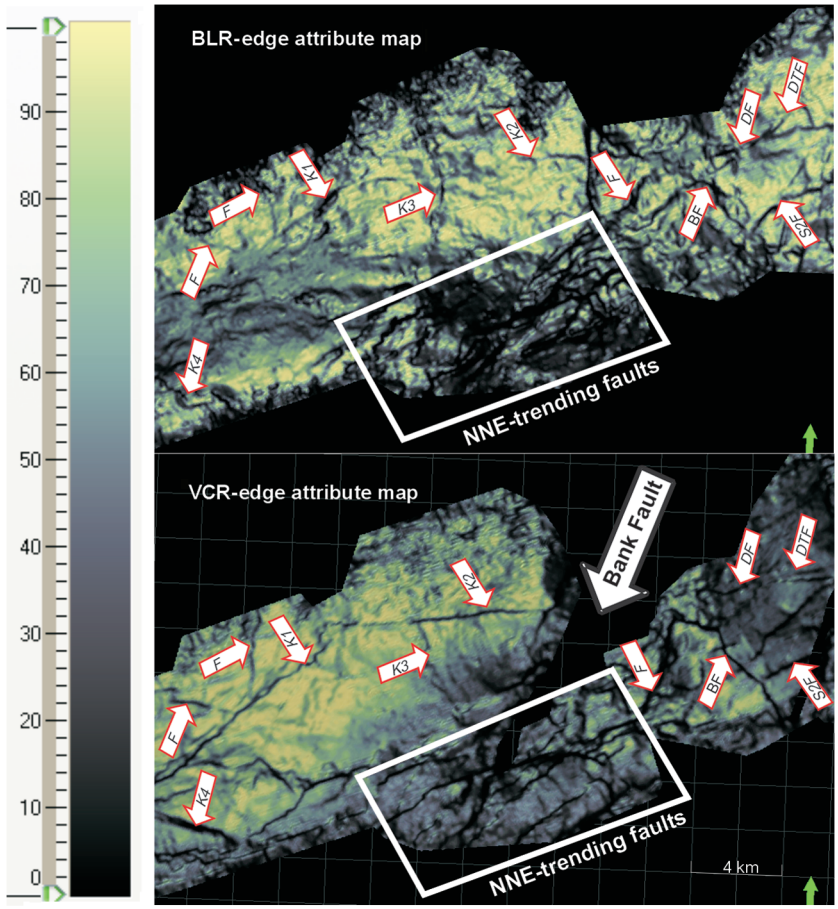


Figure 14. Propagation of faults between the BLR and VCR. BLR (top) and VCR (bottom) edge attribute maps showing high-resolution imaging of the faults. The arrows indicate structures that have propagated between the VCR and BLR horizons (color bar is given in%). DF: Danies Fault, DTF: Danies Twin Fault, BF: Boundary Fault, S2F: Shaft 2 Fault, S4F: Shaft 4 Fault, WF: Wrench Fault.

Downloaded 10 Sep 2012 to 146.141.1.82. Redistribution subject to SEG license or copyright; see Terms of Use at http://segdl.org/

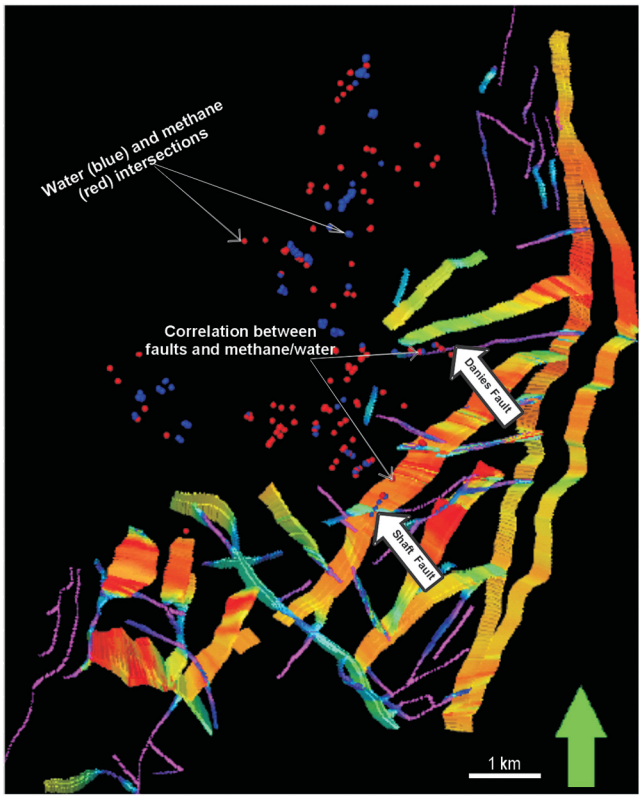


Figure 15. Seismically modeled faults and the known water-methane occurrence data in Kloof mine. There is a good correlation between methane and water, and faults, e.g., Danies Fault and Shaft Fault. Note that the northwest part of the Kloof mine has been mined out and the correlation of faults with water and methane in this area was difficult due to low S/N.

these structures could be potential conduits for water and methane. Figure 17 presents the interpreted fault surfaces, as identified by attribute analysis, differentiating between faults that are interpreted to intersect both horizons, and faults that do not intersect the BLR horizon.

DISCUSSION

Edge detection attributes have identified a wide array of structures (fault and dikes) of different orientations and variable throws that have clearly propagated between the VCR and the BLR. These structures represent either faults that were reactivated during a post-BLR deformational event, or post-BLR intrusions. Correlation between the known occurrence of fissure water and methane with geologic- and seismic-mapped faults showed that steeply dipping structures (dip>60°) are most likely to channel fluid, although this is not a particularly useful criterion because most faults in the gold fields dip steeply. However, this study has demonstrated that water and methane occur along structures that can be mapped using 3D seismics, and thus, precautions can be taken as mining progresses. Future reports of water and methane intersections on WUDLs, Driefontein, and South Deep gold mines will be correlated with the fault model derived from edge detection attributes, and used to manage the risks associated with water and methane influx.

It is clear that large volumes of water could originate from the dolomitic aquifer overlying the BLR. However, we have not been able to identify the sources of methane with confidence. Even though the Karoo sediments and coal seams no longer overlie the West Wits Line and West Rand, it is possible that methane derived from this source entered the ground water system prior to the erosion of these strata. It also is plausible that the methane is derived from igneous intrusions or from ancient algal mats.

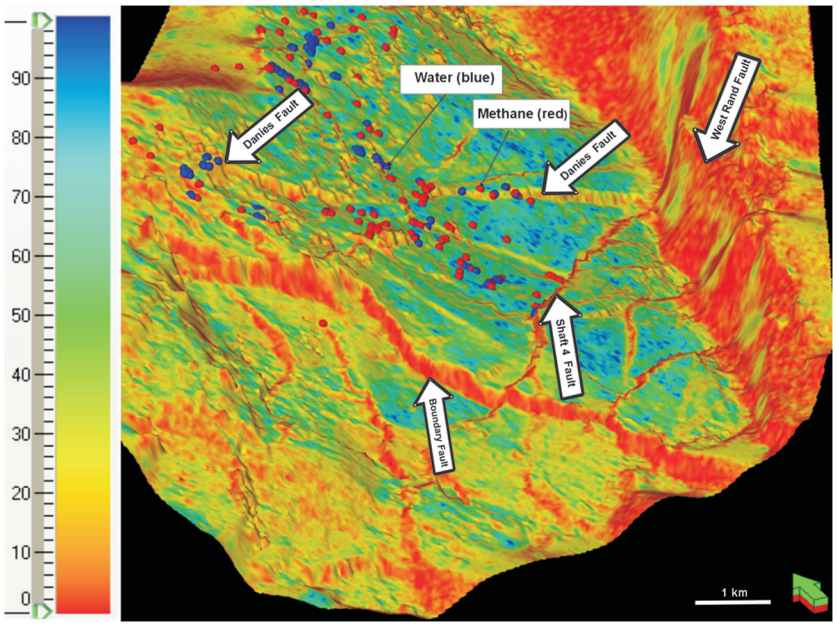


Figure 16. VCR edge attribute map of the VCR overlain with water and methane data in Kloof Mine. Structures such as Danies Fault (DF) and Shaft 4 Fault (S4F) show good correlation with water and methane data (color bar is given in %).

Downloaded 10 Sep 2012 to 146.141.1.82. Redistribution subject to SEG license or copyright; see Terms of Use at http://segdl.org/

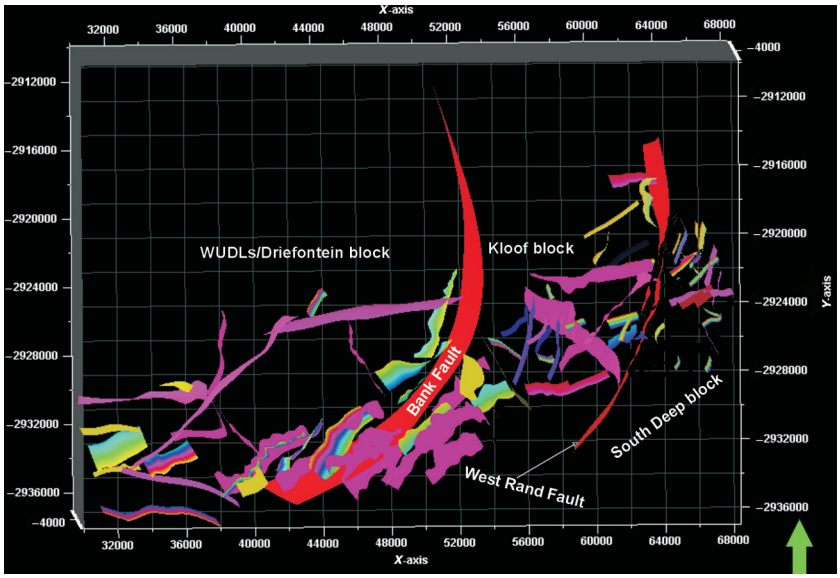


Figure 17. Fault model for WUDLs, Driefontein, Kloof, and South Deep mines using 3D seismic and edge detection attributes. The structures that have displaced the VCR and BLR are color-coded in pink.

CONCLUSION

Reflection seismics are used widely to map ore bodies in the deep gold mines of the Witwatersrand basin. Here, we have used 3D reflection seismics to mitigate the risks to mine workers posed by water inrushes and the ignition of flammable gases. To enhance the resolution of the seismic data, horizons and faults were manually picked and edge detection attributes applied. In particular, we have identified structures that displace the VCR and BLR horizons because these are the most likely to be connected to the overlying dolomitic aquifers. We correlated the mapped occurrences of water and methane with geologic- and seismic-mapped faults, and we characterized strikes and dips of these structures and their continuity and connectivity. This information could be used to assess and mitigate the risks posed by inrushes of fissure water and the ignition of flammable gases as mining proceeds to greater depths.

ACKNOWLEDGMENTS

This research was sponsored by Gold Fields Mining Ltd. We greatly acknowledge the thorough reviews and constructive comments of Alireza Malehmir and two anonymous reviewers, which improved the quality of the manuscript. The authors also thank Schlumberger for providing Petrel software, Rock Deformation Research Group, G. Smith, J. Trickett, L. Linzer, M. Gibson, M. Muller, S. Webb, and T. Owen-Smith for their major scientific contribution.

REFERENCES

Adams, D., A. G. du Plessis, S. A. Gumbie, and R. P. H. Willis, 2007, Introduction to safety practices in South Africa mines: Mine Health and Safety Council Johannesburg, 210.

Beach, A., and R. Smith, 2007, Structural geometry and development of the Witwatersrand Basin, South Africa: *in* A. C. Ries, R. W. H. Butler, and R. Graham, eds., Deformation of the continental crust: The Legacy of Mike Coward, Geological Society, Special Publication, **272**, 533–542.

Bekker, E. H., 1986, Fossil water and the associated gas mixture within and below the Ventersdorp Supergroup in the Harmony mine area, Welkom goldfield: *in* C. R. Anhaeusser, and S. Maske, eds., Mineral deposits of southern Africa: Geological Society of South Africa, **1, 2**, 731–752.

Cook, A. P., 1998, The occurrence, emission, and ignition of combustible strata gases in Witwatersrand gold mines and Bushveld platinum mines, and means of ameliorating related ignition and explosion hazards: Final project report, project GAP 504, Safety in Mines Research Advisory Committee, 89.

Cousens, R. R. M., and W. S. Garrett, 1969, The flooding at the West Driefontein mine: Journal of the South African Institute of Mining and Metallurgy, **69**, 421–463.

Coward, M. P., R. M. Spencer, and C. E. Spencer, 1995, Development of the Witwatersrand Basin, South Africa, *in* M. P. Coward, and A. C. Ries, eds., Early Precambrian processes: Geological Society, Special Publication, **95**, 243–269.

D'Agostino, N., N. Chamot-Rooke, R. Funiciello, L. Jolivet, and F. Speranza, 1998, The role of pre-existing thrust faults and topography on the styles of extension in the Gran Sasso range (central Italy): Tectonophysics, **292**, 229–254, doi: 10.1016/S0040-1951(98)00070-5.

Dalley, R. M., E. C. A. Gevers, G. M. Stampfli, D. J. Davies, C. N. Gastaldi, P. A. Ruijtenberg, and G. J. O. Vermeer, 1989, Dip and azimuth displays for 3D seismic interpretation: First Break, **7**, 86–95.

Dankert, B. T., and K. A. A. Hein, 2010, Evaluating the structural character and tectonic history of the Witwatersrand Basin: Precambrian Research, **177**, 1–22, doi: 10.1016/j.precamres.2009.10.007.

Gibson, M. A. S., S. J. Jolley, and A. C. Barnicoat, 2000, Interpretation of the Western Ultra Deep Levels 3D seismic survey: The Leading Edge, **19**, 730–735, doi: 10.1190/1.1438704.

Jackson, C. A. L., R. L. Gawthorpe, and I. R. Sharp, 2006, Style and sequence of deformation during extensional fault-propagation folding: Examples from Hammam Faraun and El-Qaa fault blocks, Suez Rift, Egypt: Journal of Structural Geology, **28**, 519–535, doi: 10.1016/j.jsg.2005.11.009.

Jolley, S. J., S. R. Freeman, A. C. Barnicoat, G. M. Phillips, R. J. Knipe, A. Pather, N. P. C. Fox, D. Strydom, M. T. G. Birch, I. H. C. Henderson, and T. W. Rowland, 2004, Structural controls on Witwatersrand Gold mineralisation: Journal of Structural Geology, **26**, 1067–1086, doi: 10.1016/j.jsg.2003.11.011.

Kritzinger, P. R., 2001, Beatrix gold mine disaster. Investigation report in terms of section 64(1) of the Mine Health and Safety Act, 1996 (Act No. 29 of 1996) into the explosion which occurred on 8 May 2001: Department of Minerals and Energy (unpublished).

Malehmir, A., and G. Bellefleur, 2009, 3D seismic reflection imaging of volvanic-hosted massive sulfide deposits: Insights from re-processing of the Halfmile Lake data, New Brunswick, Canada: Geophysics, **74**, no. 6, 209–219, doi: 10.1190/1.3230495.

Malehmir, A., C. Juhlin, C. Wijns, M. Urosevic, P. Valasti, and E. Koivisto, 2012, 3D reflection seismic imaging for open-pit mine planning and deep exploration in the Kevitsa Ni-Cu-PGE deposit, northern Finland: Geophysics (this issue).

Mambane, P. W., K. A. A. Hein, S. G. Twemlow, and M. S. D. Manzi, 2011, Pseudotachylite in the South Boundary Fault at the Cooke Shaft, Witwatersrand Basin, South Africa: South African Journal of Geology, **114**, 109–120, doi: 10.2113/gssajg.114.2.109.

Manzi, M. S. D., M. A. S. Gibson, K. A. A. Hein, N. King, and R. J. Durrheim, 2012, Application of 3D seismic techniques to evaluate ore resources in the West Wits line goldfield and portions of the West Rand goldfield, South Africa: Geophysics (this issue).

McCarthy, T. S., 2006, The Witwatersrand Supergroup, *in* M. R. Johnson, C. R. Anhaeusser, and R. J. Thomas, eds., The geology of South Africa: Geological Society of South Africa, Johannesburg/Council for Geosciences, 155–186.

Milkereit, B., E. K. Berrer, A. R. King, A. H. Watts, B. Roberts, E. Adam, D. W. Eaton, J. Wu, and M. Salisbury, 2000, Development of 3-D seismic exploration technology for deep nickel-copper deposits — A case history from the Sudbury basin, Canada: Geophysics, **65**, 1890–1899, doi: 10.1190/1.1444873.

Milkereit, B., D. Eaton, J. Wu, G. Perron, M. Salisbury, E. Berrer, and G. Morrison, 1996, Seismic imaging of massive sulfide deposits, Part 2: Reflection seismic profiling: Economic Geology, **91**, 829–834, doi: 10.2113/gsecongeo.91.5.829.

Motaung, A. H. C. H., 2000, Mponeng gold mine disaster. Investigation report in terms of section 64(1) of the Mine Health and Safety Act, 1996 (Act No. 29 of 1996) into the flammable gas explosion that occurred on 29 July 1999: Department of Minerals and Energy (unpublished).

Downloaded 10 Sep 2012 to 146.141.1.82. Redistribution subject to SEG license or copyright; see Terms of Use at http://segdl.org/

Ngcobo, T. A., 2006, The risk associated with mines in dolomite compartments: Journal of the South African Institute of Mining and Metallurgy Joernaal van die Suid-Afrikaanse Instituut vir Mynbon and Metallurgie, **106**, 251–264.
Ortlepp, W. D., 2001, The mechanism of a rock outburst in a quartzite tunnel in a deep gold mine, *in* G. Van Aswegen, R. J. Durrheim, and W. D. Ortlepp, eds., Dynamic rock mass response to mining, Proceedings of the 5th International Symposium on Rockbursts and Seismicity in Mines, South African Institute of Mining and Metallurgy Symposium Series S27, 53–58.
Pretorius, C. C., M. R. Muller, M. Larroque, and C. Wilkins, 2003, A review of 16 years of hardrock seismic of the Kaapvaal Craton, *in* D. W. Eaton, B. Milkereit, and M. H. Salisbury, eds., Hardrock seismic exploration, geophysical developments: SEG, **10**, 247–268.
Pretorius, C. C., W. H. Steenkamp, and R. G. Smith, 1994, Developments in data acquisition, processing and interpretation over ten years of deep vibroseismic surveying in South Africa: Proceedings of the 15th Congress of the Council for Mining and Metallurgical Institutions, 3, (Geology), C. R. Anhaeusser, eds., South African Institute of Mining and Metallurgy, **3**, 249–258.
Pretorius, C. C., W. F. Trewick, and C. Irons, 2000, Application of 3D-seismics to mine planning at the Vaal Reefs gold mine, number 10 shaft, Republic of South Africa: Geophysics, **65**, 1862–1870, doi: 10.1190/1.1444870.
Rijks, E. J. H., and J. C. E. M. Jauffred, 1991, Attribute extraction: An important application in any detailed 3D interpretation study: The Leading Edge, **10**, 11–19.
Robb, L. J., and V. M. Robb, 1998, Gold in the Witwatersrand Basin, *in* M. G. C. Wilson, and C. R. Anhaeusser, eds., The mineral resources of South Africa, 6th edition, Council for Geoscience, 294–349.
Rock Deformation Research, 2004, Structural and seismic appraisal of the kloof and surrounding area: Report 9350 (unpublished), 1–37.
Salisbury, M. H., G. W. Harvey, and L. Mathews, 2003, The acoustic properties of ores and host rocks in hardrock terranes, *in* D. W. Eaton, B. Milkereit, and M. H. Salisbury, eds., Hardrock seismic exploration, geophysical developments: SEG, **10**, 9–19.
Spencer, K. C., and D. M. Walter, 2000, A manual for best practice for emergency response procedures, Project Report: Turgis Technology (Pty) Ltd., 1–34.
Stevenson, F., R. M. A. Higgs, and R. J. Durrheim, 2003, Seismic imaging of precious and base-metal deposits in South Africa, *in* D. W. Eaton, B. Milkereit, and M. H. Salisbury, eds., Hardrock seismic exploration, Geophysical Development Series, SEG, **10**, 141–156.
Trickett, J. C., W. A. Duweke, and S. Kock, 2004, Three-dimensional reflection seismic: Worth its weight in platinum: International Platinum Conference 'Platinum Adding Value', South African Institute of Mining and Metallurgy, 257–264.
Vermaakt, D. T., and I. E. Chunnet, 1994, Tectono-sedimentary processes which controlled the deposition of the Ventersdorp Contact Reef within the West Wits Line, *in* C. R. Anhaeusser, ed., Proceedings of the 15th Congress of the Council for Mining and Metallurgical Institutions, **3**, (Geology): South African Institute of Mining and Metallurgy, 117–130.

Downloaded 10 Sep 2012 to 146.141.1.82. Redistribution subject to SEG license or copyright; see Terms of Use at http://segdl.org/

Tectonophysics 590 (2013) 94–105

Contents lists available at SciVerse ScienceDirect

Tectonophysics

journal homepage: www.elsevier.com/locate/tecto

Neoarchaean tectonic history of the Witwatersrand Basin and Ventersdorp Supergroup: New constraints from high-resolution 3D seismic reflection data

Musa S.D. Manzi [a,*], Kim A.A. Hein [a,1], Nick King [b,2], Raymond J. Durrheim [a,c]

[a] School of Geosciences, University of the Witwatersrand Johannesburg, PBag 3, WITS, 2050, Republic of South Africa
[b] South Deep Gold Mine, Gold Fields Limited, Republic of South Africa
[c] Council for Scientific and Industrial Research (CSIR) and University of the Witwatersrand, Johannesburg, Republic of South Africa

ARTICLE INFO

Article history:
Received 6 November 2012
Received in revised form 11 January 2013
Accepted 18 January 2013
Available online 28 January 2013

Keywords:
Neoarchaean
Witwatersrand Basin
Ventersdorp Supergroup
Seismics
Structure
Tectonics

ABSTRACT

First-order scale structures in the West Wits Line and West Rand goldfields of the Witwatersrand Basin (South Africa) were mapped using the high-resolution 3D reflection seismic method. Structural models constrain the magnitude of displacement of thrusts and faults, the gross structural architecture and Neoarchaean tectonic evolution of the West Rand and Bank fault zones, which offset the gold-bearing reefs of the basin.

The merging of several 3D seismic surveys made clear the gross strato-structural architecture of the goldfields; a macroscopic fold-thrust belt is crosscut by a macroscopic extensional fault array. These are dissected, eroded and overlain by the Transvaal Supergroup above an angular unconformity.

The seismic sections confirm that the West Rand Group (ca. 2985–2902 Ma) is unconformably overlain by the Central Rand Group (ca. 2902–2849 Ma), with tilting of the West Rand Group syn- to post-erosion at ca. 2.9 Ga. The seismic sections also confirm that an unconformable relationship exists between the Central Rand Group and the auriferous Ventersdorp Contact Reef (VCR), with an easterly-verging fold-thrust belt being initiated concomitant to deposition of the VCR at approximately 2.72 Ga. Fold-thrust formation included development of the (1) newly identified first-order scale Libanon Anticline, (2) Tandeka and Jabulani thrusts which displace the West Rand Group, and (3) parasite folds.

The fold-thrust belt is crosscut by a macroscopic extensional fault array (or rift-like system of faults) which incepted towards the end of extrusion of the Ventersdorp lavas, and certainly during deposition of the Platberg Group (2709–2643 Ma) when a mantle plume may have heated the lithosphere. The West Rand and Bank fault zones formed at this time and include (1) the West Rand and Bank faults which are scissors faults; (2) second and third-order scale normal faults in the immediate footwall and hanging wall of the faults; (3) drag synclines, and (4) rollover anticlines.

© 2013 Elsevier B.V. All rights reserved.

1. Introduction

The West Wits Line and West Rand goldfields of the Mesoarchaean Witwatersrand Basin (Fig. 1) have been the focus of renewed interest in recent years in terms of their strato-structural and geophysical architecture (Beach and Smith, 2007; Dankert and Hein, 2010; Frimmel and Minter, 2002; Mambane et al., 2011; Manzi et al., 2012a; Mashabella, 2011; Mohale, 2010). The studies undertaken by Coward et al. (1995), Beach and Smith (2007), Dankert and Hein (2010), Jolley et al. (2007) and others confirm that the basin experienced more than one episode of deformation although Dankert and Hein (2010) pointed out that surprisingly little regional-scale kinematic and structural analysis has taken place across the Witwatersrand Basin despite more than 100 years of mining of gold. However, it is generally agreed that the Witwatersrand Basin underwent inversion tectonics during and after deposition of the quartzite and conglomerate units (some auriferous) of the Central Rand Group, from extension to compression i.e. positive inversion (c.f., Beach and Smith, 2007; Dankert and Hein, 2010), and then compression to extension (i.e. negative inversion) during deposition of the Ventersdorp Supergroup (Van der Westhuizen et al., 1991).

Listric faults in the Witwatersrand Basin were recognized by Coward et al. (1995) and Vermaakt and Chunnet (1994) through studies in gold mines in the West Wits Line and West Rand goldfields, and by Beach and Smith (2007), Gibson et al. (2000, 2004) and Gibson (2005) through the interpretation of 3D seismic reflection data. Beach and Smith (2007) showed that the dominant structural styles, including major normal fault zones and their related drag folds, are those attributed to extensional tectonics that occurred during deposition of the Ventersdorp Supergroup (ca. 2709–2643 Ma) possibly during deposition of the Platberg Group.

* Corresponding author. Tel.: +27 11 717 6623.
E-mail addresses: Musa.Manzi@students.wits.ac.za (M.S.D. Manzi), kim.ncube-hein@wits.ac.za (K.A.A. Hein), nick.king@goldfields.co.za (N. King), raymond.durrheim@wits.ac.za (R.J. Durrheim).
[1] Tel.: +27 11 717 6623.
[2] Tel.: +27 83 657 9518.

0040-1951/$ – see front matter © 2013 Elsevier B.V. All rights reserved.
http://dx.doi.org/10.1016/j.tecto.2013.01.014

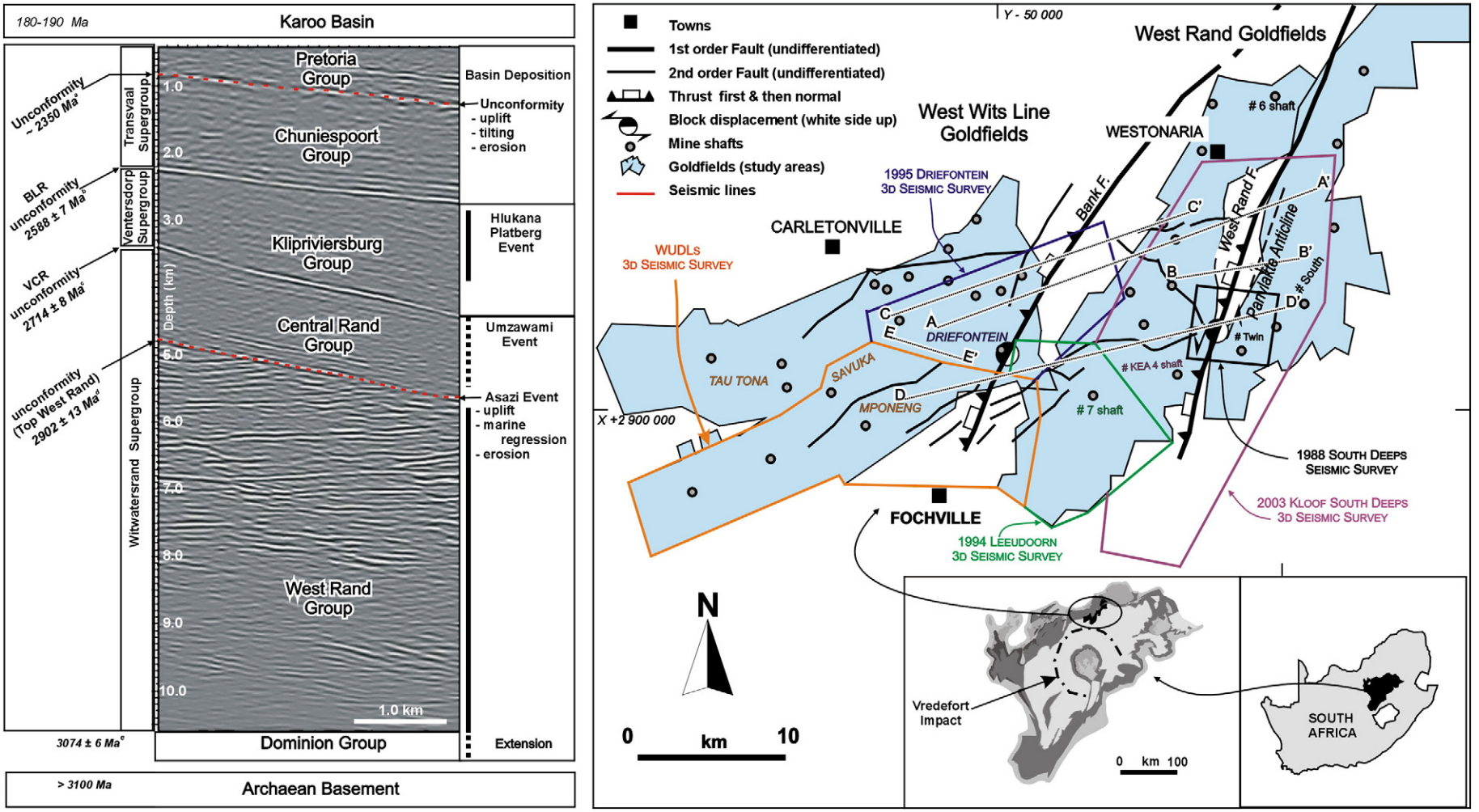


Fig. 1. Location map of the West Rand and West Wits Line (Carletonville) goldfields of the Witwatersrand Basin in South Africa, showing historical 3D seismic reflection surveys (modified after Dankert and Hein, 2010; historical surveys after Gibson et al., 2000). Generalized seismic stratigraphy and tectonic events, with dates and ages are derived from Armstrong et al. (1991), Dankert and Hein (2010), Kositcin and Krapež (2004) and Myers et al. (1989). Note that Driefontein and Kloof gold mines have been re-named KDC WEST and KDC EAST, respectively. KDC: Kloof-Driefontein Complex; WUDLs: Western Ultra Deep levels; VCR: Ventersdorp Contact Reef; BLR: Black Reef Formation. [a]Unpublished; [b]Martin et al. (1998; zircon U–Pb SHRIMP); [c,e]Armstrong et al. (1991; single zircon U–Pb SHRIMP); [d]Kositcin and Krapež (2004; zircon U–Pb SHRIMP).

Further to this, previous structural models of the Witwatersrand Basin were constrained by low resolution 3D seismic surveys that covered the region to the west of the Bank Fault (Beach and Smith, 2007; Gibson et al., 2000; Jolley et al., 2007). Little or no coverage of the eastern side of the fault (West Rand goldfields) was incorporated.

In this study, the interpretation of high-resolution 3D seismic reflection data that covers the West Wits Line and West Rand goldfields is presented, and includes studies across the Driefontein Block (now termed KDC West), the Kloof Block (now termed the KDC East), and the South Deeps Block (Fig. 1). The structural studies of the entire reprocessed and merged dataset are unique and are herein reported for the first time. The data was used to study the structural setting, mainly the first-order scale structures, but also their associated second- and third-order faults and folds. Focus was given to (1) fault geometry, fault form, and fault-throw analysis, and (2) the relative chronology of tectonic events. The results were integrated with borehole data and underground maps to validate the seismic and Neoarchaean tectonic interpretations.

The data has also been used by Manzi et al. (2012a) to map potential conduits of water and methane in the deep gold mines covered by the seismic volume. It has been used in the application of 3D seismic technique in evaluation of ore resources and is reported by Manzi et al. (2012b), and for mapping the distribution and timing of meso- to mega-scale structures and provide constraints on the ore genetic models (Malehmir et al., in press).

2. Geological setting

The Mesoarchaean Witwatersrand Basin, one of the world's premier gold regions and the greatest known source of gold on Earth, was deposited between ca. 2985 and 2849 Ma (Kositcin and Krapež, 2004) on the Kaapvaal Craton (ca. 3.6–3.2 Ga). The Witwatersrand Supergroup overlies the Dominion Group (ca. 3074 ± 6 Ma, Myers et al., 1989; U–Pb detrital zircon SHRIMP), and is made up of coarse clastic rocks and bimodal volcanic rocks. The Witwatersrand Supergroup consists of the West Rand and Central Rand groups (Fig. 1).

The West Rand Group unconformably overlies the Dominion Group with clastic and largely marine sedimentary rocks (ca. 2985–2902 Ma; Kositcin and Krapež, 2004; U–Pb detrital zircon SHRIMP). This sequence was deposited in a tectonically stable environment of the volcano-sedimentary succession of the Dominion Group (c.f., Beach and Smith, 2007; Frimmel and Minter, 2002). The West Rand Group is divided into three formations, namely the Discovery, Crown and Jeppestown formations. The Crown Formation is a seismically recognizable marker because of a relatively high acoustic impedance contrast between the overlying volcanic rocks and underlying shale units.

Unconformably overlying the West Rand Group are sandstone, conglomerate and shale units of the Central Rand Group (ca. 2902–2849 Ma; Kositcin and Krapež, 2004; U–Pb detrital zircon SHRIMP), which were deposited in a braided system of rivers of a shallow marine delta. The group hosts the majority of the auriferous reefs that are mined throughout the basin including the Elsberg, Kloof, Libanon and Kimberly reefs of the Johannesburg Subgroup, and Bird, Carbon Leader, North Leader and Middelvlei reefs of the Turffontein Subgroup (De Kock, 1964). The basin-wide Booysens Formation (sequence of laminated shale units) has been used as a stratigraphic marker to subdivide the Johannesburg Subgroup from the Turffontein Subgroup (McCarthy, 2006; Minter, 1982). Numerous erosional surfaces are hosted by the Central Rand Group dividing it into fluvial and marine repositories of sedimentation.

Synchronous to, and/or after deposition of the Central Rand Group, the sedimentary rocks of the Witwatersrand Basin were deformed with development of an easterly-verging fold-thrust belt (Beach and Smith, 2007) during the Umzawami Event (Dankert and Hein, 2010) at ca 2.73 Ga. Tectonic transport was from west to east (Beach and Smith, 2007).

The upper part of the Central Rand Group is unconformably overlain by the Ventersdorp Contact Reef (VCR) of the Venterspost Formation, which has the maximum age of 2729 ± 19 Ma (Kositcin and Krapež, 2004; U–Pb detrital zircon SHRIMP). The Venterspost Formation consists of a thin fluvial auriferous conglomerate. The VCR represents an erosional surface that formed at the end of deposition of the Central Rand Group (Frimmel et al., 1999; Gartz and Frimmel, 1999; Gibson, 2004, 2005; McCarthy, 2006; Tankard et al., 1982). It unconformably overlies and truncates approximately 2500 m stratigraphic thickness of Witwatersrand Supergroup sediments (Myers et al., 1989; Robb et al., 1991; Spencer, 1992; Winter, 1994). The depth of the VCR unconformity is approximately 3000–4200 m below surface. The conglomerates of the VCR are too thin (less than 1.5 m) to be directly resolved seismically because they fall below the tuning thickness or resolution limit, which is given by ¼ seismic dominant wavelength (λ), where $\lambda = v/f$ (Widess, 1973). Our data is characterized by the frequency (f) of 65 Hz and a mean velocity (v) of 6500 m/s, thus providing the tuning thickness of 25 m. This implies that the top and bottom of any reef with a thickness less than 25 m may not be resolved. However, the VCR unconformity coincides with a reflective interface or strong seismic reflector resulting from a major acoustic impedance contrast between metamorphosed basalts of the Klipriviersberg Group (~6400 m/s velocity) and quartzite units at the top of the Central Rand Group (~5700 m/s velocity).

Unconformably overlying the VCR is the Neoarchaean Ventersdorp Supergroup (ca. 2.72–2.63 Ga), which comprises ultramafic and mafic metavolcanic rocks of the Klipriviersberg Group, and metasedimentary rocks and bimodal metavolcanic rocks of the Platberg Group (Crow and Condie, 1988; Van der Westhuizen et al., 1991). The Klipriviersberg Group is divided into five formations, i.e. the Westonaria, Alberton, Orkney, Jeannette, and Edenville formations. The Alberton Formation is dated at 2714 ± 8 Ma (Armstrong et al. 1991; U–Pb detrital zircon SHRIMP). The emplacement of the Ventersdorp Supergroup may have coincided with global-scale mantle overturning that witnessed massive granite–greenstone belt formation in the Yilgarn and Superior cratons, and concomitant to the impingement of a superplume beneath the Kaapvaal Craton (Eriksson et al., 2007).

Bimodal metavolcanic and clastic metasedimentary rocks of the Platberg Group overlie the Klipriviersberg Group (ca. 2709 ± 8 Ma; c.f., Crow and Condie, 1988; Dankert and Hein, 2010) and Pniel Group (Jolley et al., 2004; Phillips and Law, 2000). The meta-sedimentary and meta-volcanic succession of the Platberg Group is exposed in several boreholes in the West Wits Line (De Kock, 1964). The group attains a maximum thickness of approximately 330 m and consists of boulders, cobbles, and fragments of (mainly) amygdaloidal metavolcanic rocks, with subordinate amounts of quartzite, chert and shale (Engelbrecht et al., 1986).

Unconformably overlying the Ventersdorp Supergroup is the relatively thin Black Reef Formation, which has been interpreted as the basal lithostratigraphic unit of the Palaeoproterozoic Transvaal Supergroup (ca. 2588 ± 6 Ma; Jolley et al., 2004; Krapež, 1985; Vos, 1975). The formation consists of a lower quartzite unit, with a sporadically developed conglomerate at the base, overlain by interbedded, black carbonaceous shale and dolomite beds in the upper portion. The Black Reef Formation (BLF) represents a highly reflective interface due to a major laterally extensive acoustic impedance contrast between high-velocity, high density dolomite of the Chuniespoort Group of the Transvaal Supergroup and the underlying low-velocity, less dense Ventersdorp metabasalts.

Above the BLF, the Transvaal Supergroup is divided into the Chuniespoort Group and the Pretoria Group. The Chuniespoort Group consists of carbonate (dolomite), banded iron formation and lacustrine deposits (Eriksson et al., 1995, 2007; Frimmel, 2005). The Pretoria Group (~6-7 km thick), which predominantly consists of intercalated mudstone–sandstone units, andesite and subordinate conglomerate beds, diamictite and carbonate units, non-conformably overlies the

Chuniespoort Group (Eriksson et al., 2007; SACS, 1980); a hiatus of 80 My has been proposed by Eriksson and Reczko (1995) and Eriksson et al. (1995, 2006) between the Chuniespoort and Pretoria groups. The non-conformity represents a reflective interface between the overlying low velocity volcanic rocks of the Pretoria Group and the underlying high velocity dolomites of the Chuniespoort Group.

Prior to deposition of the Transvaal Basin, the meta-sedimentary and meta-volcanic rocks of the Witwatersrand and Ventersdorp supergroups underwent extensional tectonics (c.f., Dankert and Hein, 2010; Gartz and Frimmel, 1999; Roering, 1990). Normal fault activity and extension arguably accompanied emplacement of the Klipriviersberg Group, and culminated in graben formation and deposition of the Platberg Group. The base of the BLF of the Transvaal Supergroup crosscuts earlier tectono-stratigraphy (Coward et al., 1995; Gibson et al., 2000) and a hiatus of approximately 100 Ma marks the transition from the Ventersdorp Supergroup sequences to the Transvaal Basin sequences (Dankert and Hein, 2010; Phillips and Law, 2000).

3. Methodology

The seismic dataset and the method of collection and processing are described by Manzi et al. (2012a,b). In summary, in 2003, Gold Fields Ltd conducted a high-resolution 3D seismic reflection survey, targeted at the down-dip portion of the Kloof Gold Mine (in the West Wits Line goldfield), which is located west of the West Rand Fault (Fig. 1). The survey was designed to overlap a 3D seismic survey undertaken at Leeudoorn in 1994; the Leeudoorn dataset was re-processed using the latest processing algorithms, and merged with the 2003 Kloof-South Deep data to produce a single seismic cube. This cube was merged (post-migration) with the Western Ultra Deep Levels survey (WUDLs), and incorporated into one continuous volume (>7040 km^3).

Interpretation of the Ventersdorp Contact Reef (VCR) and the Black Reef (BLR) were of particular interest in this study. They form important geophysical markers across the study area and were interpreted to constrain pre- to post-Central Rand Group age structures. Based on interval velocities, the VCR was picked as a peak because of the decrease in seismic velocity from the overlying Ventersdorp metabasalts (approx 6400 m/s) to the underlying Central Rand quartzite units (approx. 5750 m/s).

To map the first-order scale structures, the seismic sections were initially interpreted at wide-line spacing, i.e., every fifth crossline and inline of the seismic volume. Once a wide grid of picks was completed, infill picks were made at close line spacing, facilitating detailed structural interpretation. To make sure that subtle faults were not missed during the picking, each seismic line was interpreted.

However, the only faults that could be clearly seen in seismic sections during conventional interpretation were those with throws (displacements) greater than, or equal to a one-quarter dominant wavelength (λ) i.e.,

$$\frac{v}{4f}$$

where v is the mean velocity and f is the peak frequency of the wavelength (Yilmaz, 1987). The one-quarter dominant wavelength is the widely accepted seismic resolution limit for detection of faults (Lindesay, 1989; Yilmaz, 1987). The peak frequency obtained during 3D seismic acquisition over the West Wits Line and West Rand areas is 65 Hz, and 6500 m/s is a good mean velocity value observed during processing. These parameters provide 100 m dominant wavelength. By using the equation above, faults with a throw of less than 25 m fell below the seismic resolution limit.

Therefore at the scale of the goldfield (study area) the first-order scale structures refer to faults with a throw of 400 m to 2.5 km. The second-order scale structures refer to faults with a throw of less than 400 m, but greater than conventional one-quarter wavelength, i.e., 25 m. Third-order scale structures refer to faults with a throw of less than one-quarter of a wavelength; these are not visible on the original migrated seismic sections, however, they can be resolved using horizon-based attribute analysis.

4. West Rand Fault Zone (WRFZ)

The West Rand Fault Zone includes; (1) the West Rand Fault (WRF), which is approximately 1.0 km wide, (2) faults in the immediate footwall and hanging wall of the WRF, and (3) the Kloof syncline (drag) which lies parallel to the WRF in the hanging wall (Figs. 2, 3a). The fault damage zone is therefore approximately 4.2 km wide. Approximately 1.25 km below the WRF (in depth), the seismic section resolves a reverse fault that displaces and offsets the West Rand Group. The fault is hereafter named the Tandeka Thrust. The Kloof syncline, in the hanging wall to the WRF, is 4 km long and trends north–northwest (Gibson et al., 2000; McCarthy, 2006).

The WRF is north–northeast trending and west-dipping. It is listric in form; 65°–70°W in dip at 1.5 km depth; 40°W in dip at 3.0–3.5 km depth; 5°–10°W dip within shale units at the top of the West Rand Group in which it forms a décollement horizon. The WRF has a maximum normal throw of 1.6–2.0 km and an (apparent) sinistral offset of 600 m (Figs. 2, 3a). Normal fault displacement is associated with macroscopic clockwise fault block rotation and failure of the hanging wall (the Kloof Block), with development of secondary and tertiary accommodation (synthetic faults).

Displacement is unequal along the length of the WRF such that it broadly forms a scissor that is hinged in the south–southwest. In the north–northeast, near Cooke Shaft 7 (Fig. 1), second-order antithetic faults splay-off the WRF into the footwall. The graphical distribution of throw, as shown in Fig. 3b, gradually reaches zero near Kloof Shaft 3 where the Kloof and South Deep blocks are hinged. The graph suggests that the West Rand fault system has a predictable throw, but curve roughness occurs where subordinate structures form splays. Towards the north of the survey area (northeast of Kloof 6) the WRF is not imaged as a single fault but resolves two major north–northeast trending normal fault segments (dipping at ~60° to the west) that bound a 1 km long by 250 m wide VCR block.

The seismic sections show that the WRF crosscuts and offsets (normal) the West Rand Group (ca. 2985–2902 Ma), the Central Rand Group (ca. 2902–2849 Ma) and the Ventersdorp Supergroup (ca. 2714 Ma), thus constraining the relative age of the normal fault displacement to post-2714 Ma. Importantly, the WRF fault does not penetrate the base of the Chuniespoort Group (ca. 2588 Ma) of the Transvaal Basin. Thus the WRF was not active during the formation of the Transvaal Basin. Extension on the WRF is thereby restricted to the Neoarchaean, or between 2714 Ma and 2588 Ma.

5. Bank Fault Zone (BFZ)

The Bank Fault Zone (BFZ) is interpreted as the first-order scale structure that forms the boundary between the Kloof Block to the east and the Driefontein-WUDLs Block to the west (or KDC east and west, respectively). The BFZ includes; (1) the Bank Fault (BF), which is approximately 1.5 km wide, and (2) second-order faults in the hanging wall and footwall damage zones (Figs. 2, 4a). Approximately 1.5 km below the BFZ (in depth), the seismic section resolves a reverse fault that is similar in orientation to the BFZ; the fault is hereafter named the Jabulani Thrust (JT). It dips 5°–10° W.

Similar to the WRF, seismic plans and sections of the BF demonstrate it is north–northeast-trending and west-dipping. It is listric in form; 65°–75°W in dip at 3.5 km depth; 40°W in dip at 5.0–5.5 km depth; 5°–10°W in dip at 7.5 km depth in shale units of the West Rand Group in which it forms a décollement horizon. The BF has a maximum normal throw of 2.0–2.5 km and an apparent sinistral offset of 800 m (Figs. 2, 4a). Normal fault displacement was associated with macroscopic clockwise fault

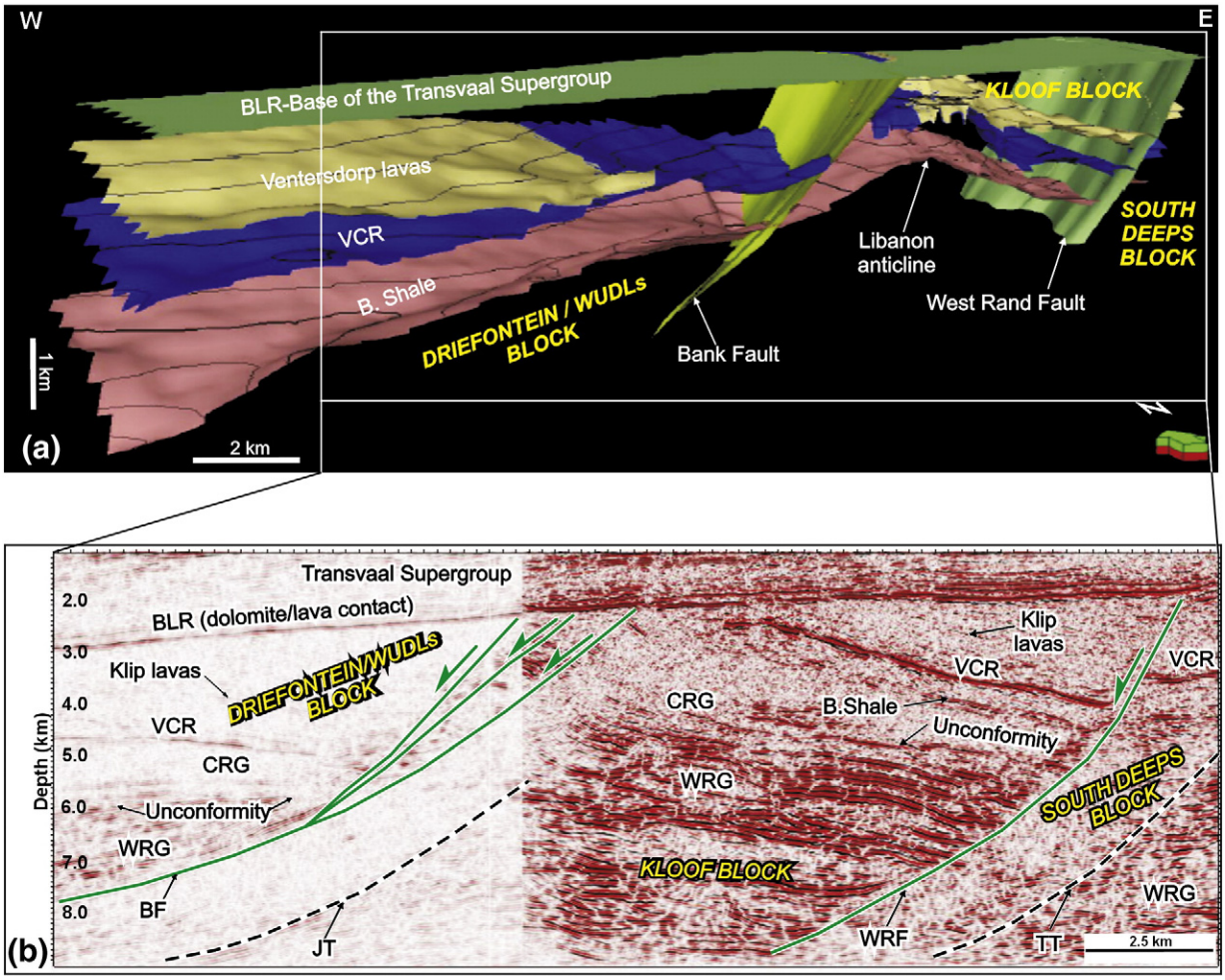


Fig. 2. Seismic model across the Witwatersrand goldfields. (a) 3D regional seismic model incorporating the BLR, Ventersdorp lavas, VCR and B. Shale. The model shows the geometry of West Rand Fault, Bank Fault and Libanon Anticline. (b) Regional crossline seismic section (line AA′ in Fig. 1) through WUDLs, Driefontein, Kloof and South Deep surveys, showing WRF and BF zones and their adjacent TT and JT, respectively. WRF: West Rand Fault; BF: Bank Fault; TF: Tandeka Thrust; JT: Jabulani Thrust; WRG: West Rand Group; CRG: Central Rand Group; Klip: Klipriviersberg; VCR: Ventersdorp Contact Reef; BLR: Black Reef Formation; B. Shale: Booysens Shale.

block rotation of the hanging wall (the Driefontein-WUDLs Block), with development of a rollover anticline (sensu-stricto).

The BF at 3.0–6.0 km depth separates high amplitude reflectors in the hanging wall to the fault from low frequency seismic events in the footwall to the fault. The origin of the high amplitude reflectors is uncertain but may characterize brecciated or mylonitised zones similar to those described by Engelbrecht et al. (1986), Fletcher and Gay (1971), Fletcher and Reimold (1989), and Vermaakt (1995) that associate with the bedding-parallel Master Bedding Fault in the West Wits Line goldfield, or may represent intrusions.

Similar to the WRF, displacement is unequal along the length of the BF; the BF broadly forms a scissor that is hinged in the south–southwest. Second-order antithetic faults also splay off the BF into the footwall to form a macroscopic breccia. The graphical distribution of throw, as shown in Fig. 4b, gradually reaches zero where the Driefontein-WUDLs and Kloof blocks are hinged. The graph suggests that the BF has a predictable throw, but curve roughness occurs where subordinate structures form splays.

In concert with the WRF, the BF crosscuts and offsets the West Rand Group, Central Rand Group and Ventersdorp Supergroup, but does not breach the base of the Transvaal Basin; normal displacement on the BF predates deposition in the Transvaal Basin. However, the evidence that the Ventersdorp Supergroup forms a wedge and possible rollover against the BF constrains the relative age of the normal faulting on the BF to between 2714 Ma and 2588 Ma.

6. South Deep Block

The South Deep block is bounded by the west-dipping WRF (Figs. 2, 3a). The South Deep Block has a consistent geometry; the dip of 5°–10° south is generally constant for all imaged stratigraphic boundaries from base of the Transvaal Basin down through to the West Rand Group. Detailed seismic interpretations indicated that a fault-parallel anticline-syncline pair (termed the Panvlakte anticline–syncline pair or PAS) subtends the WRF in the footwall. The wavelength and amplitude of the PAS is 1.6 km and 200 m, respectively. The PAS anticline is locally known as the Panvlakte Anticline (McCarthy, 2006).

The folds are open and symmetrical in form and periclinal, plunging shallowly north–northeast and south–southwest. The hinge plane of the folds lies parallel to the plane of the WRF (dipping at approximately 40°–50° W). The PAS coalesces and terminates against second-order faults near Kloof KEA Shaft in the southwest of the study area, and near Kloof Shaft 2 in the northeast of the study area. The PAS is interpreted to have formed prior to normal faulting on the WRF because the WRF crosscuts and breaches the western limb of the Panvlakte Anticline.

Furthermore, the PAS is crosscut by a series of steeply east-dipping second-order normal faults that postdate fold formation. A series of horst and grabens are resolved including the Panvlakte Horst described by McCarthy (2006) (Fig. 3a).

The PAS is also overprinted by a series of steeply-dipping northeast, north–south and east–west trending normal faults that are variously

intruded by dykes of the Klipriviersberg Group. Normal fault throw is meters to tens of meters. The faults are interpreted to have formed during instability created in the footwall block during normal displacement on the WRF and postdate formation of the PAS.

Additionally, although the Panvlakte Anticline has been interpreted as a drag or rollover fold by Mashabella (2011) and McCarthy (2006) showed that it formed by flexural-slip folding on bedding planes prior to dissection by the WRF, which means it formed during compression and not extension. It subsequently collapsed during normal displacement on the WRF and synchronous to extrusion of lavas of the Ventersdorp Supergroup.

Summarily, the gross geometry of the footwall to the WRF is that of an open anticline–syncline fold pair (PAS) that failed during extensional tectonics to form a macroscopic collapse breccia with blocks 100s of meters in size. Blocks are bounded by second- and third-order scale normal faults that resolved a horst and graben topography (including the Panvlakte Horst), while some blocks are wholly bounded by dykes of the Klipriviersberg Group. This suggests that these faults may have

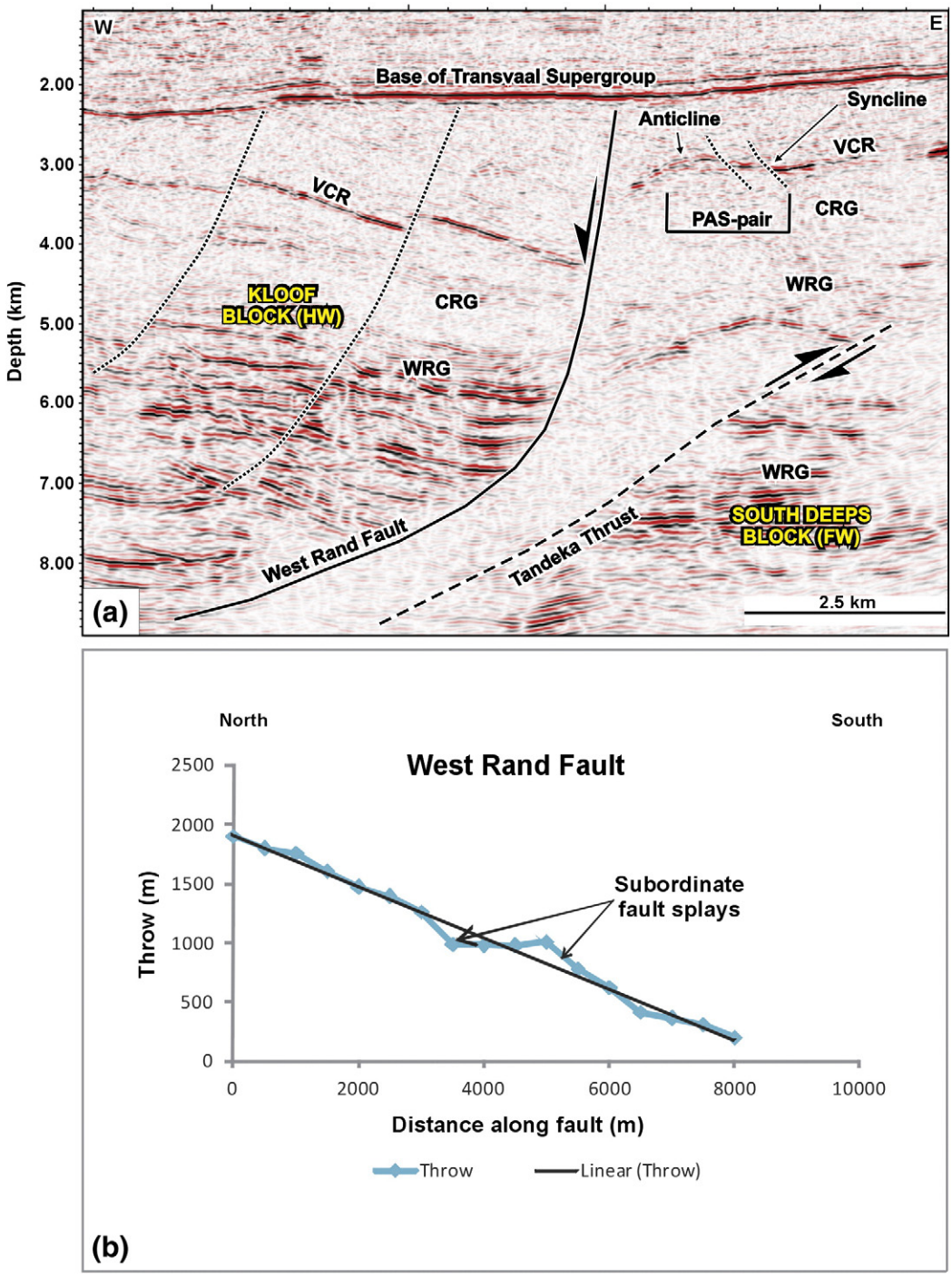


Fig. 3. (a) Seismic section (line BB′ in Fig. 1) across the listric West Rand Fault, showing the steeply dipping hanging wall (Kloof block), Tandeka Thrust and PAS-pair in the footwall block (South Deeps). (b) Displacement (throw) measured in seismic sections perpendicular to the West Rand Fault strike at 250 m interval. FW: Footwall; HW: Hanging wall; VCR: Ventersdorp Contact Reef; WRG: West Rand Group; CRG: Central Rand Group; PAS: Panvlakte Anticline Syncline.

been active syn-emplacement of the (comagmatic) Klipriviersberg lavas, but offset on some Klipriviersberg dykes may indicate that the faults were active post-emplacement as well. The age of normal faulting is thereby constrained to post-2714 Ma, which is the maximum age for the Klipriviersberg Group.

7. Kloof Block (KDC East)

The Kloof Block is situated between the WRF and the BFZ and hosts the Jabulani Thrust Complex (Figs. 2, 3a). The block hosts the northerly-trending first-order scale Libanon Anticline, the crest of which is partially decapitated by the north–northeast trending BFZ (Fig. 5). The wavelength of the anticline is greater than 8 km and the amplitude is 2 km. The eastern limb of the Libanon Anticline is dissected by a series of west-dipping reverse faults of the Jabulani Thrust. The general dip of strata in the Kloof Block is approximately 30°E for a northerly strike, but steepens to 55° E near the hinge of the Libanon Anticline, i.e., above 6.0 km depth. Below 6.0 km depth, the Libanon Anticline forms an open, symmetric, and upright fold form. The Libanon Anticline is thus disharmonic; it is likely to host bedding parallel flexural-slip faults that facilitated fold formation, but these are difficult to see in the seismic data.

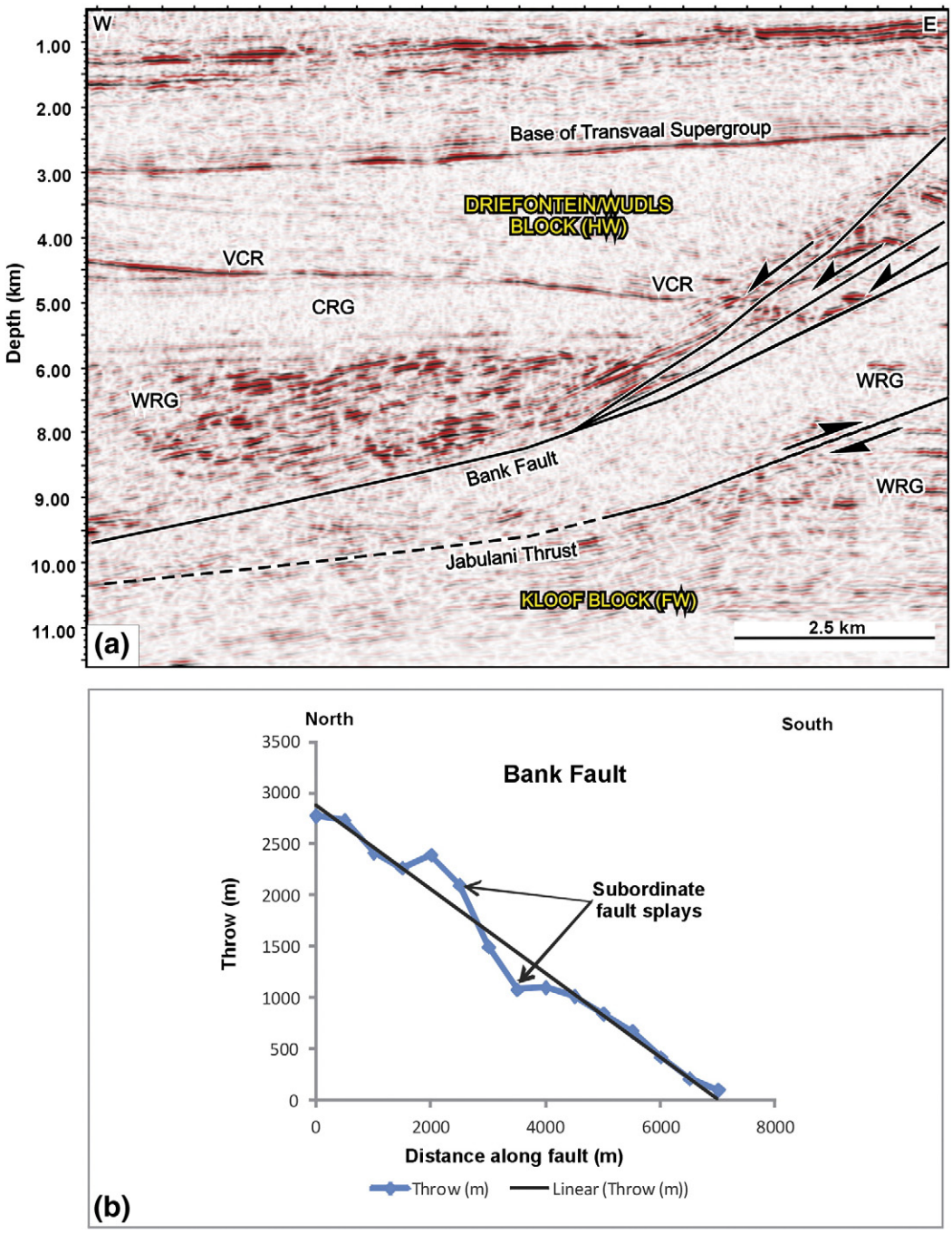


Fig. 4. (a) Seismic section (line CC′ in Fig. 1) across the listric Bank Fault, showing the hanging wall (Driefontein/WUDLs) and shallow dipping Jabulani Thrust in the footwall block (Kloof). (b) Displacement (throw) measured in seismic sections perpendicular to the Bank Fault strike at 250 m interval. FW: Footwall; HW: Hanging wall; VCR: Ventersdorp Contact Reef; WRG: West Rand Group; CRG: Central Rand Group.

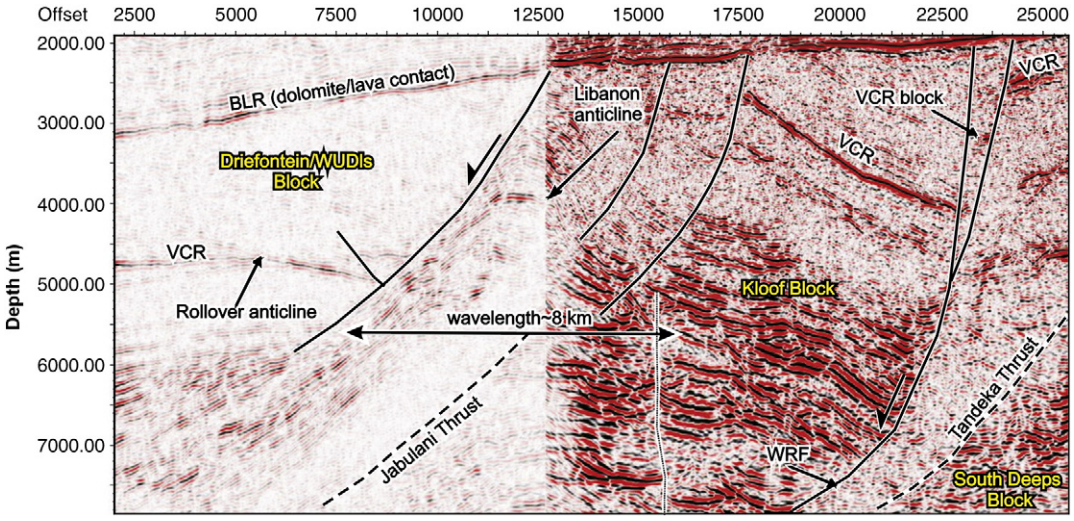


Fig. 5. Seismic section (line DD′ in Fig. 1) showing the geometry of the Libanon Anticline at the merge boundary between the footwall (Kloof) and hanging wall (Driefontein/WUDLs) blocks. The Jabulani Thrust and its subordinate faults in the footwall of the Bank Fault crosscut the Libanon Anticline. The hanging wall block hosts minor rollover anticline and a subordinate fault. FW: Footwall; HW: Hanging wall; VCR: Ventersdorp Contact Reef; WRG: West Rand Group; CRG: Central Rand Group; BLR: Black Reef Formation.

The Kloof Block is dissected by several steeply dipping conjugate normal faults (70°–80°W dip) that trend northwest and northeast. Horst and graben architectures are thereby created.

8. The Driefontein-WUDLs Block (KDC West)

The hanging wall (Driefontein-WUDLs block) to the BFZ covers a large portion of the seismic volume (a 35 km long × 10 km wide block) and hosts some parts of the deepest gold mines in the world, namely Mponeng, Tau Tona, Savuka and Driefontein gold mines. The Driefontein-WUDLs block is defined by the western limb of the Libanon Anticline (Figs. 2, 5).

In the seismic sections across the Driefontein-WUDLs block it is clear that the Booysens Shale and Turffontein Subgroup are truncated by the VCR creating a gently east-dipping angular unconformity (5°E dip in west–east seismic sections). The Turffontein Subgroup and Booysens Shale were thereby deformed and tilted prior to erosion and subsequent deposition of the VCR, i.e., at or before 2729 ± 19 Ma which is the maximum age established for the VCR (Kositcin et al., 2003).

Above the top of the West Rand Group through to the end of the Central Rand Group, the stratigraphic succession thickens to the west. Above the VCR, the Ventersdorp Supergroup forms a wedge-shaped package that thickens towards the Bank Fault. However, individual units in the Ventersdorp Supergroup do not wedge against the BF but remain relatively constant in thickness. Furthermore, the Ventersdorp Supergroup is truncated by the BLF creating an angular unconformity that dips gently west (5°–15° W dip in west–east seismic sections).

These relationships clearly indicate that the Central Rand Group was macroscopically folded and tilted (probably during formation of the Libanon Anticline), then eroded to form the VCR angular unconformity, which was then overlain by the Ventersdorp Supergroup. During or after deposition of the Ventersdorp Supergroup at ca. 2714 Ma, the Driefontein-WUDLs block was rotated clockwise (on west east-seismic sections) during normal faulting (domino block faulting) on the BF and a rollover anticline was formed McCarthy (2006). The rotated block was subsequently eroded and peneplanated before deposition of the Transvaal Supergroup at approximately 2588 Ma. The Driefontein-WUDLs block is crosscut by steeply southwest-dipping normal faults that form synthetic faults to the BF. A horst and graben architecture is thereby created.

9. Discussion

High-resolution merged 3D seismic reflection data that covers a unique 40 × 30 × 11 km seismic volume in the West Wits Line and West Rand goldfields has been used to study the strato-structural setting. Focus was given to (1) fault geometry, fault form, and fault-throw analysis, and (2) the relative chronology of tectonic events. These events were correlated with absolute geochronological data of Armstrong et al. (1991), Crow and Condie (1988), Kositcin and Krapež (2004) and Krapež (1985). The results were integrated with borehole data and underground maps to validate the seismic interpretations.

The merged data made clear the gross strato-structural architecture of the goldfields; a macroscopic fold-thrust system is crosscut by a macroscopic extensional fault array (in an interpreted rift-like system of faults). These are dissected, eroded and overlain by the Transvaal Supergroup above an angular unconformity.

The west–east seismic sections across the West Wits Line and West Rand goldfields confirm that the dominantly shale–arenite units of the West Rand Group (ca. 2985–2902 Ma, Kositcin and Krapež, 2004; U–Pb detrital zircon SHRIMP) are unconformably overlain by the Central Rand Group (ca. 2902–2849 Ma) above an angular unconformity, as proposed by Frimmel et al. (2005), Robb and Robb (1998) and SACS (1980). The unconformity juxtaposed units of the West Rand Group (which had been tilted prior to juxtaposition) against the base of the Central Rand Group. Tilting of the West Rand Group must have taken place syn- to post-erosion at ca. 2.9 Ga. The cause of tilting of the West Rand Group is not known, but it is clear that tectonic activity exposed the clastic and largely marine sediments of the West Rand Group to erosion as early as 2.9 Ga. The event is hereafter termed the Asazi Event (Asazi meaning *unknown* in the IsiZulu language).

The seismic sections also resolve an unconformable relationship between the Central Rand Group and the auriferous Ventersdorp Contact Reef (VCR), which are dated at 2942 ± 6 and 2729 ± 19 Ma (discordant U–Pb SHRIMP ages), respectively, from igneous-detrital xenotime/zircon aggregates (Kositcin et al., 2003). The VCR is interpreted as the erosional product of the Central Rand Group, as suggested by McCarthy (2006), Robb et al. (1991), Spencer (1992), Winter (1994) and others.

We interpreted the northerly-trending, upright, tight to open Libanon Anticline from the merged West Rand and 1995 historical WUDLs datasets. Parasitic folds, such as the Panvlakte anticline–syncline pair (PAS) on the eastern limb of the Libanon Anticline, and reverse faults, such as the west-dipping Tandeka and Jabulani thrusts, were

also resolved. They are interpreted as second-order structures to the Libanon Anticline, which has a wavelength of 8 km and amplitude of 2 km. The Libanon Anticline is a first-order crustal-scale fold that probably formed prior to progressive fold-thrust development, as suggested by Jolley et al. (2007).

The Libanon Anticline and parasitic folds formed syn- to post-deposition of the West Rand and Central Rand groups because they are folded about the hinges of the folds; the Tandeka and Jabulani thrusts displace the West Rand Group and thus also formed after that group. The age of fold-fault formation is best estimated from the youngest U–Pb geochronological age for the VCR at 2.7 Ga. It corresponds with (1) compressive deformation as described by Barnicoat et al. (1997), McCarthy et al. (1982) and Roering et al. (1991), (2) block faulting, folding and thrusting along the northern margin of the Witwatersrand Basin (c.f. De Wit and Tinker, 2004; Frimmel, 2005; Schmitz et al., 2004; Stanistreet et al., 1986 and others), and thrust-fold formation as detailed by Beach and Smith (2007). It also corresponds with the Umzawami Event of Dankert and Hein (2010).

We have interpreted the WRF and BF from the dataset. The WRF and BF are north–northeast trending and approximately 11 km and 20 km long, respectively. They are steeply dipping (65°–70° to the west) listric faults, flattening at the décollement horizon into the dominantly shale units of the West Rand Group.

This work confirms previous studies of Dankert and Hein (2010), Gibson et al. (2000), Gibson (2004) and Mambane et al. (2011) that these structures crosscut and offset the West Rand Group, Central Rand Group and Ventersdorp Supergroup, but do not penetrate the base of the Transvaal Basin, therefore restricting the tectonic evolution of the faults to pre-2.58 Ga. In contrast, this work contradicts studies by Coward et al. (1995) and Vermaakt and Chunnet (1994) who interpreted that the BF propagated through the BLF and displaced it by at least 200 m. A significant number of faults, identified through attribute analysis by Manzi et al. (2012a), are associated with syn- to post-Transvaal Basin development and not formation of the WRF and BF; the seismic data shows that displacement on these late faults is in the order of meters to tens of meters only.

Based on the seismic sections, and with a view to Jolley et al. (2004, 2007) and Roering et al. (1991), we propose that at the end of deposition of the West Rand Group, a tectonic event witnessed; (1) tilting and exposure of the West Rand Group at approximately 2.90 Ga by landscape uplift and marine regression during the Asazi Event (Fig. 6a); (2) landscape evolution accompanied deposition of the sandstone, conglomerate and shale units of the Central Rand Group (ca. 2902–2849 Ma) in a subaerial braided deltaic system (Fig. 6b); (3) formation of a fold-thrust belt during the Umzawami Event of Dankert and Hein (2010) at ca. 2.73 Ga, in which folding of the landscape was synchronous with the formation of thrusts, reverse and flexural-slip faults (Fig. 6c). The Libanon Anticline and its parasite folds (the PAS) are the dramatic expression of this event and are similar to macroscopic folds imaged by Beach and Smith (2007), and Frimmel and Minter (2002) in their studies for the Welkom and Klerksdorp goldfields. We confirm their findings that fold-thrust formation was progressive and directed from the west.

Furthermore, the high-resolution 3-D seismic reflection data, integrated with borehole and mapping data, has allowed us to propose a new model for the goldfields that accords with conclusions of Beach and Smith (2007) and Jolley et al. (2004, 2007) in which thrust-fold formation syn- to post-deposition of the Central Rand Group was followed by extensional collapse, initially during deposition of the Ventersdorp Supergroup (Fig. 6d,e). The extensional event is hereafter referred to as the Hlukana-Platberg Event (Hlukana meaning *tear apart* in the IsiZulu language).

The data makes clear that the WRF and BF developed as tear or scissor faults (hinged in the south–southeast) after deposition of the Klipriviersberg lavas and likely during emplacement of the Platberg Group (ca. 2.70–2.64 Ga) when a mantle plume may have heated the lithospheric mantle (Clendenin et al., 1988; Crow and Condie, 1988; Eriksson et al., 2001, 2009) causing regional crustal anatexis (Taylor et al., 2010). The formation of the WRF and BF at that time probably coincided with graben formation across the Kaapvaal craton (c.f., De Kock et al., 2012; Stanistreet et al., 1986), and perhaps with progressive pseudotachylite formation in the West Rand goldfields and elsewhere, as described by Killick and Roering (1995, 1998) and Mambane et al. (2011), as the crust and lithosphere were influenced by regional-scale extensional tectonics.

Importantly, the seismic sections do not support wedging of the Klipriviersberg lavas against the WRF or BF because individual units continue unthickened across both sides of the faults, i.e., the idea that the faults formed as growth faults (sensu stricto) during deposition of the lavas, as suggested by McCarthy (2006), is not supported. In fact, the Klipriviersberg packet thickens from east to west in restored sections (c.f., Frimmel and Minter, 2002; Tinker et al., 2002), and although they were probably emplaced in an extensional tectonic setting (Van der Westhuizen et al., 1991 and references therein), it is not likely that the WRF and BF (sensu stricto) formed at that time. Instead, we interpret that the Klipriviersberg volcanic rocks were listric-faulted during the Hlukana-Platberg Event (concomitant to graben formation) and eroded leaving a thin eroded package to the east of the WRF and a protected thick package to the west. The fold-thrust belt and extensional fault array does not penetrate the base of the Transvaal Basin (Fig. 6f).

10. Conclusion

The merging of the historical 3D seismic dataset covers mines and exploration lease areas owned by AngloGold Ashanti (Mponeng, Western Ultra-deep Levels) and Gold Fields (Kloof–Driefontein Complex—KDC; South Deep). It has enabled us to constrain the Neoarchaean tectonic history of a portion of the Witwatersrand Basin. The 3D seismic data, correlated with absolute and relative geochronology, borehole, underground mapping datasets, has characterized three Neoarchaean tectonic events:

1. Asazi Event (ca. 2.90 Ga): Exposure of the clastic and largely marine sediments of the West Rand Group during landscape uplift and tilting syn- to post-erosion, followed by the unconformable deposition of the Central Rand Group sediments.
2. Umzawami Event (ca 2.73 Ga): Compressive deformation; formation of the first-order scale thrust-fold, the Libanon Anticline and its parasitic folds, syn- to post-deposition of the Central Rand Group, and synchronous with the formation of reverse faults and thrusts such as Tandeka and Jabulani thrusts.
3. Hlukana-Platberg Event (2.70–2.64 Ga): Extensional tectonics coeval with the heating of lithosphere by mantle plume; formation of first-order scale rift-like system of faults such as the West Rand and Bank faults and their second and third-order scale normal faults that dissect and crosscut (Umzawami) fold-thrust belt towards the end of extrusion of the Ventersdorp lavas and during deposition of the Platberg Group; formation of a drag syncline and a rollover anticline in the hanging wall of the West Rand and Bank faults, respectively.

Furthermore, the throw-distance analysis on the first-order scale normal faults shows that the throw distribution exhibits a linear lateral displacement profile, but can be greatly influenced by the development of splays of the second- and third-order scale structures during the period of extensional fault activity.

This work is the first attempt to constrain the tectonic history of the West Wits Line and West Rand goldfields in the Witwatersrand Basin through the interpretation of a merged historic 3-D seismic data acquired between 1988 and 2003. In this study we propose that high-resolution 3-D seismics should be recognized as a core geophysical technique when studying the tectonic history of the region. In structurally complex domains, such as the Witwatersrand Basin, the 3-D seismic

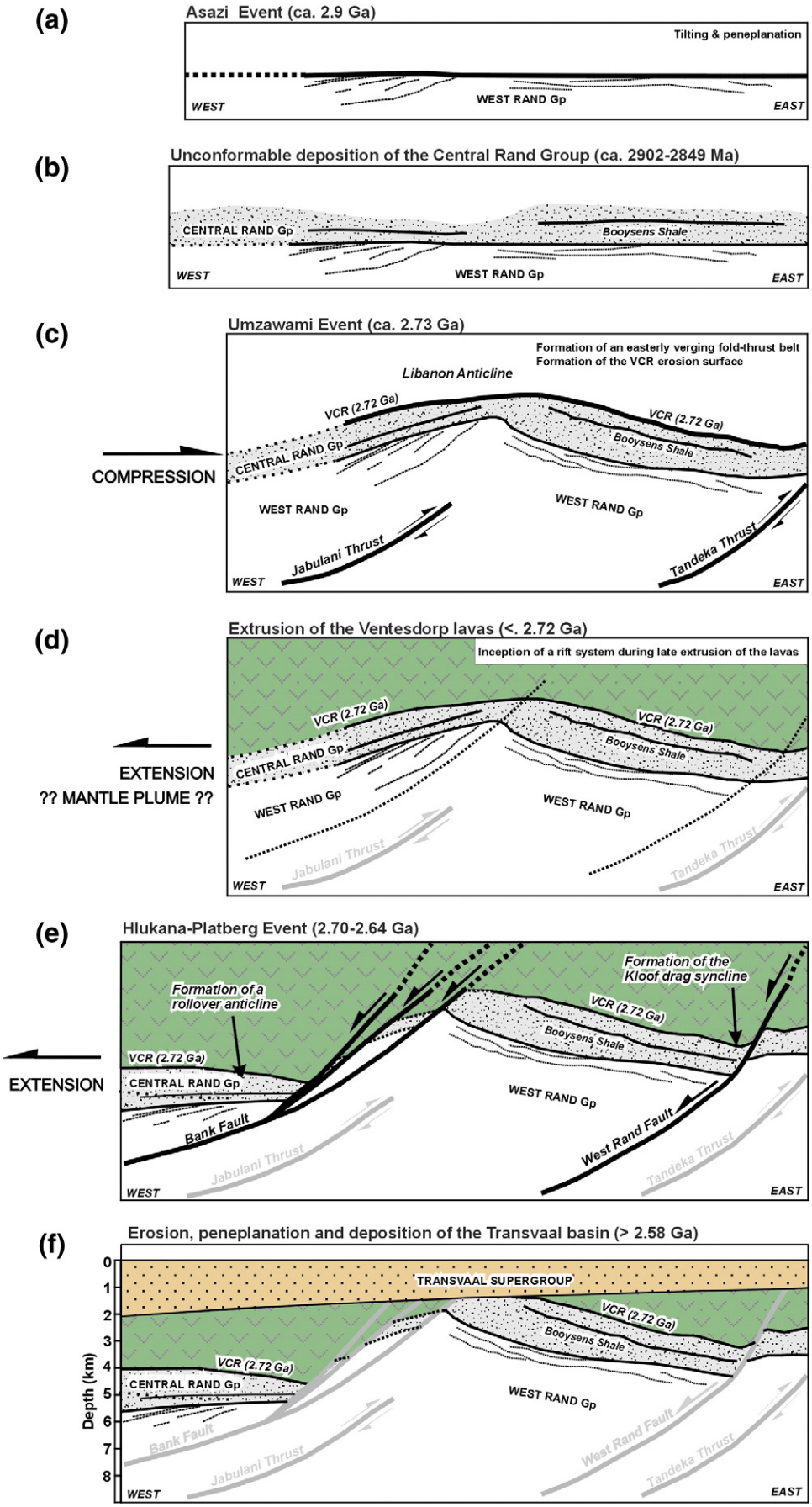


Fig. 6. Schematic model of the evolution of the Neoarchaean tectonic history of the Witwatersrand Basin and Ventersdorp Supergroup as interpreted from high-resolution 3D seismic reflection data; for explanation see text.

data correlated with borehole and underground map has fully constrained the magnitude of displacement of thrusts and normal faults, the gross structural architecture, and the tectonic evolution of the first-order scale structures. However, without kinematic analysis, 3-D seismics may not be sufficient to provide criteria that make it possible to correctly unravel the timing and the evolution of faults. Therefore, integration of kinematic data with 3-D seismics and borehole data is critical when tempting to constrain the timing of faults.

Acknowledgments

This research was supported by the University of Witwatersrand Johannesburg and sponsored by Gold Fields Mining Ltd. We wish to thank G.J. Cooper, J. Tricket and L. Lindzay for their technical contribution on this paper. We gratefully acknowledge the review of H. Frimmel and the editors for their critical and constructive comments on the paper.

References

Armstrong, R.A., Compston, W., Williams, I.S., Welke, H.J., 1991. Zircon ion microprobe studies bearing on the age and evolution of the Witwatersrand triad. Precambrian Research 53, 243–266.
Barnicoat, A.C., Henderson, I.H.C., Knipe, R.J., Yardley, B.W.D., Napier, R.W., Fox, N.P.C., Kenyon, A.K., Muntingh, D.J., Strydom, D., Winkler, K.S., Lawrence, S.R., Cornford, C., 1997. Hydrothermal gold mineralization in the Witwatersrand basin. Nature 386, 820–824.
Beach, A., Smith, R., 2007. Structural geometry and development of the Witwatersrand Basin, South Africa. In: Ries, A.C., Butler, R.W.H., Graham, R.H. (Eds.), Deformation of the Continental Crust: The Legacy of Mike Coward: Geological Society, London, Special Publications, 272, pp. 533–542.
Clendenin, C.W., Charlesworth, E.G., Maske, S., 1988. An early Proterozoic three stage rift system, Kaapvaal Craton, South Africa. Tectonophysics 145, 73–86.
Coward, M.P., Spencer, R.M., Spencer, C.E., 1995. Development of the Witwatersrand Basin, South Africa. In: Coward, M.P., Ries, A.C. (Eds.), Early Precambrian Processes: Geological Society, London, Special Publications, 95, pp. 243–269.
Crow, C., Condie, K.C., 1988. Geochemistry and origin of Late Archaean volcanics from the Ventersdorp Supergroup, South Africa. Precambrian Research 42, 19–37.
Dankert, B.T., Hein, K.A.A., 2010. Evaluating the structural character and tectonic history of the Witwatersrand Basin. Precambrian Research 177, 1–22.
De Kock, W.P., 1964. The geology and economic significance of the West Wits Line. In: Haughton, S.H. (Ed.), The Geology of Some Ore Deposits of Southern Africa, 1. Geological Society of South Africa, Johannesburg, pp. 323–386.
De Kock, M.O., Beukes, N.J., Armstrong, R.A., 2012. New SHRIMP U–Pb ages from the Hartswater Group, South Africa: implications for correlations of the Neoarchean Ventersdorp Supergroup on the Kaapvaal craton and with the Fortescue Group on the Pilbara craton. Precambrian Research 204–205, 66–74.
De Wit, M.J., Tinker, J., 2004. Crustal structures across the central Kaapvaal craton from deep-seismic reflection data. South African Journal of Geology 107, 185–206.
Engelbrecht, C.J., Baumbach, G.W.S., Mathysen, J.L., Fletcher, P., 1986. The West Wits Line. In: Anhaeusser, C.R., Maske, S. (Eds.), Mineral Deposits of Southern Africa, 1. Geological Society of South Africa, pp. 599–648.
Eriksson, P.G., Reczko, B.F.F., 1995. The sedimentary and tectonic setting of the Transvaal Supergroup floor rocks to the Bushveld Complex. Journal of African Earth Sciences 21, 487–504.
Eriksson, P.G., Hattingh, P.J., Altermann, W., 1995. An overview of the geology of the Transvaal Sequence and Bushveld Complex, South Africa. Mineralium Deposita 30, 98–111.
Eriksson, P.G., Altermann, W., Catuneanu, O., Van der Merwe, R., Bumby, A.J., 2001. Major influences on the evolution of the 2.67–2.1 Ga Transvaal basin, Kaapvaal craton. Sedimentary Geology 141–142, 205–231.
Eriksson, P.G., Mazumder, R., Catuneanu, O., Bumby, A.J., Ilondo, B.O., 2006. Precambrian continental freeboard and geological evolution: a time perspective. Earth-Science Reviews 79, 165–204.
Eriksson, P.G., Altermann, W., Hartzer, F.J., 2007. The Transvaal Supergroup and its precursors. In: Johnson, M.R., Anhaeusser, C.R., Thomas, R.J. (Eds.), The Geology of South Africa. Geological Society of South Africa, Johannesburg/Council for Geoscience, Pretoria, pp. 237–260.
Eriksson, P.G., Banjeree, S., Nelson, D.R., Rigby, M.J., Catuneanu, O., Sarkar, S., Roberst, R.J., Ruban, D., Mtimkulu, M.N., Sundur Raju, P.V., 2009. A Kaapvaal craton debate: nucleus of an early small supercontinent or affected by an enhanced accretion event. Gondwana Research 15, 354–372.
Fletcher, P., Gay, N.C., 1971. Analysis of gravity sliding and orogenic translation. Discussion Geological Society of America Bulletin 82, 2677–2682.
Fletcher, P.R., Reimold, W.U., 1989. Some notes and speculations on the pseudotachylites in the Witwatersrand Basin and Vredefort Dome. South African Journal of Geology 92, 223–234.
Frimmel, H.E., 2005. Archaean atmospheric evolution evidence from the Witwatersrand gold fields, South Africa. Earth-Science Reviews 70, 1–46.
Frimmel, H.E., Minter, W.E.L., 2002. Recent developments concerning the geological history of the Witwatersrand gold deposits, South Africa. In: Goldfarb, R., Nielsen, R.L. (Eds.), Global Exploration 2002 — Integrated Methods for Discovery. : Special Publication, 9. Society of Economic Geologists, Littleton, pp. 17–45.
Frimmel, H.E., Hallbauer, D.K., Gartz, V.H., 1999. Gold mobilizing fluids in the Witwatersrand Basin: composition and possible sources. Mineralogy and Petrology 55–81.
Frimmel, H.E., Groves, D.I., Kirk, J., Ruiz, J., Chesley, J., Minter, W.E.L., 2005. The formation and preservation of the Witwatersrand goldfields, the largest gold province in the world. In: Hedenquist, J.W., Thompson, J.F.H., Goldfarb, R.J., Richards, J.P. (Eds.), Economic Geology One Hundreth Anniversary Volume. Society of Economic Geologists, Littleton, Colorado, pp. 769–797.
Gartz, V.H., Frimmel, H.E., 1999. Complex metasomatism of an Archean placer in the Witwatersrand Basin, South Africa: the Ventersdorp Contact Reef — a hydrothermal aquifer? Economic Geology 94, 689–706.
Gibson, M.A.S., 2004. Goldfields KEA 3D Seismic Project: Final Report. Unpublished report to Gold Fields Mining, 52 pp.
Gibson, M.A.S., 2005. Interpretation of the 2003 South Deep 3D Seismic Survey. Unpublished report to Gold Fields Mining, 62 pp.
Gibson, M.A.S., Jolley, S.J., Barnicoat, A.C., 2000. Interpretation of the Western Ultra Deep Levels 3D seismic survey. The Leading Edge 19, 730–735.
Jolley, S.J., Freeman, S.R., Barnicoat, A.C., Phillips, G.M., Knipe, R.J., Pather, A., Fox, N.P.C., Strydom, D., Birch, M.T.G., Henderson, I.H.C., Rowland, T.W., 2004. Structural controls on Witwatersrand gold mineralisation. Journal of Structural Geology 26, 1026–1086.
Jolley, S.J., Stuart, G.W., Freeman, S.R., Knipe, R.J., Kershaw, D., McAllister, E., Barnicoat, A.C., Tucker, R.F., 2007. Progressive deformation of a Late Orogenic Thrust System, from duplex development to extensional reactivation and disruption: Witwatersrand Basin, South Africa. Geological Society, London, Special Publications, 272, pp. 543–569.
Killick, A.M., Roering, C., 1995. The relative age of pseudotachylite formation in the West Rand region, Witwatersrand basin, South Africa, as deduced from structural (sic) observations. South African Journal of Geology 98, 78–81.
Killick, A.M., Roering, C., 1998. An estimate of the physical conditions of pseudotachylite formation in the West Rand Goldfield, Witwatersrand Basin, South Africa. Tectonophysics 284, 247–259.
Kositcin, N., Krapež, B., 2004. Relationship between detrital zircon age-spectra and the tectonic evolution of the Late Archaean Witwatersrand Basin, South Africa. Precambrian Research 129, 141–168.
Kositcin, N., McNaughton, N.J., Griffin, B.J., Fletcher, I.R., David, I., Groves, D.I., Birger Rasmussen, B., 2003. Textural and geochemical discrimination between xenotime of different origin in the Archaean Witwatersrand Basin, South Africa. Geochimica et Cosmochimica Acta 67, 709–731.
Krapež, B., 1985. The Ventersdorp Contact placer: a gold–pyrite placer of stream and debris-flow origins from the Archaean Witwatersrand Basin of South Africa. Sedimentology 32, 223–234.
Lindesay, J.P., 1989. The Fresnel zone and its interpretive significance. The Leading Edge of Exploration 8, 33–39.
Malehmir, A., Koivisto, E., Manzi, M., Cheraghi, S., Durrheim, R.J., Bellefleur, G., Hein, K., King, N., 2013. A review of reflection seismic investigations in three major metallogenic regions: the Kevitsa Ni-Cu-PGE district (Finland), Witwatersrand goldfields (South Africa), and the Bathurst Mining Camp (Canada). Ore Geology Reviews, http://dx.doi.org/10.1016/j.oregeorev.2013.01.003.
Mambane, P.W., Hein, K.A.A., Twemlow, S.G., Manzi, M.S.D., 2011. Pseudotachylite in the South Boundary Fault at the Cooke Shaft, Witwatersrand Basin, South Africa. South African Journal of Geology 114 (2), 109–120.
Manzi, M.S.D., Durrheim, R.J., Hein, K.A.A., King, N., 2012a. 3D edge detection seismic attributes used to map potential conduits for water and methane in deep gold mines in the Witwatersrand basin, South Africa. Geophysics 77, WC133–WC147, http://dx.doi.org/10.1190/GEO2012-0135.1.
Manzi, M., Gibson, M.A.S., Hein, K.A.A., King, N., Durrheim, R.J., 2012b. Application of 3D seismic techniques in evaluation of ore resources in the West Wits Line goldfield and portions of the West Rand Goldfield, South Africa. Geophysics 77, WC163–WC171, http://dx.doi.org/10.1190/GEO2012-0133.1.
Martin, D. McB, Clendenin, C.W., Krapěz, B., McNaughton, N.J., 1998. Tectonic and geochronological constraints on late Archaean and Palaeoproterozoic stratigraphic correlation within and between the Kaapvaal and Pilbara Cratons. Journal of the Geological Society 155, 311–322.
Mashabella, S., 2011. Structural Geology of the Panvlakte Anticline in the Cooke 3 Gold Mine. Honours Thesis, University of the Witwatersrand Johannesburg, 39 pp.
McCarthy, T.S., 2006. The Witwatersrand Supergroup. In: Johnson, M.R., Anhaeusser, C.R., Thomas, R.J. (Eds.), The Geology of South Africa. Geological Society of South Africa, Johannesburg/Council for Geosciences, Pretoria, pp. 155–186.
McCarthy, T.S., Cadle, A.B., Horrocks, P., 1982. Thrusting in Witwatersrand rocks at Langerman's Kop, Johannesburg. Transactions of the Geological Society of South Africa 85, 189–201.
Minter, W.E.L., 1982. The Golden Proterozoic. (Chapter 4) In: Tankard, A.J., Jackson, M.P.A., Eriksson, K.A., Hobday, D.H., Hunter, D.R., Minter, W.E.L. (Eds.), Crustal Evolution of Southern Africa: 3.8 Billion Years of Earth History. Springer-Verlag, New York, Heidelberg and Berlin, pp. 115–150.
Mohale, M., 2010. Structural Geology of the South Boundary Fault in the Cooke 3, West Rand Goldfield. Honours Thesis, University of the Witwatersrand Johannesburg, 83 pp.
Myers, R.E., McCarthy, T.S., Stanistreet, I.G., 1989. A tectono-sedimentary reconstruction of the development of the Witwatersrand Basin, with particular emphasis on the Central Rand Group. Economic Geology Research Unit Information Circular, No. 216, pp. 497–540.
Phillips, G.N., Law, J.D., 2000. Witwatersrand gold fields: geology, genesis and exploration. In: Hagemann, S.G., Brown, P.E. (Eds.), Gold 2000 Reviews in Economic Geology 13, 439–500.
Robb, L.J., Robb, V.M., 1998. Gold in the Witwatersrand basin. In: Wilson, M.G.C., Anhaeusser, C.R. (Eds.), The Mineral Resources of South Africa. : Handbook, 16. Council for Geoscience, Pretoria, pp. 294–349.

Robb, L.J., Davis, D.W., Kamo, S.L., 1991. Chronological framework for the Witwatersrand basin and environs: towards a time-constrained depositional model. South African Journal of Geology 94, 86–95.
Roering, C., 1990. The Vredefort structure: a perspective with regard to new tectonic data from adjoining terranes. Tectonophysics 171, 7–22.
Roering, C., Berlenbach, J., Schweitzer, J.K., 1991. Guidelines for the classification of fault rocks. COMRO. User Guide, 21 (22 pp.).
SACS, South African Committee for Stratigraphy, 1980. Stratigraphy of South Africa. Part 1: Lithostratigraphy of the Republic of South Africa. South West Africa/Namibia and the Republics of Bophuthatswana, Transkei and Venda, Geological Survey of South Africa Handbook, Pretoria, 8 (690 pp.).
Schmitz, M.D., Bowring, S.A., de Wit, M.J., Gartz, V., 2004. Subduction and terrane collision stabilize the western Kaapvaal craton tectosphere 2.9 billion years ago. Earth and Planetary Science Letters 222, 363–376.
Spencer, R.M., 1992. Late Archean Tectonics and Sedimentation of the South Rand Area, Witwatersrand Basin. Ph.D. Dissertation (unpubl.), University of the Witwatersrand, Johannesburg, South Africa.
Stanistreet, I.G., McCarthy, T.S., Charlesworth, E.G., Myers, R.E., Armstrong, R.A., 1986. Pre-Transvaal wrench tectonics along the northern margin of the Witwatersrand Basin. Tectonophysics 131, 53–74.
Tankard, A.J., Jackson, M.P.A., Eriksson, K.A., Hobday, D.K., Hunter, D.R., Minter, W.E.L., 1982. Crustal Evolution of Southern Africa: 3.8 Billion Years of Earth History. Springer-Verlag, New York (523 pp.).
Taylor, J., Stevens, G., Armstrong, R., Kisters, A.F.M., 2010. Granulite facies anatexis in the Ancient Gneiss Complex, Swaziland, at 2.73 Ga: mid-crustal metamorphic evidence for mantle heating of the Kaapvaal craton during Ventersdorp magmatism. Precambrian Research 177, 88–102.
Tinker, J., de Wit, M., Grotzinger, J., 2002. Seismic stratigraphic constraints on Neoarchean-Paleoproterozoic evolution of the western margin of the Kaapvaal craton. South Africa: South African Journal of Geology 105, 107–134.
Van der Westhuizen, W.A., De Bruiyn, H., Meintjes, P.G., 1991. The Ventersdorp Supergroup: an overview. Journal of African Earth Sciences 13, 83–105.
Vermaakt, D.T., 1995. The Structural Evolution of a Portion of the Witwatersrand Basin with Special Reference to the Bank Break and Surrounding Areas. Ph.D. Dissertation (unpubl.), Rand Afrikaans University, Johannesburg, South Africa, 303 pp.
Vermaakt, D.T., Chunnet, I.E., 1994. Tectono-sedimentary processes which controlled the deposition of the Ventersdorp Contact Reef within the West Wits Line. In: Anhaeusser, C.R. (Ed.), Proceedings of the 15th Congress of the Council for Mining and Metallurgical Institutions, Volume 3 (Geology): South African Institute of Mining and Metallurgy, pp. 117–130.
Vos, R.G., 1975. An alluvial plain and lacustrine model for the Precambrian Witwatersrand deposits of South Africa. Journal of Sedimentary Petrology 45, 480–493.
Widess, M.B., 1973. How thin is thin bed? Geophysics 38, 1176–1180.
Winter, H. de La R., 1994. Foreland depobasin results of the Witwatersrand Supergroup in the Rietfontein — East Rand Region: eustatic marine parallels and tectonic continental contrasts around the proximal rim. South African Journal of Geology 97, 119–134.
Yilmaz, O., 1987. Seismic Data Processing. Society of Exploration Geophysicists.

Ore Geology Reviews xxx (2013) xxx–xxx



Contents lists available at SciVerse ScienceDirect

Ore Geology Reviews

journal homepage: www.elsevier.com/locate/oregeorev



Review

A review of reflection seismic investigations in three major metallogenic regions: The Kevitsa Ni–Cu–PGE district (Finland), Witwatersrand goldfields (South Africa), and the Bathurst Mining Camp (Canada)

Alireza Malehmir [a,*], Emilia Koivisto [b], Musa Manzi [c], Saeid Cheraghi [a], Raymond J. Durrheim [c,d], Gilles Bellefleur [e], Chris Wijns [f], Kim A.A. Hein [c], Nick King [g]

[a] Uppsala University, Department of Earth Sciences, Uppsala, Sweden
[b] University of Helsinki, Institute of Seismology, Department of Geosciences and Geography, Helsinki, Finland
[c] University of the Witwatersrand, School of Geosciences, Johannesburg, South Africa
[d] Council for Scientific and Industrial Research (CSIR), South Africa
[e] Geological Survey of Canada, Ottawa, Canada
[f] First Quantum Minerals Ltd., Perth, Australia
[g] South Deep Gold Mine, Gold Fields Limited, Johannesburg, South Africa

ARTICLE INFO

Article history:
Received 20 October 2012
Received in revised form 24 December 2012
Accepted 10 January 2013
Available online xxxx

Keywords:
Reflection seismic
Metallogeny
Kevitsa
Brunswick
Witwatersrand
Mineral deposit

ABSTRACT

Effective exploration for mineral deposits depends on a sound understanding of the processes and geological structures that contributed to their formation. The reflection seismic method has proven to be a powerful tool that provides a high-resolution image of the subsurface and information about structural and lithological relationships that control mineral deposits. The method has also become an attractive geophysical tool for deep exploration and mine planning. In this paper, we review the use of reflection seismic methods to obtain a better understanding of the architecture and ore-forming processes of three diverse mineral regions: the Kevitsa Ni–Cu–PGE district in Finland, the goldfields of the Witwatersrand Basin South Africa, and the Bathurst Mining Camp, Canada. Seismic data, both 2D and 3D, from the Kevitsa deposit clearly image the 3D geometry of the ore-bearing intrusion and provide information about its relationship to the host rock units and nearby intrusions within a larger tectonic framework. 3D seismic data from the Witwatersrand Basin not only provide clear images of major structures, including a distinct reflection that acts as a marker horizon for the gold-bearing reef, but also provide information that may be useful in resolving a long-standing controversy regarding the origin of the gold in the Basin. For example, it might be possible to show that dykes formed impermeable barriers, thereby falsifying the epigenetic hydrothermal models. 2D and 3D seismic data from the Brunswick No. 6 area in the Bathurst Mining Camp suggest that the Brunswick horizon (which contains the bulk of the massive sulfide and associated iron deposits) occurs within a reflective package that extends down to at least 6–7 km depth.

© 2013 Elsevier B.V. All rights reserved.

Contents

1. Introduction . . . 0
2. Reflection seismic methods . . . 0
3. Seismic investigations at the Kevitsa mafic–ultramafic Ni–Cu–PGE deposit . . . 0
   3.1. Kevitsa intrusion and its associated mineralization . . . 0
   3.2. Reflection seismic data . . . 0
   3.3. Seismic constraints . . . 0
4. Seismic constraints on models of ore genesis in the Witwatersrand Basin . . . 0
   4.1. Origin of the gold in the Witwatersrand Basin . . . 0

* Corresponding author. Tel.: +46 184712335; fax: +46 18501110.
E-mail addresses: alireza.malehmir@geo.uu.se (A. Malehmir), emilia.koivisto@helsinki.fi (E. Koivisto), musa.manzi@students.wits.ac.za (M. Manzi), saeid.cheraghi@geo.uu.se (S. Cheraghi), raymond.durrheim@wits.ac.za (R.J. Durrheim), gilles.bellefleur@nrcan-rncan.gc.ca (G. Bellefleur), chris.wijns@fqml.com (C. Wijns), kim.ncube-hein@wits.ac.za3 (K.A.A. Hein), nick.king@goldfields.co.za (N. King).

0169-1368/$ – see front matter © 2013 Elsevier B.V. All rights reserved.
http://dx.doi.org/10.1016/j.oregeorev.2013.01.003

ARTICLE IN PRESS

4.2. Reflection seismic mapping of the Witwatersrand Basin . . . 0
4.3. Seismic constraints on genetic models . . . 0
5. Seismic investigations at the Brunswick No. 6 base metal and associated iron deposits . . . 0
5.1. Geological background . . . 0
5.2. Seismic constraints . . . 0
6. Conclusions . . . 0
Acknowledgments . . . 0
References . . . 0

1. Introduction

Reflection seismic methods are used to provide high-resolution images of subsurface structures and lithological boundaries, as well as information about the physical properties of rocks, such as their density and seismic velocity. To date, several hundreds of 2D lines and tens of 3D surveys have been acquired and reported in major metallogenic provinces worldwide (Fig. 1, e.g., Adam et al., 2003; Campbell and Peace, 1984; Clowes et al., 1984; Dehghannejad et al., 2010, 2012a, 2012b; Durrheim et al., 1991; Eaton et al., 2010; Ehsan et al., 2012; Evans et al., 2003; Goleby et al., 2002; Juhlin et al., 2002; Korja and Heikkinen, 2005; Malehmir et al., 2006, 2007, 2009, 2011, 2012a; Milkereit and Eaton, 1998; Milkereit et al., 1996; Odgers et al., 1993; Pretorius et al., 1989; Ruskey, 1981; Stolz et al., 2004; Tryggvason et al., 2006; Urosevic et al., 2005; Williams et al., 2004).

The explorer has a range of geophysical methods to map the subsurface. His choice depends on many factors, including the physical properties and depth of the target body, the properties of the host rock and overburden, and the logistic requirements and cost of surveys. Potential field and electromagnetic methods have been widely and successfully used to search for metallic ore bodies. However, reflection seismic methods usually provide a superior trade-off between resolution and depth. This technology, especially 3D seismics, is fast becoming an established method for deep exploration and mine planning (Malehmir et al., 2012b and references therein). In addition, the present trend in exploration and exploitation of mineral resources at greater depths favors the use of seismic methods, not only for targeting deep-seated mineral deposits and for deep mine planning, but also for gaining a better understanding of the overall architecture of mineralized regions (e.g., Goleby et al., 2002; Kukkonen and Lahtinen, 2003; Kukkonen et al., 2011; Malehmir et al., 2007; Willman et al., 2010). This information is especially important when formulating strategies to explore mining camps where most shallow deposits have been found and exploited. Fig. 2 shows major base metal discoveries in Western countries until 2007. The figure clearly reveals that targets are getting deeper, especially in the so-called brownfields (i.e., mature) mining camps.

Reed (1993) provided a comprehensive review of reflection seismic surveying for mineral exploration applications. Milkereit et al. (1996) investigated the petrophysical properties of volcanogenic-hosted massive sulfide (VHMS) deposits (typically high density, and sometimes high velocity) and the application of seismic methods to explore for them. A number of papers were subsequently published presenting the successful application of seismic methods for hard rock exploration (Eaton et al., 2003 and references therein). Recently, Malehmir et al. (2012b) reviewed past and recent applications of seismic methods for mineral exploration and mine planning in Australia, Europe, Canada and South Africa. The current paper has a different focus. Here, we demonstrate how reflection seismic methods can be used to gain a better

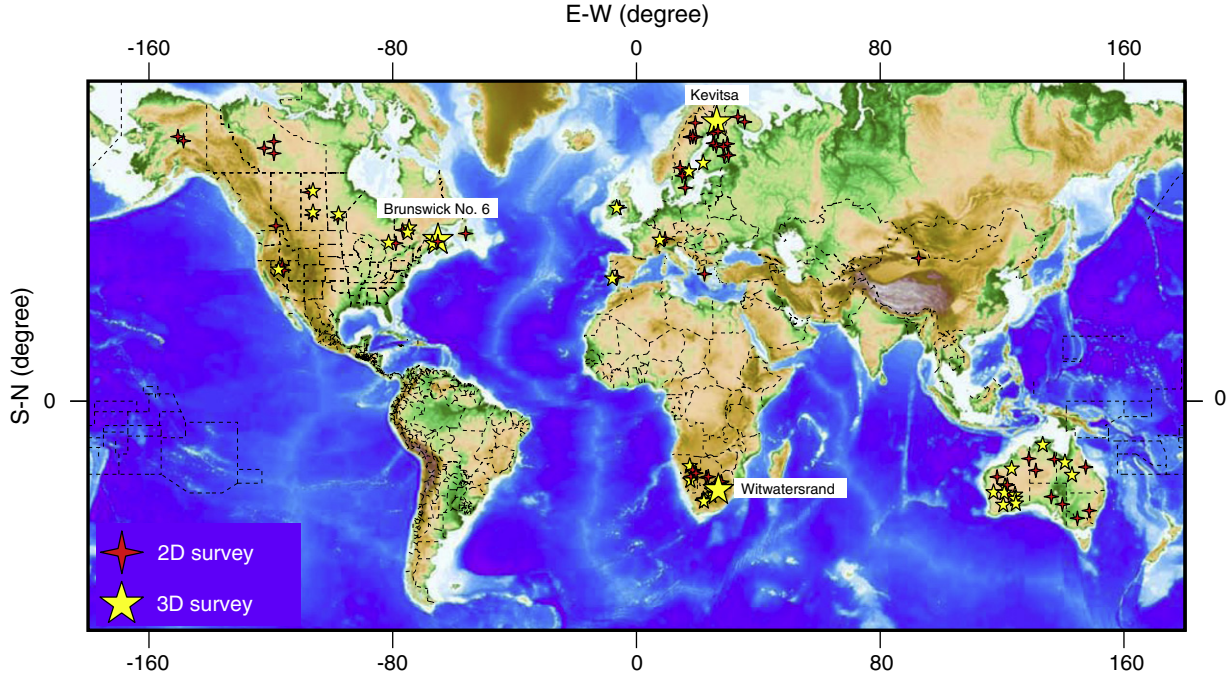


Fig. 1. World map showing locations of existing 2D and 3D hard rock seismic surveys conducted for mineral exploration, site characterizations and mine planning (modified from Malehmir et al., 2012b). Large yellow stars are locations of the 3D seismic surveys discussed in this paper. (For interpretation of the references to color in this figure legend, the reader is referred to the web version of this article.)

Please cite this article as: Malehmir, A., et al., A review of reflection seismic investigations in three major metallogenic regions: The Kevitsa Ni–Cu–PGE district (Finland), Witwatersrand..., Ore Geol. Rev. (2013), http://dx.doi.org/10.1016/j.oregeorev.2013.01.003

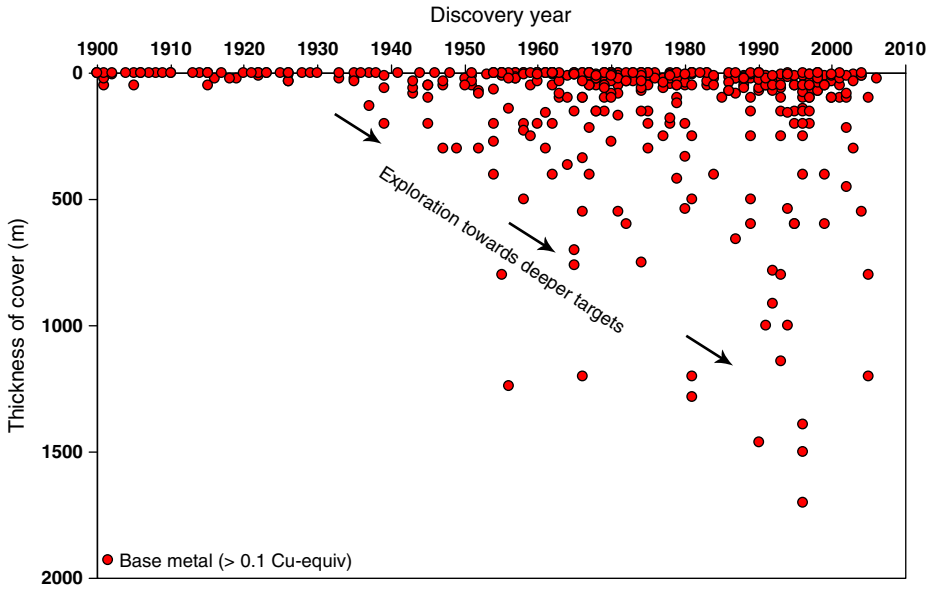


Fig. 2. Thickness of cover for major base metal mineral discoveries in the Western countries between 1850 and 2007 clearly indicating a trend towards depth while shallow deposits have still been found.
Courtesy of MinEx Consulting.

understanding the ore genesis in three major mining regions, namely the Kevitsa Ni–Cu–PGE district in northern Finland, the gold-bearing conglomerates of the Witwatersrand Basin in South Africa, and the Brunswick No. 6 base metal deposit in the Bathurst Mining Camp, Canada. These mining regions contain world-class mineral deposits, such as the super-giant Brunswick No. 12 VHMS deposit in Canada and the South Deep gold mine in the Witwatersrand goldfields. The development of the Kevitsa Ni–Cu–PGE deposit (mining commenced in summer 2012 and is planned to continue for the next 20–30 years) and the recent discovery of the nearby Sakatti Ni–Cu deposit (Jim Coppard, 2011, personal communication) are examples of favorable geological conditions in the Finnish Lapland.

We commence with a brief review of the basic principles of seismic method. We then present three case studies. In each study we (1) review existing 2D and 3D seismic data, (2) provide information about the relationships between the mineralization and structural and lithological features, and (3) analyze existing mineralization scenarios/models in the light of seismic data. For example, we show how reflection seismic data may be used to: establish a link, if any, between dykes and faults and gold mineralization in the Witwatersrand Basin; determine the depth extent of the Brunswick horizon that hosts major VHMS deposits; and map the 3D geometry of the ore-bearing Kevitsa mafic–ultramafic intrusion that controls the overall bulk mineralization, and features of its larger tectonic context.

2. Reflection seismic methods

The acquisition and processing of reflection seismic surveys depend on the site conditions (e.g., accessibility, topography, and thickness of the weathered layer) and the geology (e.g., rock properties, steepness of dips and geological complexities such as tight folding). 2D surface seismic surveys are often implemented to contain costs. However, 2D seismic data are challenging to interpret, especially in complex mining areas where the data are often acquired along crooked lines and the geological structures are in fact 3D (Malehmir and Juhlin, 2010; Malehmir et al., 2009; Nedimović and West, 2003; Wu, 1996; Zaleski et al., 1997). In these situations, the ideal solution is a 3D survey.

The strength of the seismic reflection that arises at the boundary between two geological entities depends on the contrast in the acoustic impendence (product of velocity and density). Eaton et al. (2010) discovered the strong reflective character of VHMS deposits in typical host rock environments when laboratory measurements for acoustic properties were carried out during the Lithoprobe project (Salisbury et al., 1996). Salisbury et al. (1996, 2003) systematically measured the velocities and densities of major mineral deposits and their host rocks. They showed that most metallic deposits lie far to the right of the Nafe–Drake curve in cross plots of velocity against density, mainly due to their very high density. Fig. 3 shows average velocity and density values obtained from the study areas discussed in this paper superimposed on the results of Salisbury et al. (2003). For example, note that VHMS deposits tend to place at different parts of the cross plot, depending on their mineralogy and in particular their pyrite content (Bellefleur et al., 2012; Dehghannejad et al., 2012b; Duff et al., 2012; Malehmir and Bellefleur, 2009; Malehmir et al., 2013; White et al., 2012). Also, the cross plot illustrates how host rock velocities increase from felsic to ultramafic rocks. For example, the Kevitsa main intrusion has an average P-wave velocity of 7500 m/s, while the Ventersdorp Supergroup lava and Central Rand Group quartzite (which form the hanging- and footwall of the gold-bearing Ventersdorp Contact Reef in the Witwatersrand Basin) have P-wave velocities of approximately 6500 m/s and 5700 m/s, respectively.

In addition to the prerequisite of significant acoustic impedance contrast, the successful imaging of mineral deposits and their host rock structures depends on the dimensions and geometry of the reflectors. The resolution of seismic imaging depends on the seismic wavelength, which depends on the seismic velocity of the rocks and the frequency of the seismic pulse. The Earth absorbs higher frequencies more rapidly than lower frequencies. Hence the seismic wavelength increases with depth. The seismic waves used to image a target at a depth of 1000 m typically have lengths of 50–100 m. Consequently the top and bottom of the target will only be resolved if it is thicker than about 20 m (typically a quarter of the wavelength), while the lateral extent can only be accurately determined if it is wider than 350 m (i.e., the width of the first Fresnel zone). Targets thinner than 20 m can still be detected, but their amplitude will be mainly dependent on the geometry of the target and not solely on the impedance contrast. Targets laterally shorter than 350 m can also be detected, but the response may be a combination of reflections and diffractions (Bellefleur et al., 2012; Bohlen et al., 2003;

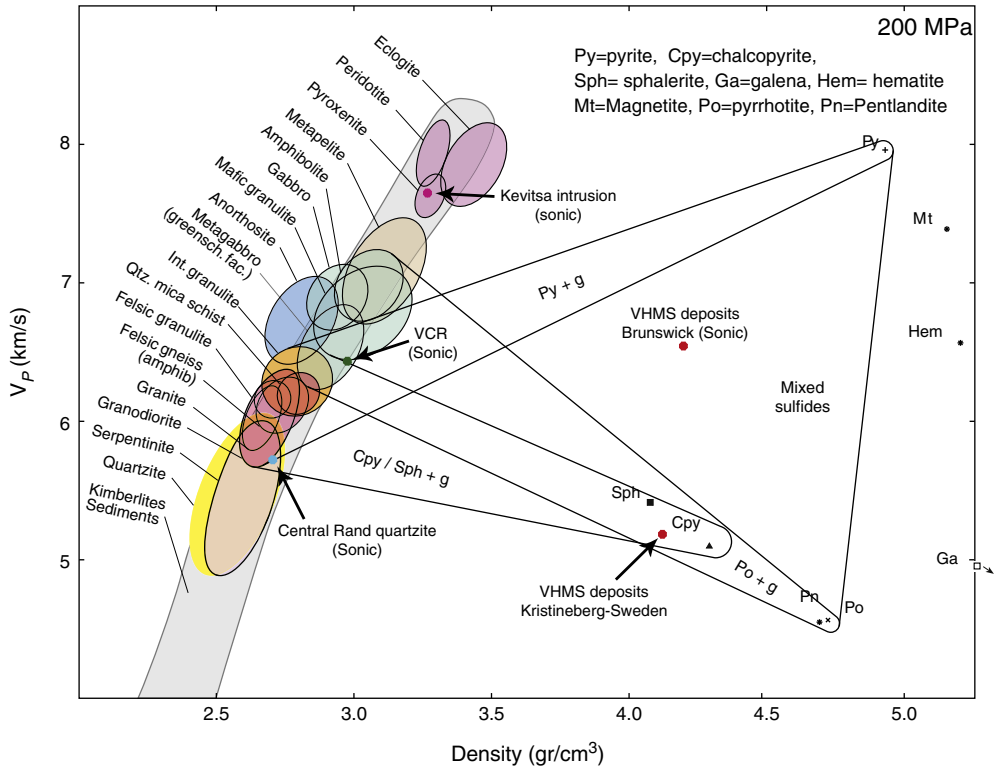


Fig. 3. Acoustic properties of most common crystalline rocks and ores (modified after Salisbury et al., 2003). Shown are also VHMS samples from the Brunswick No. 6 (Malehmir and Bellefleur, 2010) and Kristineberg mine in Sweden (Malehmir et al., 2013), Kevitsa olivine–pyroxenite (Koivisto et al., 2012; Malehmir et al., 2012a) and the lava in the hangingwall of the Ventersdorp Contact Reef (VCR) and the Central Rand quartzite in its footwall. (Manzi et al., 2012a,b).

Eaton, 1999; Malehmir and Bellefleur, 2009; Milkereit et al., 2000; White et al., 2012).

3. Seismic investigations at the Kevitsa mafic–ultramafic Ni–Cu–PGE deposit

Kevitsa is a large disseminated sulfide Ni–Cu–PGE deposit hosted by the Kevitsa mafic–ultramafic intrusion in northern Finland (Fig. 4) and dated as about 2.06 Ga old (Mutanen, 1997; Mutanen and Huhma, 2001). The Kevitsa deposit was first discovered by the Geological Survey of Finland in 1987. Open pit mining by Kevitsa Mining Oy/First Quantum Minerals Ltd. commenced in June 2012. The final pit depth is planned to be 550–600 m. The estimated ore reserves of the Kevitsa intrusion are about 240 Mt (using a nickel cut-off grade of 0.1%), with low-grade metal concentrations of Ni 0.30 wt.% and Cu 0.41 wt.% (Gregory et al., 2011). The expected life-of-mine is 20–30 years.

The Kevitsa intrusion is emplaced within layered sedimentary and volcanic rocks of the Central Lapland Greenstone Belt, and is just south of the large 2.4 Ga Koitelainen layered intrusion (Mutanen and Huhma, 2001), and west of the Satovaara intrusion (age unknown). The Kevitsa intrusive complex has an approximately oval surface expression with a northeast–southwest trending long axis. The northern part of the complex (the Kevitsa main intrusion) is characterized by olivine pyroxenites. Gabbros and pyroxenites interlayered with country rocks form the shallower southern part (Figs. 4 and 5). The disseminated sulfide Ni–Cu–PGE deposit occurs in the olivine–pyroxenite part of the Kevitsa intrusive complex, which contains up to about 5% sulfide. Most of the finely disseminated sulfides occur as granular masses interstitial to the silicate mineral crystals. The sulfides consist mainly of pyrrhotite, chalcopyrite, pentlandite, and numerous platinum group minerals of lesser economic significance. Several types of mineralization have been identified (Fig. 6): the normal or main type is disseminated, rich in nickel and copper with significant PGE and gold contents, and occurs within the main part of the intrusion; the “false ore” refers to the predominance of uneconomic pyrrhotite, and occurs mostly at the margins of the intrusion; while contact-related and possibly remobilized types are usually massive to semi-massive, and occur at or below the basal contact of the intrusion. The main mineralization is thought to be lithologically controlled, with minor structural control. Mutanen (1997) attributes the formation of the regular and false ore to contamination by variable amounts of komatiitic material and S- and C-rich metasediments. However, currently there is no consensus on the genesis.

3.1. Kevitsa intrusion and its associated mineralization

More than 400 hundred diamond holes have been drilled in the Kevitsa area, but most are concentrated close to the known deposit and do not provide a comprehensive understanding of the extent of the intrusion. The basal contact of the intrusion is penetrated by only about 30 drill holes, most of which are shallow. A better knowledge of the geometry of the intrusion would provide a framework for near-mine and deep exploration in the area. An exact knowledge of the basal contact of the intrusion would also provide an exploration target for the contact-type mineralization that is often more massive and highly rich in Ni–Cu (Fig. 6).

The Kevitsa main deposit is thought to be primarily lithologically controlled. The most recent model (Gregory et al., 2011) suggests that the Kevitsa area was the focus of multiple, laterally discontinuous and internally differentiated magma pulses with plagioclase- and orthopyroxene-rich layers at the top (often fine-grained plagioclase-bearing olivine websterite), olivine websterite in the middle, and clinopyroxene- and olivine-rich at the base (olivine pyroxenite). The mineralization is concentrated towards the base of the pulses. Thus, the extent of these pulses is an important spatial control on the extent of the economic mineralization. However, identification of the individual pulses is complicated by the presence of a rock that has been historically described as “metaperidotite” in the drill core logs. The “metaperidotite” label has

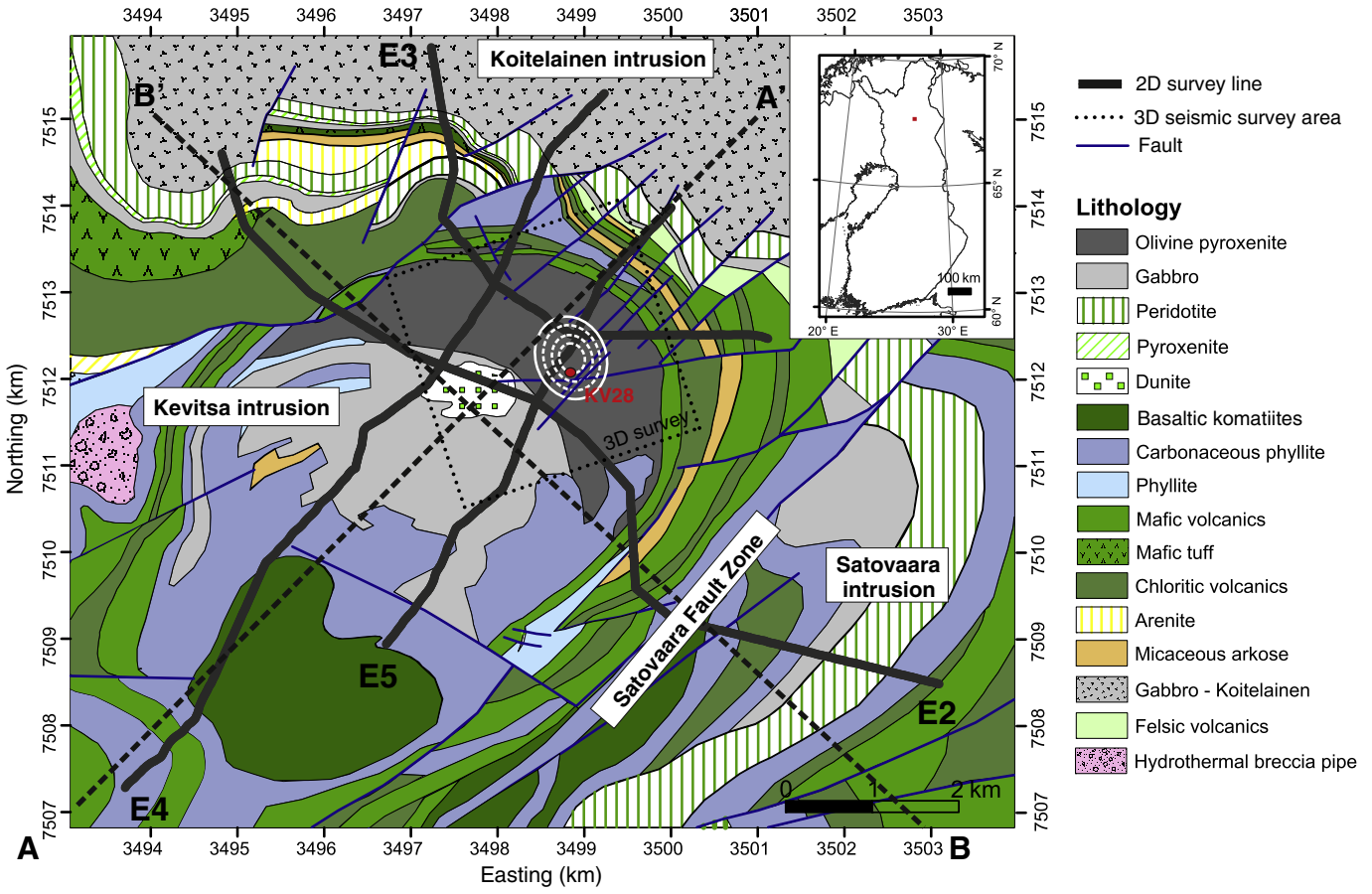


Fig. 4. Geological map of the survey area, with the Kevitsa 2D seismic survey lines E2, E3, E4 and E5 and the 3D seismic survey area. The inline and crossline sections shown in Fig. 7 are extracted from the 3D seismic volume. Location of the planned Kevitsa open-pit mine (solid and partly dashed white lines) is also shown. Bedrock geology was adapted from the Kevitsa Mining Oy/First Quantum Minerals Ltd. geologists. Dashed lines (A–A′ and B–B′) show approximate locations of the geological cross-sections shown in Fig. 5. Modified from Koivisto et al. (2012).

been mainly used for widespread amphibole-alteration of olivine–pyroxenites, but it also includes other rock protoliths. Thus, further evidence is needed in order to better understand the ore genesis at Kevitsa.

While the surface geology indicates that the Kevitsa intrusive complex is relatively undeformed along its southern and northern margins, its eastern margin was modified by the Satovaara Fault Zone (Figs. 4 and 5) during the Svecofennian orogeny at about 1.9–1.8 Ga (Gregory et al., 2011). Consequently, the Kevitsa resource area is overprinted by numerous structures that developed during the evolution of the Satovaara Fault Zone (Fig. 4). The associated shear zones and faults offset the disseminated mineralization, and the structural evolution at Kevitsa has resulted in re-mobilization of the sulfides. However, structures are not believed to be a primary control of the Kevitsa mineralization, their role being limited to local modification (Gregory et al., 2011). The exception is the location of the intrusion itself, which is thought to have been controlled by one or more major structures at depth, although these have not been identified.

On a more regional scale, questions regarding the relationship between the Kevitsa intrusion and other intrusions in its vicinity remain, in particular about its relationship to the Koitelainen intrusion to the north and the Satovaara intrusion to the east. The regional northeast–southwest trending Satovaara Fault Zone separates the Kevitsa intrusive complex from the Satovaara intrusive complex (Figs. 4 and 5). It has been suggested that the Kevitsa intrusive complex and the Satovaara complex are parts of one original intrusion (Mutanen, 1997). If so, the Satovaara intrusion could potentially host similar deposits to the Kevitsa intrusion.

3.2. Reflection seismic data

In December 2007, a series of 2D reflection seismic profiles (Koivisto et al., 2012; Kukkonen et al., 2009) was acquired in the Kevitsa area as a part of the HIRE project (High Resolution Reflection Seismics for Ore Exploration 2007–2010; Kukkonen et al., 2011) of the Geological Survey of Finland and its mining industry partners. The Kevitsa 2D seismic survey consists of four connected survey lines (lines E2, E3, E4 and E5; Fig. 4) between 6 and 11 km long (Table 1). The aims of the survey were to delineate the overall extent of the ore-bearing Kevitsa ultramafic intrusive complex, study the seismic response of the disseminated ore deposit, search for indications of new ore deposits, and to extract structural information at depth that may be associated with mineralization. In 2010, the initial positive results of the 2D seismic survey led Kevitsa Mining Oy/First Quantum Minerals Ltd. to initiate a 3D reflection seismic survey (Table 1) for mine planning and deep mineral exploration purposes (Malehmir et al., 2012a). The main objective of the 3D seismic survey was to image major fault and fracture zones critical for geotechnical planning of the mine. The 3D seismic survey is limited to the closer vicinity of the known deposit, while the 2D seismic survey was designed to provide a more regional view of the Kevitsa intrusive complex (Fig. 4). Prior to the 3D survey, a multi-offset and multi-azimuth VSP (vertical seismic profiling) survey was conducted to provide information about

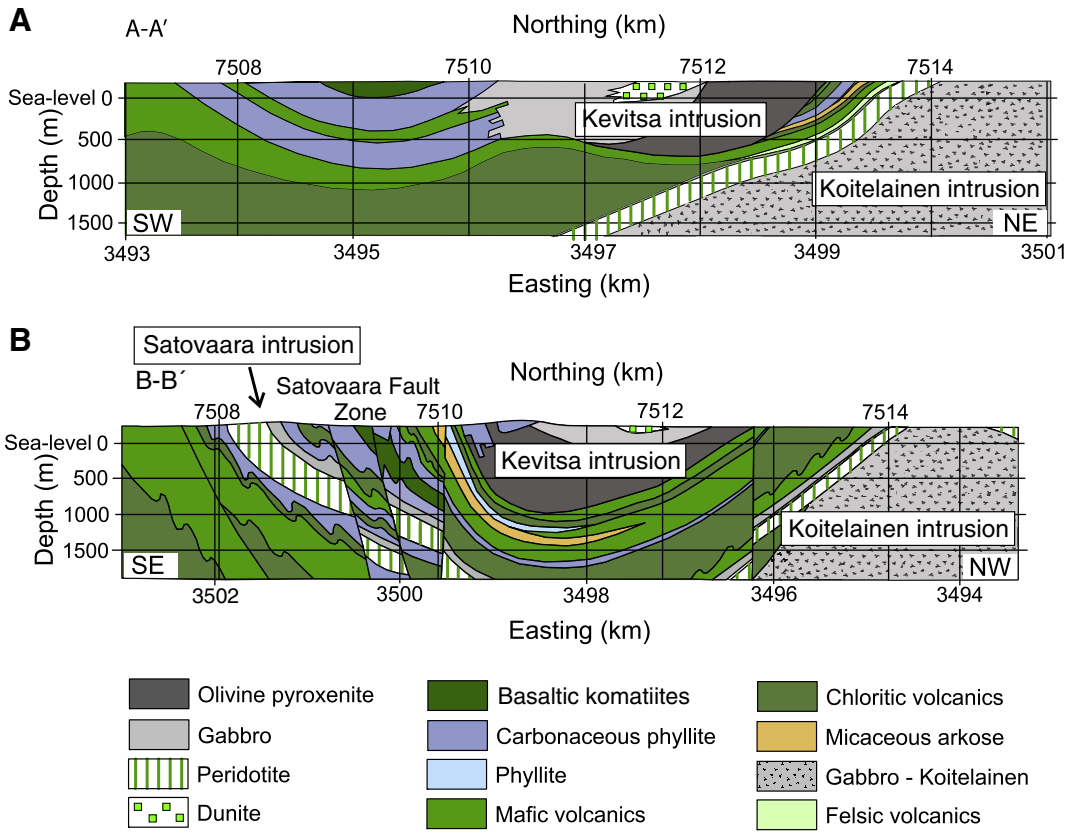


Fig. 5. (A) Simplified geologic cross-sections along southwest–northeast and (B) southeast–northwest directions showing expected geometry of the Kevitsa intrusion and fault systems (courtesy of First Quantum Minerals Ltd.).
Modified from Koivisto et al. (2012).

the steeply dipping to sub-vertical structures that could not be imaged by the 3D surface seismic data. This survey was performed in borehole KV28, the deepest borehole at the location of the planned open pit (Fig. 4). Details about the seismic data acquisition, processing and interpretation of the results can be found in Koivisto et al. (2012) and Malehmir et al. (2012a).

3.3. Seismic constraints

The main aims of the 2D and 3D seismic surveys were to delineate the shape and extent of the ore-bearing Kevitsa intrusion and the geometry of some of the host rock and surrounding units, and extract information about the larger-scale structures and structures important

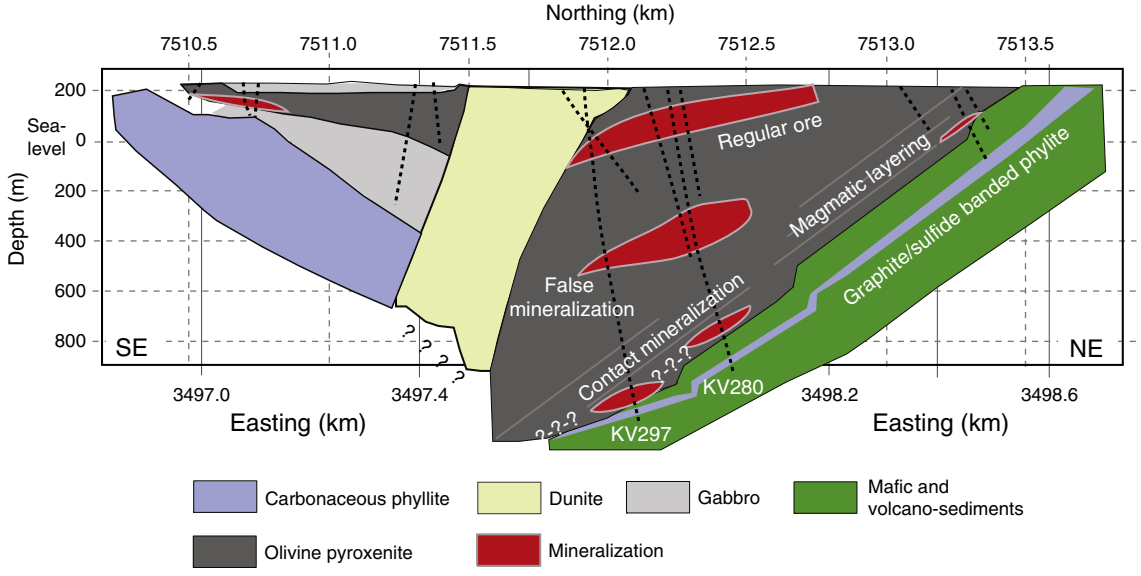


Fig. 6. Schematic cross-section constrained by deep magnetotelluric and borehole data, showing the main Kevitsa intrusion (hosting the main mineralization-regular ore) and proven massive sulfide mineralization occurring as false and contact mineralization in the study area.
Modified from Malehmir et al. (2012a).

Table 1
Main reflection seismic data acquisition parameters for the Kevitsa 2D and 3D data (2007 and 2010, respectively), Brunswick 2D and 3D data (1998 and 2000, respectively), and the Witwatersrand Basin 3D data (the 2003 Kloof–South Deep seismic surveys).

Parameter/region	Kevitsa		Brunswick No. 6		Witwatersrand Basin
Survey type	2D crooked[1]	3D orthogonal[2]	2D crooked[3,4]	3D non-orthogonal[5]	3D orthogonal[6]
Recording system	I/O-4	SERCEL408/Seistronix	SERCEL388	SERCEL388	SERCEL408
No. of active channels	402	864	481	2367 to 3456	1296
Maximum offsets	2500 to 5000 m	1700 m	4800 m	6700 m	3325 m
Total survey length/area	~33.7 km	~9 km^2	~28 km	~38 km^2	~96 km^2
Source	Dynamite	VIBSIST and dynamite	Dynamite	Dynamite	Vibroseis (4 inline 45 m array)
Charge size/depth	0.125–0.25 kg/1–2 m	0.5 kg/3 m	0.5 kg/6 m	0.5 kg/6 m	–
Source interval	50 m	45 m	40 m	60 m	50 m
No. of shots	~650	~3300	~770	~1500	~4150
Geophone frequency	10 Hz	10 Hz	10 Hz	10 Hz	10 Hz
Receiver interval	12.5 m	15 m	10 m	22 m	50 m
Nominal fold	50	60	60	100	36
No. of shot lines	–	34	–	15	45
Shot line spacing	–	80 m	–	400 m	450 m
No. of receiver lines	–	35	–	28	45
Receiver line spacing	–	70 m	–	290 m	400 m
No. of active receiver lines per patch	–	9 lines × 96 active channels	–	12 lines × 288 active channels	12 lines × 108 active channels
Sampling rate	1 ms	1 and 2 ms	2 ms	2 ms	2 ms

[1] Koivisto et al. (2012).
[2] Malehmir et al. (2012a).
[3] Malehmir and Bellefleur (2010).
[4] Cheraghi et al. (2011).
[5] Cheraghi et al. (2012).
[6] Manzi et al. (2012a).

for mine-planning purposes. The 2D and 3D seismic data were used to create a 3D lithological and structural model of the area (Koivisto et al., in preparation), thus giving valuable insight to the architecture of the whole complex (Figs. 7 and 8).

The information on the extent of the ore-bearing Kevitsa intrusion can be used for more effective exploration in the area. The base of the Kevitsa intrusion is particularly clear in the northern and western sectors where it is defined by continuous reflectors (R1 in Fig. **7**). Toward the east, the base is mostly defined by disruption of the reflectors internal to the intrusion. The 2D seismic data, which extends beyond the 3D seismic study, reveal that the prominent reflectors at the base of the intrusion continue deeper toward the south-southwest (R2 in Fig. **7**). This has been interpreted as a previously unknown southern continuation of the intrusion. Furthermore, the data reveal strong reflectors at the base of the intrusion that have been penetrated by two deep drill holes in the area. These drill holes reveal contact-type mineralization at the onset of the reflectors (KV297 and KV280 in Fig. 6). Thus, the seismic data can be directly used for exploration of the contact-type mineralization. The 3D seismic data help to define the 3D geometry of the intrusion as shown in Fig. 8A.

The use of the reflection seismic method for direct mineral exploration depends on the specific seismic signature of the mineralized targets (Fig. 3). It is unlikely that the Kevitsa deposit would be associated with distinct reflectivity solely attributed to increased sulfide contents because it is low-grade disseminated ore. Nevertheless, at the deposit scale, the economic mineralization occurs within a spatially restricted reflective zone within the ore-bearing olivine pyroxenite part of the Kevitsa intrusion (R3 in Fig. **7**). The internal magmatic layering described above is similarly restricted to the northeast of the intrusion. Outside of this area, drill holes penetrate up to 1 km of homogeneous, although altered, olivine pyroxenite, without encountering economic mineralization. We believe that the internal reflectivity in the seismic data mirrors this zone of multiple magma pulses that have been associated with the occurrence of the economic mineralization. Based on drill hole data (see details in Koivisto et al., 2012; Malehmir et al., 2012a), the often fine-grained tops (plagioclase-bearing olivine websterite) of the individual pulses could be reflective when in contact with a more coarse-grained base of another pulse with olivine pyroxenite composition (Fig. 8B). Generally, the base of a magma pulse is associated with stronger mineralization. Sulfide content increases the density, which in turn should further strengthen the contrast in acoustic impedance relative to the generally lower-density top of the next magma pulse below. Thus, the seismic data can be used to delineate a near-mine exploration envelope, based on the extent of the internal reflectivity within the olivine–pyroxenite part of the intrusion. In particular, the reflective zone continues below the known mineralization, thus indicating continuation of the mineralization at depth. Very recently, a deep zone of homogeneous, diffuse reflectivity identified on 2D line E5, similar in character to parts of the Kevitsa intrusion, has been drilled below hundreds of meters of country rock, and confirmed to be another olivine pyroxenite intrusion. At this stage no internal layering has been encountered, nor any mineralization, lending more credibility to the hypothesis that the former controls the latter.

The seismic data also reveal a complicated pattern of faults bracketing and crosscutting the Kevitsa intrusion as a whole and at the deposit scale. Some of these faults (Fig. 8) cross the planned open-pit mine at depths of about 300–500 m, and most likely continue to surface above the depth of the seismic imaging capability. These faults are therefore critical for geotechnical planning of the mine. The pit walls will be steep because of economic and environmental restrictions, and thus it is important that geologic structures transecting the open pit, in particular those sub-parallel to the pit walls, are well understood and mapped in the subsurface. On the other hand, some of the major structures identified in the seismic sections may potentially be related to the emplacement of the Kevitsa intrusion as a whole.

The 2D seismic data also indicate a possible relationship between the Kevitsa intrusive complex and nearby Satovaara complex. The reflections associated with the base of the Kevitsa intrusion are abruptly interrupted by the Satovaara Fault Zone, whereas discontinuous reflectivity characterizes the fault zone, and more continuous reflectivity appears again beneath the Satovaara intrusive complex (R4 in Fig. **7**). Our interpretation of the basal contact of the Satovaara intrusion indicates a shallower base than for the Kevitsa complex. However, the seismic data do not clearly indicate two separate intrusions, and we think that the data might actually suggest that the two complexes are parts of a once-continuous intrusive complex, now separated by the major Satovaara Fault Zone. If so, this could further indicate that the Satovaara complex potentially hosts similar deposits to the Kevitsa intrusion. However, only a few holes have been drilled into the Satovaara complex, and more holes are needed to establish

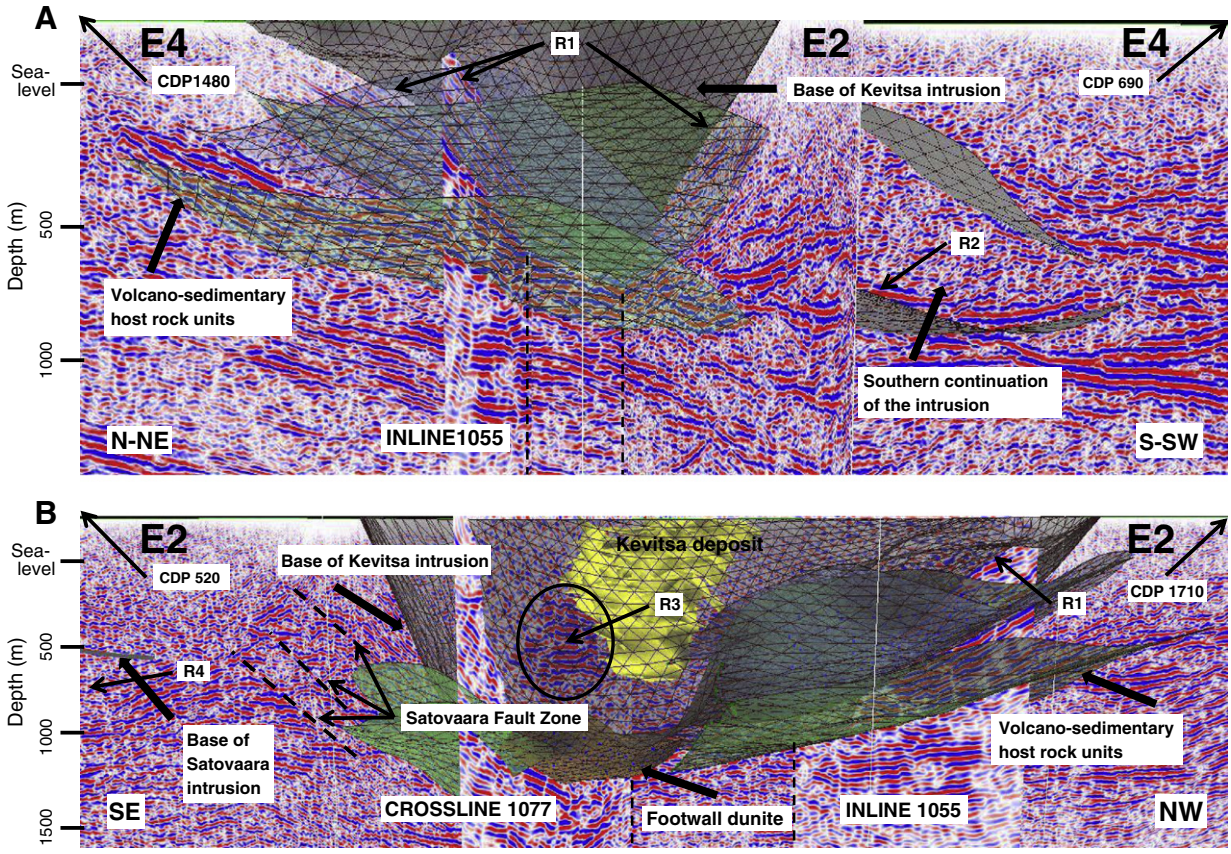


Fig. 7. (A) 3D visualization of Kevitsa 2D seismic lines E4 and E2 and an inline from the 3D seismic volume (Fig. 4) with the interpreted base of the Kevitsa intrusion, southern continuation of the intrusion, and some interpreted host rock units. Coloring of the host rock units follows the coloring on the surface geological map in Fig. 4. R1 marks the continuous reflectors at the contact to the Kevitsa intrusion and R2 the continuous reflectors, which have been interpreted as a previously unknown southern continuation of the Kevitsa intrusion (compare with the cross-sections in Fig. 5). (B) 3D visualization of Kevitsa 2D seismic line E2 and 3D seismic data (Fig. 4) with the interpreted bases of the Kevitsa and Satovaara intrusions, Satovaara Fault Zone, some host rock units and footwall dunite unit beneath the Kevitsa intrusion. Coloring of the host rock units follows the coloring on the surface geological map in Fig. 4. The Kevitsa deposit is shown in yellow (courtesy of the Kevitsa Mining Oy/First Quantum Minerals Ltd). R1 marks the continuous reflectors at the contact to the Kevitsa intrusion and R3 the reflectivity internal to the intrusion that has been interpreted to indicate spatially discontinuous magmatic layering within the intrusion. R4 indicated continuous reflectivity that is interrupted by the Satovaara Fault Zone, but continues again beneath the Satovaara intrusion.

the exact relationship of this complex to the Kevitsa intrusive complex. It should be also noted that a detailed interpretation of the Satovaara Fault Zone and continuation of the Kevitsa intrusion on E2 is complicated by a sharp curve in the survey line (Fig. 4).

4. Seismic constraints on models of ore genesis in the Witwatersrand Basin

The Mesoarchean Witwatersrand Basin of South Africa is the world's largest known accumulation of gold, and has yielded more than a third of the gold ever mined. Gold-bearing conglomerates were discovered near modern-day Johannesburg in 1886. The outcrop was traced along the perimeter of the Witwatersrand Basin, and the gravity and magnetic methods were used to explore for ore bodies where the Witwatersrand rocks were concealed by younger strata. The ore bodies were found to persist to great depths and by the 1920s mining was already taking place more than a 2 km below the surface. Gold production peaked at 1000 tonnes in 1970, and has since declined to a mere 200 tonnes in 2011. Nevertheless, the Basin is known to host substantial resources that may become attractive to exploit in the future, depending on the gold price and developments in technology.

The Witwatersrand Basin is filled with low-grade siliciclastic sediments. The gold is concentrated in quartz pebble conglomerates (known as reefs), is usually associated with pyrite, and locally associated with uraninite. On a micro-scale, most of the gold is associated with hydrothermal phases and occurs along micro-fractures (Muntean et al., 2005). The conglomerates are commonly interpreted to represent fluvial to fluvio-deltaic deposits on the basin edge. In most cases the conglomerate layers are only a few decimeters to several meters thick, but in a few instances the conglomerate layers are stacked on top of each other and give rise to massive ore bodies that are tens of meters thick. The conglomerate layers form sheets that extend for many kilometers along strike and dip.

4.1. Origin of the gold in the Witwatersrand Basin

The gold distribution is closely associated with sedimentary facies, and hence most exploration and mining geologists assumed that it was a placer deposit (e.g., Pretorius, 1981, 1989). It was assumed that the primary source of gold was the Archean basement rocks and greenstone belts in the hinterland of the foreland basin. However, the source of the vast amount of gold deposited in the basin (some 50,000 tonnes have been mined) has not been identified, although it is possible that the source rocks of the detrital gold have been eroded or are covered by younger strata. The existence of hydrothermal phases of gold was explained by remobilization over short distances (micrometers to meters) by hydrothermal fluids during a series of tectono-thermal events that have affected the basin (e.g., Frimmel et al., 2005). For example, Rasmussen et al. (2007) identified two metamorphic episodes. Firstly, a 2.03–2.06 Ga event, broadly contemporaneous with the intrusion of the Bushveld Complex, that affected

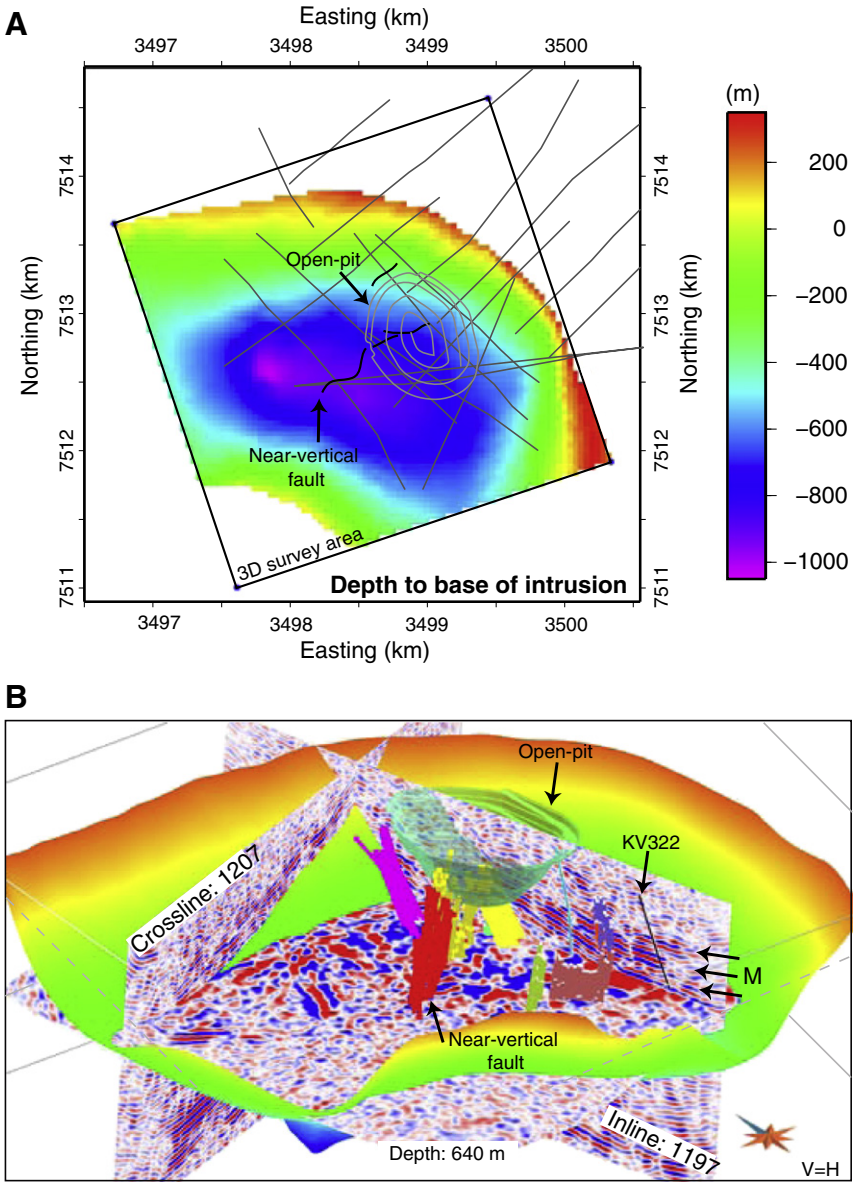


Fig. 8. (A) Depth to the base of the Kevitsa intrusion constrained by the 3D seismic and available borehole data in the study area. Solid black lines represent near-vertical faults mapped from the seismic volume. (B) 3D visualization of the seismic data with the planned open-pit mine and the picked near-vertical faults and the base of the Kevitsa intrusion. KV322 is a borehole that intersects a series of sulfide mineralization and shows a good correlation with the reflections observed in the seismic volume (see events marked as M). Modified from Malehmir et al. (2012a).

the northwestern and central parts of the basin. The intergrowth of gold and monazite in a specimen from the West Rand goldfield at 2.045 Ga was interpreted to indicate remobilization associated with the Bushveld Complex. Secondly, a 2.12–2.14 Ga event that affected the northern and central parts of the basin.

On the other hand, several workers (e.g., Barnicoat et al., 1997; Davidson, 1965; Graton, 1930; Phillips and Myers, 1989) have argued that the gold was introduced by hydrothermal fluids sometime after the sediments were deposited. It is postulated that long-range basin-wide flow of fluids was concentrated in the conglomerates because of their greater permeability, and that gold precipitated from aqueous fluids in the presence of iron sulfides. Several possible sources and events have been postulated for the source of the gold-bearing hydrothermal fluids, for example Ventersdorp-age volcanism at 2.7 Ga (Phillips et al., 1997), regional metamorphism between 2.4 and 2.0 Ga (Phillips and Myers, 1989), and the intrusion of the Bushveld Complex at ca. 2.05 Ga (Stevens et al., 1997). For example, isotope studies by Zhao et al. (2006) suggest that the source for the fluids is related to the peak metamorphism and the metamorphic fluids involved were probably derived from the basin itself, and allogenic sulfides in the Ventersdorp Contact Reef were reconstituted during fluid circulation at peak metamorphic conditions. There is no published account suggesting any direct link between the gold and, for example, deep mantle plume or subducting slab related to the gold mineralization in the basin such as those found in the other regions in the world (e.g., Lei and Zhao, 2005; Lei et al., 2009; Maruyama and Okamoto, 2007; Zhao, 2007).

This is not merely an academic debate, as the models make different predictions regarding the distribution of the ore, with significant implications for exploration strategies, the estimation of ore reserves, and mining layouts. The issue has attracted international attention. In 2005, the Society of Economic Geology (SEG) sponsored a forum where proponents of the competing modified paleoplacer and epigenetic hydrothermal models presented their views, followed by a panel discussion with audience participation. An article published in

the SEG newsletter in January 2005 provides an excellent preview of the debate (Muntean et al., 2005). Many strands of evidence must be considered to resolve the debate, ranging from micro- to meso-scale studies of the textural, geochemical and isotopic characteristics of the ore components, to macro- and mega-scale studies of the distribution of the ore bodies (Frimmel et al., 2005). Here, we demonstrate how 3D reflection seismics can be used to map the distribution and timing of meso- to mega-scale structures and provide constraints on the genetic models.

4.2. Reflection seismic mapping of the Witwatersrand Basin

The reflection seismic method was first used to explore the Witwatersrand Basin in the 1980s. Initially, 2D reconnaissance surveys were conducted to search for extensions of the basin, and blocks of ore that had either been preserved from erosion or brought to mineable depths by faulting (Pretorius et al., 1989). The first 3D survey was conducted in 1987 on the South Deep prospect (Fig. 9A, B) in the West Rand goldfield (Campbell and Crotty, 1990). South Deep

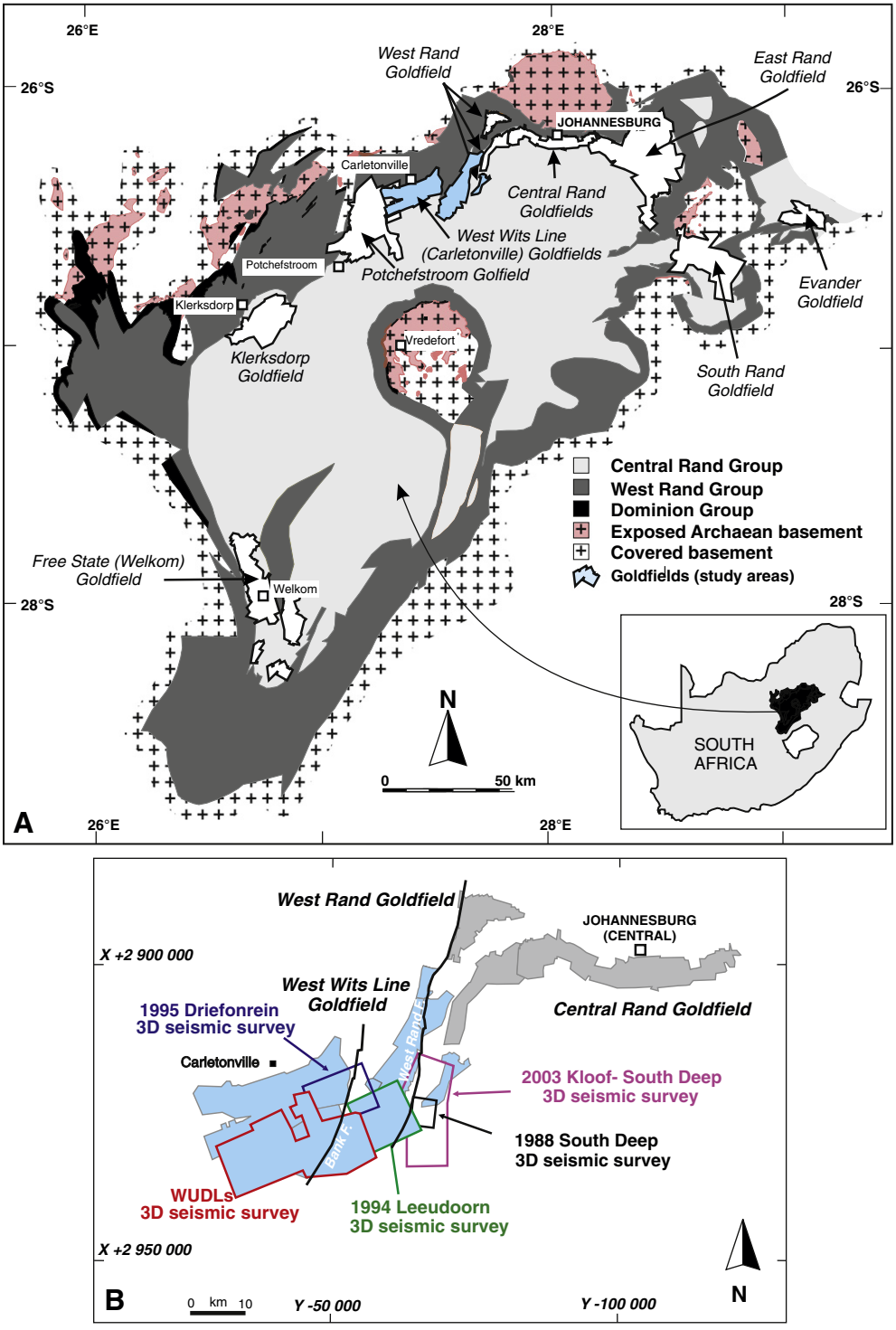


Fig. 9. (A) The location map of the West Rand and West Wits Line (Carletonville) Goldfields of the Witwatersrand Basin in South Africa (after Dankert and Hein, 2012). (B) The location of historical surveys for Kloof, South Deep, Driefontein and Western Ultra Deep Levels (WUDLs) (after Manzi et al., 2012a,b).

mine has come into production, and boasts reserves of 29 million oz and resources of 78 million oz. Since then, 3D surveys have been widely applied in the Witwatersrand Basin for final-stage exploration, bankable feasibility studies, and mine planning (Malehmir et al., 2012b; Pretorius et al., 2003).

Four surveys conducted between 1994 and 2003 (Fig. 9B) were merged and reprocessed to obtain a seismic volume that extends approximately 40 km east–west and 16 km north–south (640 km^2), with a depth extent greater than 9 km. Acquisition parameters for the 2003 surveys (the Kloof–South Deep seismic surveys covering an area of about 96 km^2) is shown in Table 1. The entire seismic data cover much of the Far West Rand goldfield and part of the West Rand goldfield, covering mines and exploration lease areas owned by Anglo-gold Ashanti (Mponeng, Western Ultra-deep Levels) and Gold Fields (Kloof–Driefontein Complex (KDC); South Deep). The spatial resolution was maximized by reprocessing the data using advanced processing techniques (Manzi et al., 2012a), enabling faults with throws as small as 10 m to be mapped. The seismic data were integrated with underground mapping and exploration drilling information on the properties of the KDC and South Deep mines. The data were reinterpreted using the latest interpretation techniques in efforts to improve the mapping of geological structures (Manzi et al., 2012a) and potential conduits for methane and water (Manzi et al., 2012b).

4.3. Seismic constraints on genetic models

3D reflection seismics is able to map the present-day geometry of reflective horizons near the ore bodies, map the geometry of faults and dykes, and place constraints on the timing of fault activity and dyke intrusions. Interpretation of the Ventersdorp Contact Reef (VCR) and the Black Reef (BLR) horizons were of particular interest, and was used to provide age limits on structures. In broad terms, if the gold was introduced during the deposition of the conglomerates (the paleoplacer model), we would expect its distribution to have been controlled by syn-sedimentary faults, and have no correlation with faults that only became active following the deposition of the Witwatersrand sediments, and/or dykes that intruded thereafter. On the other hand, if the gold was introduced at a later stage (the epigenetic hydrothermal model), the gold distribution is likely to have some association with post-Witwatersrand structures or intrusions. For example, the structures may have acted as conduits through which the ore-bearing fluid was transported, or dykes may have acted as barriers that obstructed the flow of the fluids.

Dankert and Hein (2012) evaluated the structural character and tectonic history of the Witwatersrand Basin in order to test the metallogenic models. They were able to identify fold–thrust events that terminated deposition in the Witwatersrand and Transvaal basins at ca. 2.7 and 2.2–2.0 Ga, respectively. Four basin-forming events occurred in the interim, resulting in the deposition of the volcanic–sedimentary sequences of the Klipriviersberg Group, and the sedimentary sequences of the Platberg, Chuniespoort and Pretoria Groups. These basin-forming events exploited pre-existing structures such as feeder dykes, thrust faults, normal-listric faults, and growth faults. While Dankert and Hein's analysis supports the paleoplacer model, they note that geometric, kinematic and relative chronological information was surprisingly limited.

The 3D seismic data have contributed to the understanding of the tectonic evolution of the region in several ways. The reprocessing of 1994 Leeudoorn and merging of the 1995 WUDLs surveys with the 2003 Kloof–South Deeps surveys made it possible to study regional structures on both meso-scale (meters to hundreds of meters) and mega-scale (kilometers to tens of kilometers). On a mega-scale, the seismic data resolve West Rand and Bank faults, which have maximum throws of 2 km (Fig. 10). They are north–north trending, west-dipping and listric in form (Figs. 10 and 11A). These faults displace the strata of the West Rand and Central Rand Groups (ca. 2.985–2.849 Ga) and the Ventersdorp Supergroup (ca. 2.72–2.63 Ga), and form a décollement horizon in the West Rand shales. However, the faults do not displace the strata of the Paleoproterozoic Black Reef Formation and Chuniespoort and Pretoria Groups of the Transvaal Basin sequences (ca. 2.58–2.20 Ga) (Fig. 11A). Geological and seismic data suggest that both the West Rand and Bank faults experienced reactivation (folding and thrusting) during the Umzawami Event that terminated the deposition in the Witwatersrand Basin; followed by negative inversion (i.e. a change from compression to extension) where normal faulting accompanied the extrusion of the 2.71 Ga Klipriviersberg Group lavas, culminating in the deposition of Platberg Group sediments in grabens at ca. 2.70 Ga (Dankert and Hein, 2012; Manzi et al., in press). A few kilometers below the West Rand

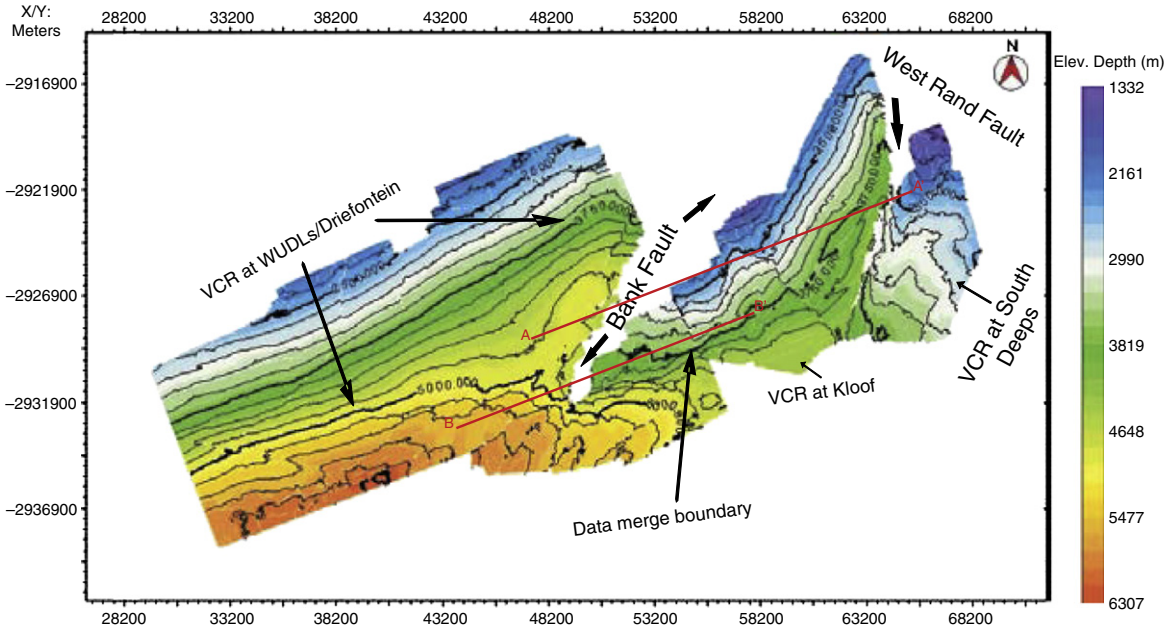


Fig. 10. Depth structure map of the Ventersdorp Contact Reef (VCR) derived from conventional picking across survey areas, showing the Bank and West Rand faults and the location of seismic sections shown in Fig. 11. The contour interval is 250 m.

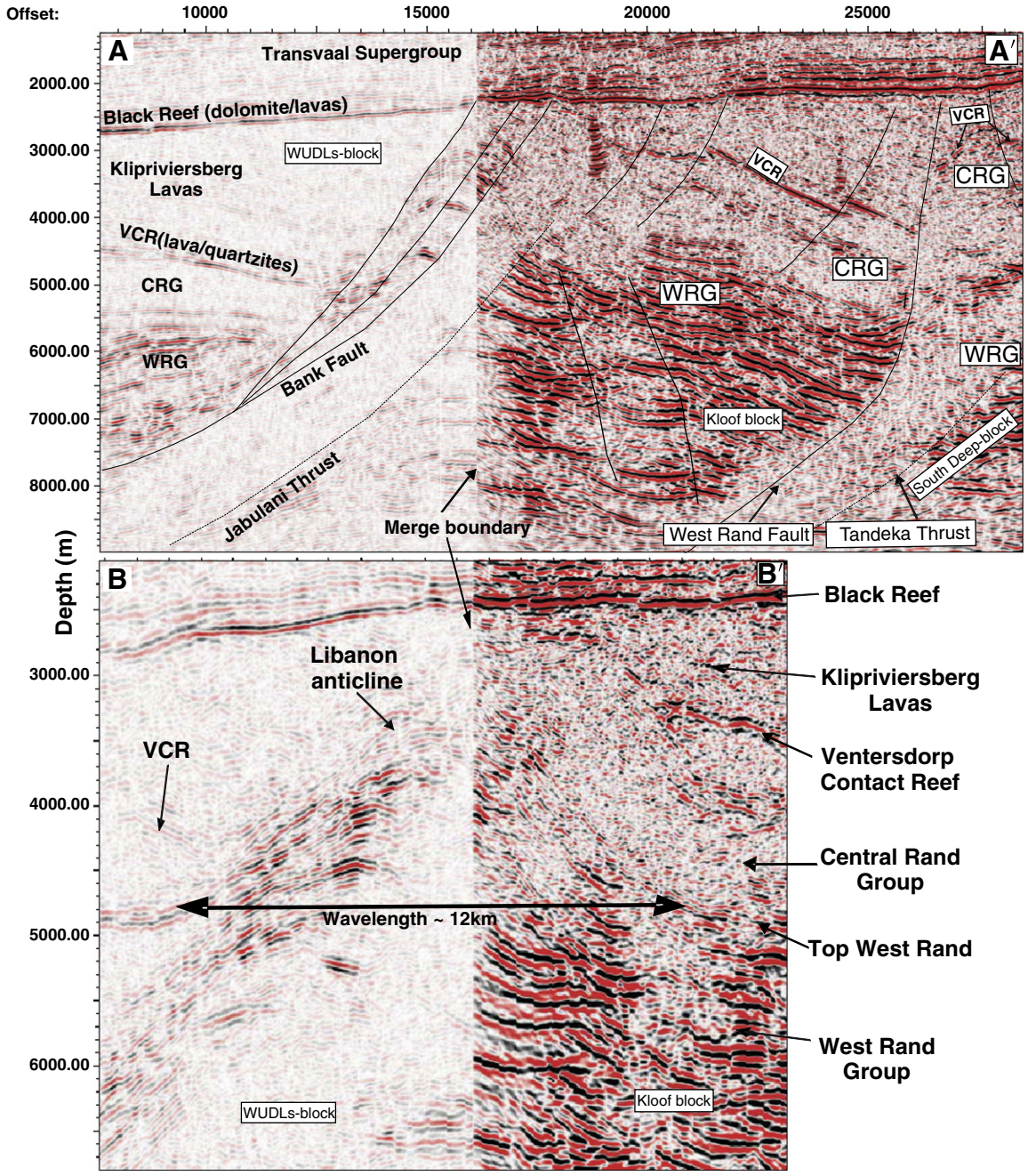


Fig. 11. (A) Seismic section (amplitude display) across the West Rand and Bank faults, showing the Jabulani and Tandeka thrusts at about 1.2 km below the Bank Fault and West Rand Fault, respectively. (B) Seismic section (amplitude display) across the major Libanon anticline at the merge boundary of the 1995 WUDLs and 2003 Kloof seismic survey. WUDLs: Western Ultra Deep Levels; WRG: West Rand Group; CRG: Central Rand Group; VCR: Ventersdorp Contact Reef. Note sharp change in the amplitudes is due to different datasets that were merged together.

and Bank Faults, the seismic data reveal the Tandeka and Jabulani thrusts, respectively (Fig. 11A). These thrusts displace and offset the West Rand Group and Central Rand Group.

More importantly, the northerly-trending Libanon anticline, which happens to lie on the eastern edge of the Western Ultra Deep Levels survey and on the western edge of the Leeudoorn survey, was identified and studied in detail for the first time (Fig. 11B). The wavelength and height of the Libanon anticline are greater than 10 km and 1.5 km, respectively. The eastern limb of the Libanon Anticline is dissected by a series of west-dipping thrust-splays of the Jubulani Fault Complex (Fig. 11b). The Libanon anticline and parasitic folds have been interpreted to have formed syn- to post-deposition of the West Rand and Central Rand groups because they are folded about the hinges of the folds. The Tandeka and Jabulani thrusts displace the West Rand and Central Rand Groups and thus also formed after them. These structural features provide important new constraints on tectonic styles and the timing of tectonic events (Manzi et al., in press). The seismic data cube was also used to compute isopach maps, and to map faults and dykes on a mega-scale. This information was used to determine the relative rates of deposition, the extent of unconformities, and the relative ages of fault activity and dyke intrusion, and the orientation and ratio of principal stresses.

Advanced signal processing techniques were used to improve spatial resolution and to map faults and dykes in plan and section on a meso-scale (meters to hundreds of meters). Edge detection techniques, in particular, were used to map fault throws as small as 10 m.

These features were correlated with known intersections of water and gas, and structures that likely acted as present-day fluid pathways were identified (Manzi et al., 2012b; Fig. 12A, B). This type of information can also be used to test genetic models. For example, Meier et al. (2009) mapped and geochemically analyzed numerous mafic dykes that cut and displaced gold reefs on a mine in the Klerksdorp goldfield. The geochemical data indicated that the dykes are the feeders of the Klipriviersberg Group flood basalts that immediately overlie the Witwatersrand rocks, while mapping indicated that they were emplaced into active or pre-existing faults. Meier et al. (2009) concluded that the dykes would have acted as barriers to regional-scale movement of fluids within the major gold-bearing conglomerate horizon in the region (the Vaal Reef), and that basin-scale gold enrichment must have occurred during sedimentation or early diagenesis. While no similar geochemical study has been conducted in the area covered by our data, the projection of dykes and faults into the VCR horizon (Fig. 13A, B) provides a ready model of barriers to fluid transport. The notion of basin-scale fluid movement caused by later tectonic or thermal events can now be tested.

5. Seismic investigations at the Brunswick No. 6 base metal and associated iron deposits

The Bathurst Mining Camp (BMC), northern New Brunswick, Canada, is a major base-metal producing region that contains the super giant Brunswick No. 12 VHMS deposit and several Zn–Pb–Cu deposits within a sub-circular area 50 km in diameter (McCutcheon, 1992). The search for additional base metal deposits in the camp requires an efficient exploration strategy based on a good understanding of the highly deformed and complex geology, combined with modern geophysical tools to provide drilling targets and to improve the understanding of the geological framework at depth. Within this context, 2D and 3D seismic surveys were acquired in two key prospecting areas of the BMC. Seismic data previously acquired by industry in the Halfmile Lake area led to the discovery of an about 6 Mt VHMS lens located at a depth of 1.2 km (Malehmir and Bellefleur, 2009; Matthews, 2002). Here, we review the main characteristics of seismic data acquired in a second area of the BMC located over the Brunswick No. 6 mine (Fig. 14). The Brunswick No. 6 deposit is located approximately 27 km southwest of the city of Bathurst in northeast New Brunswick, Canada (Fig. 14). By 1982, Brunswick No. 6 had produced about 12.2 Mt of 5.43% Zn, 2.15 wt.% Pb, 0.40 wt.% Cu, and 67 g/t Ag (Luff, 1995). Seismic reflection data (2D and 3D) were acquired in the late 1990s and early 2000s by industry to explore for new deep-seated deposits along the prospective Brunswick horizon. Re-processing and re-analysis of the data show that the Brunswick horizon occurs within a reflective package that extends down to at least 6–7 km depth (Cheraghi et al., 2011, 2012; Malehmir and Bellefleur, 2010). In addition, the seismic data provide some indications of the presence of BMC rocks beneath the Carboniferous sedimentary rocks exposed at surface east of the mining area and deeper reflections previously associated with a mafic/ultramafic dominated ophiolitic slab underlying the BMC. These results clearly demonstrate the utility of seismic reflection methods in complex mining environments.

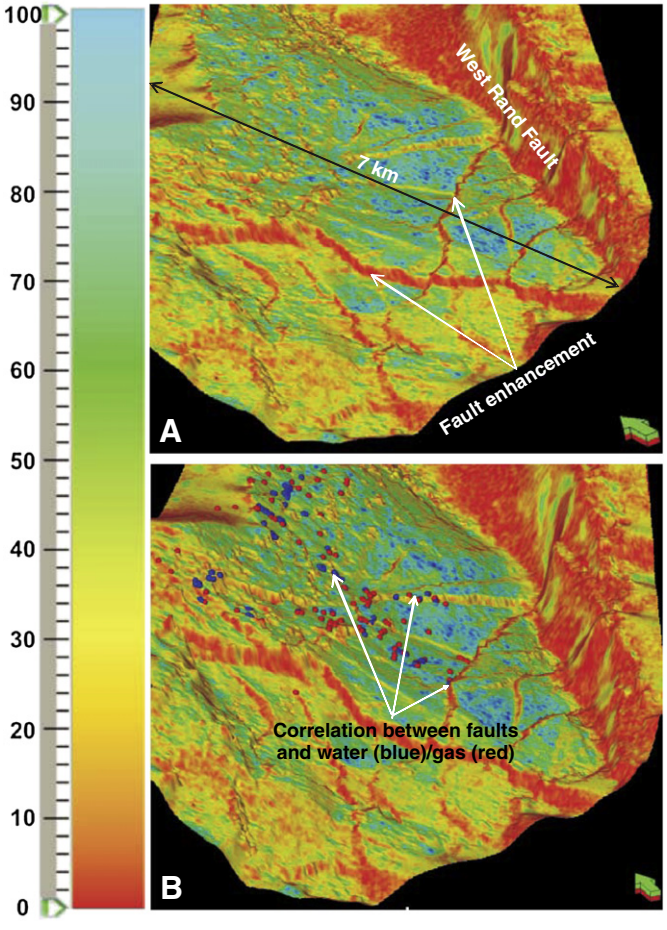


Fig. 12. (A) 3D visualization of the VCR edge attribute map at the Kloof Gold Mine. (B) Edge attribute of the VCR overlain with water and methane data from the Kloof Gold Mine. A number of minor structures show a very good correlation with water and methane data. The edge detection map is the combination of dip and azimuth maps, normalized to the local noise of the surface. The color bar is given in % where low values indicate edges such as faults and dykes. (For interpretation of the references to color in this figure legend, the reader is referred to the web version of this article.)

5.1. Geological background

The BMC is composed of several tectonic blocks and slivers that were juxtaposed during the closure of the Tetagouche-Exploits back-arc basin (van Staal et al., 2003). Fig. 15 shows a schematic cartoon of tectonic framework of the Brunswick complex in the late Ordovician–early Silurian (450–440 Ma). According to van Staal (1994), the Cambro-Ordovician clastic metasedimentary sequence of the Miramichi Group is the oldest rock in the BMC. The Brunswick complex formed during a continent–continent collision in the late Ordovician and Early Silurian. Prior to the collision, a series of oceanic–continental obductions in the early Ordovician and before that trapped large blocks of oceanic rocks (mainly ophiolite) underneath the volcanic and sedimentary rocks of the Miramichi Group (Figs. 14 and 15). The Tetagouche Group hosts the VHMS and iron deposits and is a primary target for deep exploration in the BMC. The oldest part of the Tetagouche Group is the Nepisiguit Falls Formation, which contains felsic volcanic and volcanoclastic rocks. Younger rocks of the Flat Landing Brook Formation contain rhyolite flows and rhyolitic volcanic/hyaloclastic rocks. The alkali basalt flows of the Little River Formation are the youngest part of the Tetagouche Group. The Brunswick horizon is observed in the upper part of the Nepisiguit Falls Formation and includes a mixture of sulfide, carbonate, oxide, and silicate facies. This horizon is a key target for geophysical and geochemical exploration in the camp (Gross and McLeod, 1980).

Thrusting and folding observed at surface suggest several repetitions of the geological units in the BMC (van Staal, 1987). In the study area, an example of such repetition is shown in a geological cross-section provided by Wills et al. (2006). The cross-section suggests tight and small folding structures down to deep level in the crust (Fig. 16; see A–A′ in Fig. 14 for location of the cross-section). Since the Brunswick horizon hosts most base metal deposits in this camp, it is important to image its spatial distribution and any possible repetition as detailed recognition of this prospective structure at depth could lead to new discoveries in the area.

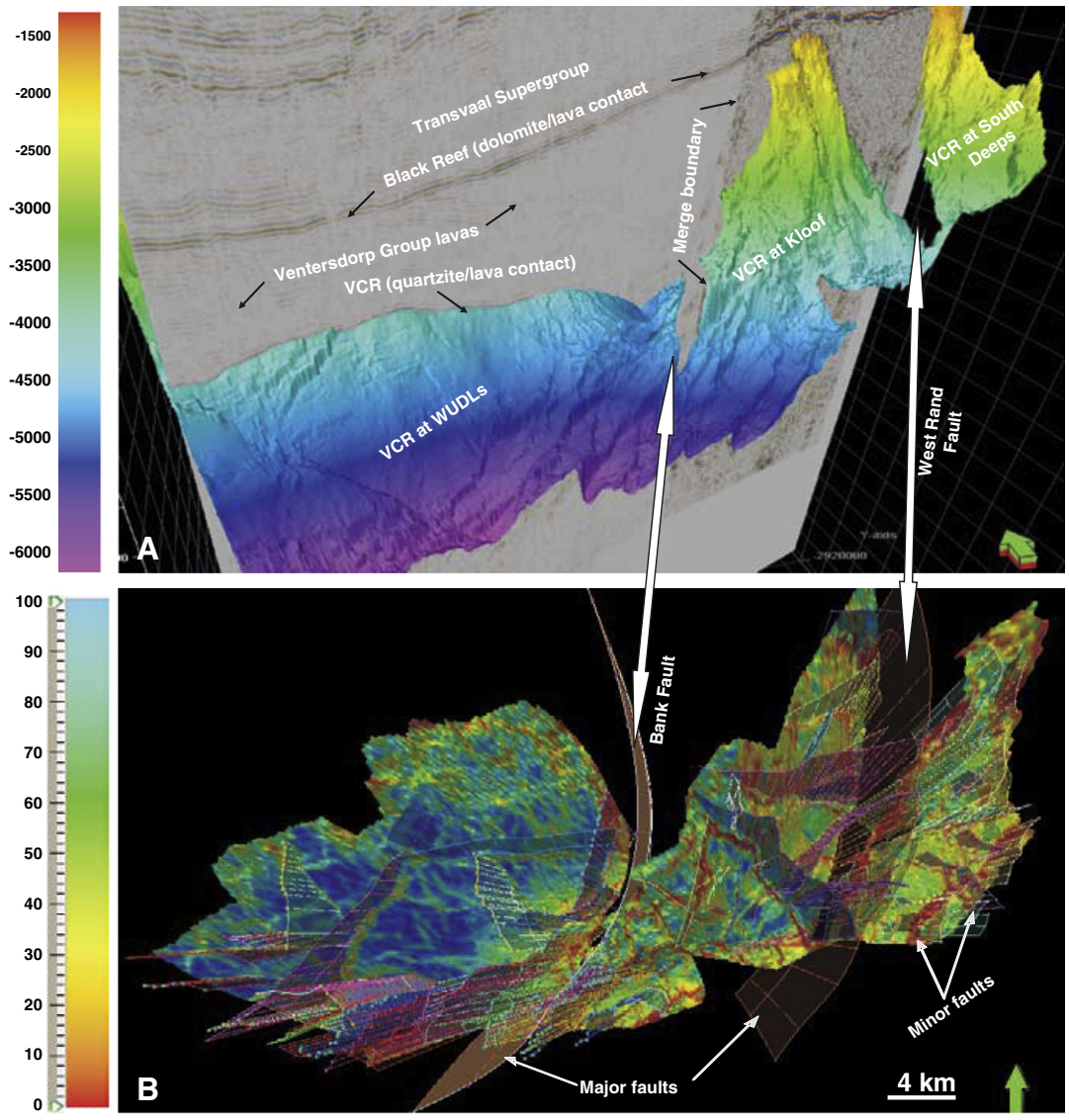


Fig. 13. (A) 3D visualization of the VCR, clearly showing the imaging of the mega-scale and meso-scale structures (color bar represents an elevation depth and is given in meters). (B) The fault framework model projected onto the VCR horizon defined from edge detection attribute (color bar represents edges and is given in % where low values indicate edges such as faults and dykes). The model incorporates the major West Rand Fault and Bank Fault, as well as a suite of minor structures. (For interpretation of the references to color in this figure legend, the reader is referred to the web version of this article.)

5.2. Seismic constraints

The available infrastructures, mining facilities, and a need to explore for new deposits at greater depths were the incentives to acquire 2D and 3D seismic data in the Brunswick area. In the late 1990s and early 2000s, Noranda Inc. (now Xstrata) acquired three 2D seismic profiles and a 3D seismic survey (Table 1) in the Brunswick No. 6 area (see Fig. 14). Details on the acquisition parameters and re-processing of the data can be found in Cheraghi et al. (2011) and (2012), Malehmir and Bellefleur (2010). Noranda Inc. and the Geological Survey of Canada also acquired wireline-logging data in a few boreholes near Brunswick No. 6 to help with the interpretation of the seismic data. The petrophysical logs showed that both the Brunswick horizon and gabbro have high acoustic impedances that contrast with the generally low acoustic impedance of the host rocks. As a result, both units produce reflections that can be observed in seismic images. In contrast, rocks of the Miramichi Group are mostly transparent to seismic waves and can help indirectly to determine the location of the reflective formations (Cheraghi et al., 2011; Malehmir and Bellefleur, 2010).

Fig. 17 shows re-processed data for the profile BRN991001 that extends 6 km from west to east just south of the Brunswick No. 6 mine (see Fig. 14). The data quality is generally good with many reflections that almost reach the surface and allow correlation with surface geological map to help the interpretation. Reflections all dip to the west in alternation with noticeable transparent sequences. A comparison between surface geological observations and shallow reflections suggests that reflective zones P1 and P2 are generated from gabbro and alkali basalts of the Little River Formation in contact with the felsic volcanic rocks of the Nepisiguit Falls Formation, and the Brunswick horizon. The P1 and P2 reflection packages are imaged down to approximately 4–5 km depth. The high amplitude reflection in P1 (see arrows in Fig. 14) is interpreted to be generated by the Brunswick horizon (Cheraghi et al., 2011; Malehmir and Bellefleur, 2010). This reflection, although clearly visible, could be hard to distinguish from gabbro reflections without the support of geological information. However, the entire reflection package can be used to guide exploration. The reflection package P2 does not reach the surface, but its projection intersects the surface at the location of the Nepisiguit Falls Formation east of the profile. Rock units of the Flat Landing

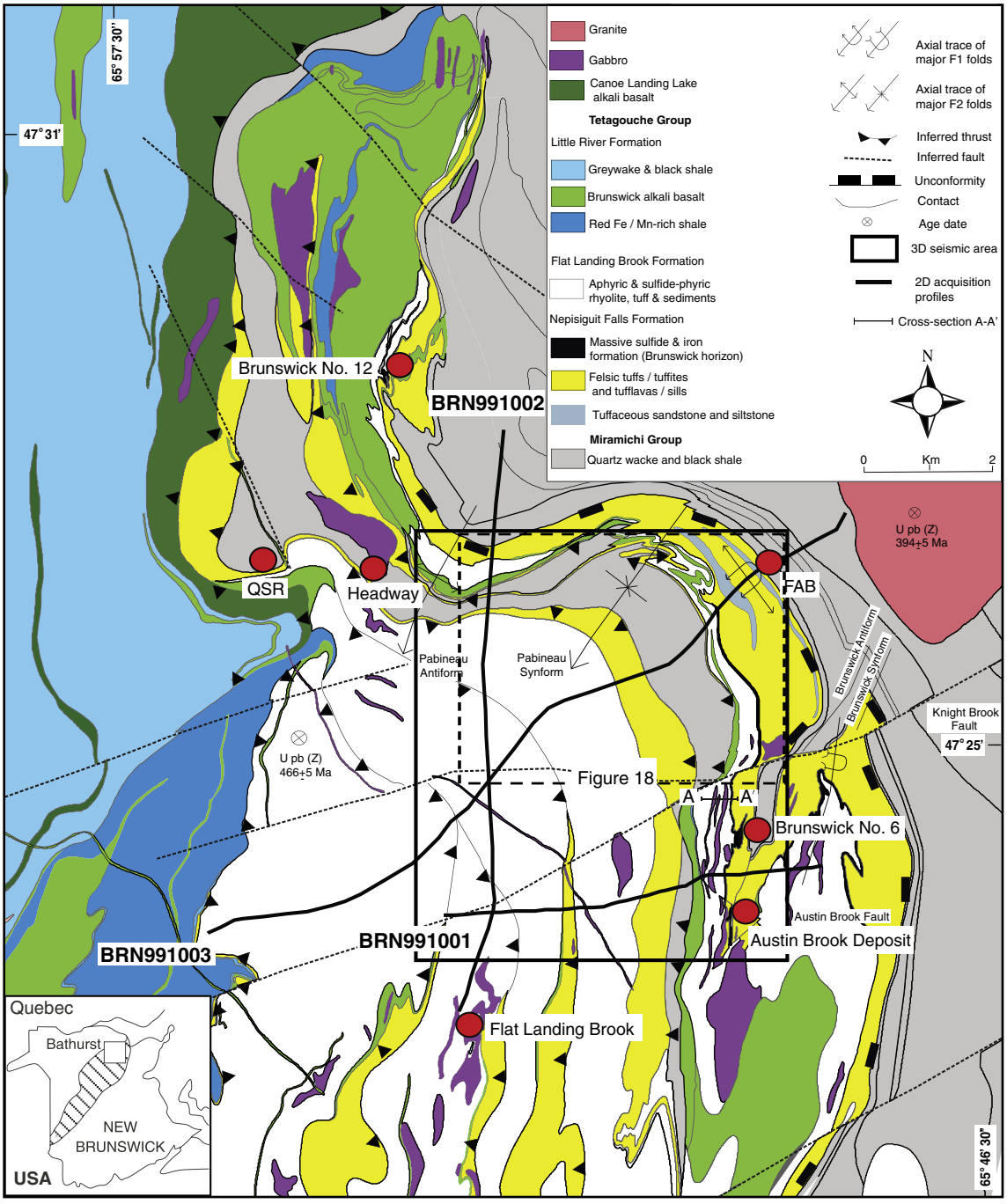


Fig. 14. Geological map of the Brunswick No. 6 area, Bathurst Mining Camp, New Brunswick (modified from van Staal et al., 2003) showing the location of major mineral deposits. The rectangle exhibits the area of the 3D seismic data. The solid black lines are 2D seismic data BRN991001, BRN991002, and BRN991003 acquired in 1999. The locations of cross-section A–A′ and a subset of the 3D seismic cube (dashed rectangle) are also shown on the map.

Brook Formation and Miramichi Group show, in general, very weak reflectivity.

The short and high amplitude reflections (R1–R4) appear to be generated by relatively thin gabbroic dykes. The correlation with gabbro dykes observed at surface is particularly convincing for R1 and R2. The discontinuous reflections at 2.25 s are interpreted as a possible repetition of BMC rocks thrust beneath the one exposed at surface. If correct, this interpretation suggests that the BMC could extend further than expected to east, and may underlie the Carboniferous sedimentary rocks exposed at surface. A short sub-horizontal reflection at approximately 2.75 s marks a change in the structural style that could indicate the lower limit of the Brunswick belt (at approximately 8 km). We associate this reflection with the mafic/ultramafic dominated ophiolitic slab possibly underlying the BMC.

When compared with the 2D profile, the 3D seismic data present lower resolution seismic image, which is mostly related to the acquisition geometry used during the survey (Cheraghi et al., 2012). However, the 3D data contain most of the elements observed on the 2D profile (Fig. 17). Fig. 18 shows a subset of the 3D volume with the P1 and P2 reflection packages. The deeper reflection observed at approximately 2.25 s (or about 6–6.5 km depth) on the 2D profile is also clear on the 3D data (Fig. 18). The attitudes of the reflections on the 3D data in the southern part of the 3D are consistent with an eastward thrusting of the BMC rocks.

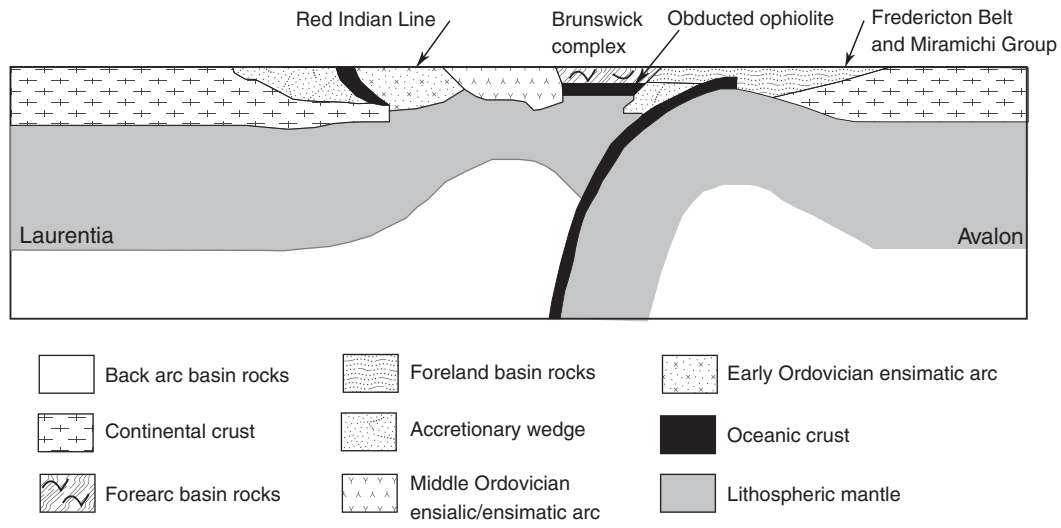


Fig. 15. Tectonic model of the Brunswick complex in the late Ordovician–early Silurian (450–440 Ma; modified from van Staal, 1994). The Brunswick horizon (massive sulfide and iron formation) is part of the Brunswick complex and is strongly folded and deformed. Note that large blocks of thrusted/obducted ophiolite rocks are expected to be trapped in the upper crust beneath the BMC.

Careful analysis of 2D and 3D seismic data, correlation of processing results with the surface geological map, and some borehole petrophysical measurements help to define the architecture of the subsurface formations in the Brunswick No. 6 area. In particular, the prospective Brunswick horizon is shown to occur within a reflection package that is imaged using the seismic data. Interpretation of deeper reflections also suggests a possible repetition of the BMC rocks at greater depths, which could also extend underneath the Carboniferous sedimentary rocks east of the mining camp. Results presented in this section of the paper demonstrate the utility of seismic methods in complex and highly deformed mining camps.

6. Conclusions

In this article, we have reviewed and presented reflection seismic data from three major mining areas of the world in order to provide information about structural and lithological relationships with mineralization. As is evident, performance and character of seismic data depend on the site conditions and geological complexities. While reflections from geological structures are often continuous and coherent in the Witwatersrand Basin, reflections are shorter and less continuous in the Brunswick No. 6 area and in Kevitsa. Nevertheless, combined with the available geological observations, seismic data from these regions

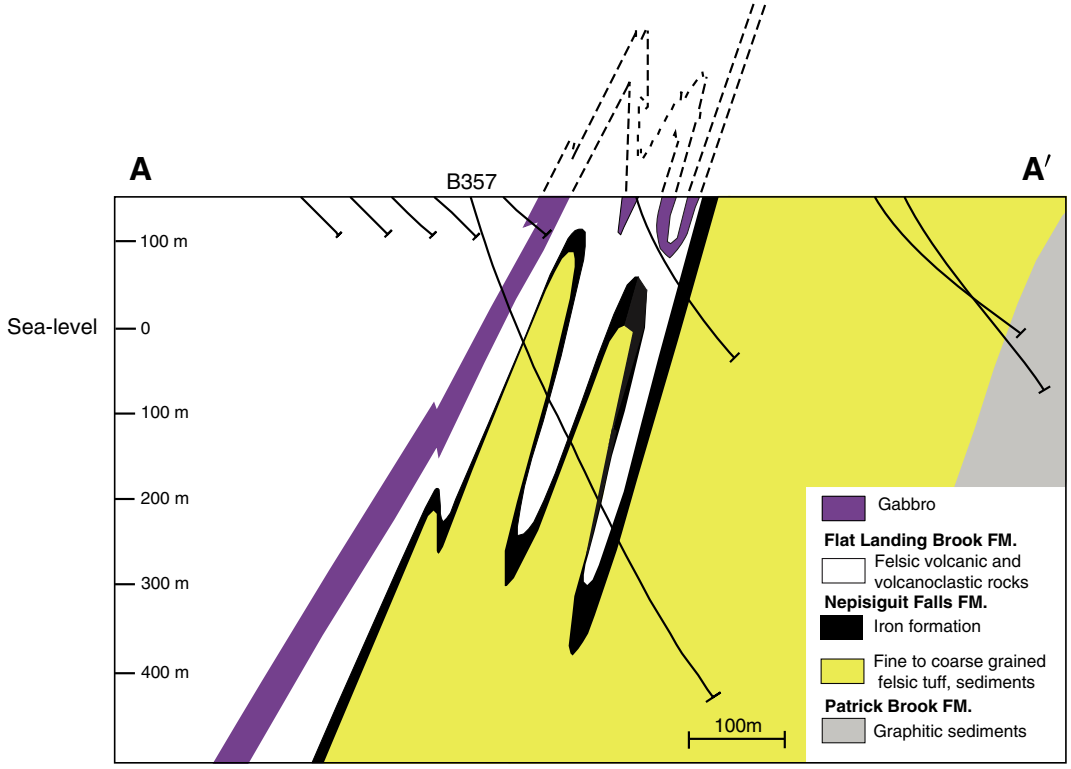


Fig. 16. Geological cross-section along the profile A–A′ shown in Fig. 14 obtained from a series of shallow and deep boreholes, including borehole B-357. The cross-section shows complex structures near Brunswick No. 6 and associated Brunswick Horizon (modified from Wills et al., 2006). Petrophysical measurements obtained from wireline logging in borehole B-357 are shown in Cheraghi et al. (2011).

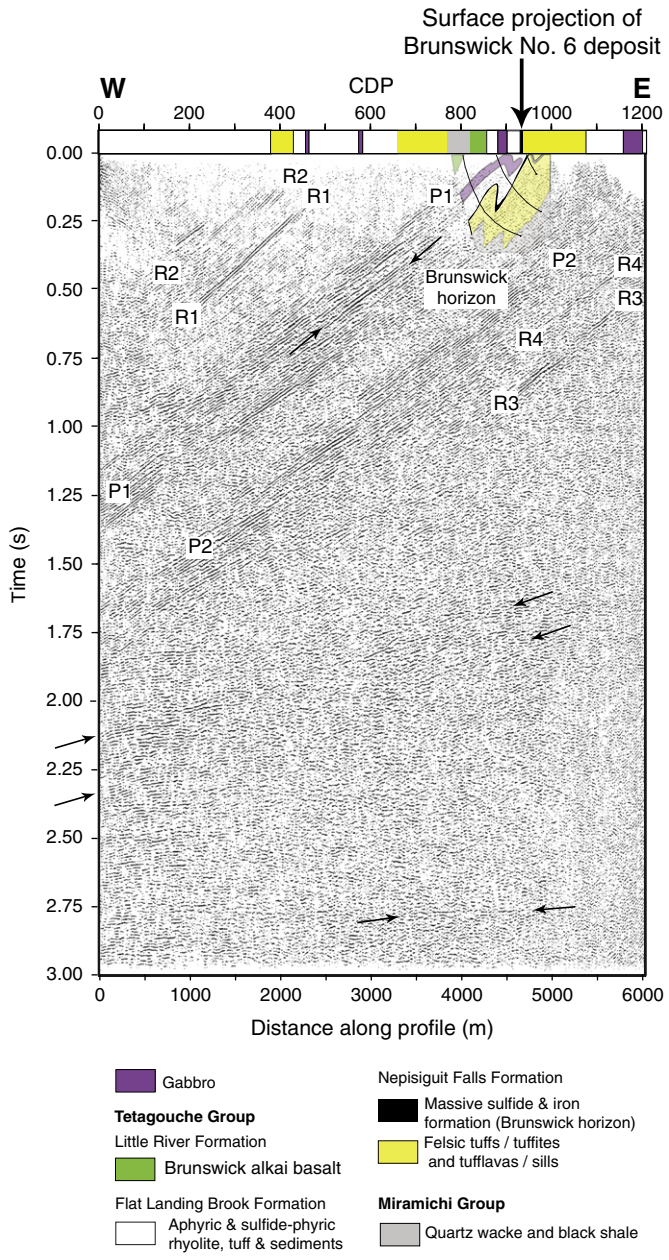


Fig. 17. Stacked section along the BRN991001 profile, showing a series of westward, steeply dipping reflections imaged down to about 1.7 s (i.e., about 5 km depth). Reflectivity pattern shows a sequence of reflective and transparent package repeating from the east to the west. The Brunswick horizon and associated structures appear within the reflective package P1. See text for interpretation of P1, P2, R1, R2, R3 and R4. See Cheraghi et al. (2011) for more details about the projected cross-section onto the profile.

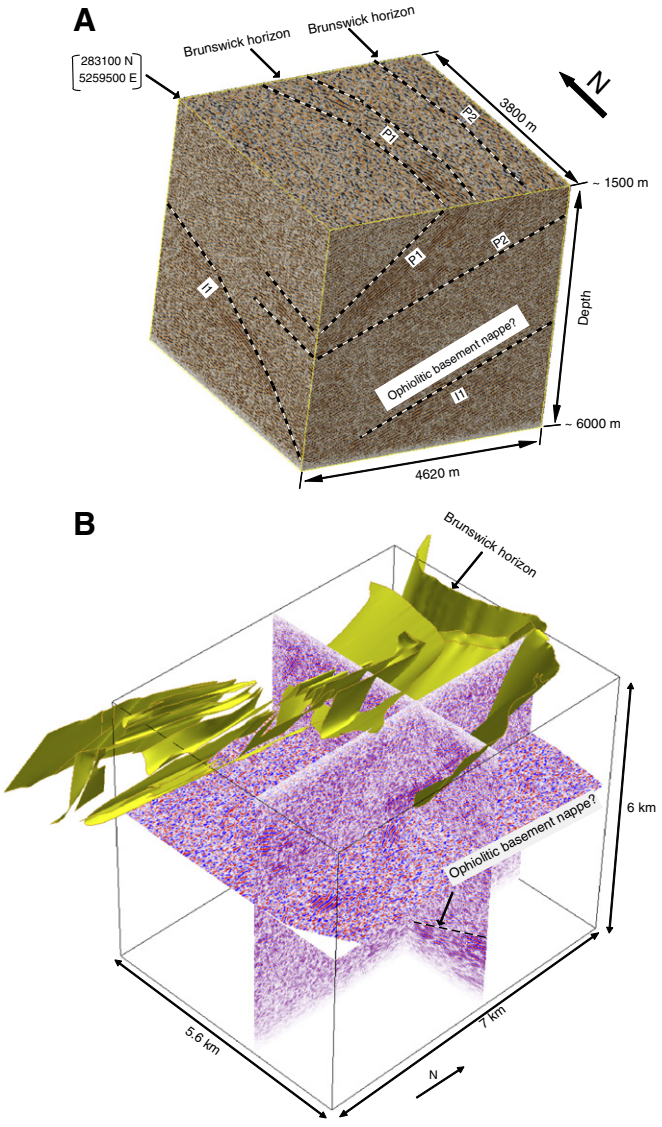


Fig. 18. 3D views from the seismic volume. (A) Unmigrated stack volume showing the depth extent of the Brunswick horizon (P1 and P2) and a high amplitude reflection (I1) interpreted to mark the base of the Brunswick volcano–sedimentary belt. (B) Migrated stacked volume and correlation of a strong high amplitude reflection with the geological model of the Brunswick horizon. A portion of the seismic cube for a time slice at 500 ms. See Fig. 14 for the surface projection of the cube and text for interpretation of events marked as P1, P2, and I1.
Figure is modified from Cheraghi et al. (2012).

provide crucial information about the overall architecture of the upper crustal structures that could be useful for future deep exploration.

Seismic data from the Kevitsa area were used to define the 3D geometry of the ore-bearing Kevitsa intrusion and the surrounding geological units, thus providing a framework for future exploration in the area. Moreover, the Kevitsa deposit is located within a part of the intrusion that is associated with distinct reflectivity of a similar spatial constraint. We believe that this reflectivity is dominantly associated with a zone of magmatic layering that controls the bulk of the economic mineralization. Thus, the seismic data can be used to delineate a near-mine exploration envelope. In particular, the reflective zone continues below the known mineralization, thus indicating continuation of the mineralization at depth. Additionally, the seismic data revealed a wealth of structures crosscutting the Kevitsa deposit and the intrusion as whole. The structures inferred from the 3D data can be critical for geotechnical planning of the mine.

The origin of the metal contained in the world's largest gold ore body, the Witwatersrand Basin, continues to be debated. We have sought to demonstrate that 3D seismic data provide a rich source of information that can be used to test the hypotheses. For example, it might be possible to show that dykes formed impermeable barriers that falsify the epigenetic hydrothermal models. We do not attempt to reach a verdict here, as a convincing model must be able to account for all relevant observations e.g. geochemistry, geochronology, and geological mapping in mine workings. In particular, the superposition of gold grades on the seismic models of stratigraphy and structure will provide an important test of the genetic models. The detailed data are regarded as strategic, and is not published at present.

Seismic data from the Brunswick No. 6 area also clearly image crustal structures down to 7–8 km depth. Of particular interest is

the Brunswick horizon that is consistently imaged within a reflective package that extends down to about 7–8 km depth. A sequence of reflective and transparent zones observed from the data would very likely represent a series of thrust faults implying a repetition of major lithological units including BRN horizon.

Future studies should aim at linking these rather shallow but high-resolution seismic data from the upper crust with deeper structures and provide further insights about the overall structures of the crust and upper mantle in these highly rich mineralized regions. Until such data are available, these reflection seismic data serve a basis for our understanding of the major geological structures associated with the mineralization.

Acknowledgments

We would like to thank First Quantum Minerals Ltd. for allowing us to publish the seismic results. We also thank Xstrata for providing access to the 2D and 3D seismic data in the Brunswick No. 6 area. Consolidated Mineral and Gold Fields are acknowledged for allowing us to show the seismic images from the Wits Basin. A. Malehmir and R. Durrheim acknowledge funding provided by the Swedish International Development Cooperation Agency (SIDA) and Meeting Points Mining to review research in the mineral exploration industry in Sweden and South Africa. R. Durrheim acknowledges support from the DST/NRF South African Research Chairs program. Several local geologists from Kevitsa Mining Oy provided useful input to the interpretation of the seismic data from the Kevitsa mining area. We acknowledge comments and suggestions provided by two anonymous reviewers and the Editor M. Santosh.

References

Adam, E., Perron, G., Arnold, G., Matthews, L., Milkereit, B., 2003. 3D seismic imaging for VMS deposit exploration, Matagami, Quebec. In: Eaton, D.W., Milkereit, B., Salisbury, M.H. (Eds.), Hardrock Seismic Exploration. SEG, Tulsa, Oklahoma, pp. 229–246.

Barnicoat, A.C., Henderson, J.H.C., Knipe, R.J., Yardley, B.W.D., Napier, R.W., Fox, P.C., et al., 1997. Hydrothermal gold mineralization in the Witwatersrand Basin. Nature 386, 820–824.

Bellefleur, G., Malehmir, A., Müller, C., 2012. Elastic finite-difference modeling of volcanic-hosted massive sulfide deposits: a case study from Halfmile Lake, New Brunswick, Canada. Geophysics 77 (5), WC25–WC36. http://dx.doi.org/10.1190/GEO2011-0445.1.

Bohlen, T., Müller, C., Milkereit, B., 2003. Elastic wave scattering from massive sulfide orebodies: on the role of composition and shape. In: Milkereit, B., Eaton, D., Salisbury, M. (Eds.), Hardrock Seismic Exploration. SEG, Tulsa, Oklahoma, pp. 70–89.

Campbell, G., Peace, D.G., 1984. Seismic reflection experiments for gold exploration, Wits Basin, Republic of South Africa. Paper presented at 46th Meeting and Technical Exhibition. European Association of Exploration Geophysicists, London (June 19–22).

Campbell, G., Crotty, J.H., 1990. 3-D seismic mapping for mine planning purposes at the South Deep Prospect. In: Ross-Watt, D.A.J., Robinson, P.D.K. (Eds.), SAIMM Symposium Series S10, 2: Proc. Internat. Deep Mining Conf. pp. 569–597.

Clowes, R.M., Green, A.G., Yorath, C.J., Kanasewich, E.R., West, G.F., Garland, G.D., 1984. LITHOPROBE — a national program for studying the third dimension of geology. J. Can. Soc. Explor. Geophys. 20, 23–39.

Cheraghi, S., Malehmir, A., Bellefleur, G., 2011. Crustal-scale reflection seismic investigations in the Bathurst Mining Camp, New Brunswick, Canada. Tectonophysics 506, 55–72. http://dx.doi.org/10.1016/j.tecto.2011.04.011.

Cheraghi, S., Malehmir, A., Bellefleur, G., 2012. 3D imaging challenges in steeply dipping mining environment: new lights on acquisition geometry and processing from the Brunswick No. 6 seismic data, Canada. Geophysics 77 (5), WC109–WC122. http://dx.doi.org/10.1190/GEO2011-0475.1.

Dankert, B.T., Hein, K.A.A., 2012. Evaluating the structural character and tectonic history of the Witwatersrand Basin. Precambrian Res. 177, 1–22.

Davidson, C.F., 1965. The mode and origin of banket orebodies. Institute of Mining and Metallurgy. Transcripts 74, 319–338.

Dehghannejad, M., Malehmir, A., Juhlin, C., Skyttä, P., 2012a. 3D constraints and finite-difference modeling of massive sulfide deposits: the Kristineberg seismic lines revisited, northern Sweden. Geophysics 77 (5), WC69–WC79. http://dx.doi.org/10.1190/GEO2011-0466.1.

Dehghannejad, M., Bauer, T., Malehmir, A., Juhlin, C., Weihed, P., 2012b. Crustal geometry of the central Skellefte district, northern Sweden — constraints from reflection seismic investigations. Tectonophysics 524–525, 87–99. http://dx.doi.org/10.1016/j.tecto.2011.12.021.

Dehghannejad, M., Juhlin, C., Malehmir, A., Skyttä, P., Weihed, P., 2010. Reflection seismic imaging of the upper crust in the Kristineberg mining area, northern Sweden. J. Appl. Geophys. 71, 125–136. http://dx.doi.org/10.1016/j.jappgeo.2010.06.002.

Duff, D., Hurich, C., Deemer, S., 2012. Seismic properties of the Voisey's Bay massive sulfide deposit: insights into approaches to seismic imaging. Geophysics 77, WC59–WC68.

Durrheim, R.J., Nicolaysen, L.O., Corner, B., 1991. A deep seismic reflection profile across the Archean–Proterozoic Witwatersrand Basin, South Africa. In: Meissner, R., et al. (Ed.), Continental lithosphere: deep seismic reflections. Am. Heophys. Geodynamics Series 22, 213–224.

Eaton, D.W., Adam, E., Milkereit, B., Salisbury, M., Roberts, B., White, D., et al., 2010. Enhancing base-metal exploration with seismic imaging. Can. J. Earth Sci. 47, 741–760.

Eaton, D.W., Milkereit, B., Salisbury, M., 2003. Hardrock seismic exploration: mature technologies adapted to new exploration targets, Foreword to Hardrock Seismic Exploration. In: Eaton, D.W., Milkereit, B., Salisbury, M.H. (Eds.), Hardrock Seismic Exploration. SEG, Tulsa, Oklahoma, pp. 1–6.

Eaton, D.W., 1999. Weak elastic-wave scattering from massive sulfide ore bodies. Geophysics 64, 289–299.

Ehsan, S.A., Malehmir, A., Dehghannejad, M., 2012. Re-processing and interpretation of 2D seismic data from the Kristineberg mining area, northern Sweden. J. Appl. Geophys. 80, 43–55. http://dx.doi.org/10.1016/j.jappgeo.2012.01.004.

Evans, B.J., Urosevic, M., Taube, A., 2003. Using surface-seismic reflection to profile a massive sulfide deposit at Mount Morgan, Australia. In: Eaton, D.W., Milkereit, B., Salisbury, M.H. (Eds.), Hardrock Seismic Exploration. SEG, Tulsa, Oklahoma, pp. 157–163.

Frimmel, H.E., Groves, D.I., Kirk, J., Ruitz, J., Chesley, J., Minter, W.E.L., 2005. The formation and preservation of the Witwatersrand goldfields, the world's largest gold province. Econ. Geol. 769–797 (100th Anniversary Volume).

Graton, L.C., 1930. Hydrothermal origin of the Rand gold deposits. Part I. Testimony of the conglomerates. Econ. Geol. 25 (Suppl. 3) (185 pp.).

Gregory, J., Journet, N., White, G., Lappalainen, M., 2011. Kevitsa Copper Nickel Project Finland: Technical Report for the Mineral Resources and Reserves of the Kevitsa Project. First Quantum Minerals Ltd.(52 pp.).

Gross, G.A., McLeod, C.R., 1980. A preliminary assessment of the chemical composition of iron formations in Canada. Can. Mineral. 18, 223–229.

Goleby, B., Korsch, R., Fomin, T., Bell, B., Nicoll, M.G., Drummond, B.J., et al., 2002. Preliminary 3-D geological model of the Kalgoorlie region, Yilgarn Craton, Western Australia, based on deep seismic-reflection and potential-field data. Aust. J. Earth Sci. 49, 917–933.

Juhlin, C., Elming, S.Å., Mellqvist, C., Öhlander, B., Weihed, P., Wikström, A., 2002. Crustal reflectivity near the Archaean–Proterozoic boundary in northern Sweden and implications for the tectonic evolution of the area. Geophys. J. Int. 150, 180–197.

Koivisto, E., Malehmir, A., Heikkinen, P., Heinonen, S., Kukkonen, I., 2012. 2D reflection seismic investigations at the Kevitsa Ni–Cu–PGE deposit, northern Finland. Geophysics 77 (5), WC149–WC162. http://dx.doi.org/10.1190/GEO2011-0496.1.

Koivisto, E., Malehmir, A., Voipio, T., in preparation. 3D lithological and structural modeling of the Kevitsa 2D and 3D seismic data sets.

Korja, A., Heikkinen, P., 2005. The accretionary Svecofennian orogen-insight from the BABEL profiles. Precambrian Res. 136, 241–268.

Kukkonen IT, Lahti I, Heikkinen P, 2009. HIRE Working Group. HIRE Seismic Reflection Survey in the Kevitsa Ni–PGE deposit, North Finland. Espoo, Finland: Geological Survey of Finland, Unpublished report Q 23/2008/59.

Kukkonen, I.T., Lahtinen, R., 2003. Finnish Reflection Experiment FIRE 2001–2005. Special Paper, 43. Geological Survey of Finland, Espoo, Finland (247 pp. ISBN 951-690-963-9).

Kukkonen, I.T., Heikkinen, P., Heinonen, S., Laitinen, J., HIRE Working Group, 2011. Reflection seismics in exploration for mineral deposits: initial results from the HIRE project. In: Nenonen, K., Nurmi, P.A. (Eds.), Geoscience for Society 125th Anniversary Volume. Special Paper, 49. Geological Survey of Finland, Espoo, Finland, pp. 49–58.

Lei, J., Zhao, D., 2005. P-wave tomography and origin of the Changbai intraplate volcano in Northeast Asia. Tectonophysics 397, 281–295.

Lei, J., Zhao, D., Su, Y., 2009. Insight into the origin of the Tengchong intraplate volcano and seismotectonics in southwest China from local and teleseismic data. J. Geophys. Res. 114, B05302. http://dx.doi.org/10.1029/2008JB005881.

Luff, W.M., 1995. A history of mining in the Bathurst area, northern New Brunswick, Canada. CIM Bull. 88, 63–68.

Malehmir, A., Andersson, M., Lebedev, M., Urosevic, M., Mikhaltsevitch, V., 2013. Experimental estimation of velocities and anisotropy of a series of Swedish crystalline rocks and ores. Geophys. Prospect. 61, 153–167. http://dx.doi.org/10.1111/j.1365-2478.2012.01063.x.

Malehmir, A., Juhlin, C., Wijns, C., Urosevic, M., Valasti, P., Koivisto, E., 2012a. 3D reflection seismic investigation for open-pit mine planning and exploration in the Kevitsa Ni–Cu–PGE deposit, northern Finland. Geophysics 77 (5), WC95–WC108. http://dx.doi.org/10.1190/GEO2011-0468.1.

Malehmir, A., Durrheim, R., Bellefleur, G., Urosevic, M., Juhlin, C., White, D., et al., 2012b. Seismic methods in mineral exploration and mine planning: a general overview of past and present case histories and a look into the future. Geophysics 77 (5), WC173–WC190. http://dx.doi.org/10.1190/GEO2012-0028.1.

Malehmir, A., Dahlin, P., Lundberg, E., Juhlin, C., Sjöström, H., Högdahl, K., 2011. Reflection seismic investigations in the Dannemora area, central Sweden: insights into the geometry of poly-phase deformation zones and magnetite–skarn deposits. J. Geophys. Res. 116, B11307. http://dx.doi.org/10.1029/2011JB008643.

Malehmir, A., Bellefleur, G., 2010. Reflection seismic imaging and physical properties of base-metal and associated iron deposits in the Bathurst Mining Camp, New Brunswick, Canada. Ore Geol. Rev. 38, 319–333. http://dx.doi.org/10.1016/j.oregeorev.2010.08.002.

Malehmir, A., Juhlin, C., 2010. An investigation of the effects of the choice of stacking velocities on residual statics for hardrock reflection seismic processing. J. Appl. Geophys. 72, 28–38. http://dx.doi.org/10.1016/j.jappgeo.2010.06.008.

Malehmir, A., Bellefleur, G., 2009. 3D seismic reflection imaging of volcanic-hosted massive sulfide deposits: insights from re-processing Halfmile Lake data, New Brunswick, Canada. Geophysics 74, B209–B219. http://dx.doi.org/10.1190/1.3230495.

Malehmir, A., Thunehed, H., Tryggvason, A., 2009. The Palaeoproterozoic Kristineberg mining area, northern Sweden: results from integrated 3D geophysical and geologic modeling, and implications for targeting ore deposits. Geophysics 74, B9–B22. http://dx.doi.org/10.1190/1.3008053.

Malehmir, A., Tryggvason, A., Lickorish, H., Weihed, P., 2007. Regional structural profiles in the western part of the Palaeoproterozoic Skellefte ore district, northern Sweden. Precambrian Res. 159, 1–18.

Malehmir, A., Tryggvason, A., Juhlin, C., Rodriguez-Tablante, J., Weihed, P., 2006. Seismic imaging and potential field modeling to delineate structures hosting VHMS deposits in the Skellefte Ore District, northern Sweden. Tectonophysics 426, 319–339.

Manzi, M.S.D., Gibson, M.A.S., Hein, K.A.A., King, N., Durrheim, R.J., 2012a. Application of 3D seismic techniques in evaluation of ore resources in the West Wits Line goldfield and portions of the West Rand goldfield, South Africa. Geophysics 77, WC163–WC171.

Manzi, M., Durrheim, R.J., Hein, K.A.A., King, N., 2012b. 3D edge detection seismic attributes used to map potential conduits for water and methane in deep gold mines in the Witwatersrand Basin, South Africa. Geophysics 77, WC133–WC147.

Manzi, M.S.D., Hein, K.A.A., King, N., Durrheim, R.J., in press. Neoarchaean tectonic history of the Witwatersrand Basin and Ventersdorp Supergroup: new constraints from high-resolution 3D seismic reflection data. Tectonophysics http://dx.doi.org/j.tecto.2013.01.014/j.tecto.2013.01.014.

Maruyama, S., Okamoto, K., 2007. Water transportation from the subducting slab into the mantle transition zone. Gondwana Res. 11, 148–165.

Matthews, L., 2002. Base metal exploration: looking deeper and adding value with seismic data. Can. Soc. Explor. Geophys. Rec. 27, 37–43.

McCutcheon, S.R., 1992. Base-metal deposits of the Bathurst–Newcastle district: characteristics and depositional models. Explor. Min. Geol. 1, 105–119.

Meier, D.L., Heinrich, C.A., Watts, M.A., 2009. Mafic dykes displacing Witwatersrand gold reefs: evidence against metamorphic–hydrothermal ore formation. Geology 37, 607–610.

Milkereit, B., Berrer, E.K., King, A.R., Watts, A.H., Roberts, B., Adam, E., et al., 2000. Development of 3-D seismic exploration technology for deep nickel–copper deposits — a case history from the Sudbury Basin, Canada. Geophysics 65, 1890–1899.

Milkereit, B., Eaton, D., 1998. Imaging and interpreting the shallow crust. Tectonophysics 286, 5–18.

Milkereit, B., Eaton, D.W., Wu, J., Perron, G., Salisbury, M.H., Berrer, E., et al., 1996. Seismic imaging of massive sulphide deposits: part II. Reflection seismic profiling. Econ. Geol. 91, 829–834.

Mutanen, T., 1997. Geology and ore petrology of the Akanvaara and Koitelainen mafic layered intrusions and the Keivitsa–Satovaara layered complex, northern Finland. Bulletin, 395. Geological Survey of Finland, Espoo, Finland (Report available at: www.arkisto.gsf.fi/bul/BT395.pdf).

Muntean, J.L., Frimmel, H.E., Phillips, N., Law, J., Myers, R., 2005. Controversies on the origin of world-class gold deposits, part II: Witwatersrand gold deposits. Soc. Econ. Geol. Newsl. 60, 7–19.

Mutanen, T., Huhma, H., 2001. U–Pb geochronology of the Koitelainen, Akanvaara and Keivitsa mafic layered intrusions and related rocks. In: Vaasjoki, M. (Ed.), Radiometric Age Determinations from Finnish Lapland and Their Bearing on the Timing of Precambrian Volcano–Sedimentary Sequences. : Special Paper, 33. Geological Survey of Finland, Espoo, Finland, pp. 229–246.

Nedimović, M.R., West, G.F., 2003. Crooked-line 2D seismic reflection imaging in crystalline terrains: part 1, data processing. Geophysics 68, 274–285.

Odgers, A.T.R., Hinds, R.C., von Gruenewaldt, G., 1993. Interpretation of a seismic reflection survey across the southern Bushveld Complex. S. Afr. J. Geol. 96, 205–212.

Phillips, G.N., Myers, R.E., 1989. The Witwatersrand goldfields: part II. An origin for Witwatersrand gold during metamorphism and associated alteration. Econ. Geol. Monogr. 6, 598–608.

Phillips, G.N., Law, J.D.M., Stevens, G., 1997. Alteration, heat and Witwatersrand gold: 111 years after Harrison and Langlaagte. S. Afr. J. Geol. 100, 377–392.

Pretorius, C.C., Muller, M.R., Larroque, M., Wilkins, C., 2003. A review of 16 years of hard rock seismics on the Kaapvaal Craton. In: Milkereit, B., Eaton, D., Salisbury, M. (Eds.), Hardrock Seismic Exploration. SEG, Tulsa, Oklahoma, pp. 247–268.

Pretorius, D.A., 1981. Gold and uranium in quartz–pebble conglomerates. Econ. Geol. 117–138 (75th Anniversary Volume).

Pretorius, C.C., Jamison, A., Irons, C., 1989. Seismic exploration in the Witwatersrand Basin, Republic of South Africa. Proceedings of Exploration, 87. Ontario Geol. Sur, pp. 241–253 (Spec. 3).

Pretorius, D.A., 1989. The sources of Witwatersrand gold and uranium: "A continued difference of opinion". Information Circular no. 206.Economic Geology Research Unit, University of Witwatersrand, Johannesburg (43 pp.).

Rasmussen, B., Fletcher, I.R., Muhling, J.R., Mueller, A.G., Hall, G.C., 2007. Bushveld-aged fluid flow, peak metamorphism, and gold mobilization in the Witwatersrand Basin, South Africa: constraints from in situ SHRIMP U–Pb dating of monazite and xenotime. Geology 35, 931–934.

Reed K., 1993. Seismic reflection surveying for mining exploration applications, a review of practice past and current with an outlook for the future. Unpublished report. Mineral Industry Technology Council of Canada. 219 pp.

Ruskey, F., 1981. High resolution seismic methods for hard rock mining. Premining Investigations for Hardrock Mines: Proc. U.S. Bureau of Mines Technology Transfer Seminar. Denver, pp. 4–28.

Salisbury, M.H., Milkereit, B., Bleeker, W., 1996. Seismic imaging of sulfide deposits: part I. Rock properties. Econ. Geol. 91, 821–828.

Salisbury, M.H., Harvey, C.W., Matthews, L., 2003. The acoustic properties of ores and host rocks in hardrock terranes. In: Milkereit, B., Eaton, D., Salisbury, M. (Eds.), Hardrock Seismic Exploration. SEG, Tulsa, Oklahoma, pp. 9–19.

Stevens, G., Gibson, R.L., Droop, G.T.R., 1997. Midcrustal granulite facies metamorphism in the central Kaapvaal Craton: the Bushveld Complex connection. Precambrian Res. 82, 113–132.

Stolz, E., Urosevic, M., Connors, K., 2004. Reflection seismic surveys at St Ives gold mine, WA. Preview 111, 79.

Tryggvason, A., Malehmir, A., Rodriguez-Tablante, J., Juhlin, C., Weihed, P., 2006. Seismic reflection investigations in the western part of the Palaeoproterozoic Skellefte Ore District, northern Sweden. Econ. Geol. 101, 1039–1054.

Urosevic, M., Stoltz, E., Massey, S., 2005. Seismic Exploration for Gold in a Hard Rock Environment — Yilgarn Craton, Western Australia. 67th Meeting, EAGE, Expanded Abstracts, G009.

van Staal, C.R., 1987. Tectonic setting of the Tetagouche group in northern New Brunswick: implications for plate tectonic models of the northern Appalachians. Can. J. Earth Sci. 24, 1329–1351.

van Staal, C.R., 1994. Brunswick subduction complex in the Canadian Appalachians: record of the Late Ordovician to Late Silurian collision between Laurentia and the Gander margin of Avalon. Tectonics 13, 946–962.

van Staal, C.R., Wilson, R.A., Rogers, N., Fyffe, L.R., Langton, J.P., McCutcheon, S.R., et al., 2003. Geology and tectonic history of the Bathurst Supergroup, Bathurst Mining Camp and its relationships to coeval rocks in southwestern New Brunswick and adjacent Maine — a synthesis. In: Goodfellow, W.D., McCutcheon, S.R., Peter, J.M. (Eds.), Massive sulfide deposits of the Bathurst Mining Camp, New Brunswick, and northern Maine: Economic Geology Monograph, 11, pp. 37–60.

Williams, N.C., Lane, R., Lyons, P., 2004. Regional constrained 3D inversion of potential field data from the Olympic Cu–Au province, South Australia. Preview 109, 30–33.

Willman, C.E., Korsch, R.J., Moore, D.H., Cayley, R.A., Lisitsin, V.A., Rawling, T.J., et al., 2010. Crustal-scale fluid pathways and source rocks in the Victorian Gold Province, Australia: insight from deep seismic reflection profiles. Soc. Econ. Geol. 105, 895–915.

Wills, A.O., Lentz, D.R., Roy, G., 2006. Chemostratigraphy at the Brunswick No. 6 volcanic-sediment-hosted massive sulfide deposit, New Brunswick: resolving geometry from drill core in deformed felsic volcanic rocks. Explor. Min. Geol. 15, 35–51.

White, D.J., Secord, D., Malinowski, M., 2012. 3D seismic imaging in the Flin Flon VMS mining camp: part I — seismic results. Geophysics 77, WC47–WC58.

Wu, J., 1996. Potential pitfalls of crooked-line seismic reflection surveys. Geophysics 61, 277–281.

Zaleski, E., Eaton, W.D., Milkereit, B., Roberts, B., Salisbury, M., Petrie, L., 1997. Seismic reflections from subvertical diabase dikes in an Archean terrane. Geology 25, 707–710.

Zhao, D., 2007. Seismic images under 60 hotspots: search for mantle plumes. Gondwana Res. 12, 335–355.

Zhao, B., Robb, L.J., Harris, C., Jordaan, L.J., 2006. Origin of hydrothermal fluids and gold mineralization associated with the Ventersdorp Contact Reef, Witwatersrand Basin, South Africa: constraints from S, O, and H isotopes. Geol. Soc. Am. Spec. Pap. 405, 333–352. http://dx.doi.org/10.1130/2006.2405(17).

Seismic attribute analysis to enhance detection of thin gold-bearing reefs: South Deep gold mine, Witwatersrand basin, South Africa

M.S.D. Manzi[1]✉, K.A.A. Hein[2], R.Durrheim[3], and N.King[4]

[1] School of Geosciences, University of the Witwatersrand Johannesburg, PBag 3, WITS, 2050, Republic of South Africa; E-mail: musa.manzi@students.wits.ac.za

[2] School of Geosciences, University of the Witwatersrand Johannesburg, PBag 3, WITS, 2050, Republic of South Africa; E-mail: kim.ncube-hein@wits.ac.za

[3] School of Geosciences, University of the Witwatersrand Johannesburg, PBag 3, WITS, 2050, Republic of South Africa; E-mail: raymond.durrheim@wits.ac.za

[4]South Deep gold mine; Gold Fields Limited, Republic of South Africa; Email: nick.king@goldfields.co.za

ABSTRACT

The gold-bearing Upper Elsburg Reef clastic wedge (UER) in the South Deep gold mine in the Witwatersrand basin (South Africa) hosts the highly auriferous basal conglomerate known as the Elsburg Conglomerate (EC) reef. The reef is less than 20 m thick and together with quartzite and conglomerate beds in the UER (1-120 m thick) is below the seismic tuning thickness, or the dominant quarter wavelength. They are extremely difficult to identify on migrated seismic sections using traditional amplitude interpretations. In order to enhance the detection of the EC reef and its subcrop position against the overlying Ventersdorp Contact Reef (VCR), complex-trace seismic attributes, or instantaneous attributes and volume attribute analysis were applied on prestack time migrated (PSTM) seismic sections. In particular, the instantaneous phase and paraphase allowed the clear identification of the continuity of the EC reef, and overlapping and interfering wavelets produced by the convergence of VCR and the EC reef. In addition, these attributes increased confidence in the interpretation of the EC, in particular its offsets (faults), and its depth. A high correlation between the seismically determined depth of the EC reef and borehole intersections was observed, with several depth discrepancies below the vertical seismic resolution limit (~ 25 m). This information can now be incorporated into the current mine geological model, thus improving the resource evaluation of the Upper Elsburg Reef in the South Deep gold mine.

Key words: Witwatersrand basin, 3D seismic method, seismic attributes, seismic resolution, tuning thickness

1. Introduction

The 3D seismic reflection technique had its origin in the oil industry in the 1960s, where it was used to locate oil and gas reservoirs. In recent years, the 3D reflection seismic technique has played an important role in the exploration of the Witwatersrand basin in South Africa, being used to image and evaluate gold-bearing horizons for mine planning and production purposes, and for better imaging of faults that act as conduits for methane and water to the mining levels (Campbell and Crotty, 1988; Weder, 1994; Gibson et al., 2000; Pretorius et al., 2000; Salisbury et al., 2003; Stevenson et al., 2003; Gibson, 2005; Manzi et al. 2012a, b). To date, 3D seismic surveys have been acquired and reported in major metallogenic provinces worldwide, being used to explore for ore deposits and constrain regional tectonic interpretations that play a key role in understanding ore metallogenesis (Pretorius et al., 2003; Jolley et al., 2004; Trickett et al., 2004; Dehghannejad et al., 2012; Duff et al., 2012; Malehmir et al., 2012; Malinowski et al., 2012; Manzi et al., 2012a; Malehmir et al., 2013; Manzi et al., 2013).

In 3D seismic studies by Manzi et al. (2012a, b), many conventional and new interpretation techniques (mainly horizon-based attribute analysis), such as dip, azimuth and edge detection, were used to detect fault offsets that displaced the Ventersdorp Contact Reef (VCR) and Black Reef (BLR) in the West Wits Line goldfields by as little as 10 m. However, in the South Deep development areas, which are situated west of the Kloof gold mine in the West Rand goldfields, Manzi et al. (2012a) found it difficult to identify and consistently track thin Elsburg reefs on conventional amplitude displays due to severe destructive interference resulting from overlapping wavelets, and because the thickness of the reefs is below the vertical seismic resolution limit (tuning thickness). The problem of detecting thin-reefs, wavelet doublets and interference is well known in the oil and gas industry where attempts to

image the top and bottom of thin reservoirs has proved challenging (Widess, 1973; Chopra et al., 2006; Chopra et al., 2009; Purnomo and Harith, 2010). Several techniques including seismic inversion have been developed to try and address the problem (Kallweith and Wood, 1982; Russel, 1988; Chopra et al., 2006; Hall, 2006; Zeng, 2009). However, the use of complex-trace seismic attribute analysis to enhance detection of gold-bearing reefs with thicknesses below the seismic resolution limit, such as the Elsburg Conglomerate reef (EC ~ 20 m) in the South Deep gold mine (Fig. 1), has not been attempted before.

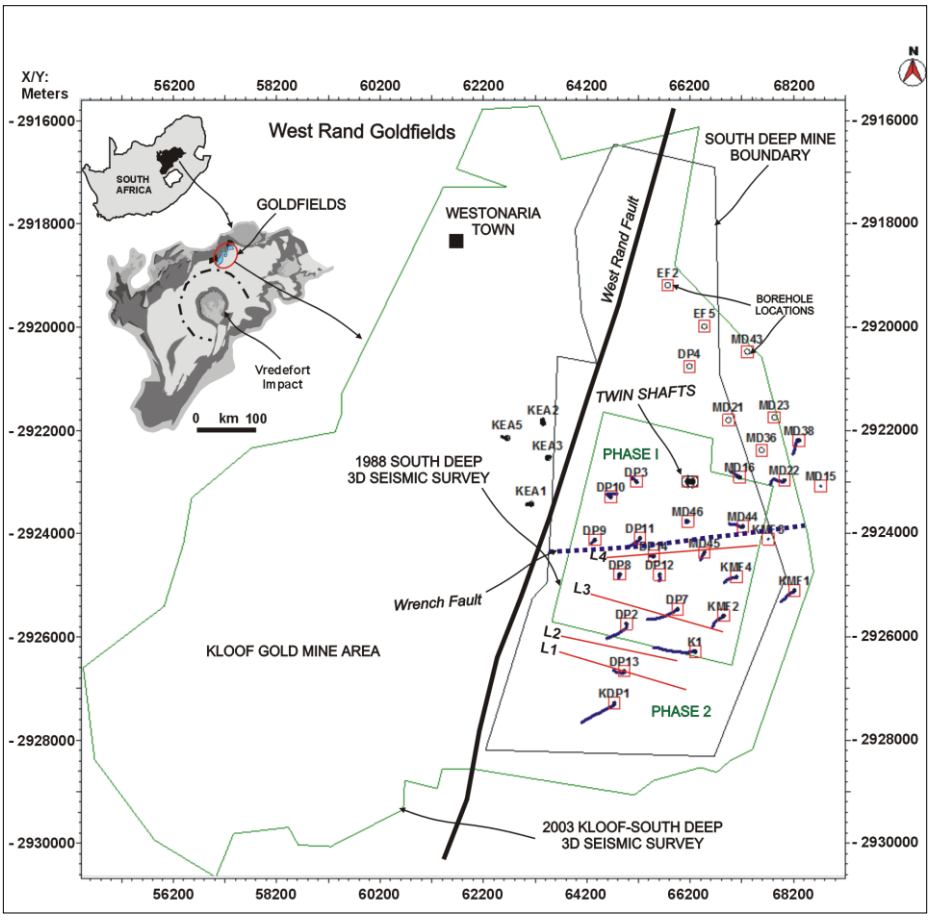


Fig. 1. *The geological map showing the study area (top left) (after Dankert and Hein, 2010). The seismic base map showing the location of the 2003 Kloof-South Deep 3D seismic survey and 1988 South Deep 3D seismic survey. The red rectangles and lines (L1-L4) represent the borehole locations and seismic sections across the South Deep seismic survey, respectively.*

Seismic resolution is determined by the seismic wavelength (λ), which, in turn, depends on the seismic velocity (v) of the rocks and the frequency (f) of the seismic wavelet. Vertical seismic resolution is defined as the ability to distinguish two close reflectors at different depths (Liu and Marfurt, 2006; Zhang et al., 2009). The loss of resolution is caused by the convolution of the seismic wavelets with the Earth's reflectivity. Seismic wavelet is not a narrow beam or a sharp impulse, but a disturbance with a finite duration. Also, the Earth acts as a low pass filter. High frequencies are more rapidly absorbed, and thus the dominant seismic wavelength increases with depth, resulting in poor resolution of thin horizons (Chung and Lawton, 1991; Yilmaz et al., 2001; Chopra and Marfurt, 2008; Purnomo and Harith, 2010). Furthermore, the strength of the seismic reflection that arises at the lithological boundaries depends on the contrast in the acoustic impendence.

The one-quarter dominant seismic wavelength ($\lambda/4$) is often described as the tuning thickness, which is the thickness where constructive interference occurs between the wavelet reflected from the top and base of the layer (Chopra et al., 2006; Hanneing and Paton, 2012).

The South Deep gold mine seismic data are characterized by a seismic wavelet with the dominant peak frequency of 65 Hz, an average velocity of 6500 m/s, and wavelength of 100 m (Manzi et al., 2012 a). Thus the top and bottom of the gold-bearing reefs, with a thickness less than 25 m, may not be detected through conventional amplitude-derived interpretations. This is because seismic amplitude variations are related to the seismic waves resulting from thin conglomerate units confined within unconformably overlying and underlying rocks (Fig. 2). Moreover, it is difficult to identify the subcrop position, which is a position in the seismic section where overlapping seismic wavelets interfere due to a smaller separation between

reflecting horizons. Thus conventional picking on seismic traces with interfering wavelets can lead to misinterpretations (Fig. 3).

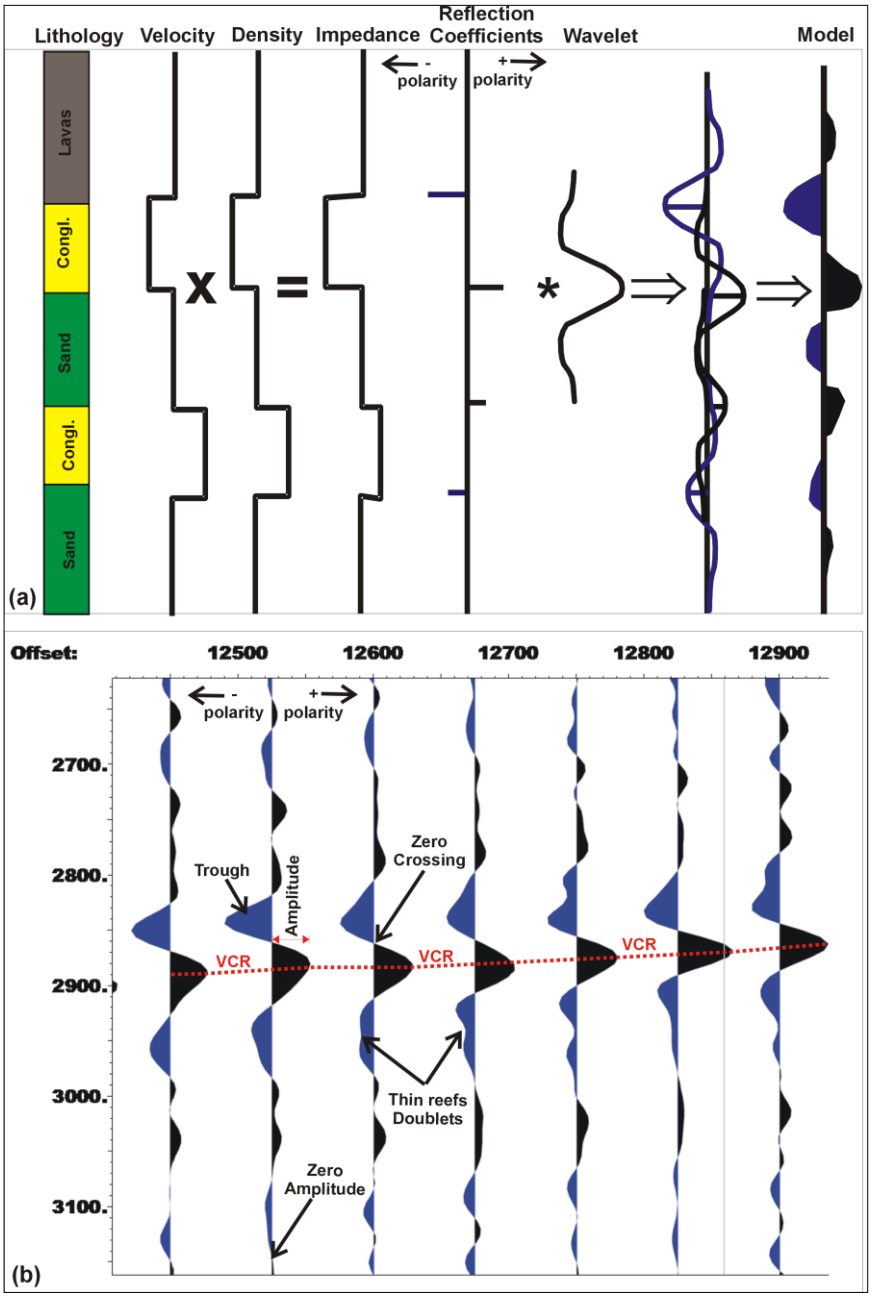


Fig. 2. *(a) The model showing reflection coefficient (RC) series as defined from lithological boundaries. The convolved RC with the field wavelet produces a simulated raw field trace showing both a trough and peak of the wavelet. (b) Wiggle trace section extracted from South Deep data volume. The composite trace has a reflection with 90° phase. Black is a positive polarity and blue is a negative polarity. The highest amplitude event corresponds to the top of the Ventersdorp Contact Reef (VCR) and the summed wavelets, or doublets correspond to the thin reefs.*

The upper Elsburg Reef clastic wedge package (UER) of the South Deep gold mine lies at a depth of 2900 m to 3500 m below the surface. It forms the footwall to the gold-bearing Ventersdorp Contact Reef (VCR ~1.5 m thick) and can be best described as an east-dipping, divergent clastic wedge that hosts a low acoustic-impedance package of stacked gold-bearing reefs (Fig. 4), the richest being the EC at the base of UER. The UER thickens to 120 m near the eastern boundary of the mining permit (Fig. 4; Erismann, 2007; Anonymous, 2011).

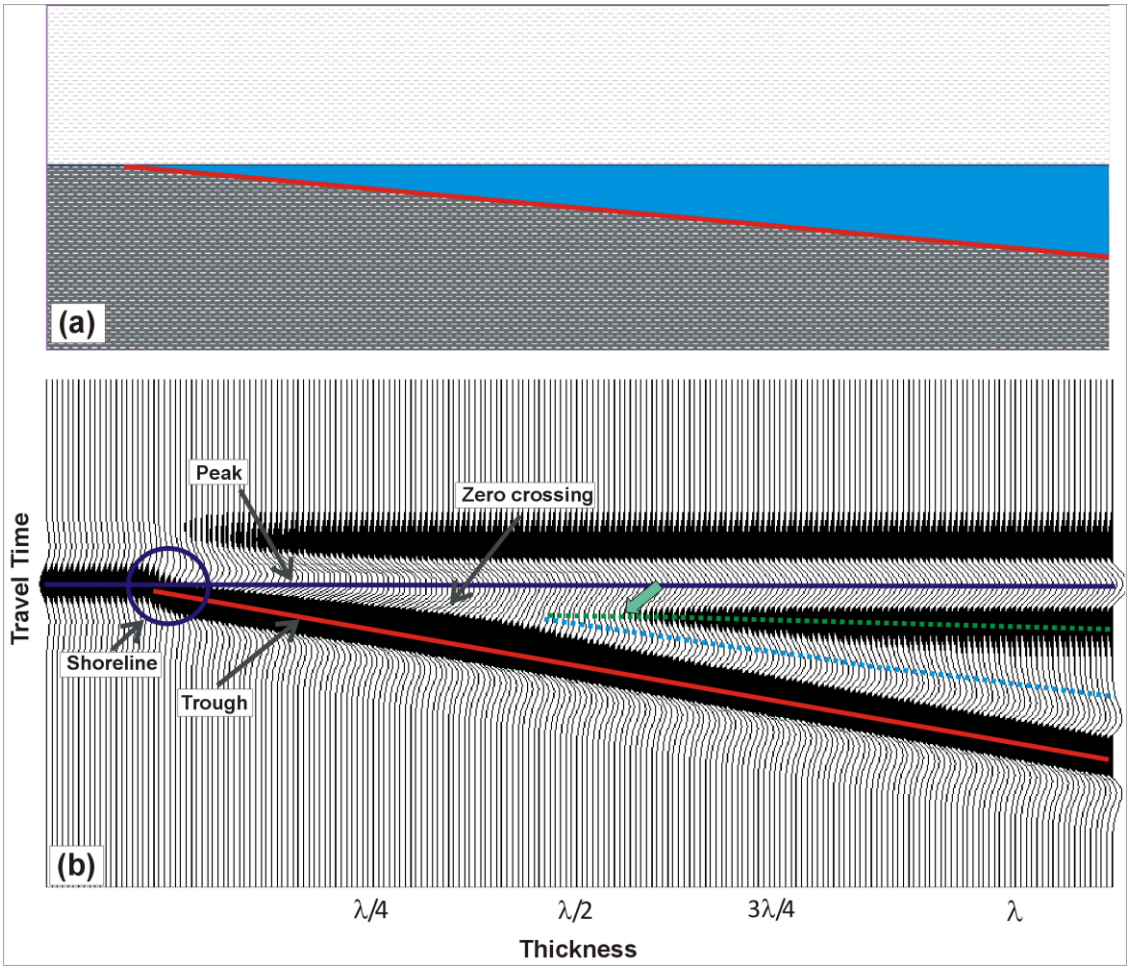


Fig. 3. *(a) Geological wedge-shaped models. The top layer is the metabasalts of the Klipriviersberg (white); the layer below is quartzite (black) and the middle layer (blue) is the alternation of sand, quartzite and conglomerates. (b) Synthetic seismic section of the wedge model, with a wavelet dominant frequency of 65 Hz. The wedge thickness ranges from λ/4 (close to the shoreline or subcrop position) to λ (away from the shoreline position).*

The UER package is unconformably overlain by the higher-impedance layers of the Ventersdorp Contact Reef (VCR), which are in turn overlain by metabasalts of the Klipriviersberg Group. The UER is underlain by quartzites of the Elsburg Formation, with the higher-impedance layers of Booysens Shale Formation lying deeper in the footwall (Fig. 4).

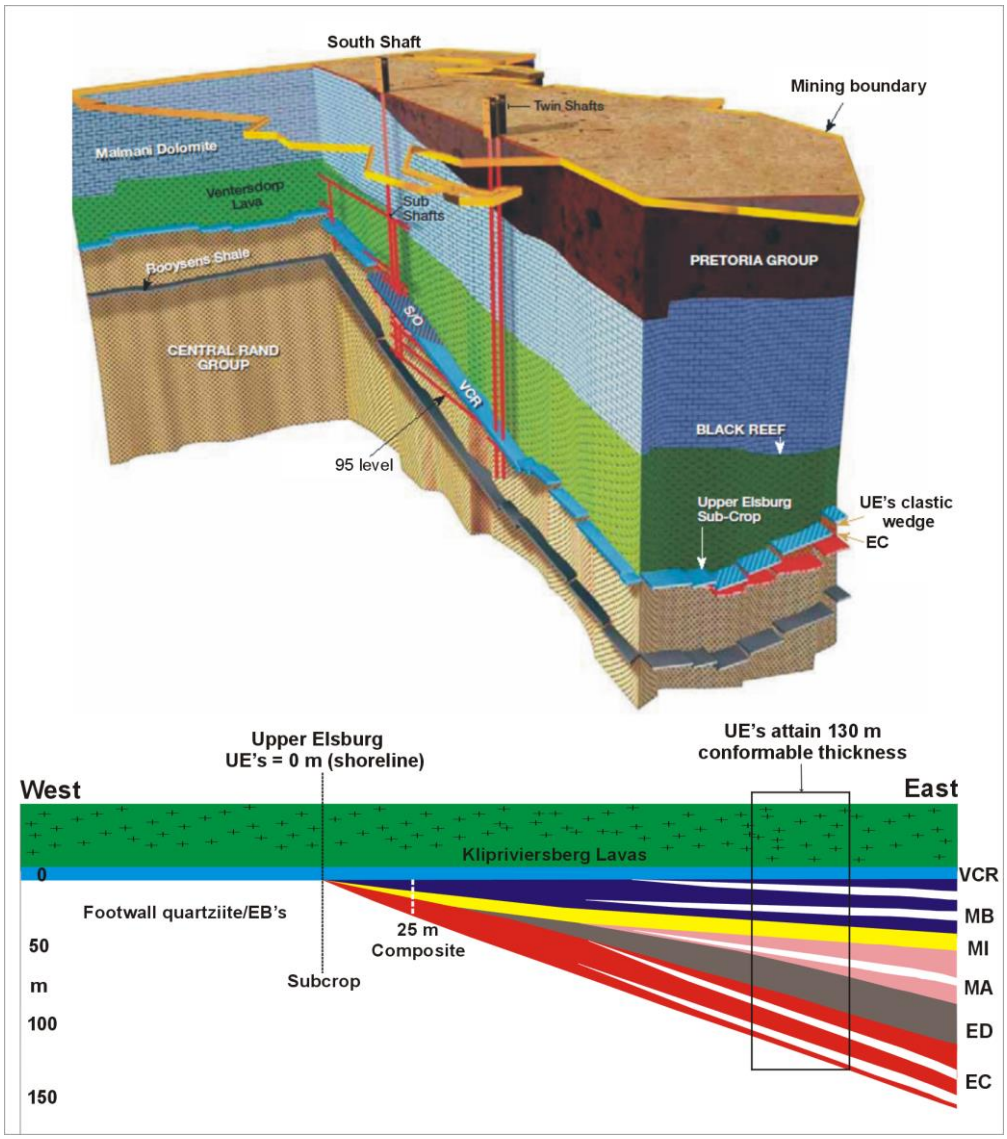


Fig. 4. *Three (top) and two (bottom) dimensional schematic illustration of an easterly divergent Upper Elsburg clastic wedge (UER) with low acoustic-impedance package of multi-stacked gold-bearing reefs. The maximum thickness of the wedge is approximately 120 – 130 metres in the eastern boundary of the mine (After Erismann, 2007; South Deep Gold Mine, 2007).*

Additionally, the metabasalts of the Klipriviersberg Group (~6400 m/s velocity and ~2.90 g/cm^3 density) of the Ventersdorp Supergroup and the quartzite units (~5700 m/s velocity and 2.67 g/cm^3 density) of the Central Rand Group provide a major and laterally extensive impedance contrast, generating a very strong and continuous seismic reflection which coincides well with the mapped position of the VCR (Figs. 2-4). Thus the VCR is detected seismically. This is not the case for the gold-bearing reefs of the UER. A decrease in acoustic impedance or interference due to stratigraphic variations between interbedded quartzite and conglomerate units makes an individual reef within the UER undetectable by seismics. This is particularly evident in the western half of the mining area where the UER package is excised and the gold-bearing EC comes close to, or subcrops (contacts) against the VCR and the overlying metabasalts (Arthur et al., 1990; Erismann, 2007) (Figs. 3-4).

In fact, as the EC reef in the UER subcrops against the VCR, the wavelet of the negative reflection from the top of the VCR constructively interferes with the negative reflection from the top of EC reef (Arthur et al., 1990; Erismann, 2007). The UER reaches tuning thickness ($\lambda/4$) where the interbedded quartzite and conglomerate reefs converge against the base of the VCR (known locally as the shoreline), and is also where constructive interference reaches a peak (Figs. 3-4). Below the tuning thickness, the conventional amplitude attribute display is not able to detect subtle and significant changes between the wavelets.

In this study, we look closely at the effect of wavelets on the highly auriferous but thin EC reef, and subsequently show how the complex-trace seismic attribute displays, such as instantaneous phase and paraphrase, can enhance the detection of this reef. In addition, we use these attributes to (i) identify the subcrop position of the EC against the VCR, and (ii) detect the continuity of faults between VCR and EC levels. Volume attributes (e.g. zero-

crossing) and isopach maps were also used to constrain the position of the EC subcrop that had partially been constrained during routine mine underground mapping (Fig. 5).

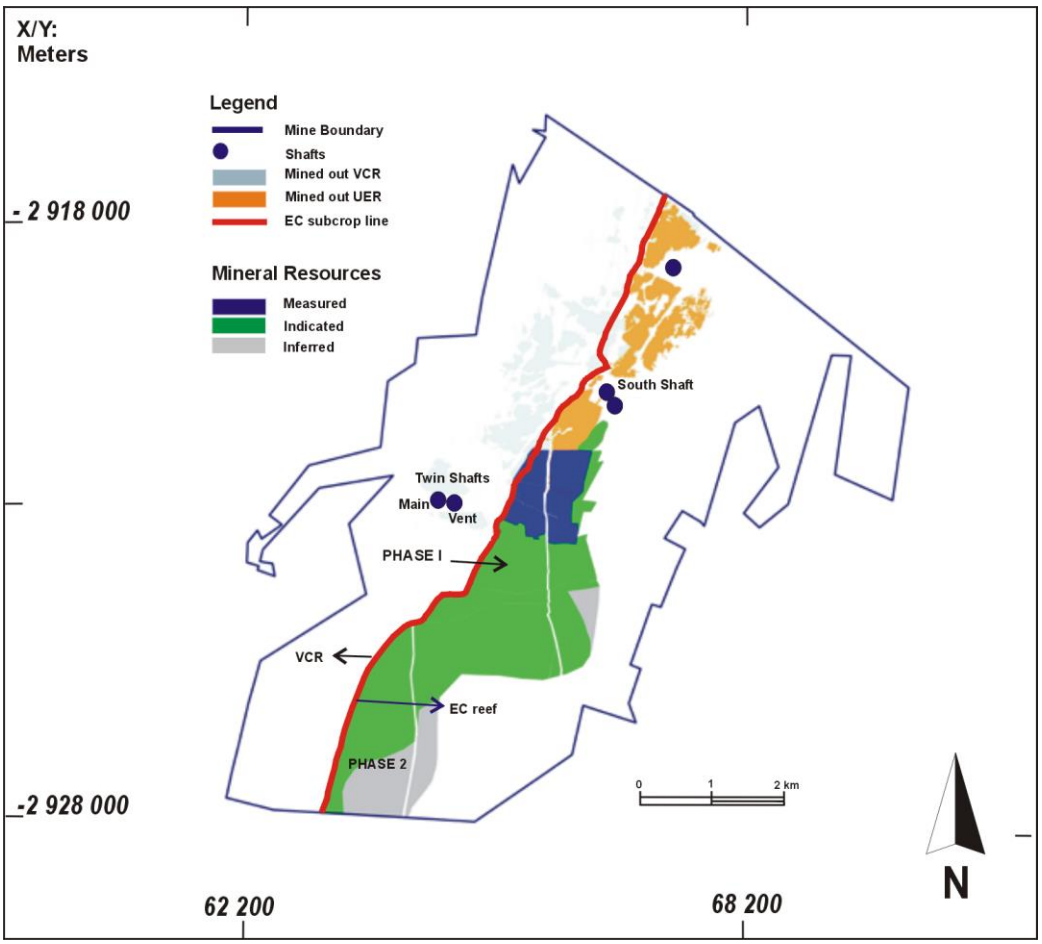


Fig. 5. *South Deep underground resource model showing the Elsburg Conglomerate (EC) subcrop positioning, mined-out and development areas.*

2. South Deep gold mine and gold-bearing reefs

The South Deep ore body is one of the largest known gold deposits in the Archean Witwatersrand basin and is owned and operated by Gold Fields Ltd. The Witwatersrand basin is the world's largest gold producing region, having yielded about 40% of all the gold ever mined. The Witwatersrand gold ore bodies occur in fluvial conglomerate beds termed reefs (Krapež, 1985; Arthur et al., 1990; Jolley et al., 2004; Erismann, 2007). The gold generally occurs together with pyrite, uranite and bitumen on degradational surfaces. High gold grades occur in massive, clast-supported, and gravel-sized oligomict to polymict conglomerates, while low grades are found on scour surfaces in pebbly sands (Engelbrecht et al., 1986; Robb and Meyer, 1995; Pretorius et al., 2000).

The South Deep gold mine is situated in the West Rand goldfield on the northern margin of the Archean Witwatersrand basin (see Fig. 1). The mine lies east of the West Rand Fault (WRF) and is wholly situated in its faulted and folded footwall. The WRF trends north-northeast, with a steep dip of 65°-70° west. It has been defined as a tear or scissor fault by Manzi et al. (2013). It has a maximum normal offset of 1.5 km and maximum sinistral offset of 600 m, but is hinged in the south-southeast.

The South Deep gold mine is serviced by the Twin Shaft Complex and South Shaft Complex, with its main shaft and two sub-vertical shafts (Fig. 5). The mining area is subdivided into Phase I and Phase II, which are development areas to the north and south of the Wrench Fault system, respectively (Figs. 1 and 5). The VCR of the Venterspost Conglomerate Formation, and the UER of the Central Rand Group are the major economic sources of gold in the South Deep gold mine, with resources of 81.4 Moz. and mineral

reserves at 39.6 Moz. and an estimated Life of Mine that extends to 2080 (Anonymous, 2011). The UER makes-up approximately 93% of the reserve of the South Deep gold mine, while the VCR (~1.5 m thick conglomerate unit) makes up 7%. The EC provides the best gold grades and value within the mine (Arthur et al., 1990; Erismann, 2007).

A generalized stratigraphic column through the South Deep Phase II area is shown in Fig. 6, and detailed descriptions of the geology and seismic stratigraphy of the Witwatersrand basin has been reported by Vermaakt and Chunnet (1994), Gibson et al. (2000), Jolley et al. (2004; 2007), Dankert and Hein (2010), Mambane et al. (2011), and Manzi et al. (2012 a, b; 2013) and others. In summary, the Central Rand Group is divided into the lower Johannesburg Supergroup and upper Turffontein Subgroup. The basin-wide Booysens Shale Formation (sequence of laminated shale units), is situated at the top of the Johannesburg Subgroup and forms a sequence stratigraphic boundary that separates the Johannesburg and Turffontein subgroups. The Booysens Shale Formation is a prominent stratigraphic and reflective seismic marker (Minter, 1982; McCarthy, 2006; Manzi et al., 2012a).

The Turffontein Subgroup is divided into the Kimberley, Elsburg and Mondeor formations. The Elsburg Formation is dated at 2914 ± 12 Ma (Armstrong, 1991; youngest U-Pb detrital zircon SHRIMP age; Robb and Meyer, 1995), and subdivided into the (lower) Waterpan and (upper) Modderfontein members (Figs. 4-6). The Waterpan and Modderfontein members are known locally as the Upper Elsburg Individuals and Upper Elsburg Massives, respectively (Anonymous, 2011).

The Upper Elsburg Individuals consists of well-defined conglomerate units known as EA, EB, EC and ED units; these are interbedded with quartzwackes (Arthur et al., 1990;

Erismann, 2007; Anonymous, 2011). In contrast, the Upper Elsburg Massives are made up of the conglomerate packages that are known as MA, MI and MB units (Figs. 4-6). Collectively, the Upper Elsburg massives are seismically transparent.

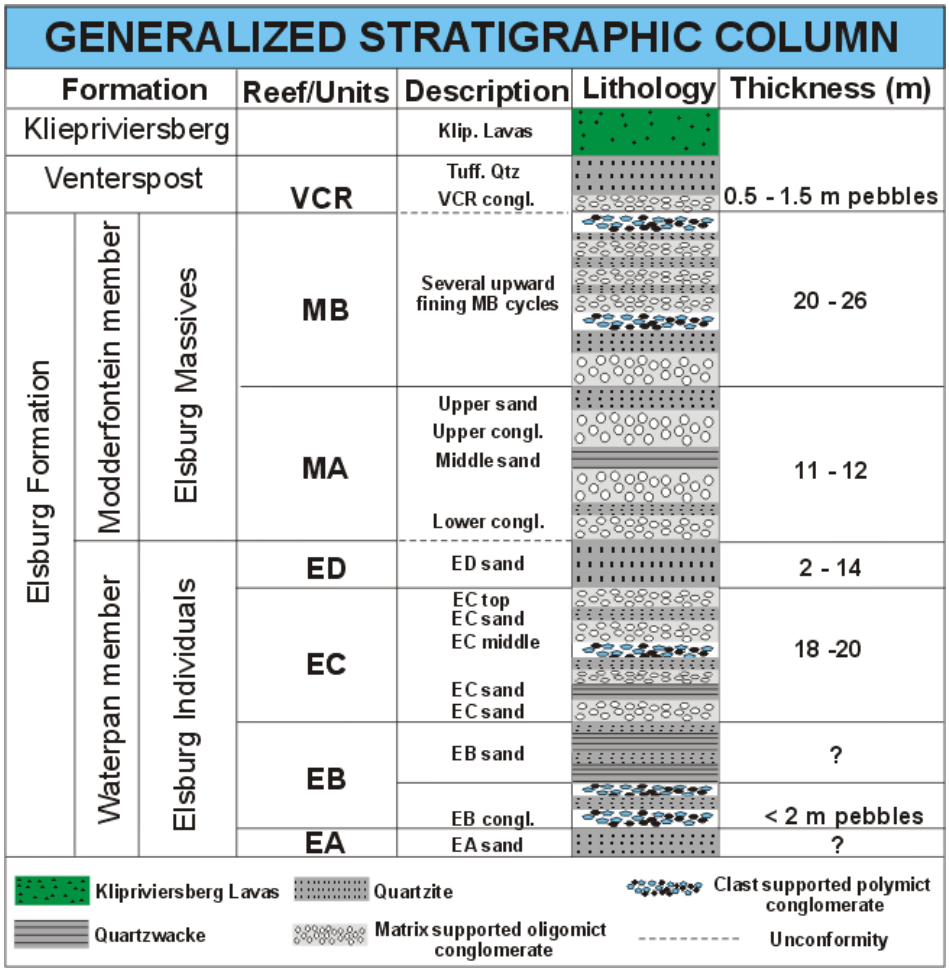


Fig. 6. *Generalized stratigraphic column of the South Deep gold mine (After Erismann, 2007).*

The EC reef of the Upper Elsburg Individuals is a major exploration target in the South Deep Mine because of its high gold grade. The EC conglomerate is well sorted and clast supported, with an oligomictic base (Erismann, 2007; Anonymous, 2011). It is overlain by the ED quartzwacke and is thus a very poor reflective interface.

The Ventersdorp Contact Reef (VCR) unconformably overlies the UER with an approximately 5 degrees divergent angle of unconformity (McCarthy, 2006; Anonymous, 2011; Manzi et al., 2012a). The top of the VCR is a strong, laterally continuous seismic reflective interface. The position where the gold-bearing EC conglomerate subcrops against the VCR, and also where the Upper Elsburg reefs converge/merge is locally known to as the shoreline (Gibson, 2005; Erismann, 2007) (Fig. 4 and 5). The zone immediately east of the shoreline, where the conglomerate and quartzites of Upper Elsburg package are closely packed, is referred to as the shoreline composites (Gibson, 2005; Erismann, 2007; Anonymous, 2011). The eastward divergence of the Elsburg reefs, and their juxtaposition against the base of the VCR, has resulted in characteristic wedge-shaped package of metasedimentary rocks that exerts a primary control on ore volumes (Arthur et al., 1990; Erismann, 2007). Gold grades decrease as the wedge increases in thickness. This is concomitant to a decrease in the percentage of conglomerate pebbles with increasing distance away from the shoreline composites (Arthur et al., 1990; Erismann, 2007). The clastic wedge reaches 120 m in thickness near the eastern boundary of the mine permit.

3. Application of 3D seismic to South Deep gold mine

The first ever 3D seismic survey acquired in South Africa in 1988 (Campbell and Crotty, 1988; 1990) played an important role in the discovery and establishment of the South Deep gold mine in 1990. Since then the 3D seismic technique has been used for strategic mine planning and design in South Africa.

The 2003 3D seismic reflection survey was shot by Compagnie Générale de Géophysique (CGG) and processed by Velseis Processing Pty in Brisbane (Australia). The principal focus of the survey was to target the VCR orebody in the Kloof area to the west of the South Deep

Mine, as well as the VCR orebody in the South Deep Phase I and Phase II blocks. The purpose of achieving coverage over the South Deep Phase II block was to delineate the UER package (Figs. 4 and 6). The survey consisted of 4155 shot points recorded over an area of approximately 96 km^2 covering the Kloof area (~57 km^2), South Deep mine Phase I and II (~28 km^2), and Meerkat Extension areas (~22 km^2). The design and acquisition parameters are summarized by Manzi et al. (2012a; b) and the processing parameters are presented in Table 1. At least fifty boreholes and one VSP dataset were used to calibrate, constrain and validate the seismic interpretation (e.g., positions of seismic horizons at depth).

In 2004, Velseis produced a prestack time migrated (PSTM) volume that imaged relatively strong horizons with frequency content of approximately 20 to 65 Hz. The prestack time migration cube serves as the basis for the extraction of high-quality seismic attributes. The seismic volume covering the South Deep project area extends to approximately 9 km depth, with an east–west extent of 4 km and north–south extent of 16 km, or 576 km^3.

Table 1: Processing parameters for 2003 3D Kloof-South Deep and 1994 Leeudoorn seismic data sets.

Processing Route	Parameters
Data reformat	From SEGD to Promax internal format
Trace editing	Air-blast attenuation applied
Geometry application	Source, receiver, offsets, etc assigned to each trace
Gain recovery: spherical divergence correction	1/(TV^2), where V=5500 m/s
Surface consistent spiking deconvolution	Operator design window at 0 m offset: 100 – 2500 ms, operator length: 120 ms, white noise stabilization: 1%
Zero phase spectral whitening	8 frequency windows, 500 ms sliding window
3D refraction statics correction	Surface layer V0=1200 m/s (constant), seismic datum elevation: 15000 m a.m.s.l
Statics application	Smooth processing datum
1st pass interactive velocity analysis	Every 600 m in both cross line and in line directions
1st pass surface consistent residual statics	Maximum power autostatics, 300 ms time gate around flattened horizons
Interim stack: Leeudoorn and Kloof-South Deep	Data sets stacked separately, 35% stretch mute and 500 ms AGC applied
Prestack phase rotation and time-shift to match Leeudoorn and Kloof data sets	Leeudoorn data: time shift of -8 ms and 90˚ phase shift
Prestack merge of Kloof-South Deep and Leeudoorn data sets	Refraction statics calculated on the merged data and tied to upholes
Second pass interactive velocity analysis	Every 600 m in both cross line and in line directions
Second pass surface consistent residual statics application	Maximum power autostatics, 300 ms time gate around flattened horizons
CDP trim statics	Non-surface consistent CDP statics
Dip moveout (DMO) velocity analysis	Full 3D Kirchoff DMO using 50 m in line and cross line distance
Prestack time migration (PSTM) flow	
First pass PSTM velocity analysis	DMO velocities removed and PSTM velocities picked
PSTM	Full 3D Kirchoff using velocity model from smoothed first pass PSTM velocities
Second pass PSTM velocity analysis	Second pass PSTM velocities picked
Normal moveout (NMO) correction	Second pass PSTM velocities applied
Stack	
Bandpass frequency filter	Time varient Ormsby zero phase filter, 0-1400 ms: 15/20-80/90 Hz
Depth conversion	Using interval velocities derived from borehole data and Black Reef and VCR time horizons
WUDLS data merge	Kloof-South Deep data depth shifted to 1830 m a.m.s.l datum and re-gridded to match WUDLs orientation

4. Seismic attribute analysis

More than 50 different seismic trace attributes have been developed since their introduction in 1970s (Taner et al., 1979; Sheriff, 1991; White, 1991; Brown, 1996; Rock Solid Images, 2003). Seismic attributes are derived from the seismic data and mathematical manipulation of seismic wave components such as amplitude, frequency and phase (Sheriff, 1991). These tools have played an integral part in improving the quality and efficiency of 3D seismic interpretations. They are typically extracted along seismic traces to reveal information that is hidden in the migrated seismic sections (Justice et al., 1985; Knapp, 1990; Barnes, 1991; Taner, 2001; Chopra et al., 2006; Chopra and Marfurt, 2007).

In this study, instantaneous attributes (post-stack attributes), one of eight categories defined by Barnes (1992; 1999); Brown (2001) and Taner (2001) have been used. Instantaneous attributes describe the characteristics of the seismic trace at each signal point (Taner et al., 1979; White, 1991; Barnes, 1993; Fomel, 2007). They may be used to identify the presence of thin reefs, and can help to enhance detection of their extent, continuity and resolution (Rock Solid Images, 2003). In general terms, a complex seismic trace ($g(t)$) with a real trace component ($x(t)$) and an imaginary (quadrature) trace component ($y(t)$), can be expressed as:

$$g(t) = x(t) + iy(t) \tag{1}$$

where $y(t)$ is derived from $x(t)$ using the Hilbert Transform ($H(x(t))$) defined by Taner and Sheriff (1977) as:

$$y(t) = \frac{1}{\pi t} * x(t) \tag{2}$$

The Hilbert Transform shifts the seismic trace ($x(t)$) by 90°, and therefore $y(t) = H(x(t))$. From equation (1), the instantaneous amplitude ($A(t)$) (which is the length of the vector that intercepts the complex-trace, $g(t)$) can be calculated as:

$$A(t) = \sqrt{x^2(t) + y^2(t)} \tag{3}$$

The instantaneous amplitude or reflection strength is a phase-independent vector that measures the acoustic impedance. Thereby it can identify changes in lithological character between geological layers. The instantaneous phase (angle of a rotating vector, ($\theta(t)$)) can be derived from equation (1) and (2). This phase is measured from -180° to +180°, and is described by Sheriff and Geldart (1995) as:

$$\theta(t) = \tan^{-1} \frac{y(t)}{x(t)} \tag{4}$$

The instantaneous phase defines the continuity of thin and weak seismic events, and may change in response to wavelet interference. The attribute provides an instantaneous amplitude independent display and is useful to identify the continuity of weak events, subtle faults and dipping events. From equation (4), the paraphrase (which is a complementary attribute for instantaneous phase) can be expressed by:

$$\beta(t) = \cos(\theta(t)) \tag{5}$$

Paraphase represents, for each seismic reflection event, the full 180 degree rotation of phase (from peak to trough) without any representation of amplitude. This attribute has no seismic amplitude information and event values range from 0 to 1 and hence all events are represented and this makes the events look continuous. Zero phase events are represented as either 0 or 1. It is mainly used to identify reflecting events from thin boundaries and wave interference caused by bed truncations (Artun et al., 2005). Paraphase is continually smoother than instantaneous phase, since it avoids +/- 180° discontinuity that occurs in the instantaneous phase. Thus strong and weak seismic reflection events exhibit equal

amplitude strength, that is, amplitude peaks and troughs retain their position. Instantaneous frequency, the first derivative of the instantaneous phase ($\theta(t)$), can be expressed by:

$$\omega(t) = d\theta(t)/dt \tag{6}$$

Instantaneous frequency is a measure of how the instantaneous phase changes, that is, how quickly the seismic wavelet goes from zero crossing to zero-crossing or peak to trough. It is independent of instantaneous phase and amplitude, and is useful to find out thickness change and lateral changes in lithological boundaries. Depending on signal-to-noise of the data, the lower frequencies can be interpreted as a thicker reflector. Equation (4) also shows that the instantaneous phase and frequency attributes are intrinsically related, implying that phase anomalies coincide with seismic events of low instantaneous frequencies.

Another important attribute is the Average Energy ($E(k)$), which is the ratio between the sum of the squared reflection strength, or amplitude within a specified user's time window. This attribute is superior to amplitude (or reflection strength) in the detection of lithological contrast. It can be computed from the energy values averaged for the zones between paraphase peaks (Taner and Sheriff, 1977). It is given by:

$$E(k) = \sum_{i}^{k} a_i^{\,2} / k \tag{7}$$

where k represents number of samples with amplitude (a) within a window. It can be used as a good predictor of seismic events in low impedance layers.

5. Methodology

The attribute analysis work flow was conducted using the Seismic Micro-Technology (SMT) Kingdom Suite and Petrel software packages. These two packages facilitated the interpretation of seismic, borehole and mapping datasets in a single environment. Horizons and faults were interpreted along the in-lines, cross-lines, various arbitrary lines and depth slices. Reflectors were selected for picking based either on their geological significance or because the wavelets were clear and strong, with a constant phase. A seismic reflector was picked as a peak or trough depending on the impedance change over a lithological contact. Generally, a decrease in seismic velocity over a lithological contact correlated with a peak on the seismic section, while an increase in velocity correlated with a trough (e.g., Figs. 2 and 3). Whenever two or more strong amplitude (peak) seismic events of the same character were shown, the event could be followed where it was continuous. Where discontinuities such as faults were encountered, the event was broken, and the fault was interpreted manually. It was necessary to know the amount of vertical displacement on both sides of the fault in order to be able to continue an event to the opposite fault block.

Furthermore, the nature of reflectors was expected to change laterally as different beds subcropped, or onlapped against the unconformity. Thus closely spaced thin layers could have been summed causing wavelets doublets, or one reflector could have continued over a fault into a different reflector (Fig. 2). However, with careful picking, each reflector was correlated with a stratigraphic boundary throughout the study area. The seismic attributes were extracted for each section to enhance strato-structural interpretations. Existing borehole data were used to ground-truth the data and constrain seismic phase shifts in seismic attribute displays. Isopach maps and volumetric attributes were computed for the interval between VCR and markers in the metabasalts of the Klipriviersberg Group to identify and locate the EC's subcrop position against VCR

6. Mapping of the VCR-unconformity

The VCR was picked as a peak because of the decrease in impedance from the overlying high velocity and high density metabasalts of the Klipriviersberg Group (approximately 6400 m/s) to the underlying low velocity quartzite units of the Central Rand Group (approximately 5750 m/s). The impedance produced a reflective interface that could be imaged by a seismic method. The color coded amplitude display of the seismic section exhibited a very strong and continuous VCR peak across the South Deep block, which correlated very well with borehole data (Fig. 7a). Table 2 Lists of selected South Deep in-mine borehole intersections points (TVD seismic) and their corresponding VCR surface and EC horizon. The correlation between EC reef and boreholes was derived as observed from the seismic section, while the VCR and borehole correlation was computed from the VCR gridded surfaces and borehole control.

The depth discrepancies between VCR/EC and reefs and borehole formation tops were calculated (Table 2). The depth discrepancy values highlighted in red represent very huge depth miscorrelations (> 2×bin size of the survey) between boreholes and horizons. The empty spaces represent the boreholes that had not intersected the EC horizon. On average, boreholes drilled from underground had a good tie (0 - 20 m) with the VCR reflector, although the VCR at some depths is slightly deeper than the actual depths of the borehole formation tops (Table 2). In contrast, the depth-discrepancies between boreholes drilled from surface and more than 1 km apart, and the VCR reflector, were greater than 50 m. These large depth misties are attributed to the greater distance between these boreholes, and errors in the velocity field used for depth conversion and/or borehole deviation at depth. These depth errors were considered in the final structural model.

Table 2: South Deep in-mine borehole intersections points (TVD seismic) and their corresponding VCR surface and EC horizon.

VCR: Ventersdorp Contact Reef; EC: Elsburg Conglomerate.

BH Control	VCR Top TVD seismic (m)	VCR Horizon TVD seismic (m)	EC top Seismic section (m)	EC top TVD seismic (m)	VCR Discrepancy (m)	EC Discrepancy (m)
SD1	2560	2542	2650	2630	18	-20
SD2	2540	2526			14	
SD3	2567	2534			33	
SD4	2569	2540			29	
SD5	2566	2548			18	
SD6	2539	2507			32	
SD7	2546	2529	2749	2758	17	9
SD8	2574	2553	2750	2769	21	19
SD9	2559	2524			35	
SD10	2580	2558			22	
SD11	2587	2558			29	
SD12	2589	2563			26	
SD13	2593	2568			25	
SD14	2603	2570	2690	2759	33	69
SD15	2624	2572			52	
SD16	2630	2572			58	
SD17	2630	2573			57	
SD18	2633	2576			57	
SD19	2639	2587	2720	2700	52	-20
SD20	2633	2569			64	
SD21	2553	2575			-22	
SD22	2502	2518			-16	
SD23	2555	2518			37	
SD24	2555	2533			22	
SD25	2542	2519			23	
SD26	2485	2539			-54	
SD27	2494	2530			-36	
SD28	2459	2492	2565	2560	-33	-5
SD29	2435	2504			-69	
SD30	2492	2533			-41	
SD31	2482	2528			-46	
SD32	2487	2530			-43	
SD33	2492	2533	2530	2560	-41	30
SD34	2497	2492			5	
SD35	2502	2505			-3	
SD36	2507	2506			1	
SD37	2512	2506			6	
MD 45	2620	2615	2731	2735	5	4
K1	2630	2600	2740	2750	30	10

The VCR surface across the South Deep block has an average dip of 5° to the south. However, the VCR elevation map, as presented in Fig. 7b, supports conclusions of Gibson (2005) that the South Deep block is dissected by the prominent second-order scale west-trending Wrench Fault (WF), which has a maximum dextral strike-slip offset of 175 m. The Wrench Fault divides the South Deep mine between a structurally complex area (Phase I) to

the north, and a comparatively less structurally complex area (Phase II) to the south. The seismic data indicates that in fact, the VCR in Phase I dips approximately ~7° to the south, in contrast to an average dip of 11° to the south in Phase II. Furthermore, the VCR elevation map shows optimum imaging of a second-order north-south trending, low amplitude, long wavelength (~1.5 km wavelength) fold couplet, locally termed the Panvlakte anticline-syncline (PAS) pair by Manzi et al. (2013) (Fig. 7b). Thus the VCR surface is variable in dip across the South Deep block.

The VCR in the Phase II area was a priority target for this study. The VCR map derived from Root Mean Square (RMS) amplitude (which measures the seismic reflectivity within a specified time window) identified numerous faults in the Phase II area, as well as amplitude anomalies that coincided with the location of stopes and shaft infrastructure (Fig. 8). The amplitude anomalies result from high acoustic impedance contrast between rocks and air in the excavation. The faults trend predominantly north-northeast and are too complex to see on migrated cross sections. These include complex multi-segments of the Panvlakte Fault (40 - 350 m throw) and Waterpan Fault (25 - 80 m throw) (Fig. 8). These faults were not mapped adequately in the conventional depth-structure map.

The variations in dip angle of the VCR sub-blocks, the constraints on fault orientations across the mining areas, and the presence of the Panvlakte anticline-syncline (PAS) pair are significant and must be factored into mine planning and development.

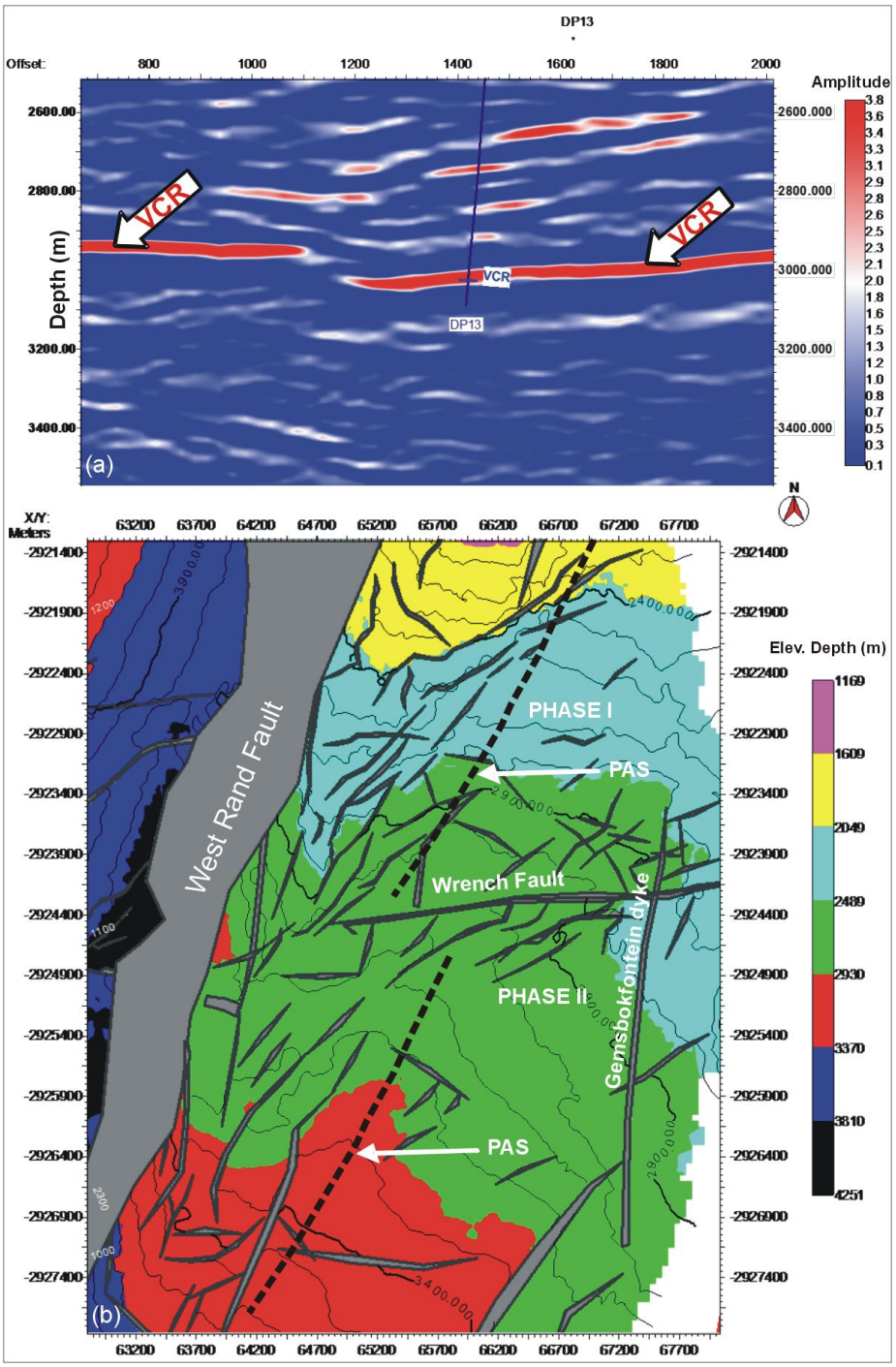


Fig. 7. (a) *Amplitude display of the seismic section showing strong and consistent VCR horizon, constrained by borehole (DP13). (b) Depth structure contour map of the VCR horizon showing fault polygons and prominent West Rand and Wrench faults. PF: Panvlakte Fault; WPF: Waterpan Fault.*

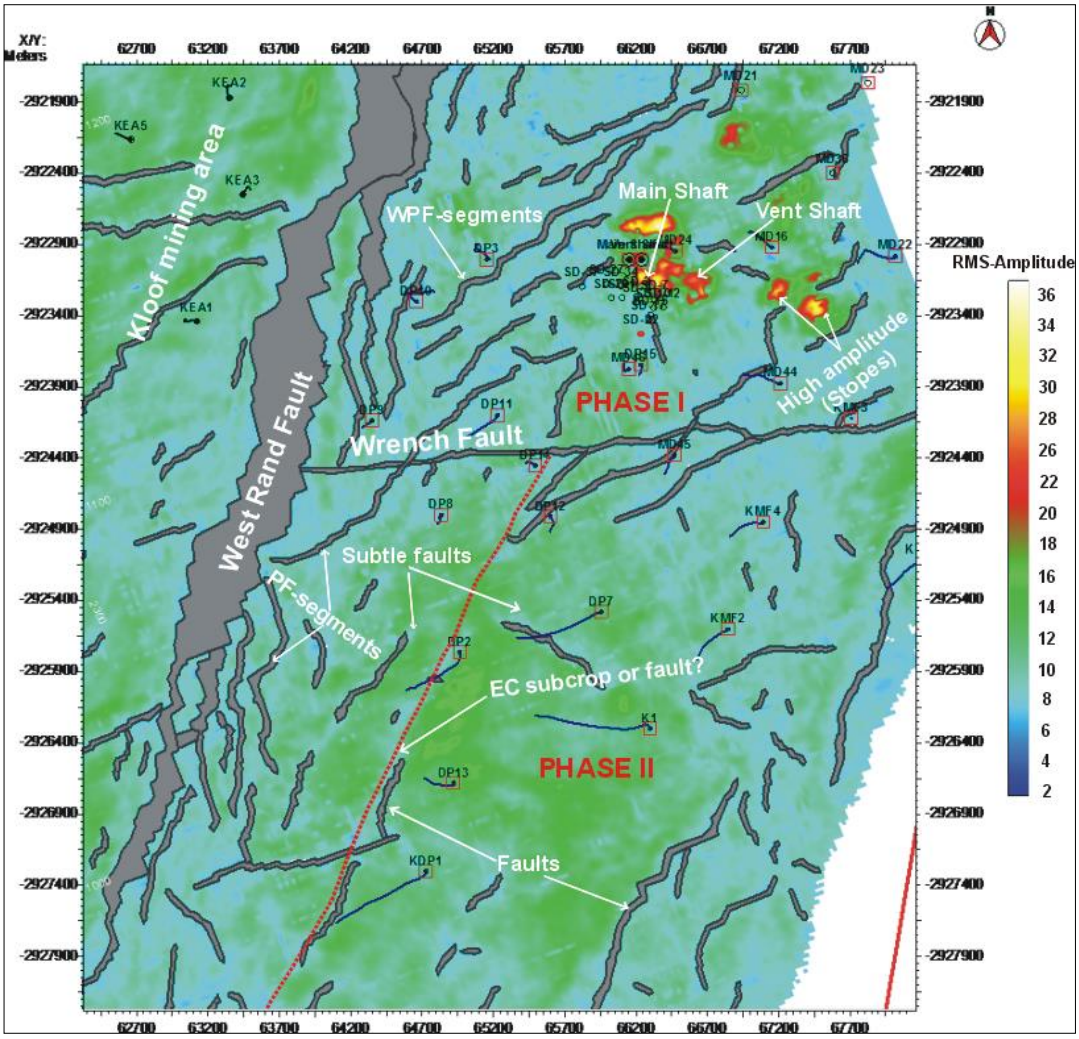


Fig. 8. *The VCR map derived from the Root Mean Square (RMS) Amplitude attribute. The map shows detection of subtle faults that fall below seismic resolution limit and location of shaft infrastructures. PF: Panvlakte Fault; WPF: Waterpan Fault.*

7. Enhancement of the Elsburg Conglomerate Reef

To enhance the detection of the EC reef, complex-trace attributes were extracted along each PSTM section (Line 1-4 in Fig. 1) at regular intervals across the Phase II area, and perpendicular to the geologically-defined trend line of the EC subcrop (Fig. 5).

Line 1 **-** The instantaneous attributes extracted from the seismic volume included reflection strength, average energy, frequency, and paraphase (Fig. 9a-d). These attribute displays clearly show optimum imaging of the lateral continuity of the VCR, with the average energy (square of RMS amplitude) exhibiting more contrast than the reflection strength (Fig. 9a and b). Exploration borehole DP 13 (Fig. 9) shows a good depth correlation with the VCR, which was intercepted at approximately 3.50 km. The optimum imaging of the VCR horizon by average energy is interpreted to be, in part, related to the length (close to dominant wavelength) of the chosen window for the seismic signal (Fig. 9b). Unfortunately, these attributes, reflection strength in particular, failed to detect thin reefs within the UER package. In addition, the instantaneous frequency (Fig. 9c), which represents the mean amplitude of the wavelet, was also not able to identify and distinguish low amplitude events, such as thin reefs. The increase in instantaneous frequency values indicated reef thinning and/or truncations. Since instantaneous frequency is the first derivative of the phase. It is very sensitive to noise associated with either low amplitudes or zero-crossing. As a result, reflections that are interpreted as thin reefs are highly disrupted and discontinuous. This is evident in Fig. 9c where low amplitude events are wrapped with high frequency dipping coherent noise throughout the section. As a result, instantaneous frequency, although much better than amplitude, does not provide a high degree of confidence that what is seen on the seismic section is the result of lithological changes rather than noise.

Furthermore, the paraphase display (Fig. 9d), which is the cosine of the instantaneous phase, better enhanced continuity of weak thin Elsburg events and VCR/EC interference. The ringing and high frequency background noise in the frequency display (that tended to distort the full migrated image) was removed, making it much easier to map thin events and reflectors. The continuity of the EC reef was well defined and its associated wavelets stood-out above the dipping incoherent noise. Thereby, paraphase display proved to be particularly effective in the enhancement of the EC reef.

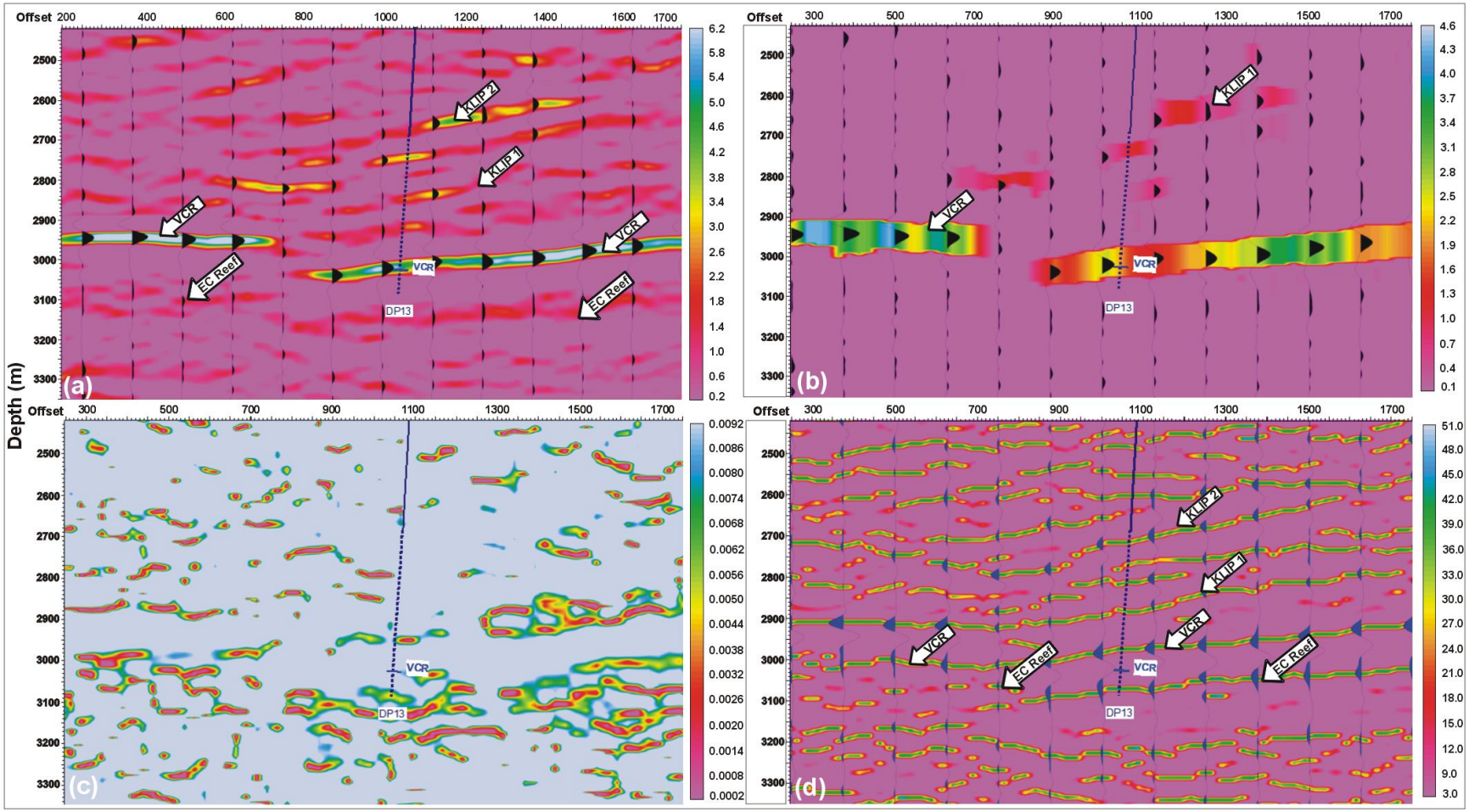


Fig. 9. *Seismic section (L1 in Figure 1) (a) Reflection strength display (wiggle trace) showing strong seismic amplitude related to the VCR imaging. (b) Average energy display (wiggle trace) showing optimum imaging of the VCR but poor EC reef imaging. (c) Instantaneous frequency display showing poor imaging for both VCR and EC reef. (d) Paraphase display (wiggle trace) highlighting lateral continuity of the EC reef and enhancement of minor faults. The color overlays exhibit more information than is visible on traditional black and white seismic sections. VCR: Ventersdorp Contact Reef; EC: Elsburg Conglomerate; KLIP: Klipriviersberg*

Line 2 – The reflection strength, frequency, phase, and paraphase displays for seismic Line 2 are presented in Fig. 10a-d. The amplitude display (overlain by wiggle traces) shows the strength of reflection and continuity associated with the EC horizon. However, it is difficult to consistently track the event through the seismic section due to its limited lateral extent or highly variable reflection character (Fig. 10a). The instantaneous frequency, on the other hand, only defined the VCR horizon (Fig. 10b). Moreover, the instantaneous frequency attributes suffered from low signal-to-noise ratio and wavelet interference arising from the VCR interface and other weaker events below. The doublets are characteristic of the shoreline composite and are probably caused by multiple, closely-spaced reefs within the UER. The inconsistency and reduction in frequency in the seismic sections could be related to destructive interference caused by prestack processing artifacts such as velocity analysis, spectral whitening, and refraction statics corrections. In contrast, the instantaneous phase highlights the lateral continuity of EC horizons and weaker events below the VCR (Fig. 10c). The instantaneous phase is independent of the trace reflection magnitude and is thus the best indicator of lateral continuities of the thin layers. Unfortunately, the instantaneous phase showed abrupt changes at +90 and -90 degrees. This is not surprising, since the attribute was computed from the arctan function (Eq. 4).

In contrast, the paraphase attribute display (Fig. 10d) enhanced the detection of the shape, character and continuity of the EC horizon, as well as subtle faults that were not well defined clearly on the amplitude and frequency attribute displays. This suggests that paraphase is not only useful in emphasizing the physical properties of the thin reefs within the composite shoreline, but is also useful at enhancing their continuity, as well as fault offsets. Although, paraphase is similar to phase, the peaks and troughs do not align with peaks and troughs in the original seismic section. Therefore, care needs to be taken during the tracking and picking of these events. Although no well data are available to evaluate the nature of these

reefs, they were interpreted with high confidence since their continuity and strength are prominent throughout the phase and paraphrase displays.

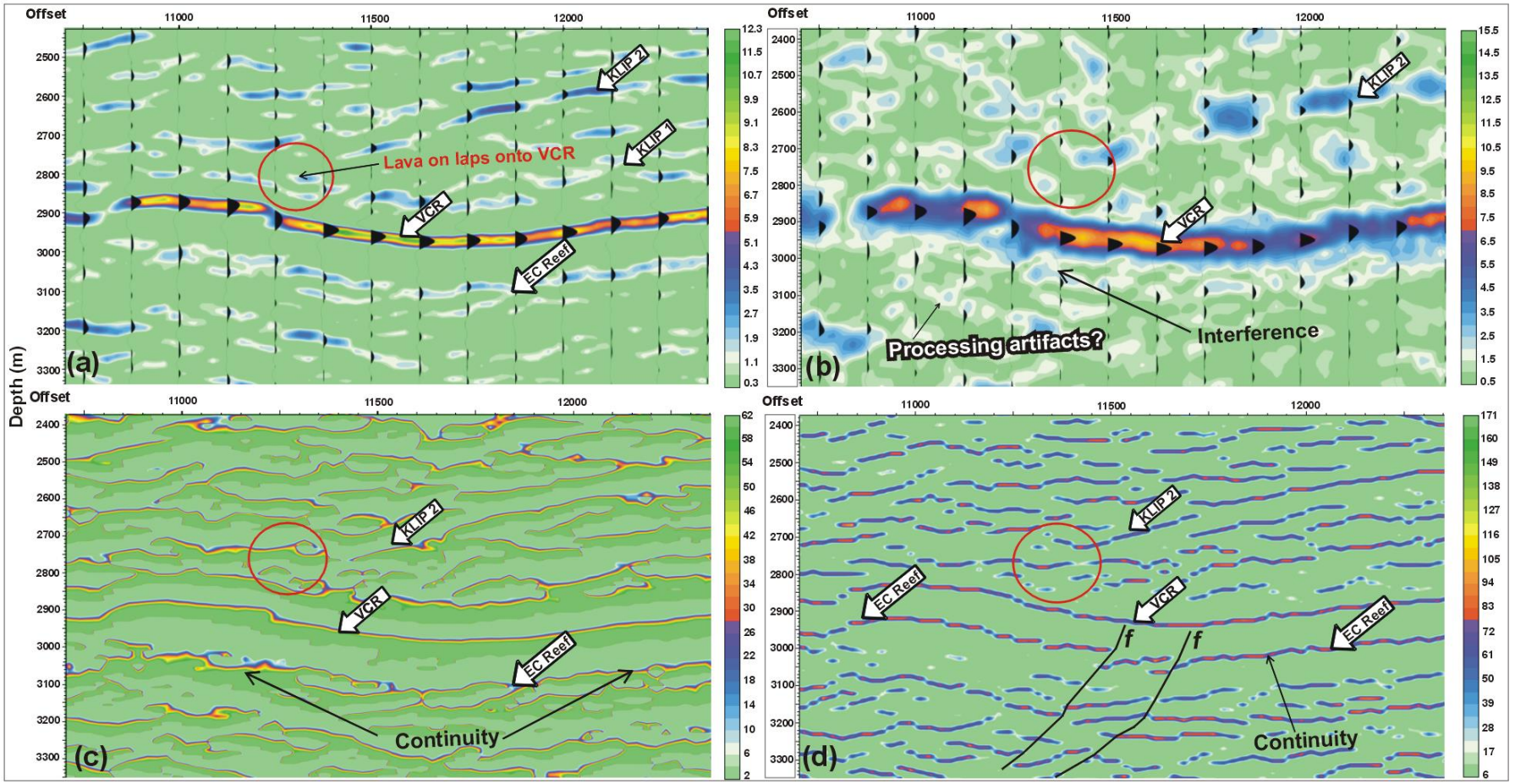


Fig. 10. *Seismic section (L2 in Figure 1) (a) Reflection strength display (wiggle trace) highlighting the KLIP l horizon event onlapping onto the VCR and VCR continuity. (b) Instantaneous frequency display (wiggle trace) showing noisy spikes associated with thin seismic events and poor imaging of the VCR when comparing to Figure 10 (a). (c) Instantaneous phase display continuous events associated with VCR and EC reef. (d) Paraphase display providing much better imaging of the EC reef. Observe the imaging of faults in Figure 10 (d) that was not prominent in other attribute displays. VCR: Ventersdorp Contact Reef; EC: Elsburg Conglomerate; KLIP: Klipriviersberg.*

More importantly, paraphase display clearly shows the reflection termination patterns (e.g., onlap, truncations, etc) that define the genetic reflection package. In particular, the metabasalts of the Klipriviersberg Group appear to onlap or terminate against an initially inclined VCR near the shoreline, which is a junction of the Klipriviersberg Group seismic markers and lower VCR. Within the metabasalts of the Klipriviersberg Group, we have identified two relatively strong seismic markers, namely Klip 1 (lower) and Klip 2 (upper). Various suggestions on the causes of these onlap developments have been suggested by Gibson (2005). The upper Klip 1 is interpreted as the horizontal surface, whereas the lower VCR is an inclined erosional surface. As these horizons converge at the shoreline, wedge-shaped UER package accommodation is formed. According to Gibson (2005), these onlaps imply that the UER package accommodation was expanded into landward direction of which sediments are derived. The detailed discussion concerning causes of such accommodation development is beyond the scope of this article.

Line 3 – The amplitude and frequency displays on this section did not detect the EC reef successfully (Fig. 11a and b). The instantaneous frequency display was contaminated by high noise spikes from low amplitude events, thus providing poor detail on the UER. The VCR is also poorly defined by this attribute. With reasonably high quality reflection amplitudes and high signal-to-noise on this section, frequency display would be expected to offer much better enhancement of the VCR. Surprisingly, this attribute shows even more chaotic and less continuous signature than those observed in the amplitude display.

In contrast, the instantaneous phase and paraphase displays (Fig. 11c and d), provide a much improved resolution and continuity of the reflection events, especially the EC unit. The interference of seismic events cannot be clearly seen on the phase, but it is clear on the paraphase display. When displayed with suitable color bars, these attributes made strong seismic events easy to distinguish from weak seismic events, in terms of amplitude or

frequency in relation to peaks and troughs. The peaks from the instantaneous phase display have a constant phase of 0°, while troughs for the same display have constant phase of 180°, and zero-crossings with a phase of ± 90°. These characteristics make it easier to see interference, especially in seismic sections that are characterized by low amplitudes, stratigraphic terminations, complex faulting and low signal-to-noise ratio. The exploration borehole DP 7, which was drilled about few metres east of the shoreline position, provided good opportunity to verify whether or not the thin reflections seen on seismic sections are in fact thin reefs. Figure 11d shows a very good correlation between EC reef and DP 7.

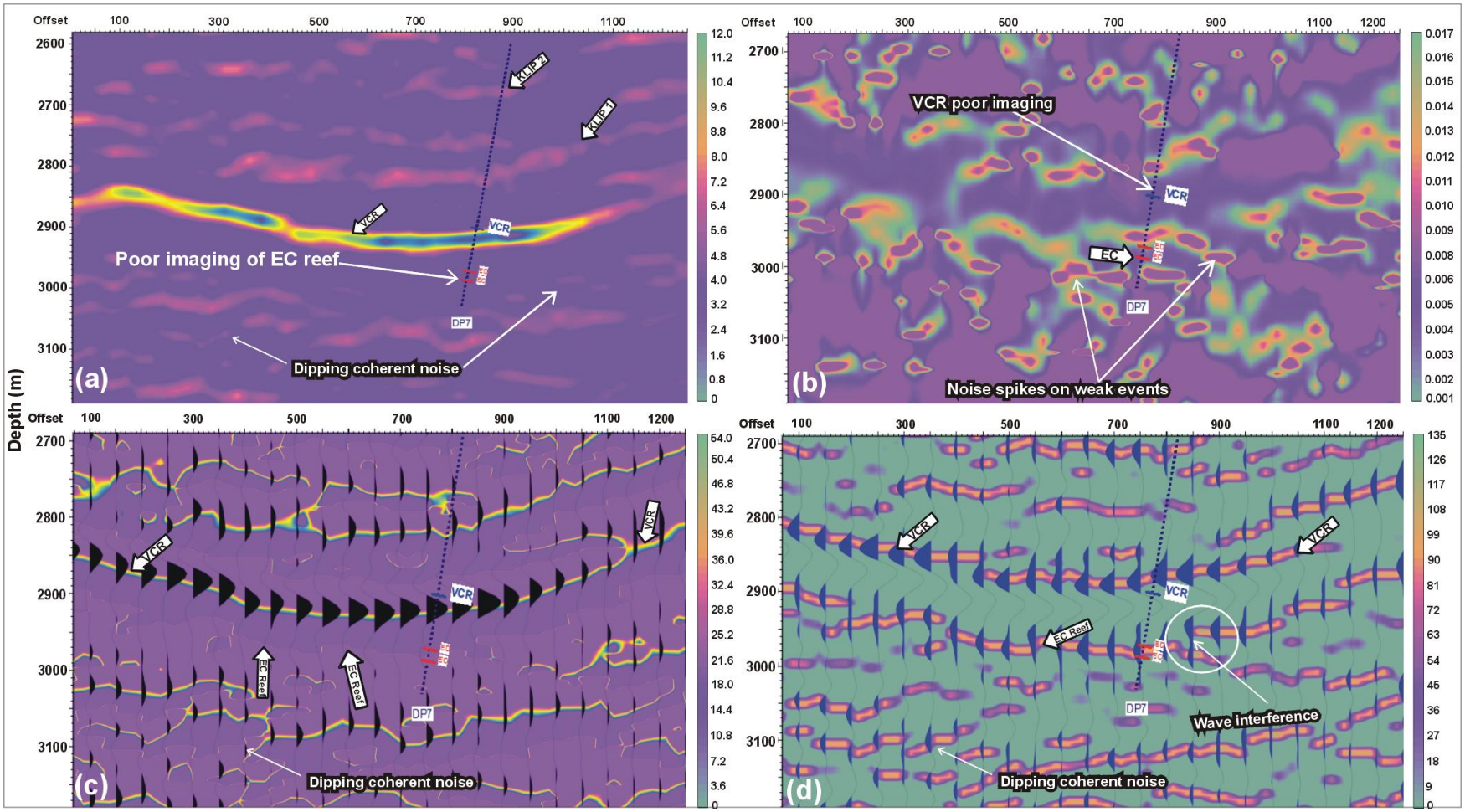


Fig. 11. *Seismic section (L3 in Figure 1) (a) Amplitude display showing strong and continuous VCR horizon. (b) Instantaneous frequency contaminated by noise and showing poor detection of weak events (c) Instantaneous phase (wiggle trace) highlighting weak events as thin and continuous reflections. (d) Paraphase display making weaker events much stronger and continuous. Notice how well the EC reef ties with the borehole control (DP7). VCR: Ventersdorp Contact Reef; EC: Elsburg Conglomerate.*

Line 4 – The amplitude display shows poor detection of the EC reef (Fig. 12a). The paraphase attribute (Fig. 12a), on the other hand, was extremely powerful in the enhancement of the constant phase associated with EC reef. The paraphase provided a better tie between EC and ED units with the borehole controls. High values of paraphase were associated with troughs that corresponded to low amplitude events, while distortion in the data due to interference on the seismic wavelets was represented by low phases. However, these attributes, showed significant variations and variability in character with respect to faults; many faults appeared less coherent due to a low signal-to-noise ratio on the data. In fact, it is not easy to verify whether or not these discontinuities represent real faults, and their interpretation depends on our subjective opinion. Generally, as was the case with the VCR, the depth discrepancy between underground borehole and EC reef was approximately 11 m (equivalent to ½ bin size of the survey), although the EC reef was slightly above the actual borehole depth, while depth discrepancy between surface boreholes and seismic EC reef was greater than 50 m, owing to the borehole deviations at depths (Table 2).

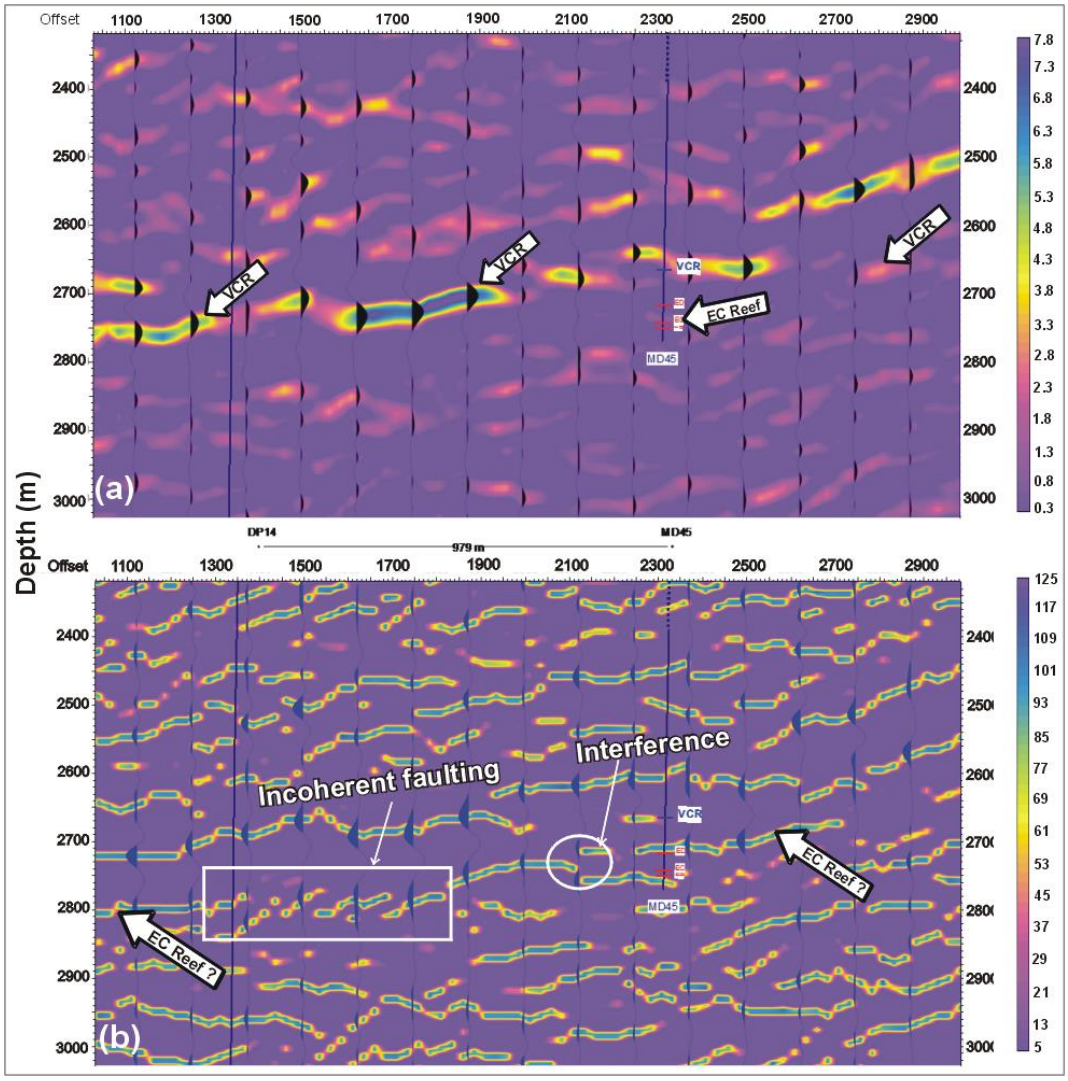


Fig. 12. *Seismic section (L5 in Figure 1) with major faulting and low signal-to-noise ratio (a) Amplitude display (b) Paraphase display. Notice how well the EC reef is enhanced by paraphase attribute. VCR: Ventersdorp Contact Reef; EC: Elsburg Conglomerate.*

8. EC reef subcrop position

The identification of the EC subcrop against the VCR could provide an important economic control as it forms the western boundary of the UER orebody. Two distinct seismic markers were imaged within the metabasalts of the Ventersdorp Supergroup, the lower of which is termed KLIP 1 and is situated 200-1000 m above the VCR. The upper marker is termed the KLIP 2 and is situated 200-2000 m above the VCR (Figs. 9-12).

To locate and interpret the EC subcrop, the isopach map was computed between the VCR and KLIP 1 because geological mapping in the South Deep mine had shown that the EC subcrop position occurred at a location where the KLIP 1 onlapped the VCR surface. Therefore, computing the VCR-KLIP 1 isopach constrained the EC subcrop line (Fig. 13). The seismic sections presented in Figs. 9-11 confirmed that the metabasalts of the Klipriviersberg Group onlap the VCR surface, which accords with the classification by SACS (1980) that the metabasalts unconformably overlie the Venterspost Conglomerate Formation, including the VCR. To confirm the EC subcrop position, the zero-crossing attribute was examined in addition to constructing an isopach map (Figs. 13 and 14). The zero-crossing is one of the volume attributes, and simply describes the zero point (interference or convergent point) that has been crossed by the seismic wavelets (Rana et al., 2006). This attribute is capable of indicating a greater degree of vertical lithological complexity (e.g., subcrop, onlap, toplap, truncations or terminations). This attribute, when computed between two horizons, is expected to provide a resolution below the tuning thickness of approximately 20-25 m. Although this is very difficult to interpret, the distinct zero-crossing north-northeast trending lineament is clearly seen in the zero-crossing map computed between VCR and KLIP 1 in Fig. 14 (red trend). The lineament represents areas of more zero crossings and hence is likely to be indicative of EC subcrop position.

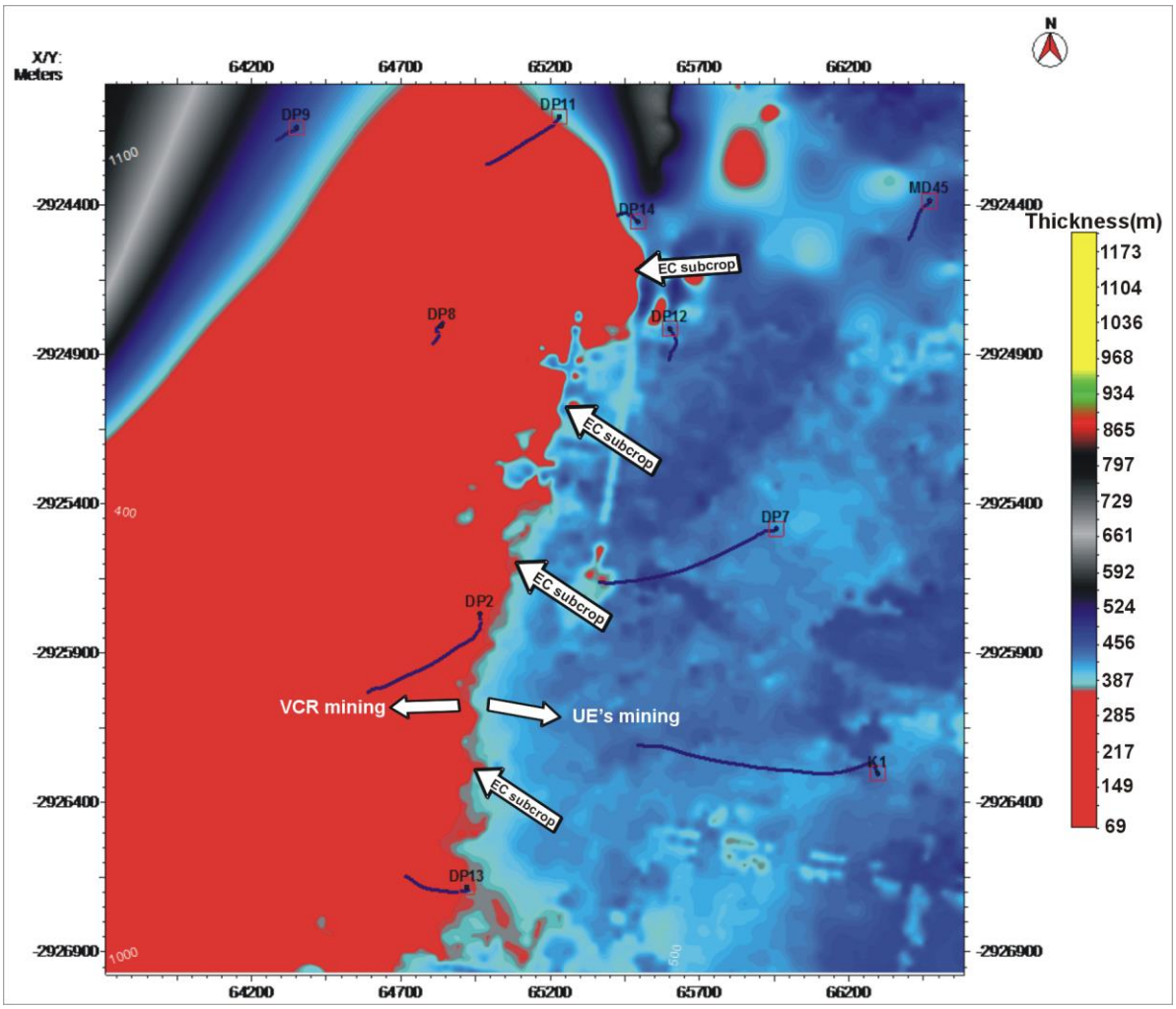


Fig. 13. *VCR-Klip 1 Isopach map showing EC subcrop position. Notice how the isopach thins to the west of the mining area, coinciding with the interference zone where the Klip1 onlaps onto the VCR surface.*

The zero-crossing attribute also proved a good complementary tool for the location of subcropping EC reef position. The zero-crossings observed between KLIP 1 (top) and VCR (base) are represented by odd numbers, which is not surprising since KLIP 1 and VCR were picked as a trough and peak, respectively. It can thus be inferred that the north-northeast trending lineament corresponds to the EC subcrop position. In comparison to the current geologic model presented by South Deep gold mine (Fig. 5), the seismic maps report exactly

the same trend, location and orientation of the EUR subcrop as that given by the mine geology model.

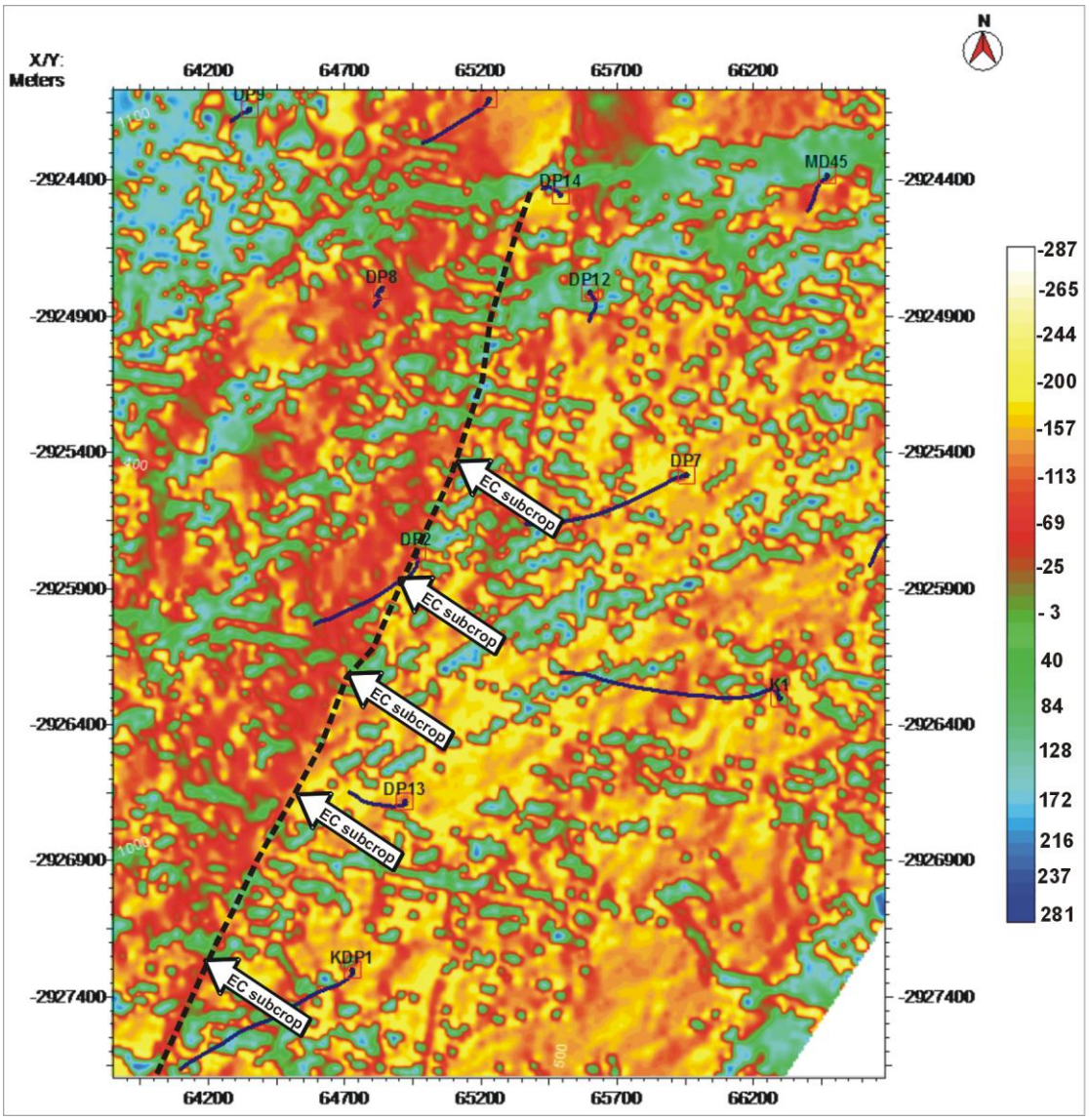


Fig. 14. The zero-crossing attribute map between Klip 1 and VCR confirming the Elsburg Conglomerates subcrop position and its orientation as predicted by isopach map in Fig. 13 and the mine model in Fig. 5.

9. Discussion

Conventional seismic interpretations based on wavelet amplitude do not provide enough information to detect thin gold-bearing reefs. This is because the amplitude is sensitive to the tuning thickness, i.e., it decreases as the thickness of the thin reefs decreases.

Seismic attributes are sensitive to noise in the seismic data from which they are derived. The noise in data may be coherent or incoherent and have different sources. The noise tends to interfere with the thin reflectors and complicate the seismic interpretations. For example, the dipping coherent noise can cause linear features on seismic attribute displays, which are not easily distinguishable from real features. The seismic sections shown in Figs. 10 and 11 serve to demonstrate that low-frequency coherent noise and interference features are present on seismic attribute displays, and that only detailed borehole control and underground geological mapping can verify the observed reefs and faults, respectively. Below the VCR, at depths between 2.9 and 3 km, several dipping low-frequency coherent noise seem to interfere with the EC reef. These interferences are so strong that they make it almost impossible to clearly identify the actual reefs.

The cause for dipping coherent noise in the data is not known, but it is very likely that much of this noise is related to processing artifacts (such as migration velocity errors) and acquisition footprints (such as those due to geometry, fold, azimuths and offsets). Significant migration velocity errors, in particular, can cause overlapping reflector signals to produce discontinuity and tuning artifacts that may overwhelm corresponding seismic events associated with the reefs. The complex geology, such as truncations and onlaps, within the UER wedge package may also cause such noise interferences. The noise interferences caused by truncations and subcropping of reefs are simply related to the fact that the

seismic processing cannot easily resolve the ambiguity when two seismic signals interfere with each other. Furthermore, this seismic survey was shot using old acquisition systems, which may, in part, explain the low signal-to-noise ratio in some areas. The subsequent seismic processing may also not have been able to reduce the effects of system-induced noise. Similar noise signatures are observed by the authors in seismic sections across the West Rand and West Wits line goldfields and are a major concern for detailed seismic interpretations. Since it is beyond the scope of this study to discuss in detail the seismic acquisition and processing parameters for this survey, the reader is referred to the articles published by the authors from these data (e.g., Manzi et al., 2012 a; Manzi et al., 2012b; Manzi et al., 2013).

Although the acquisition and processing steps undertaken for Gold Fields Limited 3D seismic data offered great advantages for accurate VCR and BLR interpretation West Wits Line gold mines, the conventional interpretation techniques did not allow for exploitation of the data to its full potential in the South Deep gold mine. For example, subtle faults and reefs with thicknesses far below tuning could not be recognized on the migrated seismic sections. However, seismic attributes derived from these data are a novel way of enhancing the detection of these features in the data. This suggests that the high-resolution prestack time migrated volume used in this study serves as the basis for high-level generation of seismic attributes. For example, the most important economic gold-bearing reefs in the South Deep block, the VCR and EC reef, have been mapped with high confidence using instantaneous attributes. The position and orientation of structures (faults/dykes) that offset the reefs were mapped with high level of confidence, as well the depth of the VCR and EC reefs.

Due to the presence of abundant different noise signatures on several seismic sections, it was necessary to rely strongly on the borehole control and underground geological map data

to confirm the depth positions of the interpreted reefs and faults. This study has demonstrated that instantaneous attributes, with special color coding, can improve the detection of thin reefs. Conventional seismic amplitude displays were not able to locate the position of the EC subcrop. The main reason for this was that the UER thins towards its contact with the VCR and is thereby impossible to distinguish. Through utilization of seismic trace attributes, correlated with several boreholes from South Deep gold mine, it has been possible to confidently interpret the extent of the EC reef.

However, in complex areas, such as those characterized by major faults or low signal-to-noise ratio, seismic trace attribute analysis may fail to provide useful information in the seismic sections. In such cases, borehole controls are needed to validate the interpretation. The amplitude attribute also suffers from wavelet interference and phase problems in the data. Seismic attributes that are not amplitude dependent can enhance interpretations, thus improving the enhancement of thin reefs.

Of all attributes computed on the PSTM sections, the phase and paraphase were the most valuable. These are capable of highlighting even weak events because of their insensitivity to the reflection strength. Paraphase, in particular, enhanced the contrast between reflectors having minor differences in velocity and density. Subtle and distinct changes in phase and paraphase attributes were associated with changes at minor lithological boundaries. However, it is important to note that phase and paraphase attributes are only completely reliable when correlated with boreholes. It is also imperative to carefully choose attributes to enhance interpretation of thin reefs because their effectiveness varies, depending on the type of the reef and its geometry.

Generally, the discrepancies or misfits computed between the logged positions of the VCR/EC events and boreholes fall within the positional accuracy of the seismic survey of ± 25 m vertical resolution (considering the seismic bin size of 25 m). Based on this study, it should be possible, with a relatively high signal-to-noise ratio, to distinguish reefs below tuning thickness within a wedge shaped package of clasltic metasedimentary rocks using complex-trace attribute analysis.

Zero-crossing attribute and isopach analysis were also used to detect the interference wavelets or subcrop position of the EC reef against the VCR. Based on these analyses, and in conjunction with geologic model, it may be concluded that the negative values and low thickness values in the zero-crossing and isopach map, respectively, represent the interference point, or the point where EC subcrops against the VCR. Although zero-crossing and isopach maps are completely independent, they provide remarkably similar results. The advantage of these methods over complex-trace attributes is that no borehole control is needed to constrain the interpretations.

This seismically-defined EC subcrop position can now be factored into the current mine model, thereby improving the resource evaluation of the UER in the South Deep mine. In addition, structural data provided by the 3D seismic survey can be exported from Petrel into CADS-Mine to assist the shaft geologists in development of robust geological model. This has the potential to (1) reduce drilling risks, (2) improve prospection of the UER units, and (3) increase the value of the new 3D seismic data. Based on this study, it can be concluded that the behaviour of seismic attributes is not unique, and therefore it should be emphasized that a single attribute approach is not desirable in seismic interpretations.

10. Conclusions

In an effort to re-examine the existing 3D seismic data over South Deep mine project areas, instantaneous attribute analysis has been applied successfully in the detection of thin gold-bearing reefs, which fall below the tuning thickness.

While the surface boreholes deliver accurate gold grades and depths at the points where they intersect the reef; structural models derived from boreholes always suffer from uncertainties. This is because boreholes are a two-dimensional (linear) sample of a three-dimensional Earth. Borehole data must be projected between points of control using geostatistical assumptions about dip and strike and geostatistically-constrained conceptual geological models. Structures between boreholes are not sampled, and maybe missed, or erroneously projected. However, by applying seismic trace attribute analysis to the 3D seismic data cube, it is possible to accurately identify structures, locate many subtle faults and delineate gold-bearing reefs below the seismic tuning thickness.

Interpretations of the VCR with various techniques, such as isopach and zero-crossing analysis, have assisted in refining the trace of the UER shoreline across the South Deep permit area. More importantly, it has been shown that the complex-trace attribute analysis can enhance the detection of the thin reefs within the UER clastic wedge.

It is worth noting that the resolution of thin reefs is not simply dependent on one-quarter dominant seismic resolution criteria, or the use of seismic attributes, but on other factors such as signal-to-noise ratio, impedance of the materials above and below, complexity of the adjacent layers, and the accuracy of the velocity fields used for migration. All these factors limit the geological information that can be interpreted from seismic sections. Since the

South Deep gold mine data is relatively good in quality, there is little doubt that thin reflectors detected through instantaneous attribute analysis represent real reefs. Finally, unless the borehole data are presented to verify and constrain seismic interpretations, any interpretation using seismic attributes must be treated with care.

Acknowledgements

This research was sponsored by Gold Fields Mining Ltd. The authors would like to thank J. Tricket, L. Lindzay and M. Gibson for their major scientific contribution towards this project. Useful input from discussions with N. Buthelezi is highly appreciated. The article has benefited from review by A. Malehmir and another anonymous reviewer.

References

Anonymous, 2011, South Deep gold mine, Unpublished internal technical short report, 22 pp.

Artun, E., Mohaghegh, S. D., Toro, J., Wilson, T., Sanchez., A., 2005, Reservoir characterization using intelligent seismic inversion, SPE 98012, 2005 SPE Eastern Regional Meeting, Sept. 14–16, Morgantown, West Virginia.

Armstrong, R.A., Compston, W., Retief, E.A., Williams, I.S., Welke, H.J., 1991. Zircon ion microprobe studies bearing on the age and evolution of the Witwatersrand triad. Precambrian Research 53, 243-266.

Arthur, D. L., 1990. Report of the stratigraphy and sedimentology of the upper Elsburg strata in the South Deep Project Area. Unpublished Internal report, Western Areas Gold mine, 52 pp.

Barnes, A. E., 1991. Instantaneous frequency and amplitude at the envelope peak of a constant phase wavelet. Geophysics 56, 1058-1060.

Barnes, A.E., 1992. The calculation of instantaneous frequency and instantaneous bandwidth. Geophysics 57, 1520–1524.

Barnes, A.E., 1993. Instantaneous spectral bandwidth and dominant frequency with applications to seismic reflection data. Geophysics 58, 419–428.

Barnes, A.E., 1994. Theory of two-dimensional complex seismic trace analysis. 64th Annual International Meeting. Society of Exploration Geophysics. Expanded Abstracts 94, 1580-1583.

Barnes, A.E., 1999. Seismic attributes past, present, and future. Society of Exploration Geophysics. Expanded Abstracts 18, 892.

Brown, A.R., 1996. Seismic attributes and their classification. The Leading Edge, 10, 1090.

Brown, A.R., 2001. Understanding seismic attributes. Geophysics 66, 47-48.

Campbell, G., Crotty, J. H.,1988. The application of 3-D seismic surveys to mine planning: South African Chamber of Mines MINTEK Seminar, 4th March 1988.

Campbell, G., Crotty, J. H., 1990. 3-D seismic mapping for mine planning purposes at the South Deep Prospect. In: Ross-Watt, D.A.J., Robinson, P.D.K. (Eds.), Proceedings International Deep Mining Conference: SAIMM Symposium Series S10, 2, 569–597.

Chopra, S., Castagna, J.P., Portniaguine, O., 2006. Seismic resolution and thin-bed reflectivity inversion. CSEG Recorder 31, pp. 19-25.

Chopra, S., Marfurt, K.J., 2007. Seismic attributes for prospect identification and reservoir characterization. Society of Exploration Geophysicists, Tulsa, pp. 456.

Chopra, S., Marfurt, K.J., 2008. Emerging and future trends in seismic attributes. The Leading Edge 27, 298-318.

Chopra, S., Castagna, J., Xu., Y., 2009. Thin-bed reflectivity inversion and some applications. First Break 27, 17-24.

Chung, H., Lawton, D., 1991. Some properties of thin beds. Society of Exploration Geophysics, Expanded Abstracts 10, 224.

Dankert, B.T., Hein, K.A.A., 2010. Evaluating the structural character and tectonic history of the Witwatersrand basin. Precambrian Research 177, 1-22.

Dehghannejad, M., Malehmir, A., Juhlin, C., and Skytta, P., 2012. 3D constraints and finite-difference modelling of massive sulphide deposits: The Kristineberg seismic lines revisited, northern Sweden. Geophysics 77, WC69-WC79, doi: 10.1190/GEO2011-0466.1.

Duff, D., Hurich, C., and Deemer, S., 2012. Seismic properties of the Voisey's Bay massive sulphide deposit Insights into approaches to seismic imaging. Geophysics 77, WC59-WC68, doi: 10.1190/GEO2011-0483.1.

Engelbrecht, C.J., Baumbach, G.W.S, Mathysen, J.L., Fletcher, P., 1986. The West Wits Line. In: Anhaeusser, C.R., Maske, S. (Eds.), Mineral Deposits of Southern Africa, Geological Society of South Africa 1, pp. 599-648.

Erismann, F., 2007. The South Deep Au-U ore deposit Witwatersrand basin, Republic of South Africa, Fluid inclusions and hydrothermal processes: MSc thesis, Eidgenössische Technische Hochschule (ETH) Zürich and final report to joint venture partners of South Deep Mine, pp. 87.

Fomel, S., 2007. Local seismic attributes. Geophysics 72, 29-33.

Gibson, M.A.S., Jolley, S.J., Barnicoat, A.C., 2000. Interpretation of the Western Ultra Deep Levels 3D seismic survey. The Leading Edge 19, 730-735.

Gibson, M.A.S., 2005. Interpretation of the 2003 South Deep 3D seismic survey. Unpublished internal report to Gold Fields Mining, 62 pp.

Hall, M., 2006. Predicting bed thickness with cepstral decomposition. The Leading Edge 25, 199-204.

Hanneing, A., Paton, G., 2012. Understanding thin beds using 3D seismic analysis workflows, attributes: New views on seismic imaging - their use in exploration and

production, 31st Annual GCSSEPM Foundation Bob F. Perkins Research Conference 1, pp. 322-341.

Jolley, S.J., Freeman, S.R., Barnicoat, A.C., Phillips, G.M., Knipe, R.J., Pather, A., Fox, N.P.C., Strydom, D., Birch, M.T.G., Henderson, I.H.C., and Rowland, T.W., 2004. Structural controls on Witwatersrand gold mineralization. Journal of Structural Geology 26, 1026-1086.

Jolley, S.J., Stuart, G.W., Freeman, S.R. Knipe, R.J., Kershaw, D., McAllister, E., Barnicoat, A.C., Tucker, R.F., 2007. Progressive Deformation of a Late Orogenic Thrust System, From Duplex Development to Extensional Reactivation and Disruption: Witwatersrand basin, South Africa. Geological Society. London. Special Publications 272, 543–569.

Justice, J.H., Hawkins, D.J., Wong, G., 1985. Multidimensional attribute analysis and pattern recognition for seismic interpretation: Pattern Recognition 18, pp. 391.

Kallweith, R.S., Wood, L.C., 1982. The limits of resolution of zero-phase wavelets. Geophysics 47, 1035-1046.

Knapp, R. W., 1990. Vertical resolution of thick beds, thin beds, and thin-bed cyclothems. Geophysics 55, 1183-1190.

Krapež, B., 1985. The Ventersdorp Contact placer: a gold-pyrite placer of stream and debris-flow origins from the Archaean Witwatersrand basin of South Africa. Sedimentology 32, 223-234.

Liu, J., Marfurt, K. J., 2006. Thin bed thickness prediction using peak instantaneous frequency. 76th Annual International Meeting. Society of Exploration Geophysicists. Expanded Abstracts, 968-972.

Malehmir, A., Durrheim, R., Bellefleur, G., Urosevic, M., Juhlin, C., White, D., Milkereit, B., Campbell, G., 2012. Seismic methods in mineral exploration and mine planning: a general overview of past and present case histories and a look into the future. Geophysics 77, WC173–WC190, doi:10.1190/GEO2012-0028.1.

Malehmir, A., Koivisto, E., Manzi, M., Cheraghi, S., Durrheim, R. J., Bellefleur, G., Wijns, C., Hein, K. A.A., and King, N., 2013. A review of reflection seismic investigations in three major metallogenic regions: The Kevitsa Ni–Cu–PGE district (Finland), Witwatersrand goldfields (South Africa), and the Bathurst Mining Camp (Canada). Ore Geology Reviews, Witwatersrand goldfields (South Africa), and the Bathurst Mining Camp (Canada). Ore Geology Reviews, http://dx.doi.org/10.1016/j.oregeorev.2013.01.003.

Malinowoski, M., Schetselaar, E, White, D.J., 2012. 3D Seismic imaging of volcanogenic massive sulphide deposits in the Flin Flon mining camp, Canada: Part 2-Forward modeling. Geophysics 77, WC81-WC93, doi: 10.1190/GEO2011-0474.1.

Mambane, P.W., Hein, K.A.A., Twemlow, S.G., Manzi, M.S.D., 2011. Pseudotachylite in the South Boundary Fault at the Cooke Shaft, Witwatersrand basin, South Africa. South African Journal of Geology 114, 109-120.

Manzi, M.S.D., Gibson, M.A.S., Hein, K.A.A., King, N., Durrheim, R.J., 2012a. Application of 3D seismic techniques to evaluate ore resources in the West Wits line goldfield and portions of the West Rand goldfield, South Africa. Geophysics 77, WC163–WC171, doi:10.1190/GEO2012-0133.1.

Manzi, M.S.D., Durrheim, R.J., Hein, K.A.A., King, N., 2012b. 3D edge detection seismic attributes used to map potential conduits for water and methane in deep gold mines in the Witwatersrand basin, South Africa. Geophysics 77, WC133–WC147, doi: 10.1190/GEO2012-0135.1.

Manzi, M.S.D., Hein, K.A.A., King, N., Durrheim, R.J., 2013. Neoarchaean tectonic history of the Witwatersrand basin and Ventersdorp Supergroup: New constraints from high resolution 3D seismic reflection data. Tectonophysics 590, 94-105, doi: 10.1016/j.tecto.2013.01.014.

McCarthy, T.S., 2006. The Witwatersrand Supergroup. In: Johnson, M. R., Anhaeusser, C.R., Thomas, R.J. (Eds.), The Geology of South Africa: Geological Society of South Africa, Johannesburg/Council for Geosciences, Pretoria, pp. 155-186.

Minter, W.E.L., 1982. The Golden Proterozoic (Chapter 4). In: Tankard, A.J., Jackson, M.P.A., Eriksson, K.A., Hobday, D.H., Hunter, D.R., Minter. W.E.L., (Eds.), Crustal evolution of Southern Africa: 3.8 Billion Years of Earth History. Springer-Verlag, New York, Heidelberg and Berlin, pp. 115-150.

Pretorius, C.C., Steenkamp, W.H., Smith, R.G., 1994. Developments in data acquisition, processing and interpretation over ten years of deep vibroseismic surveying in South Africa. In: Anhaeusser, C.R. (Eds.), Proceedings of the 15th Congress of the Council for Mining and Metallurgical Institutions 3, South African Institute of Mining and Metallurgy, 249–258.

Pretorius, C.C., Trewick, W.F., Fourie, A., Irons, C., 2000. Application of 3-D seismics to mine planning at Vaal Reefs gold mine, number 10 shaft, Republic of South Africa. Geophysics 65, 1862-1870.

Pretorius, C.C., Muller, M.R., Larroque, M., Wilkins, C., 2003. A review of 16 years of hardrock seismic of the Kaapvaal Craton. In: Eaton, D.W., Milkereit, B., Salisbury, M.H. (Eds.), Hardrock Seismic Exploration, Geophysical Developments10: Society of Exploration Geophysicists, pp. 247-268.

Purnomo, E.W., Harith, Z.Z.T., 2010. Combination of minimum-maximum (m-m) attribute and zero-intens-difference (z-i-d) attribute for estimating seismically thin-bed thickness. ITB Journal of Engineering Science 43, 78-100.

Rana, S., Burley, S.D., Chowdhury, S., 2006. The application of hierarchical seismic attribute combination to high precision infill well planning in the South Tapti Field, offshore Western India. Geohorizons, Journal of Society of Petroleum Geophysicists 11, 32-38.

Robb, L.J., Meyer, F.M., 1995. The Witwatersrand basin, South Africa: Geological frame work and mineralization processes. Ore Geology Reviews 10, 67-94.

Rock Solid Images, 2003. Seismic trace attributes and their projected use in prediction of rock properties and seismic facies, Houston, Texas, pp. 1-4.

Russel, B.H., 1988. Introduction to seismic inversion methods. Society of Exploration Geophysicists, SEG course notes 2, pp. 90.

SACS (South African Committee for Stratigraphy), 1980. Stratigraphy of South Africa. Part 1: Lithostratigraphy of the Republic of South Africa. South West Africa/Namibia and the Republics of Bophuthatswana, Transkei and Venda. Geological Survey of South Africa Handbook 8, pp. 690.

Salisbury, M.H., Harvey, G.W., Mathews, L., 2003. The acoustic properties of ores and host rocks in hardrock terranes. In: Eaton, D.W., Milkereit, B., Salisbury, M.H. (Eds.), Hardrock Seismic Exploration, Geophysical Developments Series 10. Society of Exploration Geophysicists, pp. 9-19.

Sheriff, R.E., Geldart, L.P., 1995, Exploration seismology, Cambridge University press, pp. 592.

Sheriff, R.E., 1991. Encyclopedic Dictionary of Exploration Geophysics. SEG, Tulsa.

Stevenson, F., Higgs, R.M.A., Durrheim, R.J., 2003. Seismic imaging of precious and base-metal deposits in South Africa. In: Eaton, D.W., Milkereit, B., Salisbury, M.H. (Eds.), Hardrock Seismic Exploration, Geophysical Development Series 10, Society of Exploration Geophysicists, pp. 141-156.

Taner, M.T., Koehler, F., Sheriff, R.E., 1979. Complex seismic trace analysis. Geophysics 44, 1041-1063.

Taner, M.T., Sheriff, R.E., 1977. Application of amplitude, frequency, and other attributes to stratigraphic and hydrocarbon determination: Section 2. Application of seismic reflection configuration to stratigraphic interpretation, AAPG Memoir 26, 301-327.

Taner, M.T., 2001. Seismic attributes, Canadian Society of Exploration Geophysicists Recorder, 48-56.

Trickett, J.C., Duweke W.A., Kock, S., 2004. Three-dimensional reflection seismic: worth its weight in platinum: International Platinum Conference 'Platinum Adding Value', South African Institute of Mining and Metallurgy, 257-264.

Vermaakt, D.T., Chunnet, I.E., 1994. Tectono-sedimentary processes which controlled the deposition of the Ventersdorp Contact Reef within the West Wits Line. In: Anhaeusser, C.R. (Eds.), Proceedings of the 15th Congress of the Council for Mining and Metallurgical Institutions 3, South African Institute of Mining and Metallurgy, 117-130.

Weder, E.E.W., 1994. Structure of the area south of the Central Rand gold mines as derived from a gravity and vibroseis surveys, Proceedings of the 15th CMMI Congress, South African Institute of Mining and Metallurgy, 271-281.

White, R. E., 1991. Properties of instantaneous seismic attributes. The Leading Edge 10, 26–32.

Widess, M.B., 1973. How thin is thin bed? Geophysics 38, 1176-1180.

Yilmaz, O., Tanir I., Cregory, C., 2001. A unified 3D seismic work flow. Geophysics 66, 1699-1713.

Zeng, H., 2009. How thin is a thin bed? An Alternative Perspective. The Leading Edge 28, 1192-1197.

Zhang, P., Shen, Z., Shen, H., 2009. Discussions on resolution limit in seismic inversion: CPS/SEG Beijing international geophysical conference and exposition, pp. 259, doi: 10.1190/1.3603784.

The Ventersdorp Contact Reef model in the Kloof Gold Mine as derived from 3D seismics, geological mapping and exploration borehole datasets

Musa S.D. Manzi[1✉], Kim A.A. Hein[1], Raymond J. Durrheim[2, 3] and Nick King[4]

Seismic and Structural appraisal

[1 ✉] Corresponding Author; School of Geosciences, University of the Witwatersrand Johannesburg, PBag 3, WITS, 2050, Republic of South Africa; Tel +27-11-7176623; E-mail: Musa.Manzi@students.wits.ac.za

[1] School of Geosciences, University of the Witwatersrand Johannesburg, PBag 3, WITS, 2050, Republic of South Africa; Tel: +27-11-7176623; E-mail: kim.ncube-hein@wits.ac.za

[2] School of Geosciences, University of the Witwatersrand Johannesburg, PBag 3, WITS, 2050, Republic of South Africa; Tel: +27 11 717 6579; E-mail: Raymond.Durrheim@wits.ac.za

[3] CSIR Centre for Mining Innovation, Republic of South Africa.

[4] South Deep Gold mine; Gold Fields Limited, Republic of South Africa; Tel: +27-82-374 2060; Email: nick.king@goldfields.co.za

Abstract

A model of the Ventersdorp Contact Reef (VCR) orebody at Kloof Gold Mine was derived by integrating 3D reflection seismic data with information derived from underground mine mapping and exploration drilling. The study incorporated the depth-converted prestack time migrated (PSTM) seismic cube, the mine geomodel, faults and dikes mapped in excavations, mine development infrastructure, and intersections of the VCR by surface and underground exploration drilling. The 3D seismic data provide an accurate geometric model of the VCR orebody and its offsets. The underground mapping datasets help to define minor faults and dikes that are below seismic resolution limits. The integration of the these datasets allowed (1) for better mapping of fault architectures and distributions within the lease area, (2) definition of the likely zones of difficult ground conditions around seismically imaged dikes and faults, and (3) better predictions of the number and spacing of faults that offset the VCR within minable blocks. The model is useful in mitigating both economic and safety risks of deep mining.

1. Introduction

The Archaean Witwatersrand Basin of South Africa is the world's largest known gold deposit since its discovery in 1886. Almost 60 kt of gold has been mined, with a retained reserve estimated at 35 kt gold [1]. Gold occurs in conglomerate units known as reefs, which vary in thickness from 10 cm to 5 m. Gold mining in several goldfields takes place at depths ranging from about 500 m to 4500 m below surface [1], [2], [3] and [4].

Initially orebody models were based on geological mapping, exploration drilling, and interpretation of gravity and magnetic data [5], [6], [7] and [8]. However, these techniques lacked the resolution and areal coverage needed to generate robust geological models of deep ore bodies [8] and [9]. In the late 1980s, the 3D reflection seismic method became the core tool for final stage exploration and feasibility studies [10].

The application of 3D seismic techniques in the Witwatersrand gold mines has been reported by Gibson et al. [4], Pretorius et al. [6-7], and Malehmir et al. [10-11], among others. A multitude of processing, interpretation and structural modeling techniques have been developed in recent decades, making it worthwhile to re-process, interpret and model old 3D seismic datasets. By using these techniques, it is now possible to generate a state-of-the-art 3D orebody model that unravels structural complexities such as intersecting and cross-cutting faults. However, the 3D seismic technique, like any other geophysical prospecting technique, has its specific limitations [12].

Firstly, many seismically-derived horizon models suffer from major depth misties when correlated with the borehole controls. This is commonly the result of inaccurate velocity fields that are used for migration (either pre- or post-stack) and the conversion of travel times to depth during processing. In structurally complex areas such as the Witwatersrand Basin, lateral velocity variations make the velocity analysis a challenging task [13]. This is because seismically-derived models are fundamentally developed from the seismic travel time data that has been corrected for depth using complex velocity fields. A constructed geological model is therefore dependent on how well the velocity fields have been approximated at various seismic processing stages. Furthermore, the velocity fields for migration and subsequent time-to-depth conversion processes are, in turn,

dependent on the number and distribution of boreholes. A variety of techniques have been proposed to improve velocity analysis in complex areas during prestack migration processing stages [13] and [14]. Unfortunately, apart from the reprocessing of the datasets, there is currently little that can be done to correct for the large uncertainties of depth misties between seismic horizon models and borehole controls, especially when the inaccurate seismic velocity field has been used for migration and subsequent time-to-depth conversion.

Secondly, the resolution of fault imaging is primarily a function of the dominant frequency and the signal-to-noise ratio (S/N) of the field data. The seismically-derived ore horizon models are also dependent in the S/N of the picked seismic horizons. Faults have a number of effects, almost always undesirable, on underground gold mining. These effects include: (1) physical displacement of gold-bearing reefs that may make the reefs impractical to mine, (2) reducing the stability of the mining hangingwall in underground workings, and (3) they may act as conduits for ingress of water and flammable gas into underground workings. Faults have their origin and evolution in a range of processes such as compression and extension. It is important to effectively recognize faults in the seismic data and determine their orientation and amount of vertical displacement (throw). This type of information can assist in (1) the unraveling the fault generation mechanisms and timing, (2) mitigating the risk of falls of ground or rockbursts ahead of mining. Furthermore, faults can exhibit complex structural architectures such as multi-fault segments that bound orebody blocks, multiple bifurcations from a single plane to form a branched fault array, and late faults that crosscut and offset fault systems. These features have significant impact on mine development. Failing to identify fault (and dike) arrays is risky in terms of mine planning and design.

In studies by Manzi et al. [15-16], various seismic interpretation techniques, including edge detection attribute analysis, were used to image faults with throws as small as 10 m. However, [4], [15], [16], and [17] showed that regardless of the quality of the seismic data, there are always smaller faults that offset the orebody that cannot be imaged, and have a significant impact on mine development. Even with a very good 3D seismic survey design, state-of-art processing and interpretation capabilities, features such as thin dikes, near-vertical faults, subtle faults with offset as low as 1-2 m and which displace the gold-bearing reef by more than the stoping height, cannot be

directly imaged by seismics because they are well below seismic resolution limit. For example, seismic data with dominant frequency of 50 Hz and high S/N can resolve faults with throws as small as 5-10 m, while seismic data with low S/N can only resolve faults with throws of 25-30 m.

Thirdly, structural imaging and fault horizon models derived solely from seismic data depend on factors such as the 3D seismic survey design, the skills and experience of seismic processor and interpreter; and the time given to perform the interpretation. Therefore, taking a 3D geological model constructed from seismic data only as a true and final geological model may be inaccurate. Faced with a wide range of uncertainties, it is necessary to incorporate other models based on, for example, datasets such as underground mapping and exploration boreholes. Quality geological mapping data, in particular, is extremely useful when attempting to model faults and dikes that fall below seismic resolution limits.

In this study we derive the model of the Ventersdorp Contact Reef (VCR) orebody in Kloof Gold Mine, by integrating 3D seismics, geological mapping and exploration borehole datasets. To generate a robust orebody model we, (1) minimize the impact of depth misties in the seismic defined VCR ore horizon through the application of a depth-error gridding method, and (2) correct for lateral mis-positioning of structures in the seismic model by testing errors between seismic amplitude and underground infrastructures such as shafts and excavations.

Importantly, given that a prolonged period of mining and associated mine mapping has occurred across a large area of the Kloof Gold Mine, we extend studies by [18] in using 3D seismics to interpret the stoped-out areas adjacent to development areas. By doing so, we are able to assess and estimate how many of the seismically invisible structures are likely to be present in development areas and use these data to enhance a geological model of the VCR orebody. To achieve this goal, we determine and then apply a series of fault statistics from well-mapped structures immediate to the area of interest. These statistics include measuring the size-frequency distribution of faults (mainly normal faults), computation of fault attributes (e.g. dip), fault spacing, fault throw (vertical component of the displacement) and fault heave (horizontal component of the displacement) for various geometries across the study area. These statistics are important when attempting to define likely face advancement rates, scheduling and ultimately bulk production rates and tonnages. They also help

define the zones around the seismically-imaged structures where difficult ground conditions are expected, and predict the number and spacing of faults that offset the orebody within minable blocks. This type of statistical analysis is undertaken for the first time in the Witwatersrand Basin.

In the past two decades, it has become clear that there are well-defined fractal relationships between fault throw and the size-frequency distribution of faults [19] and [20]. These values vary greatly between different suites and the age of structures. The historic geological mapping data from Kloof Gold Mine provide a superb database from which to derive these statistics.

2. Kloof Gold Mine

2.1. Mining history and prospects

The Kloof Gold Mine is owned and operated by Sibanye Gold (subsidiary of Gold Fields Limited). The mine is the product of an amalgamation that took place in April 2000 of the Libanon, Kloof, Leeudoorn and Venterspost mines under Gold Fields Limited, and forms the western part of the Kloof-Driefontein Complex (KDC). Prior to the amalgamation, the Kloof Gold Mine operated as a separate entity and was granted a lease to mine down-dip of the Libanon mine at depths between 2.5 and 3.7 km.

Kloof Gold Mine is a critical asset of Sibanye Gold. Of its 83 million ounce resource base, approximately 29 million ounces are situated below current shaft depths. The 3D seismic survey explores these areas, which are critical to ensuring long-term sustainability beyond 2021.

Geographically, the Kloof Gold Mine is located in the West Wits Line goldfield of the Witwatersrand Basin, 65 km southwest of the city of Johannesburg (Fig. 1). The major portion of the mining lease area is situated in the West Wits Line goldfield, but the northerly portion straddles the boundary of the West Rand goldfield (see Fig. 1). Four gold-bearing reefs are exploited, namely the Ventersdorp Contact Reef (VCR), Kloof Reef (KR), Libanon Reef (LR) and Middelvlei Reef (MR). The VCR represents 93% of the reserve portfolio, while 4% comes from MR and 3% from the KR and LR collectively. The VCR is one of the richest ore horizons in the Witwatersrand Basin goldfields.

The mining area in Kloof comprises five producing shafts that mine varied contributions from remnant pillars and virgin reefs. The Kloof Gold Mine has an estimated reserve of 44.1 Mt for a Life of Mine (LoM) head-grade of 13.9 g/t gold. These are planned for depletion by 2021 at an average production rate of 170,000 t/month. The deepest mining level of the orebody is at 3.347 km below surface and the total gold production is averaged at 1,667 kg per month at an average yield grade of 6.0 g/t.

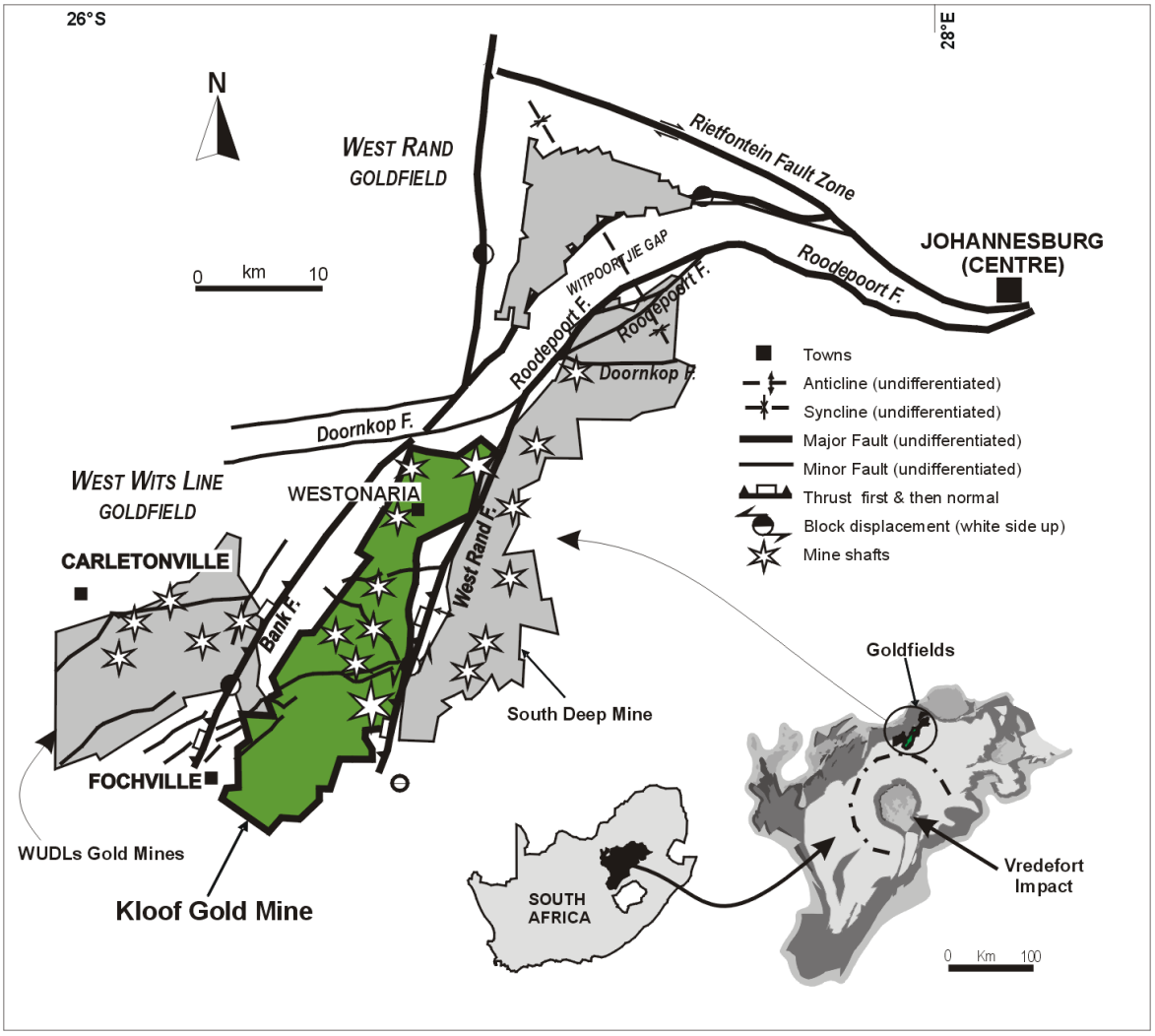


Fig. 1. *The location map of the West Rand and West Wits Line (Carletonville) goldfields of the Witwatersrand basin in South Africa, showing the Kloof Gold Mine (modified after Dankert and Hein, 2010).*

2.2. Geology

The geology of the Witwatersrand Basin has been described by Malehmir et al. [11], Beach and Smith [21], Jolley et al. [22], Dankert and Hein [23], Mambane et al. [24] and others. The generalized stratigraphy of the basin is presented in Fig. 2. The VCR orebody was deposited at an angular unconformity between metasedimentary rocks (quartzite and conglomerate units) of the Central Rand Group of the Witwatersrand Supergroup (Fig. 2) and metabasaltic rocks of the Ventersdorp Supergroup [4] and [23]. The unconformity is characterized by an auriferous thin fluvial conglomerate referred to as the Venterspost Conglomerate Formation or VCF [25], [26], [27], and [28] and [29], or the Venterspost Formation [30] and [31]. The (basal) auriferous conglomeratic lithofacies of the VCF is referred to as the Ventersdorp Contact Reef (VCR) and is dated at 2729 ± 19 Ma (discordant U-Pb SHRIMP ages) from igneous-detrital xenotime/zircon aggregate [32]. The Kloof Gold Mine is situated on the eastern limb of the first order crustal-scale Libanon Anticline [18]. It is bounded to the west and east by the Bank and West Rand faults, respectively (Fig. 1).

In the West Wits Line, the VCR is separated from the Witwatersrand Supergroup by an angular unconformity [27], [33], [34] and [35] that is interpreted as a degradational surface by [36], [37] and [38]. Where present in the central and southern portion of the Witwatersrand Basin, the VCR is conformable with the metasedimentary rocks of the Central Rand Group [26], [39] and [40].

The VCR at the Kloof Gold Mine is approximately 1.5 m thick. The orebody dips at 25° to the southeast for a north-northeast strike, and lies at 1 km to 4.2 km depth (Fig. 2). The VCR orebody is divided into two major reef types namely, plateau and channel reefs [37]. These reef types are further subdivided into facies types, which consist of a complex series of intercalated oligomictic and polymictic conglomerates of varying thicknesses and differing average gold grade [41].

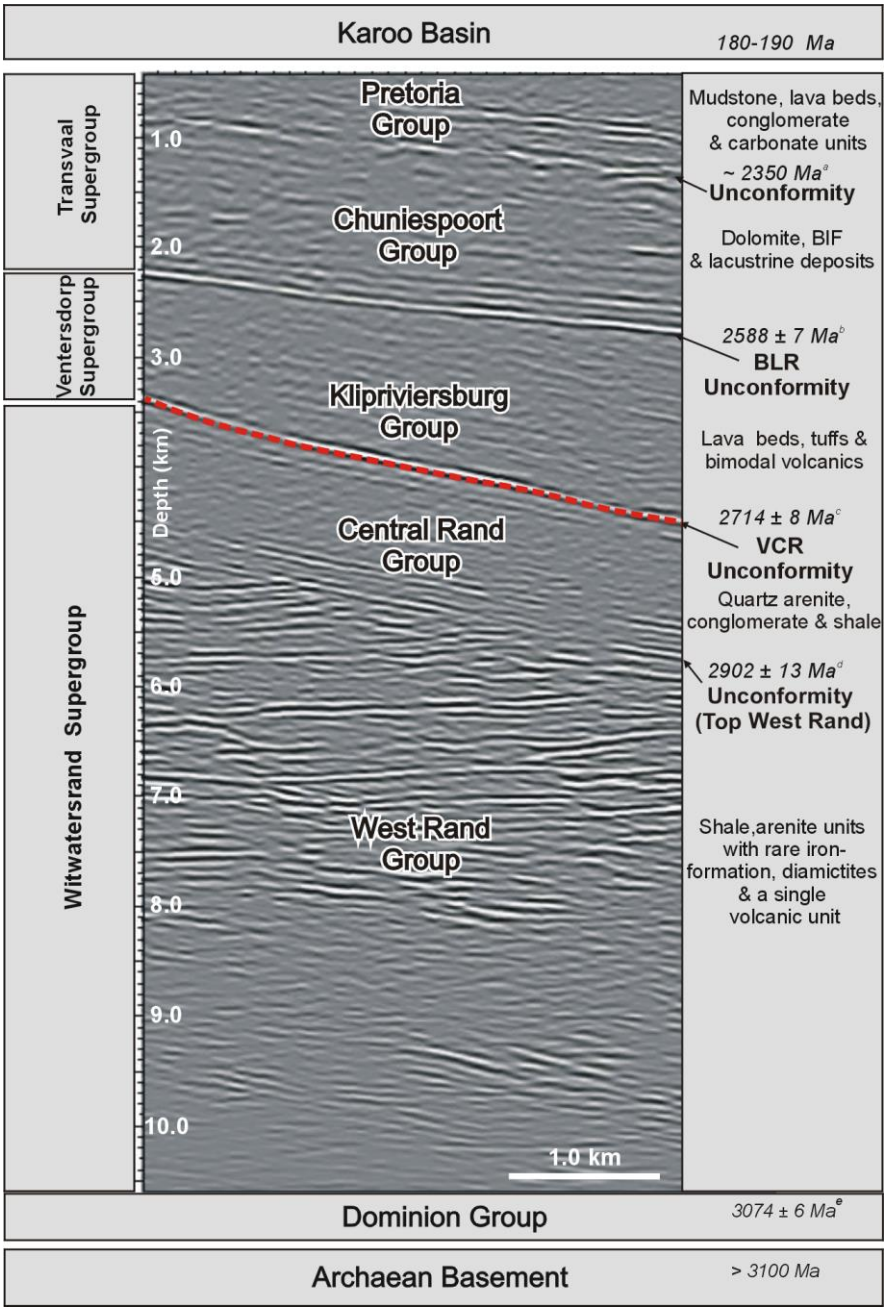


Fig. 2. *Generalized seismic stratigraphy, with dates and ages are derived from Krapež [32], Myers et al. [61], Armstrong et al. [62], Kositcin and Krapež [63] and Dankert and Hein [23]. VCR: Ventersdorp Contact Reef; BLR: Black Reef Formation. [a]Unpublished; [b]Martin et al. (1998; zircon U-Pb SHRIMP) [64]; [c,e]Armstrong et al. (1991; single zircon U-Pb SHRIMP); [d]Kositcin and Krapež (2004; zircon U-Pb SHRIMP).*

3. 3D seismic survey

3.1. Acquisition

The Kloof 3D seismic survey, the most recent 3D survey of the Witwatersrand Basin, was acquired in 2003 over those areas deemed prospective, which covers much of the area where the VCR is deeper than the current shaft infrastructure at the Kloof Gold Mine (Fig. 3a, b). These areas are known as Kloof Extension areas (KEA) and the 3-Shaft drop-down areas (Fig. 3b). Through the reprocessing of the 1994 Leeudoorn seismic data, and merging with the 2003 Kloof survey, the coverage of 7-Shaft decline and Eastern Boundary Area (EBA) was achieved (Fig. 3a, b). The details of the seismic data acquisition and processing have been reported by Manzi et al. [15-16].

The 2003 Kloof seismic survey was designed to image the VCR orebody over the depth range of 3.0-4.2 km. The orebody is too thin to be directly imaged by the seismic method. However, it coincides with a major acoustic impedance contrast between relatively high–velocity/dense metabasalts of the Klipriviersberg Group (~6400 m/s velocity and ~2.90 g/cm^3 density) and underlying low-velocity/dense quartzite units (~5700 m/s velocity and ~2.67 g/cm^3 density) of the Central Rand Group that produces a strong seismic reflector. The survey objectives were to image (i) the cut-off of the VCR on the steeply-dipping (65°-70° W) West Rand Fault; (ii) the extent of the VCR in the South Deeps lease area. This was to provide the basis for early and accurate mine design and scheduling for new projects, ensuring realistic production ramp-ups and gold production profiles.

The current 3D seismic dataset maybe globally the largest 3D seismics from hardrock environment with a surface footprint of 85 km^2, and is possibly the most cost-effective Witwatersrand Basin survey completed to date (Fig. 3b). A programme of exploration drilling and underground mapping was completed at the same time as the survey to determine the gold grade and delineate areas of structural risk, thus optimizing future mine development (see Fig. 4 for the location of boreholes). These sources of information meant that expansion of Kloof into development areas could be done with a high level of confidence. The merged 3D seismic reflection dataset was provided as a depth-converted prestack time migrated (PSTM) volume. The Kloof depth-converted prestack time

migrated (PSTM) volume (Fig. 4), incorporating the Leeudoorn dataset, covers an area of 12 x 16 km and projects to a depth of 11 km.

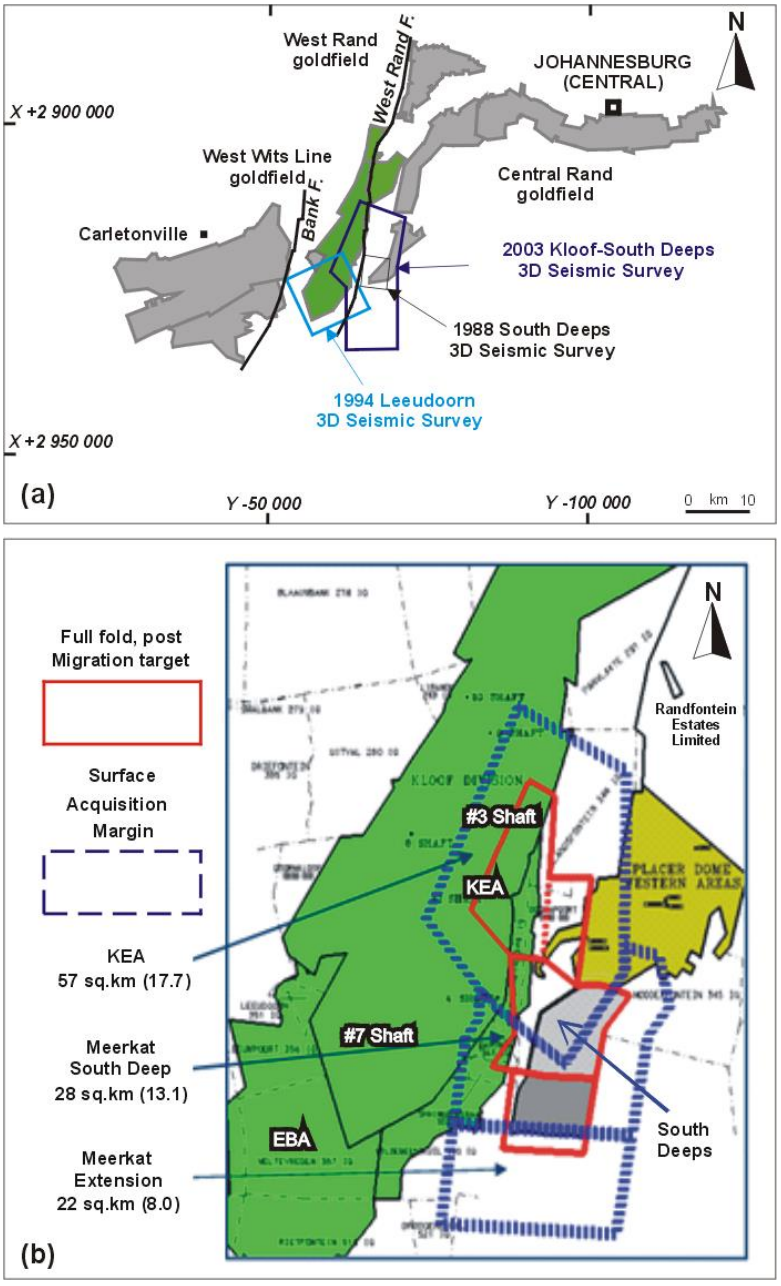


Fig. 3. *(a) The location map showing the historical surveys overlain by the 2003 3D Kloof-South Deep seismic survey (after Gibson et al., 2000; Manzi et al., 2012a). (b) Kloof Development area and South Deeps seismic survey acquisition margin and targeted areas (after Manzi et al., 2012b). KEA: Kloof Extension areas, EBA: Eastern Boundary Area.*

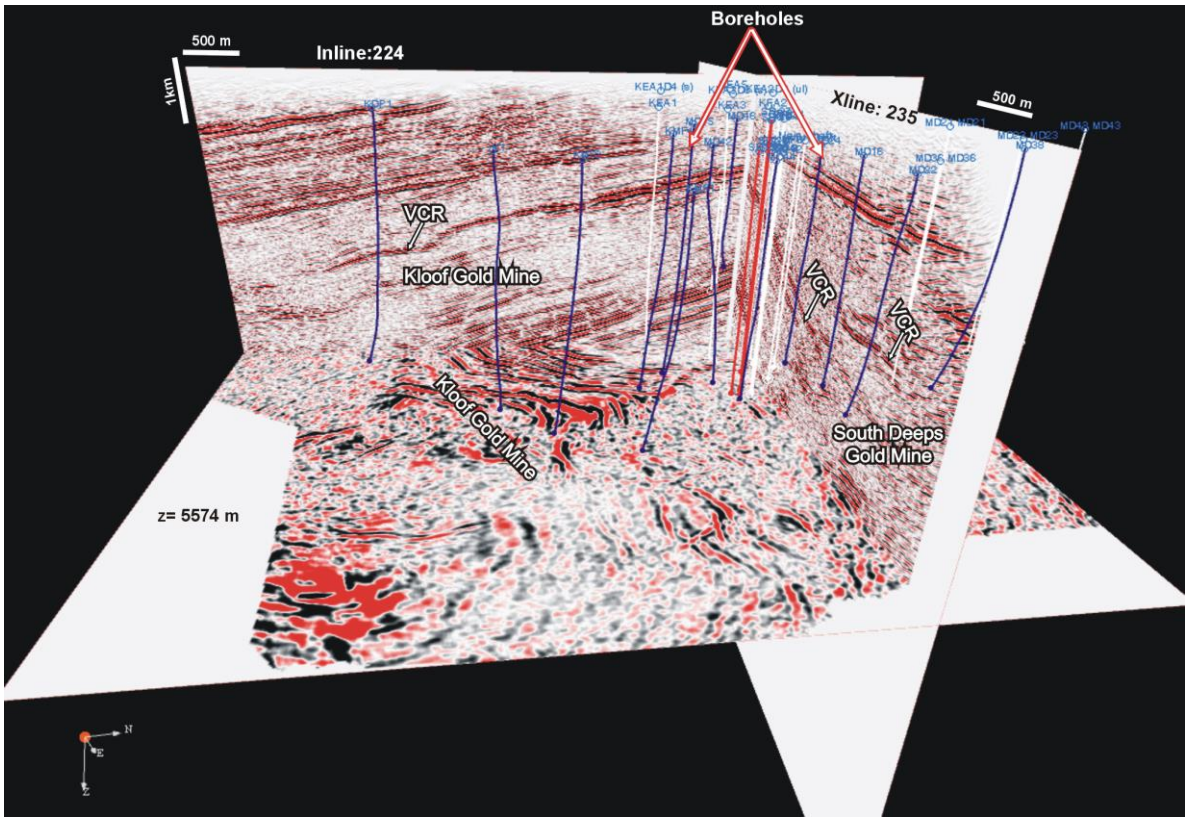


Fig. 4. *3D depth-converted prestack time migrated seismic cube (amplitude display) covering Kloof and South Deeps Gold mines, showing location of exploration boreholes.*

3.2. Seismic resolution limits

The survey parameters, such as bin size, horizontal and vertical resolution, fold of coverage, source and receiver configurations were carefully chosen to achieve the optimum imaging of the VCR and geological features. The seismic resolution limit, comprising the vertical and horizontal resolution, is a critical parameter for the optimum imaging of the orebody and realistic modeling. The vertical resolution is defined as the ability to distinguish two close seismic events at different depth levels, and is defined in terms of seismic dominant wavelength;

$$\lambda = v / f \qquad (1)$$

where v and f are the mean velocity and dominant frequency, respectively [42]. Based on the survey parameter trials conducted prior to the commencement of the 3D seismic survey, the observed dominant frequency (f) of 50 Hz and mean velocity (v) of 6200 m/s provided 124 m dominant wavelength (λ). According the Widess criteria [43], the vertical resolution limit, for the data with

low (S/N) is 1/4 seismic dominant wavelength (λ). However, previous studies by Gibson et al. [4], Manzi et al. [15-16] and Jolley et al. [22] of the deep mine workings showed that vertical resolution limits for feature detection are closer to 1/8 of the dominant wavelength, i.e., the Widess criteria [43] for the data with sufficiently high S/N. Therefore, for $\lambda/4$ and $\lambda/8$ Widess criteria, the achievable resolution limits are 31 m and 15.5 m, respectively. Although the S/N of these data is high, it was thought that features less than ~16 m would not be resolved.

The horizontal resolution is simply described as the ability to detect two laterally displaced features as two distinct adjacent events [44]. The most traditional estimate of the horizontal resolution is derived from the size of the Fresnel zone, and is strongly correlated to the bin size of the survey. The Fresnel zone is the subsurface area where the reflected energy arrives at the surface within the time interval equal to half the dominant period [42]. Using the Fresnel zone criterion for depths of 1000 m and 4000 m, the horizontal resolution varies between 250 m and 500 m, respectively. Therefore, geological features with spacing below these limits may not be discernible. However, after migration, the limit of resolvability can be enhanced to approximately the dominant wavelength, which is 124 m [45]. Therefore, features with spacing much less than the Fresnel zone can be detected, assuming a good velocity model and high S/N of the data. Since the Kloof Gold Mine is characterized by moderately dipping stratigraphy (~ 30° E), a proper bin size was chosen to avoid spatial aliasing. Spatial aliasing is an ambiguity that rises if the survey bin size is too large, for example, steeply dipping reflectors or stratigraphy can be incorrectly imaged and reconstituted to a shallow dip. The bin size is the function of the root mean square average velocity (V_{rms}) to the target, peak frequency (f_{max}), and the dip angle (α) of the structural element. It is given by [46] as:

$$\Delta x \leq V_{rms} \Big/ (4 f_{\max} \times \sin(\alpha)) \qquad (2)$$

By taking into consideration these parameters, the largest bin size that will not cause aliasing is 62 m. However, 25 m bin size was an adequate and safer sampling detection limit to record the maximum lateral resolution of 124 m diameter (the dominant wavelength). This bin size was used to avoid spatial aliasing up to a maximum stratigraphic dip of 35° and a frequency of 100 Hz, which matches the maximum dip of the VCR at Kloof Gold Mine and the highest source frequencies used. It

should, however, be noted that other parameters such as source and receiver geometry can also affect the design of the bin size.

4. Seismic imaging of the VCR

The VCR seismic horizon was picked manually on every single inline and crossline (25 m interval) and depth slices of the PSTM seismic cube using a variety of seismic attribute displays. The VCR was picked as a peak (maximum positive amplitude) originating from the reflection produced at the contrast between the metabasalts at the bottom of Ventersdorp Supergroup (~ 6400 m/s velocity) and quartzite units at the top of the Central Rand Group (~ 5700 m/s velocity). Discontinuities such as faults were manually picked on every third inline and crossline of the seismic sections (75 m interval). Faults were also picked on the VCR surface. The confidence with which fault parameters (location and offset) were interpreted was controlled by the amplitude of the VCR horizon reflection. Therefore, in order to pick faults on the VCR seismic horizon, breaks needed to be visible. The amplitude attribute computed for the VCR horizon provided a first pass indication of the likely imaging ability for any structures that were present in the data (Fig. 5). The amplitude measures the seismic acoustic impedance and thus helps to identify changes in lithological characteristics in the data. The results resolved a variability in the quality of the VCR picks due to the amplitude of the signal returned to the surface, which is a function of the reflectivity at the acoustic boundaries [42]. The VCR amplitude display was divided into two domains based on the S/N (Fig. 5). The part of the survey with high S/N corresponded to the development areas, Kloof Extension area (KEA) and Extension Boundary Area (EBA) (Fig. 5). The KEA included areas east of stopes nearby Shaft #1 and #3, and areas surrounding the Shaft #4, #9 and #7 complexes. The EBA is the southwestern part of KEA. The low confidence (poor S/N) areas included the western part of the EBA, and areas to the north of the Shaft #8 complex and northwest of the Shaft #7 complex (Fig. 5). It is important to note that the areas characterized by low S/N were near the survey boundaries (mainly northern part of the survey), implying that the poor quality of the data was due to low fold-of-coverage and poor migration at the edges of the survey (Fig. 5). In addition, the poor quality of the data in the northern

part of Shaft #8 complex is unavoidable because of outcropping dolomite rocks, which hampered seismic acquisition [15]. The areas where the S/N deteriorated required more careful re-picking of the VCR before being confidently assigned as robust picks.

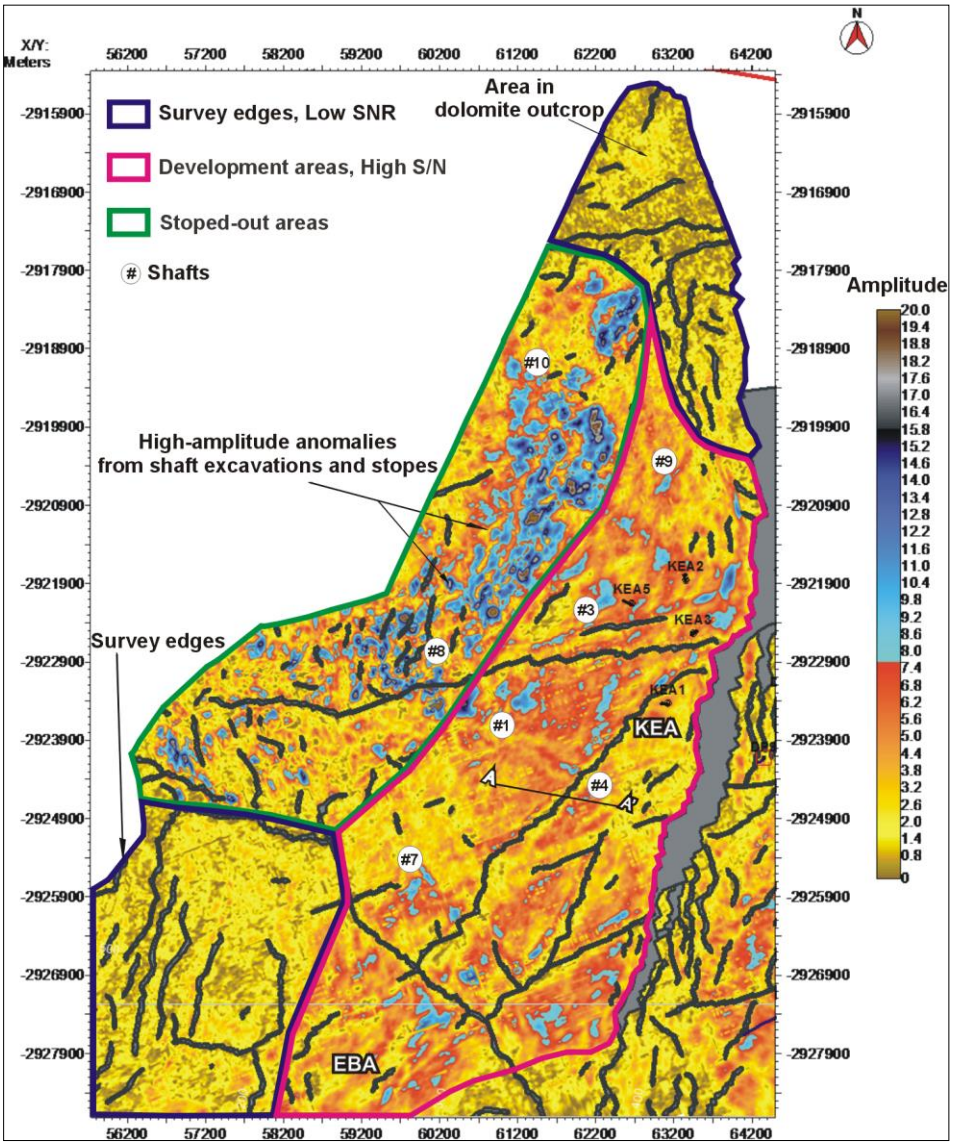


Fig. 5*. Amplitude attribute computed for the VCR horizon across the Kloof survey area. The map shows the location of shaft excavations, stoped-out and development areas, and the imaging faults.*

High-amplitude anomalies coincided with stoped-out areas immediate to Shaft #8 and #10 complexes, and corresponded with infrastructure including development drives, workshops, hoisting, pump chambers, and stopes (Fig. 6). Therefore, structural interpretation in these areas was challenging. Excavations, and in particular stopes, were expected to produce high-amplitude reflections due to an acoustic impedance contrast between the surrounding rocks and air in the excavation (Fig. 5 and 6). The average stoping height is of the order of approximately 1-2 m [47]. The high-amplitude reflections were also evident on the migrated inline and crossline sections (Fig. 6), precisely coinciding with shaft excavations. Apart from the stoped-out areas, the amplitude map resolved variations in the frequency of structural elements throughout the survey area. Areas with erratic amplitudes were interpreted to be the result of either low S/N or structural complexity. Areas with dimmed amplitude anomalies were interpreted to be due to waveform interference and scattering of the seismic energy. The data from underground mapping was therefore used to reduce the ambiguity. By projecting faults mapped in the stoped-out areas to the development areas, it was found that most faults were represented by amplitude diminutions.

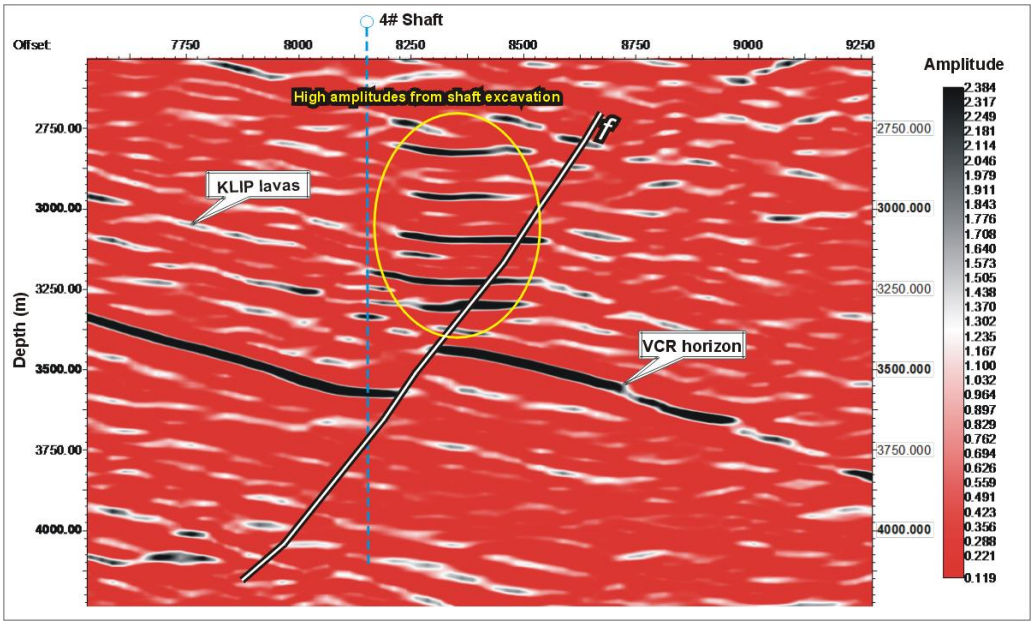


***Fig. 6**. Seismic section (amplitude display) showing the imaging of shaft locations, coinciding with high amplitude reflection events. Note that the #4 Shaft intercepts the fault at depth of about 3.5 km below surface.*

The detailed structural interpretation of the VCR depth map is shown in Fig. 7. The depth-converted seismic data has improved the structural interpretation. The VCR pick, as shown in any west-east seismic section, is clear across the survey area, showing a minor depth mistie (~ 12 m) with the borehole control (Fig. 7b).

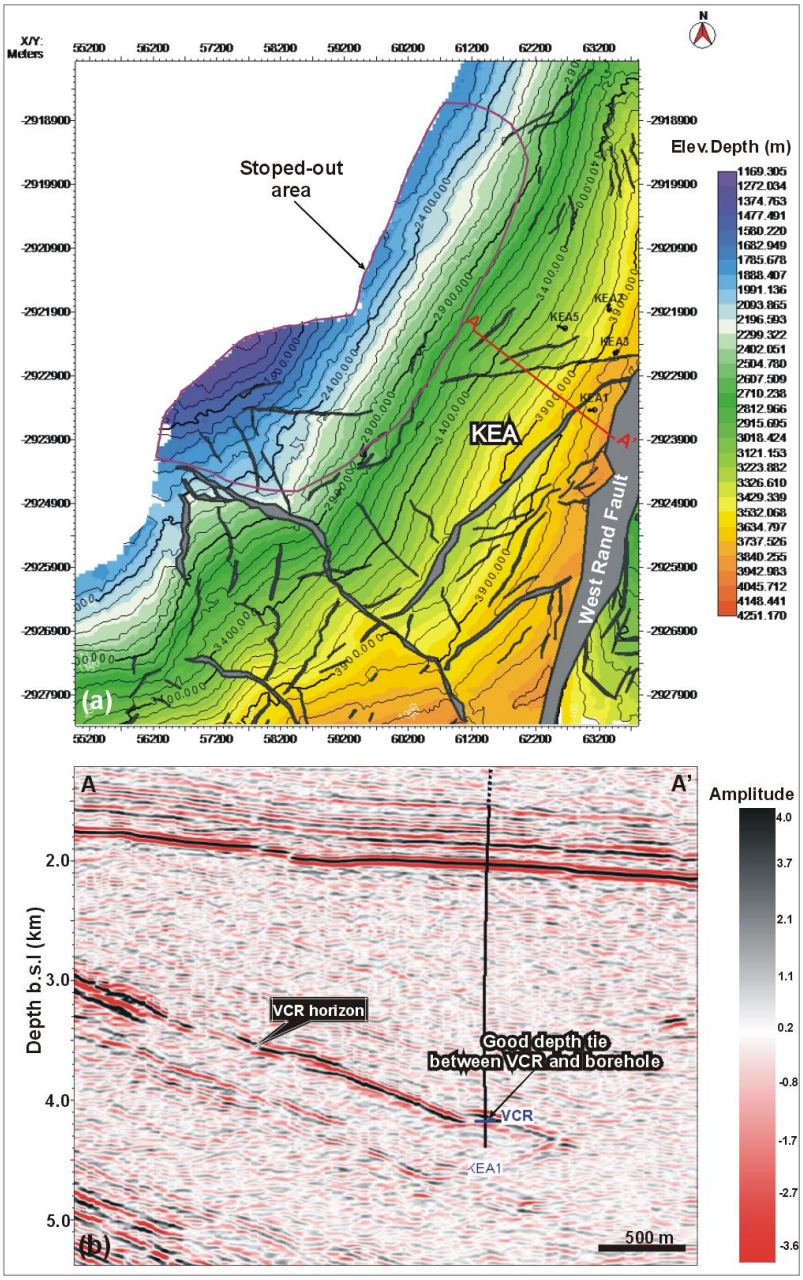


Fig. 7. *(a) VCR depth structure map. (a) Seismic section (amplitude display) showing good depth tie between VCR and a borehole. The VCR horizon cut-off lines, defined by 'fault-polygons', are incorporated in the initial phase of 3D modeling as input data.*

After picking the VCR horizon in 2D seismic sections, the 3D fault surfaces and VCR horizon were created and integrated. The noise introduced during picking was smoothed using post-fault interpolation smoothing operators such as the bi-harmonic smoothing algorithm [48]. These operators seek to remove the isolated surface noise, but retain linear breaks (faults). Subsequently, the fault-horizon projection was enhanced using edge detection attribute analysis. These techniques provided maximum resolution for the identification and location of faults, eliminated errors resulting from false complex geometries created by conventional picking around faults, and thus minimized unrealistic 3D fault-horizon geometries. Generally, faults picked manually on seismic sections do not exactly match breaks in the horizon. The fault surfaces developed were therefore modified and modeled using newly developed modeling techniques to give tight correlation with the seismically-defined VCR breaks. The 3D fault-horizon network formed the basis of a realistic model.

5. Data integration and comparison

The data that were integrated and utilized in the development of the VCR orebody model includes 3D seismic data, 3D seismic interpretation, mine geomodels that incorporate faults and dikes mapped in underground workings, intersections of the VCR by surface and underground exploration boreholes (~50 holes), and mine development infrastructure maps. The datasets were integrated into the mine planning process using the AutoCAD package. The final output was a robust geological framework model for the VCR orebody constrained by the borehole, seismic and mapping data.

5.1. Comparison of seismic model and geomodels

The interpretations based on mapping and seismic data are presented in Fig. 8. There are clearly more faults and dikes present in the geomodel when compared with the seismic model for the development areas. Some faults and dikes resolved in the geomodel do not appear in the seismics, and vice versa (Fig. 8a, b). For example, north-northeast trending dikes and faults are not resolved by the seismics (Fig. 8a). Therefore, the geomodel clearly adds an important dimension to the final VCR orebody model.

Similarly, seismics shows high resolution imaging of many faults that are not present in the geomodel, particularly in the unmapped areas (Fig. 8b). Furthermore, there are a number of faults and dikes that match in seismic and geomodels. In fact, some faults in the geomodel extend beyond the stoped-out areas to the development areas (Fig. 8a). It may be concluded that underground mapping and seismic datasets complement each other.

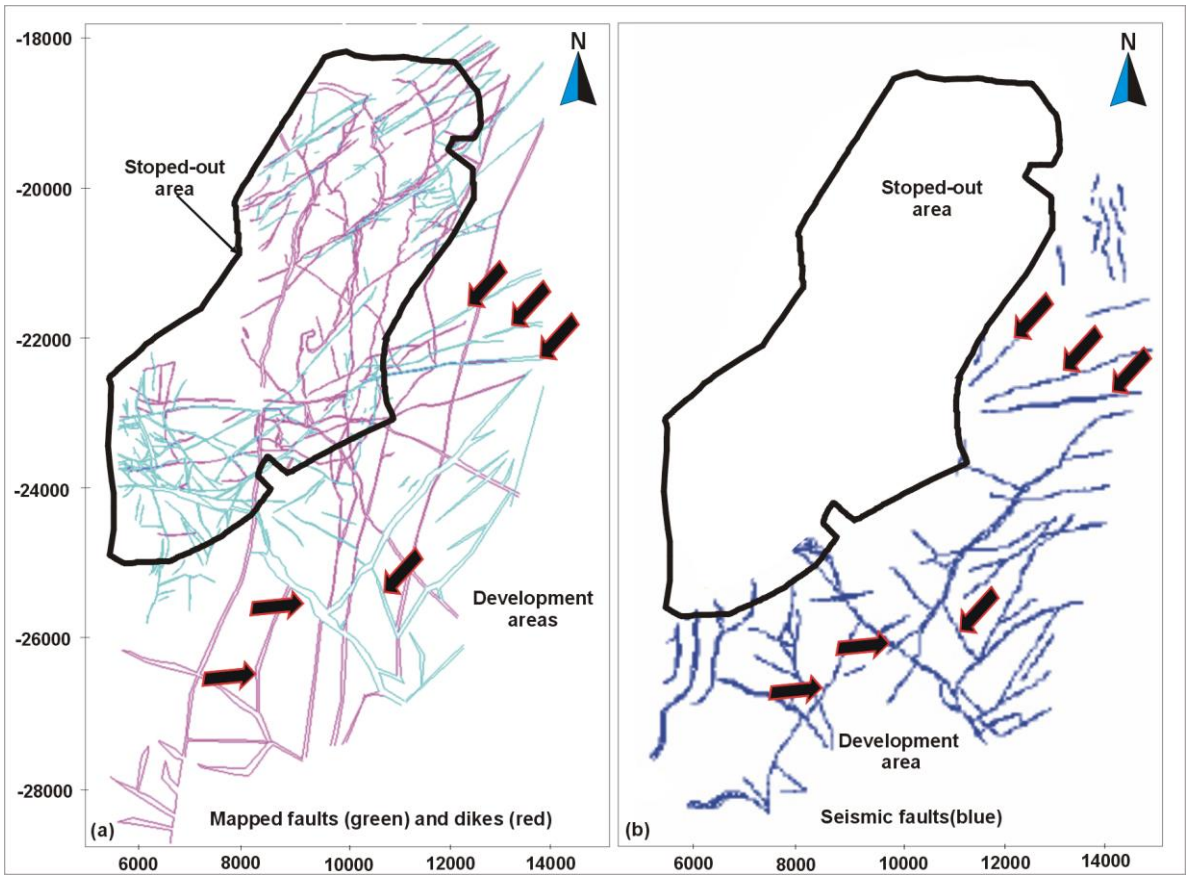


Fig. 8. *The comparisons between seismic and mine underground mapped faults and dikes. (a) Faults mapped underground (green) and dikes mapped underground (red). (b) The seismically defined faults from development area. Note the structures that are present in both models as shown by arrows.*

However, when the geomodel is overlain on the amplitude-derived VCR seismic horizon to compare the two models, miscorrelations occur. In most cases, the underground mapped structures are located within 50 m of their seismic equivalent, or equivalent to 2 bins of the seismic data. Thus mapping data provides positional accuracy on structures imaged by seismic and seismic data provides an important extra control on the underground positioning of structures.

To assess and test the depth correlation between the VCR seismic horizon and geomodel, the depth misties were computed. The depth misties were variable from north to south in the survey area. The seismic model in the northern area places the VCR deeper than the geomodel. The southern area resolves large but variable depth misties between VCR geomodel and seismic model. These misties may be the result of low S/N of the seismic data and the poor velocity model used for prestack time migration.

5.2. Comparison of seismic model and borehole intersections

Surface and underground borehole data, initially used for migration and two-way travel time-to-depth conversion, and one Vertical Seismic Profile (VSP), were utilized as a control during seismic interpretation and VCR orebody modeling. The surface boreholes were drilled on a widely-spaced grid (> 1 km), while underground boreholes were drilled in a tight grid (<100 m). The mistie computed between seismically-defined VCR horizon and borehole control was large (~100 m) but varied across the survey area (Fig. 9a). The depth mistie grid showed that there was a consistent error in the depth conversion. Such misties between the seismic model and borehole control confirmed that the velocity field used for migration and time-to-depth conversion of the seismic data was in error. Furthermore some depth misties of several meters occurred where boreholes were drilled in faulted areas.

To tackle the problem of depth misties, the anomalous errors that resulted from the computed mistie between seismically-defined VCR and borehole control points, were removed. The data was then gridded and the error grid was used to depth-tie the seismic horizon data, which proved successful (Fig. 9b, c). However, a potential problem with this approach is that although it provides

better results, it does not take into account the true reason for the error, which is the wrong velocity model used for the PSTM and subsequent depth conversion.

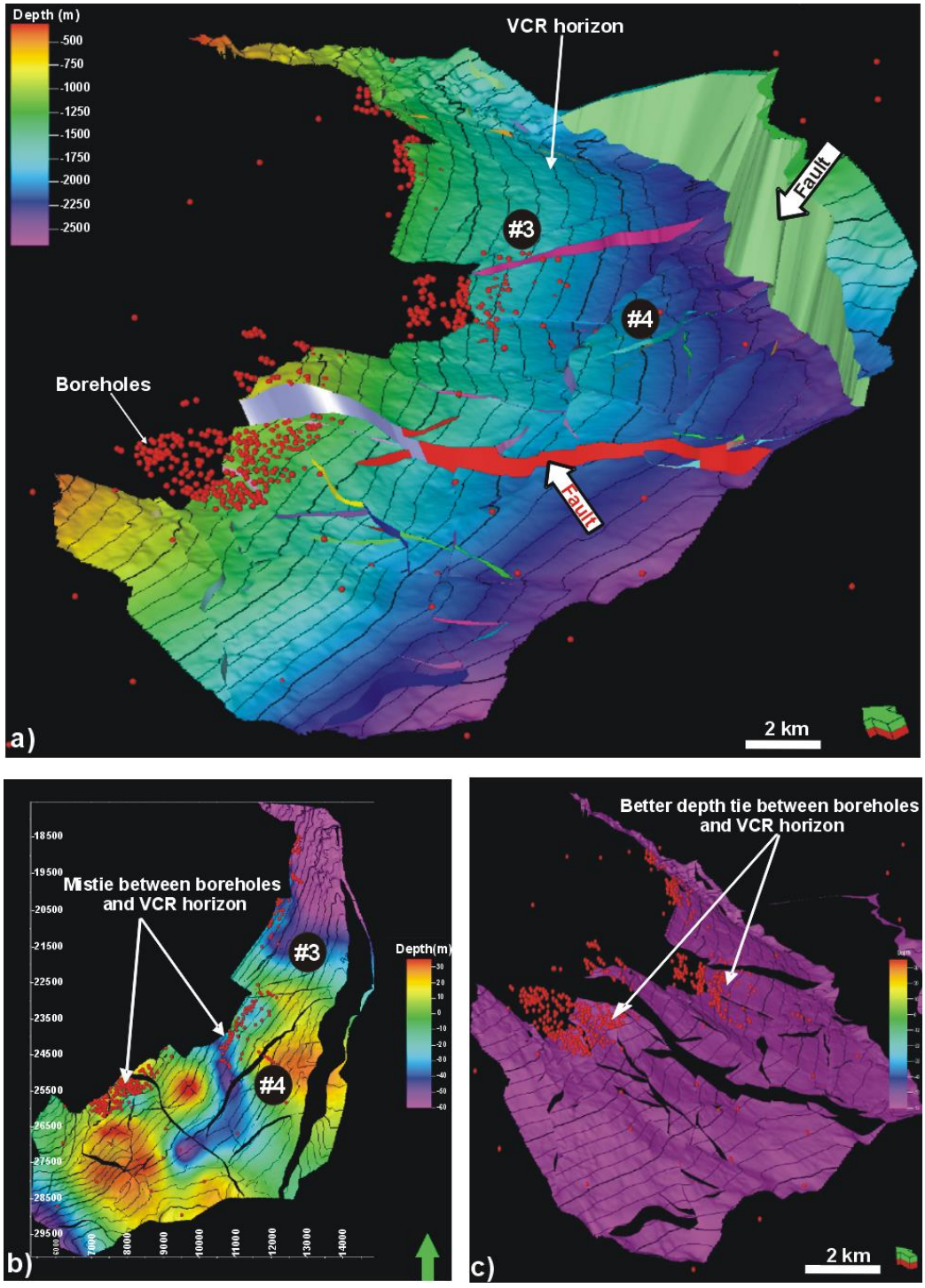


Fig. 9. *The tieing of the VCR to the exploration boreholes. (a) VCR depth mistie with boreholes. Note how the borehole intersections to the north (around #3 Shaft) are generally below the VCR. Some holes in the northwest of #3 Shaft are located in the faulted zones, thus causing major misties (b) De-spiked error grid. Note the misties between the boreholes and the seismically defined VCR surface. (c) Depth corrected model. Note how the borehole VCR intersections (red spheres) coincide with the VCR surface.*

5.3. Comparison of seismic model and infrastructure

The purpose of tieing the seismic data and infrastructure, such as shaft barrels, was to provide a better lateral position resolution for the seismic imaging. This was achieved through the computation of thick slice seismic volume amplitudes. These attributes are horizontal sections extracted at constant time coordinate of the 3D seismic volume [49]. The root-mean-square amplitudes, in particular, are useful in increasing horizontal resolution. They provide more consistent results than local seismic amplitudes, which tend to be dominated by local geological and structural variations [49]. The thick slice (~ 500 m) volumetric variation in the amplitude character of the data (Fig. 10), computed through the metabasalts of the Klipriviersberg Supergroup, provided better control on the lateral resolution between infrastructure and seismic than vertical seismic sections. The root mean-square high amplitudes of isolated bodies also coincided with stopes and shaft barrels in Shaft #4, although the seismic anomaly was offset from the expected position by 200 m to the west and approximately 40 m to the north (Fig. 10).

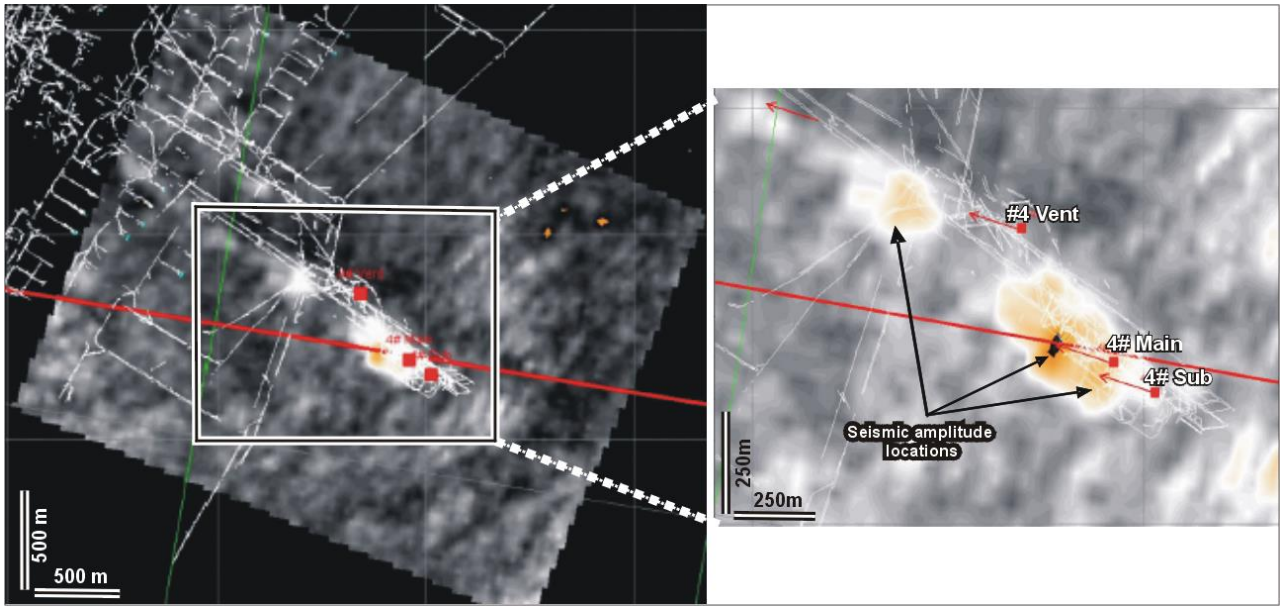


Fig. 10. *Seismic volume slice amplitude versus 4 Shaft infra-structure. The multiple high amplitude (hot colours) isolated bodies appear to tie with the shaft barrels but the seismic appears to offset by ~200m to the west and ~40m, to the north.*

Based on these seismic anomalies, it was then assumed that seismics had a bias of about 200 m and 40 m to the west and north, respectively. The bias and discrepancies between the seismics and infrastructure needed to be taken into account for all seismically-imaged structures. It is interpreted that the major depth-borehole and lateral position misties are very likely to be related, because these are controlled by the velocity assigned to the metabasalts of the Klipriviersberg Supergroup.

Infrastructure clearly provides key reference points for imaged underground structures within 200 m and 40 m from the shafts. However, the major challenge with these results is that amplitude anomalies resulting from large excavations can be several bins in size. Consequently, there is always a difficulty in trying to correctly place the excavations within the resulting anomaly; shafts are vertical and typically 1/2 the diameter of the seismic bin size (~25 m).

6. Structural analysis

The VCR orebody at the Kloof Gold Mine is characterized by a series of complex normal faults and dikes. The fault characteristics that are critical to VCR orebody mining include fault distribution patterns, position, continuity, strike, dip, dip direction, pitch and hade, fault length, fault spacing (compartmentalization), fault offset (throws) and fault heave. These characteristics are interdependent. Fault/dike complexity can be resolved as (1) multiple segments that bound discrete VCR blocks; (2) multiple bifurcations from a single plane to form a branched fault/dike array; and (3) faults/dikes which crosscut and/or offset older faults, or fault/dike systems (Fig. 11). The identification of these fault/dike arrays and sections of the mine that may be considered risky in terms of fault/dike frequency, as well as fault/dike-bounded VCR blocks, is critical to a robust financial valuation of the orebody and Life of Mine planning. To avoid misinterpretations, and ensure robust orebody modeling, it is desirable to assess accurately the impact that arrays of faults and dikes can have on the mining of the orebody. Fortunately, the latest improved modeling techniques enhance the ability to handle and incorporate complex structural architectures into models, and thereby ultimately optimize ore resource evaluation and production rates.

Fault geometric attributes, especially dip, are a major consideration in rock stability estimates. For example, orebody blocks bound by shallowly-dipping normal (0°-45°) faults are considered to be

more unstable than blocks bounded by steeply-dipping (60°-80°) normal faults [50], [51], [52] and [53]. This is because shallowly-dipping normal faults are prone to gravity failure and mining-induced seismicity [54]. The dip, strike and fault throw maps for seismically modeled structures in the development areas are presented in Fig. 12.

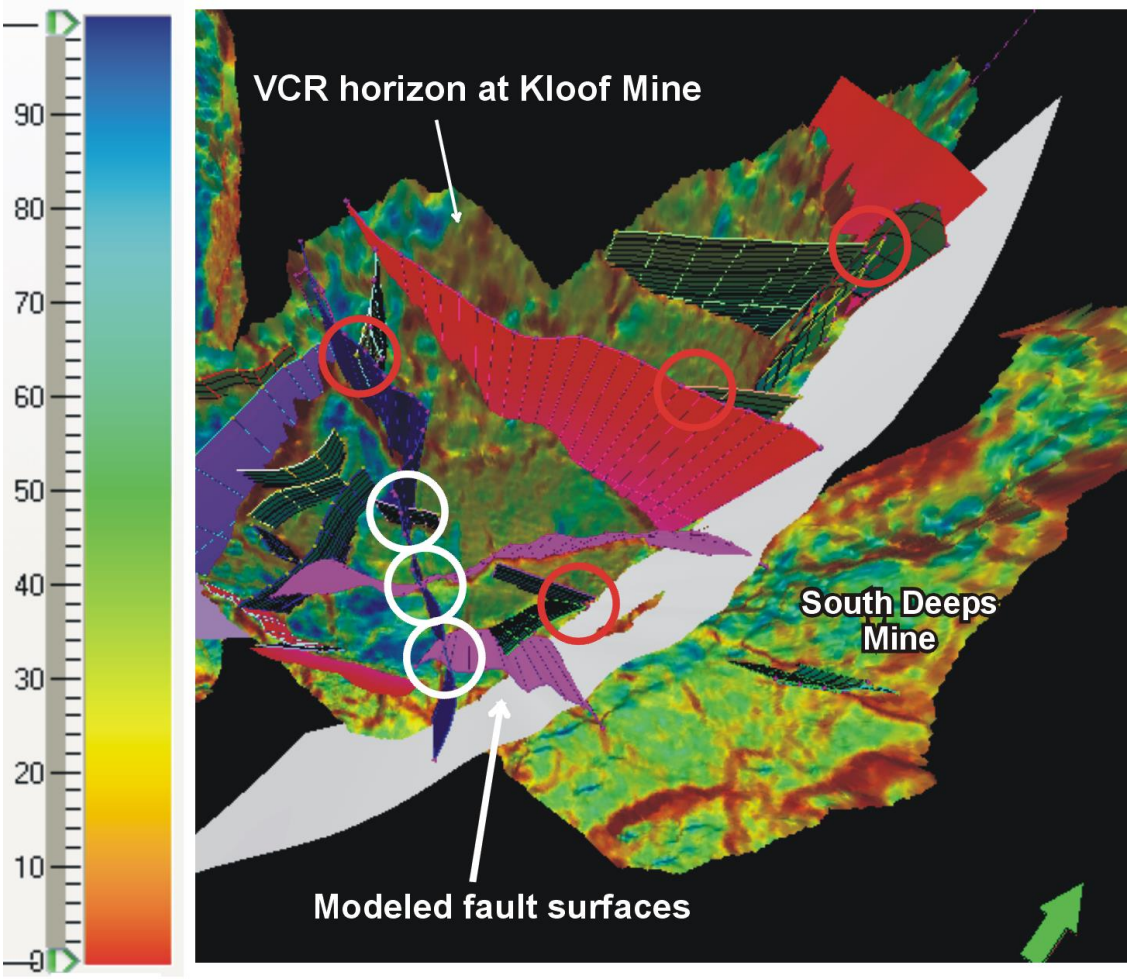


Fig. 11. *VCR horizon-fault framework defined from edge detection seismic attribute. Model shows bifurcation of faults from a single plane into two branches (red circles) and cross-cutting relationship between faults (white circles).*

6.1. Fault throw

Fault throw is an important geometrical attribute in structural analysis because it provides information about the relative vertical displacement between fault blocks. To estimate the appropriate fault throw, the 3D fault planes were mapped for the entire length of the fault in the development area. Frequently, it is assumed that there is little variation in throw along the length of a simple fault, while increased variability and abrupt changes indicates the presence of fault intersections or branching fault segments [54], [55], [56], [57] and [58]. This tenet seems to hold true for the 3D seismic data in the study area to some degree. However, near or at the point of intersection of some faults with others, the throw is below the seismic resolution limit, while further along individual fault planes (away from the intersection point), the throw is above the seismic limit (and thus can be estimated). This is interpreted to mean that fault throw is indeed variable along fault planes, but that variability decreases at points of intersection of some faults (and not the converse). A simple model of fault throw may thus not be ideal and a potential source of error into the orebody modeling.

Faults interpreted from the development areas using 3D seismics have been compared to faults from the stoped-out areas using the geomodel (Fig. 12c). The majority of faults exhibit throws of less than 16 m and predominately in the range of 6-8 m. However, faults that exhibit throws in the range of 16-30 m form a neat extensional array and are tightly orientated northeast, east and southeast. Where they intersect, a complex series of (mapped and seismically-imaged) minor faults is produced with throws of less than 4-6 metres. These are oriented north-northeast, east-northeast and southeast. It should also be noted that steeply dipping faults (and dikes) are not well imaged in the seismic data and thus are under-sampled as witnessed by the many steep faults mapped in the stoped-out area, but their frequency was extrapolated to the development areas by using fault frequency data from the stoped-out areas.

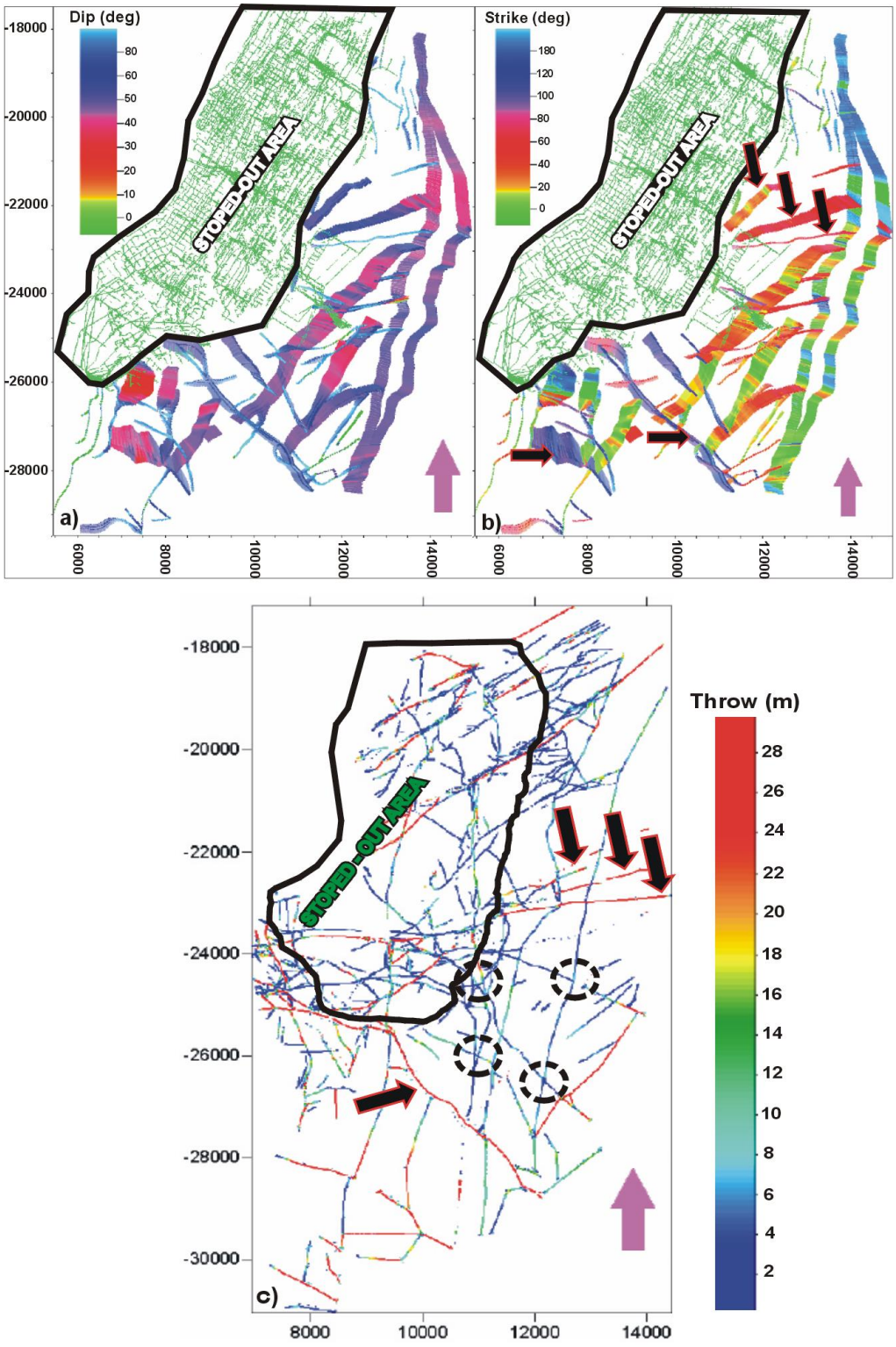


Fig. 12. *Geometrical attributes for the seismically imaged faults. (a) Faults colour coded for dip. (b) Faults colour coded for strike. (c) Fault throw map for stoped-out and development area showing throw linear colour gradient. Note that the structures that are present in the model developed from mapping (geomodel) (c) and seismics (a) are indicated as red arrows.*

6.2. Fault spacing

Faults and dikes can severely compartmentalize the orebody. The spacing between faults/dikes or ‘fault spacing’ is one of the major parameters that define whether or not the orebody block is accessible for mining. The larger the compartment, the more accessible the ore, provided that the gold grade is suitable for recovery, and the cost and risk of ore recovery is acceptable. Fault spacing is simply the distance to the nearest fault intersection across the orebody [59]. Cowie and Roberts [57], Wines and Lilly [59], and Soliva and Benedicto [60] have shown that regular fault spacing is the result of limited horizontal extent of the shear stress reduction zone around faults.

In this study, fault spacing or compartment maps were computed for stoped-out and development areas to ascertain the size of the VCR orebody blocks using techniques (implemented in Petrel interpretation software packages) as applied by Rock Deformation Research (RDR). To do this, the distance from a grid point to the nearest fault intersection across the orebody is calculated automatically.

Fault and dike spacing for stoped-out and development areas were computed, analysed and compared (Fig. 13). In all maps, the statistical average fault spacing, which was measured perpendicular to the fault strike for each locality, ranges from 0-500 m. Comparison of the faults imaged by seismic with those included in the geomodel shows a significant difference. In particular, seismically-defined faults are characterized by smaller spacing relative to faults in the geomodel (see Fig. 13b, c).

To evaluate the accuracy in the mapping of the compartment sizes, the geomodel faults were combined with seismically imaged faults (Fig. 14a). The results suggested that the seismic data predicts overly large unfaulted compartments, indicating that the technique currently under-estimates the number of dikes present in the development areas.

To further enhance the resolvability of compartments, the geomodel dikes, geomodel faults and dikes, and seismically-mapped faults were integrated and combined (Fig. 14b). The final map resolved small compartments when compared to the large compartments initially predicted from seismics. Complex intersection points resolved 0-50 m wide fault-bounded compartments and zones that may not be ideal for mining. Furthermore, faults and dikes on seismic and geomodel that are

disconnected, and/or terminated, were actually continuous in the integrated model. The number of seismically-defined compartments was one-half to one-third the number of compartments presented in the geomodels.

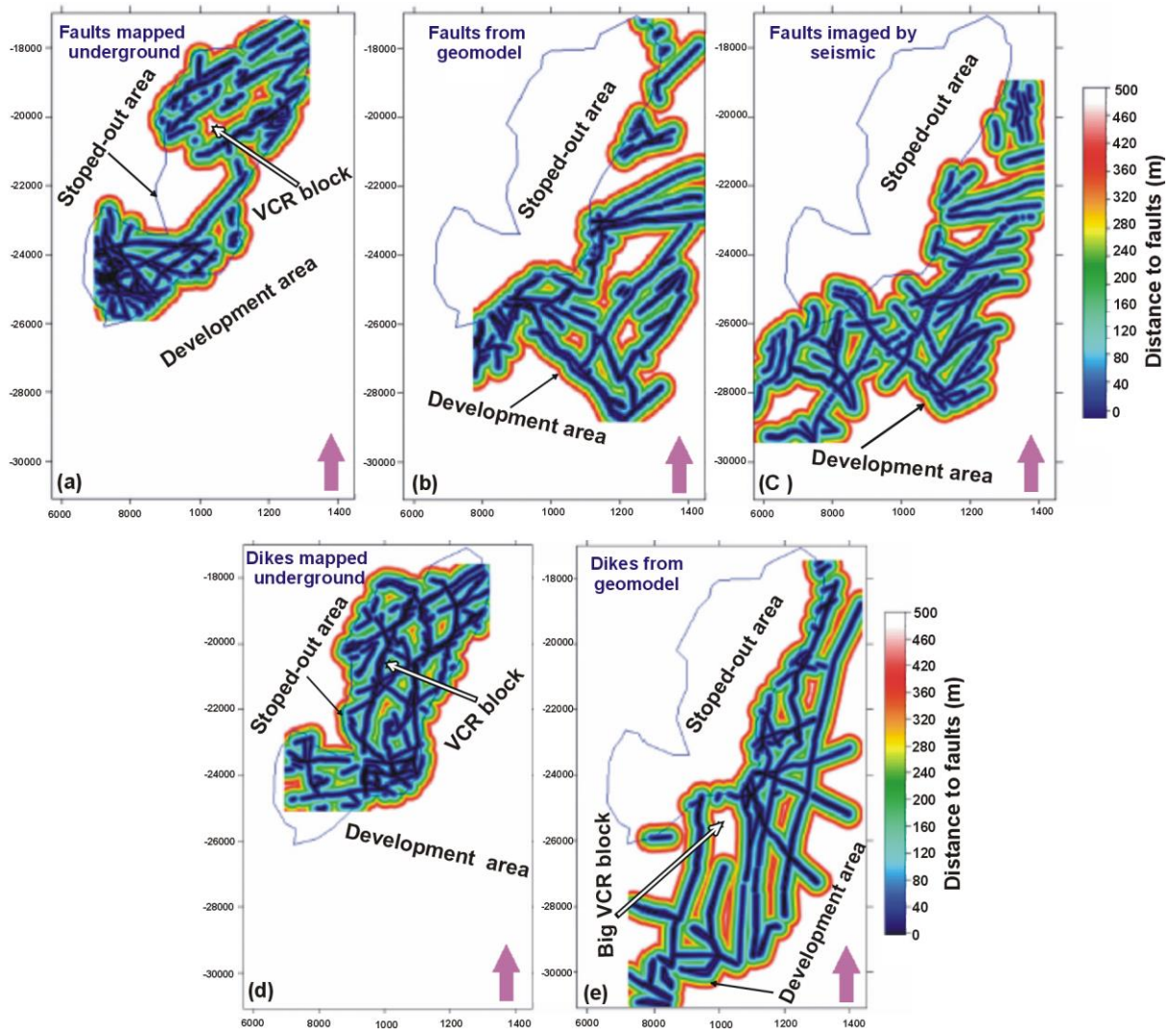


Fig. 13. *Fault spacing maps (compartment sizes) for the various structural elements. (a) Faults mapped underground in the stoped-out area. (b) Faults from geomodel in the development area. (c) Seismically-imaged fault in the development areas, note the larger compartment sizes in the seismic model. (d) Dikes mapped underground in the stoped-out areas. (e) Dikes from geomodel in development area.*

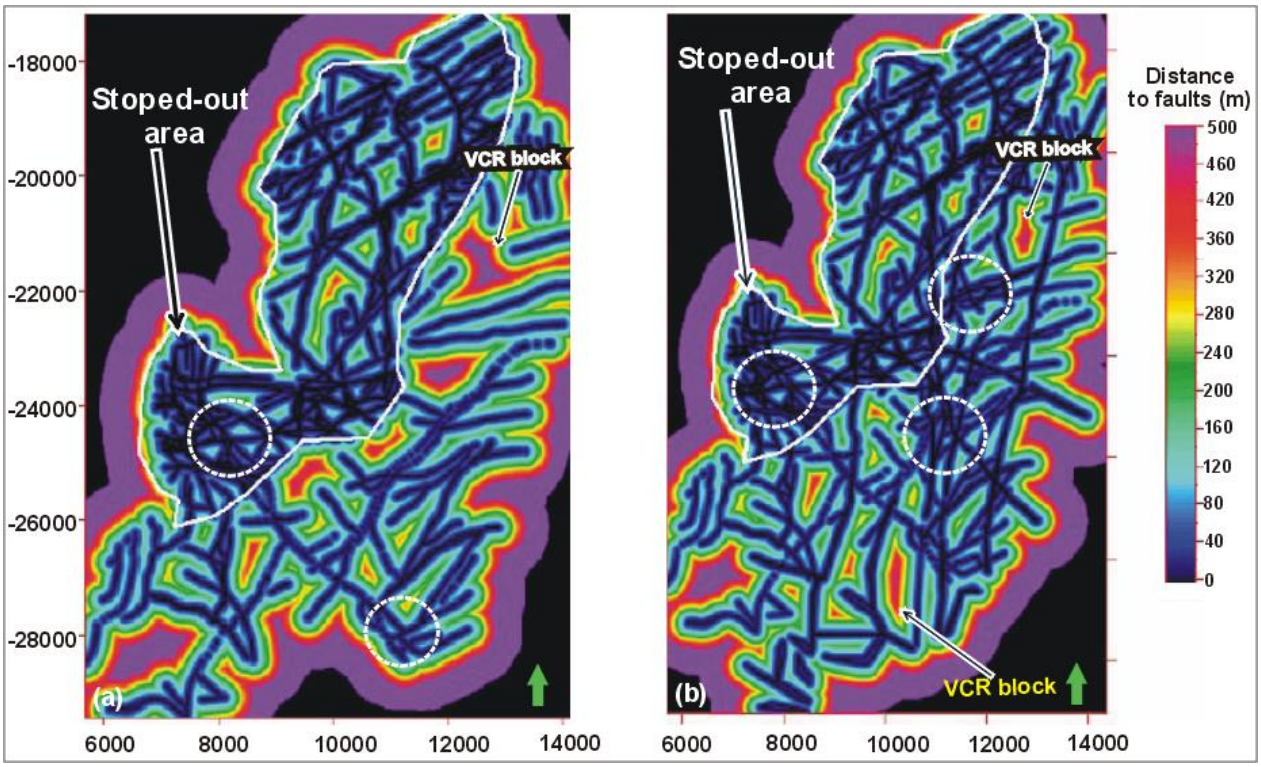


Fig. 14. *Compartment size maps for all structures. (a) Seismically imaged faults and underground mapped structures from stoped-out areas. (b) The integration of seismically imaged faults with underground mapped faults and dikes from both stoped-out and development areas. White circles represent the zones of complex ground conditions that are not ideal for mining.*

6.3. Integrated structural analysis

The overall results show that seismically-imaged faults subdivide the VCR orebody into an array of block sizes ranging from 150 to 500 m, while geomodel faults and dikes resolve compartment block sizes ranging from 50 to 500 m. These results clearly show that seismics fail to detect fault-bounded compartments falling below the seismic dominant wavelength, of 124 m.

In summary, the power that the 3D seismic data has over the geomodel (which retroactively maps faults/dikes while it is stoped-out) is that the 3D seismic method effectively ”sees” in advance of mine development and accurately constrains the location, strike, dip, dip direction, fault spacing and compartmentalization of a development block. The 3D seismic fault model has some limitations. Steeply dipping faults are not well imaged unless they have a throw greater than seismic resolution limit, and compartment sizes below seismic wavelength are not resolved. Combined with the application of modern geometric, kinematic and analytical structural techniques, the 3D seismic method can identify zones of risk with the consequence that it will improve mine planning. Finally,

the orebody model which incorporated seismic data, complex fault and dyke architectures derived from seismic and underground mapping, was transferred into mine software packages for future mine planning and designs (Fig. 15).

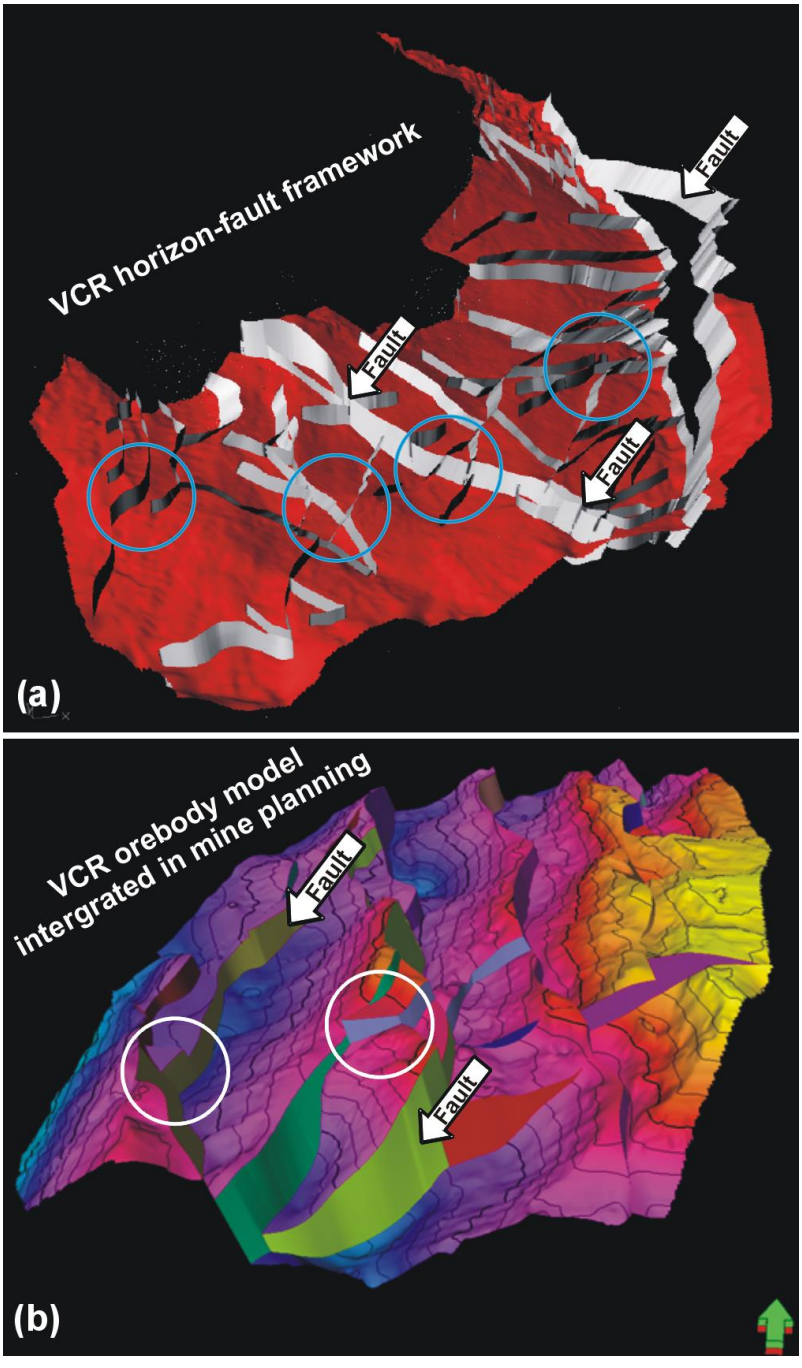


Fig. 15. *Final orebody model integrated into data mine packages. (a) The VCR surface and faults are in Auto Cad package in the mine datum. (b) Direct integration in mine planning.*

7. Discussion

The integration of borehole, seismic, mine underground mapping data has produced an improved VCR orebody model, even in the areas with low S/N, such as the 7 Shaft drop-down area and EBA. The correlation of seismic data with mine development infrastructure, such as shafts and excavations, has proven to be a good test of the lateral accuracy of the seismic data. The misties observed between developments (excavations) and seismic are probably due to the fact that the shafts are vertical and approximately half the diameter of the seismic bin; therefore they do not resolve a clear anomaly on the seismic amplitude maps.

The current seismic interpretation has been depth matched against all available surface and underground borehole control. We used a heuristic approach to minimize the depth discrepancies that occur between seismically-derived VCR horizon and borehole controls. The errors between depth-tied VCR horizon and borehole intersections were mostly less than 1 m, compared with the depth mistie variations of ~ 100 m. Errors of several meters that remained after depth mistie correction are confined boreholes drilled in faulted areas. Although a heuristic approach produced a better depth tie, it should be noted that this method does not take into account the actual cause for the depth misties, which is the inaccuracy of the velocity field used for the PSTM and depth conversion.

Assessment of the fault statistics for extension ground mapping, mine mapping and seismic data for the entire Kloof ground indicated that new seismic techniques are able to accurately predict faults in advance of development better than the geomodel based on geological mapping and borehole logs. In fact, this and previous studies by [10] and [22] in the deep mine workings show that seismic resolution limits for fault throw detection can be as small as 1/8 of the dominant wavelength.

It should be noted that the seismics undersamples a series of minor structures (mainly dikes) that have been predicted by the underground mapping. Nevertheless, statistics, show that the fault loss (reef loss) determined by underground mapping agrees with that seen in the seismic data. However, a series of dikes shown by underground mapping may add an additional reef loss to the seismic area, where dikes were undersampled. This implies that taking only a seismically defined model, or mapping model, as a true geological model may be detrimental to mine planning and designs.

Through fault spacing analysis, the distribution of fault networks and the widths of stable unfaulted block sizes have been successfully determined.

The VCR orebody is compartmentalized by a variety of fault architectures including antithetic, synthetic, cross-cutting and bifurcating faults. These have been modeled and can be incorporated into existing plans of development areas.

8. Conclusions

This study has demonstrated the value of an integrated geological, structural and geophysical approach to exploration mapping and ore resource modeling. The 3D seismic method is established as a very effective tool for mineral exploration. Here we show the application of 3D seismics to mine planning and orebody modeling. However, because of seismic imaging limitations, it is essential that the seismic technique is integrated with other geological datasets such as underground mine mapping and borehole logs. We have developed a reasonably 3D orebody model of the Kloof Gold Mine by integrating 3D seismics, logs of exploration boreholes, and underground mapping information. Newly developed seismic attributes and modeling techniques were used to interpret and model complex structural architectures. We used horizon-based edge attribute analysis to incorporate structural complexity in the model beneath the threshold of seismic resolution. This model will be used to select shaft positions and plan the micro-layout of tunnels and stopes. The statistical analysis of faults has helped to predict the frequency and displacement of small faults within Kloof Gold Mine.

Acknowledgements

Gold Fields Mining Ltd is acknowledged for funding this project and providing permission to publish the results. We wish to thank Schlumberger for providing the Petrel® interpretation software, Rock Deformation Research (RDR), Compagnie Générale de Géophysique (CGG), G. Cooper, G. Smith, J. Trickett, L. Linzer and N. Buthelezi for their major contribution in this study.

References

[1] Safonov YuG, Prokofèv VYu. Gold-bearing reefs of the Witwatersrand Basin: A model of synsedimentation hydrothermal formation. Geol. Ore Deposit 2006; **48**: 415–447.

[2] Vieira FMCC, Diering DH, Durrheim RJ. Methods to mine the ultra- deep tabular gold-bearing reefs of the Witwatersrand Basin, South Africa. In: Bullock RL, Hustrulid W, editors. Underground mining methods, engineering fundamentals and international case studies. Society for mining, metallurgy, and exploration 2001; 691-704.

[3] Vieira FMCC, Durrheim RJ. Probabilistic mine design methods to reduce rockburst risk, South Africa. J. S. Afr. Inst. Min. Metal. 2002; 231-242.

[4] Gibson MAS, Jolley SJ, Barnicoat AC, Interpretation of the Western Ultra Deep Levels 3D seismic survey: The Leading Edge 2000; **19**: 730-735.

[5] Durrheim RJ. Recent reflection seismic developments in the Witwatersrand basin. In: Barazangi M, Brown L, editors. Reflection Seismology, a global perspective: Geodynamics Series, Washington: American Geophysical Union; 1986; **13**: 77-83.

[6] Pretorius DA, The sources of Witwatersrand gold and uranium: "A continued difference of opinion": Johannesburg, Economic Geology Research Unit, University of Witwatersrand, Information circular, 1989. p. 43.

[7] Pretorius CC, Muller MR, Larroque M, Wilkins C. A Review of 16 years of Hardrock Seismics on the Kaapvall Craton. In: Eaton DW, Milkereit B, Salisbury MH, editors. Hardrock seismic exploration, Geophysical Developments. Soc. Explor. Geophys. 2003**; 10**: 247-268.

[8] Trickett JC, Duweke WA, Kock S. Three-dimensional reflection seismic: worth its weight in platinum, International Platinum Conference 'Platinum Adding Value', South Africa. J. S. Afr. Inst. Min. Metal. 2004; 257-264.

[9] Stevenson F, Higgs RMA, Durrheim RJ. Seismic imaging of precious and base-metal deposits in South Africa. In: Eaton DW, Milkereit B, Salisbury MH, editors. Hardrock Seismic Exploration. Geophysical Developments 2003; **10**: 141-156.

[10] Malehmir A, Durrheim R, Bellefleur G, Urosevic M, Juhlin C, White DJ, Milkereit B, Campbell G. Seismic methods in mineral exploration and mine planning: A general overview of past and present case histories and a look into the future. Geophysics 2012; **5**: 173-190.

[11] Malehmir A, Koivisto E, Manzi M, Cheraghi S, Durrheim R J, Bellefleur G, Wijns C, Hein KAA, King N. A review of reflection seismic investigations in three major metallogenic regions: The Kevitsa Ni–Cu–PGE district (Finland), Witwatersrand goldfields (South Africa), and the Bathurst Mining Camp (Canada). Ore Geol. Rev. in press.

[12] Cheraghi S., Malehmir A, Bellefleur G. 3D imaging challenges in steeply dipping mining environment: new lights on acquisition geometry and processing from the Brunswick No. 6 seismic data, Canada. Geophysics 2012; **5**:109–122.

[13] Milkereit B, Spencer C. A new method for migration velocity analysis of noisy seismic data: Signal Process. 1988; **15**: 237-247.

[14] Alaei B. An integrated procedure for migration velocity analysis in complex structures of thrust belts. J. Appl. Geophys. 2006; **59**: 89-105.

[15] Manzi MSD, Gibson MAS, Hein KAA, King N, Durrheim RJ. Application of 3D seismic techniques to evaluate ore resources in the West Wits line goldfield and portions of the West Rand goldfield, South Africa: Geophysics 2012a; **5**: 1-9.

[16] Manzi MSD, Durrheim RJ, Hein KAA, King N. 3D edge detection seismic attributes used to map potential conduits for water and methane in deep gold mines in the Witwatersrand basin, South Africa: Geophysics 2012b; **5**: 1-16.

[17] Anonymous. Structural and seismic appraisal of the Kloof and surrounding area, Report: 9350. Leeds: Unpublished 2004. p. 1-37.

[18] Manzi M, Hein KAA, King N, Durrheim RJ. NeoArchaean tectonic history of the Witwatersrand Basin and Ventersdorp Supergroup: New Constraints from high-resolution 3D seismic reflection data. Tectonophysics 2013; **590**: 94-105

[19] Wines DR, Lilly PA. Measurement and analysis of rock mass discontinuity spacing and frequency in part of the Fimiston Open Pit operation in Kalgoorlie, Western Australia: case study, Int. J. Rock Mech. Min. Sci. 2002; **39**: 589-602.

[20] Morris AP, Ferrill DA, McGinnis RN. Fault frequency and strain. Lithosphere 2009; **1**:105-109.

[21] Beach A, Smith R. Structural geometry and development of the Witwatersrand Basin, South Africa. In: Ries AC, Butler RWH, Graham RH, editors. Deformation of the Continental Crust: The Legacy of Mike Coward. Geological Society, London, Spec. Pub. 2007; **272**: 533-542.

[22] Jolley SJ, Stuart GW, Freeman SR, Knipe RJ, Kershaw D, McAllister E, Barnicoat AC, Tucker RF. Progressive Deformation of a Late Orogenic Thrust System, From Duplex Development to Extensional Reactivation and Disruption: Witwatersrand Basin, South Africa. Geological Society. Spec. Pub. 2007; **272**: 543–569.

[23] Dankert BT, Hein KAA. Evaluating the structural character and tectonic history of the Witwatersrand Basin. Precambrian Res. 2010; **177**: 1-22.

[24] Mambane PW, Hein KAA, Twemlow SG, Manzi MSD. Pseudotachylite in the South Boundary Fault at the Cooke Shaft, Witwatersrand Basin, South Africa: S. Afr. J. Geol. 2011; **114**: 109-120.

[25] Winter H, de la R. A cratonic foreland model for Witwatersrand Basin development in a continental back-arc, plate-tectonic setting. S. Afr. J. Geol. 1987; **90**: 409-427.

[26] Winter H, de la R. The Ventersdorp Contact Reef in relation to the Witwatersrand Basin and overlying Ventersdorp volcanic rocks. S. Afr. J. Geol. 1994b; **97**: 260-278.

[27] Els GB. Sedimentary characteristics of a bedrock placer: the VCR at Stilfontein Gold mine, 'Other Reefs' Symposium. Extended Abstracts. Johannesburg: Geol. Soc. S. Afr. 1989. p. 87-91.

[28] Frimmel HE. Archaean atmospheric evolution: evidence from the Witwatersrand gold fields, South Africa: Earth-Sci. Rev. 2005; **70**:1-46.

[29] Frimmel HE, Groves DI, Kirk J, Ruiz J, Chesley J, Minter WEL. The formation and preservation of the Witwatersrand goldfields, the largest gold province in the world. In: Hedenquist JW, Thompson JFH, Goldfarb RJ, Richards JP, editors. Economic Geology One Hundreth Anniversary Volume. Littleton, Colorado: Soc. Econ. Geol.; 2005. pp. 769-797.

[30] McCarthy TS, Stanistreet IG, Cadle AB, Durrheim R. The geology of the Ventersdorp Supergroup (Bezuidenhout Valley) outlier to the east of Johannesburg and its relevance to the tectonics of a Witwatersrand Basin margin. S. Afr. J. Geol. 1990b; **93**: 289-309.

[31] SACS. Task Group for the Witwatersrand Supergroup. A revised stratigraphic framework for the Witwatersrand Supergroup. Lithostratigraphic Series South African Committee for Stratigraphy, 2006. p. 42.

[32] Kositcin N, McNaughton NJ, Griffin BJ, Fletcher IR, David I, Groves DI, Birger Rasmussen B Textural and geochemical discrimination between xenotime of different origin in the Archaean Witwatersrand Basin, South Africa. Geochimica et Cosmochimica Acta 2003; **67**: 709–731.

[33] Antrobus ESA, Brink WCJ, Brink MC, Caulkin J, Hutchison RI, Thomas DE, Van Graan JA, Viljoen JJ. The Klerksdorp goldfield. In: Anhaeusser C, Maske S, editors. Mineral Deposits of Southern Africa, Vol I. Johannesburg: The Geol. Soc. S. Afr., 1986. pp. 549-59.

[34] Vermaakt DT. The structural evolution of a portion of the Witwatersrand Basin with special reference to the Bank Break and surrounding areas. PhD Thesis. Rand Afrikaans University, Johannesburg; 1995.

[35] Van der Westhuizen WA, De Bruiyn H, Meintjes PG. The Ventersdorp Supergroup. In: Johnson, MR, Anhaeusser CR, Thomas RJ, editors. The Geology of South Africa. Pretoria: Geol. Soc. S. Afr., Johannesburg/Council for Geoscience; 2007. pp. 187-208.

[36] De Kock M. The geology and economic significance of the West Wits Line. In: Haughton SH, editors. The Geology of Some Ore Deposits in Southern Africa. Johannesburg: Geol. Soc. S. Afr.; 1964, p. 323-386.

[37] Krapež B. The Ventersdorp Contact placer: a gold-pyrite placer of stream and debris- flow origins from the Archaean Witwatersrand Basin of South Africa. Sedimentology1985; **32**: 223-234.

[38] McCarthy TS. The tectono-sedimentary evolution of the Witwatersrand Basin with special reference to the occurrence and character of the Ventersdorp Contact Reef - A review. S. Afr. J. Geol. 1994; **97**: 247-259.

[39] Tucker RF, Viljoen RP. The geology of the West Rand goldfield, with special reference to the southern limb. In: Anhaeusser C, Maske S, editors. Mineral deposits of Southern Africa, Vo 1. Johannesburg: The Geol. Soc. S. Afr., 1986. pp. 649-688.

[40] Linton PL, McCarthy TS, Brown CA. The sequential eruption and tectonic history of the Kilpriviersberg Group as illustrated by the distribution of geochemical units. S. Afr. J. Geol. 1994; **97**: 196-204.

[41] Anonymous. Technical short form report. Unpublished 2011. p. 26.

[42] Yilmaz O. Seismic data analysis: Processing, inversion, and interpretation of seismic data: Soc. Explor. Geophys., Tulsa, Oklahoma 2001. p. 2027.

[43] Widess MB. How thin is a thin bed?: Geophysics 1973; **38**:1176–1180.

[44] Brown AR. Interpretation of three-dimensional seismic data, 5th edition. AAPG Memoir 42, Tulsa Oklahoma, 1999. p. 514.

[45] Stolt RH, Benson AK. Seismic migration: Theory and practice: Geophys. Press; 1986. pp. 382.

[46] Yilmaz O. Seismic Data Processing: Soc. Explor. Geophys., Tulsa, Oklahoma; 1987. pp. 526.

[47] Viera FMCC, Durrheim RJ. Probabilistic mine design methods to reduce rockburst risk, J. S. Afr. Inst. Min. Metall. 2002; 231-242.

[48] Manzi MS, Hein KAA, Durrheim RJ. 3D modeling of the orebody structural complexities: KDC East Gold Mine, South Africa. In: Proceedings of the 12th SGA Biennial Meeting, Mineral deposit research for a high-tech world. Uppsala, Sweden; 12–15 August 2013, p. 85-87.

[49] Zeng HM, Backus M, Barrow KT, Tyler N. Stratal slicing, Part 1: Realistic 3-D seismic model: Geophysics 1998; **63**: 502-513.

[50] Esterhuizen GS. Preliminary study of the effects of fault properties and mining geometry on the stiffness of the loading system in fault slip seismic events as a basis for identifying situations prone to seismic activity, SIMRAC; 1994. p. 1-20.

[51] Wernicke B. Low-angle normal faults and seismicity: A review. J. Geophys. Res. 1995; **100**: 159-174.
[52] Ofoegbu GI, Ferril DA. Mechanical analyses of listric normal faulting with emphasis on seismicity assessment. Tectonophysics 1998; **284**: 65-77.

[53] Westaway R. The mechanical feasibility of low-angle normal faulting, Tectonophysics 1999; **308**: 407-443.
[54] Marrett R, Allmendinger RW. Estimates of strain due to brittle faulting: sampling of fault populations. J. Str. Geol. 1991; **13**: 735-738.

[55] Cowie PA, Scholz CH. Physical explanation for the displacement-length relationship of faults using a post-yield fracture machanics model. J. Str. Geol. 1992; **14**: 1133-1148.
[56] Scholz CH, Dawers NHYuJZ, Anders MH, Cowie PA. Fault Growth and Fault Scaling Laws: Preliminary Results. J. Geophys. Res. 1993; **98**: 951-961.

[57] Cowie P A, Roberts G P. Constraining slip rates and spacing for active normal faults. J. Str. Geol. 2001; **14**: 1133-1148.

[58] Cowie PA, Normal Fault Growth in Three-Dimensions in Continental and Oceanic Crust. J. Geophys. Res. 1998; **103**: 325-346.

[59] Wines DR, Lilly PA. Measurement and analysis of rock mass discontinuity spacing and frequency in part of the Fimiston Open Pit operation in Kalgoorlie, Western Australia: case study, Int. J. Rock Mech. Min. Sci. 2002; **39**: 589-602.

[60] Soliva R, Benedicto A. Geometry, scaling relations and spacing of vertically restricted normal faults. J. Str. Geol. 2005; **27**: 317-325.

[61] Myers RE, McCarthy TS, Stanistreet IG. A tectono-sedimentary reconstruction of the development of the Witwatersrand Basin, with particular emphasis on the Central Rand Group. Economic Geology Research Unit Information Circular 1989; **216**: 497-540.

[62] Armstrong RA, Compston W, Retief EA, Williams IS, Welke HJ. Zircon ion microprobe studies bearing on the age and evolution of the Witwatersrand triad. Precambrian Res. 1991; **53**: 243-266.

[63] Kositcin N, Krapež B. SHRIMP U-Pb detrital zircon geochronology of the late Archean Witwatersrand Basin, relation between zircon provenance age spectra and basin evolution. Precambrian Res. 2004; **129**: 141-168.

[64] Martin DMcB, Clendenin CW, Krapež B, McNaughton NJ. Tectonic and geochronological constraints on late Archaean and Palaeoproterozoic stratigraphic correlation within and between the Kaapvaal and Pilbara Cratons, J. Geol. Soc. 1998; **155**: 311-322.

3D modelling of the ore body structural complexities: KDC East Gold Mine, South Africa

Musa M.S. Manzi
University of the Witwatersrand Johannesburg, SOUTH AFRICA

Kim A.A. Hein
University of the Witwatersrand Johannesburg, SOUTH AFRICA

Raymond J. Durrheim
University of the Witwatersrand Johannesburg, SOUTH AFRICA

Abstract. Complex faults and dykes can sub-divide ore-bearing reefs (or ore bodies) into compartments, which may not be ideal for deep underground mining. The Ventersdorp Contact Reef (VCR) at the Kloof-Driefontein Complex (KDC) East Gold Mine is crosscut by a complex arrangement of faults and dykes. These faults and dykes include; (1) multi-fault segments that bound discrete VCR blocks; (2) multiple bifurcations from a single plane to form a branched fault array and; (3) faults that crosscut and offset older faults, or fault systems. This paper presents the VCR ore body model at KDC East Gold Mine as derived from 3D seismic reflection data, faults and dykes mapped in excavations, as well as intersections of the VCR from both surface and underground exploration boreholes. To ensure robust VCR ore body modelling we used Non-Uniform Rational B-Splines (NURBS) and biharmonic based techniques to handle and incorporate complex structural architectures, which are not easy to model through conventional techniques.

Keywords. KDC East Gold Mine, VCR ore body, compartmentalization, structural modelling, 3D seismics

1 Introduction

The geologically complex Witwatersrand Basin of South Africa is the largest gold depository in the history of mining. Gold mining in the goldfields takes place at depths ranging from 500 to 4500 m below surface. There are about 20 or more gold ore bodies (quartz pebble conglomerates) that have been mined, or are currently in production. The Ventersdorp Contact Reef (VCR~1.5 m in thickness) in particular, is one of the richest ore bodies in the basin. The orebody is too thin to be directly imaged by the seismic method. However, it coincides with a major acoustic impedance contrast between relatively high–velocity/dense metabasalts of the Klipriviersberg Group and underlying low-velocity/dense quartzite units of the Central Rand Group that produces a strong seismic reflector. In this paper we present a state-of-the-art model of the VCR ore body for the Kloof-Driefontein Complex (KDC) East Gold Mine (Fig. 1), as developed from new modelling techniques.

At KDC East Gold Mine, the VCR lies at 1.0 to 4.2 km depth and presents 97% of the reserve portfolio of Sibanye Gold (a subsidiary of Gold Field Ltd). With the VCR becoming increasing difficult to mine at greater depths, the technical challenge for mining engineers is to design new techniques to optimize the remaining ore reserves. Understanding the complex geometric attributes of faults (i.e., fault dip, dip direction, spacing, throw, and heave) and dykes that crosscut the VCR ore body is critical for its quantitative modelling. Improved seismic interpretations and structural modelling techniques enhance our ability to effectively 'see' faults with throws beyond seismic resolution limits, and model complex distribution of faults and dykes.

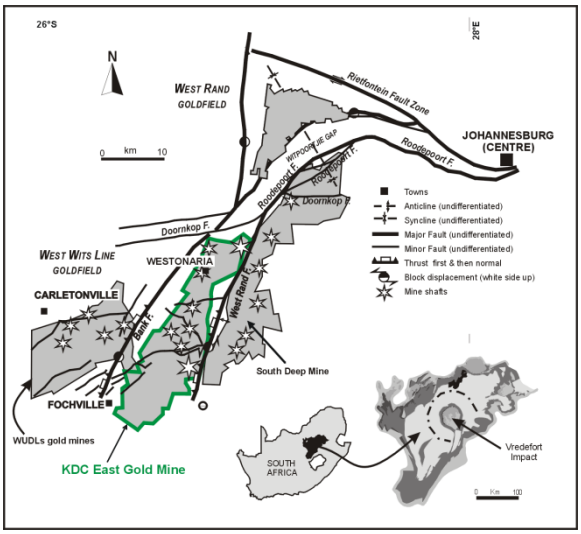


Figure 1. Location map of the KDC East Gold Mine of the Witwatersrand Basin. Modified after Dankert and Hein (2010).

2 3D seismic and structural complexities

The modelling of the VCR began with the 3D seismic imaging of the VCR horizon, and faults and dykes that crosscut it (Figs. 2a, b and c). The 3D seismic data for the KDC East Gold Mine, which was acquired in 2003, is characterized by a seismic wavelet with the dominant peak frequency of 65 Hz and an interval velocity of 6500 m/s (Manzi et al, 2012a). Thus, faults with throws of less than a quarter of the seismic dominant wavelength (~25 m in this case) are difficult to detect through conventional interpretation. Furthermore, subsequent to seismic data migration, faults and dykes with spacing much less than the seismic dominant wavelength (~100 m in this case) may also not be resolvable.

After picking the VCR horizon data points in 2D seismic sections, the noise introduced during picking was smoothed using post-fault interpolation smoothing operators such as the bi-harmonic smoothing algorithm developed by Halenbrook (2001). This algorithm is used

in seismic interpretation to detect subseismic faults, to filter-out the isolated horizon noise, and to separate gross structural configurations (long wavelength) from faults and dykes (short wavelength) (Fig. 2c). It also tends to maximize the resolution for the identification and location of faults, eliminate errors resulting from false complex geometries created by conventional picking around faults, and thus minimizes unrealistic fault-horizon geometries (Fig. 2c). The advantage of applying this algorithm post-fault projection is that filtering only occurs within the horizon rather than across the faults. However, care must be taken not to filter out the faults and dykes, since the bi-harmonic smoothing algorithm is capable of filtering-out noise in addition to real faults and dykes, which can significantly affect the fault geometry.

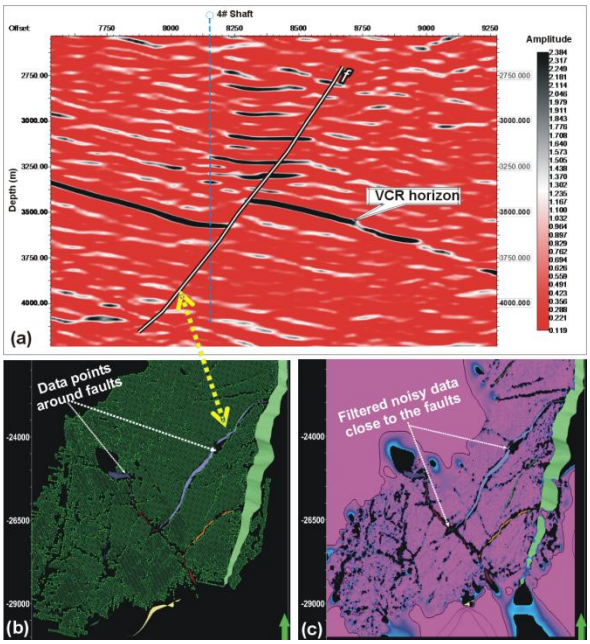


Figure 2. (a) Seismic section (amplitude display) showing a strong reflective VCR horizon. (b) Picked seismic horizon data points and fault polygons. (c) Smoothed horizon-fault projection by bi-harmonic smoothing algorithm.

3 3D fault-horizon projection modelling

The VCR ore body at the Kloof Gold mine is characterized by a series of complex normal faults. The geometric complexities that present challenges in the generation of the VCR ore body modelling include; (1) multi-fault segments that bound discrete VCR blocks; (2) multiple bifurcations from a single fault plane to form a branched fault array and; (3) faults that crosscut and offset older faults or fault systems. The newly developed modelling and interpolation technique 'Non-Uniform Rational B-Splines (which is implemented in Petrel software packages) is capable of modelling complex faulted ore bodies and provides flexibility in designing and modelling different geometries (Rock Deformation Research, 2004; Piegl and Tiller, 1997). Conventional modelling techniques only model the faults with linear interpolation between fault pillars, i.e., they restrict fault-pillars (Fig. 3a, b) in moving along specific degrees and planes. This often creates horizon geometries that are jagged. NURBS, in contrast, is a tetrahedral volume modelling technique, i.e., it allows multi degrees of movement through fault pillars during interpolation.

To avoid unrealistic VCR ore body modelling, the fault pillars (derived from seismics) were modified to give tight correlation with the seismically defined VCR horizon (Figs. 3c, d). The data was then gridded (using Kriging gridding algorithm), and the faults were re-modelled using NURBS repeatedly until the stable VCR ore body geometry was achieved (Fig. 4a, b and c).

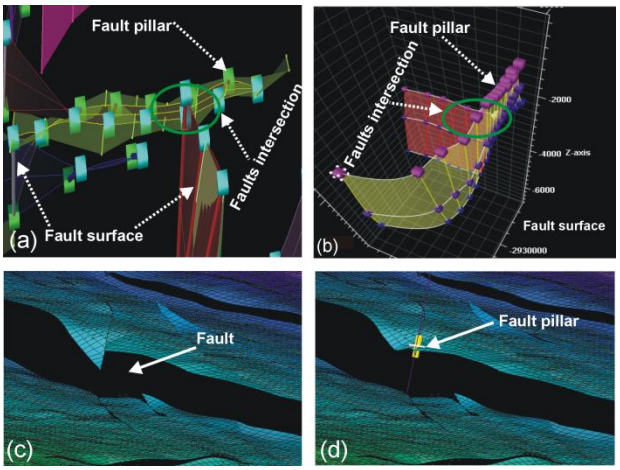


Figure 3. (a) Modelled fault surfaces and fault pillars (changed dip of faults from vertical) using NURBS. (b) Modelled fault surfaces showing fault intersections. (c) Horizon modelling around the fault zones. (d) Projection of fault pillars into horizon breaks (faults).

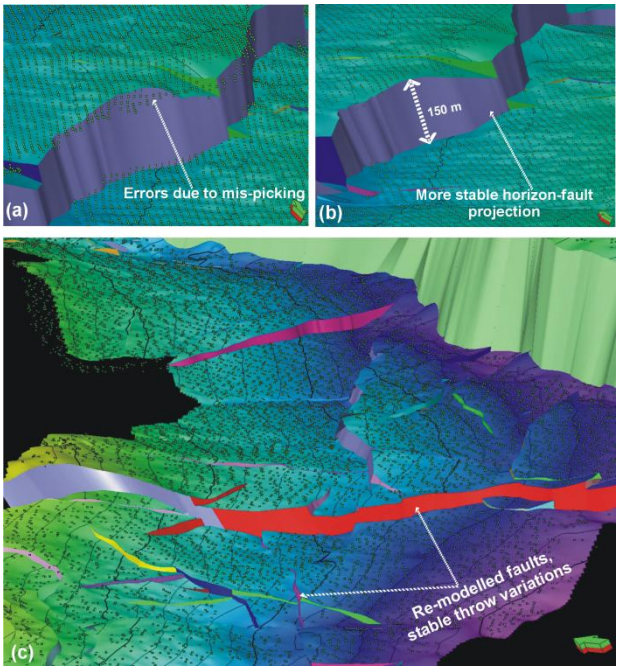


Figure 4. (a) Seismic horizon data points overlap across the fault throw, the dip of the fault is thus in error. (b) Horizon is projected in a sensible manner to the fault. (c) Re-modelled faults and horizon, showing the stable throw variations.

4 3D edge detection attributes

Generally, fault sticks that were picked manually on seismic sections did not exactly correspond to VCR horizon breaks in 3D environments (Fig. 5a). The fault-

horizon projection was therefore enhanced using edge detection attribute analysis. The application of this technique ultimately allowed for tieing of uncorrelated fault sticks to their appropriate positions (Fig. 5b). The edge-detection algorithm is the combination of dip and azimuth variations, normalized to the local noise surface, which overcomes the difference in detectability between the dip and dip azimuth attributes. This technique also improves the lateral resolution of the fault traces, which aids in characterizing fault continuity and connectivity, and thus minimizes unrealistic 3D fault-horizon geometries (Manzi et al., 2012b).

Some of the interpretation techniques are sensitive to the fault trend, so care was taken to ensure that trend is correctly modelled. When a VCR horizon on either side of a fault was significantly offset near the fault boundary, the application of the attributes allowed for the projection of one fault onto another (Fig. 5b), allowing gaps between a branching fault and its stem fault to be closed.

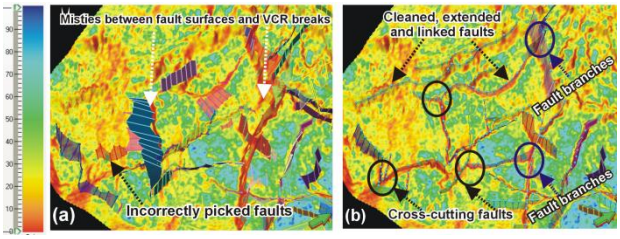


Figure 5. (a) Picked fault surfaces show no correlation with the VCR horizon breaks (faults) derived from edge attributes. (b) Re-modelled faults showing cleaned, extended and linked fault surfaces.

5 Ore body compartment sizes

Faults and dykes can severely compartmentalize ore bodies in the KDC East Gold Mine. The spacing between faults/dykes or 'fault spacing' is one of the major parameters that define whether or not VCR ore body blocks are accessible for mining, thus compartment sizes were incorporated into the fault-horizon model. Arguably, the larger the compartment, the more accessible the ore, provided that the gold grade is suitable for recovery, and the cost and risk of ore recovery is acceptable.

The compartment maps derived from seismic and underground mapping data are presented in Fig. 6a and Fig. 6b, respectively. The results show that seismically-imaged faults subdivide the VCR ore body into compartment sizes ranging from 150 to 500 m. However, structural maps from the stoped-out areas resolve compartment sizes ≤ 50 (which is equivalent to 2 bins of the seismic survey). It follows that seismics fail to detect fault-bounded compartments falling below the seismic dominant wavelength (124 m). This means that it is inaccurate to use a 3D geological model based only on seismic data as the final geological model. Rather, it is prudent to incorporate other models based on datasets, such as underground mine maps and exploration boreholes, to arrive at a robust ore body model. Quality geological mapping data, in particular, is extremely useful when attempting to model faults and dykes that fall below seismic resolution limit.

Finally, the ore body model which incorporated the seismic data, and complex fault-dyke architectures extracted from seismic and underground mapping, was transferred into mine software packages for future mine planning and design (Fig. 7a, b).

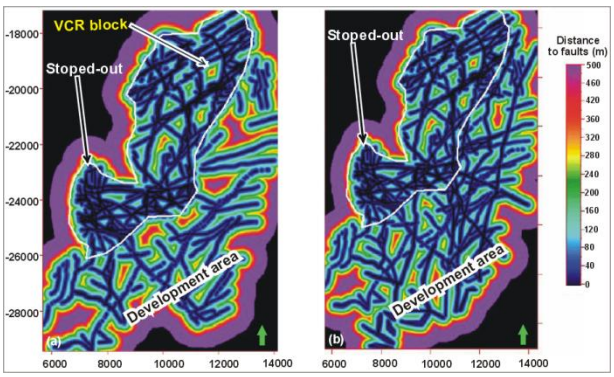


Figure 6. (a) Compartment size maps derived from seismically defined faults; (b) Compartment size maps derived from the integration of seismically defined faults and underground mapped faults and dykes.

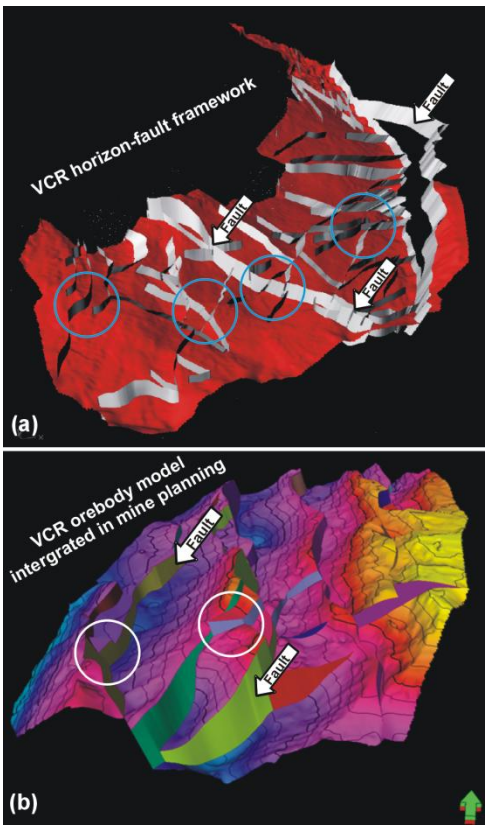


Figure 7. (a) Seismically defined fault-horizon projection. (b) Integration of the 3D structural ore body model into mine software packages (e.g. AutoCAD).

6 Conclusion

We have presented a geologically reasonably 3D ore body model of the KDC East Gold Mine, as derived from 3D seismics, exploration holes and underground mapping information. The newly developed modelling techniques were used to manage complex structural architectures that are impossible to model using traditional modelling tools. Moreover, we used unique horizon-based edge attribute analysis (post fault-horizon

projection) to incorporate subseismic structural complexity in the model. This model has been factored into future mine development strategies for better placement of shafts and improved life-of-mine planning; i.e., the high degree of structural resolution afforded by these modelling techniques will guide future exploration drilling activities and enable the layout of tunnels and stopes to be optimized.

Acknowledgements

We greatly acknowledge Gold Fields Ltd for allowing the publication of these results, in particular R. Segage (Schlumberger), N. King (South Deep Mine, Gold Fields Ltd), N. Buthelezi (University of Witwatersrand), S. Freeman (Rock Deformation Research), G. Smith, J. Trickett, L. Linzer, M. Gibson, and M. Muller.

References

Dankert, B.T., and K.A.A. Hein, 2010. Evaluating the structural character and tectonic history of the Witwatersrand Basin: Precambrian Research, 177, 1-22.

Halenbrook, B.T., 2001. Mesh deformation using the biharmonic operator. International Journal for Numerical Methods in Engineering 2, 1-30.

Manzi, M., Durrheim, R.J., Hein, K.A.A., King, N., 2012a. 3D edge detection seismic attributes used to map potential conduits for water and methane in deep gold mines in the Witwatersrand Basin, South Africa. Geophysics 77(5), WC133–WC147.

Manzi, M.S.D., Gibson, M.A.S., Hein, K.A.A., King, N., Durrheim, R.J., 2012b. Application of 3D seismic techniques in evaluation of ore resources in theWestWits Line goldfield and portions of the West Rand goldfield, South Africa. Geophysics 77(5), WC163–WC171.

Piegl, L., Tiller W., 1997. The NURBS Book, 2nd Edition, Springer, 646 p.

Rock Deformation Research, 2004, Structural and seismic appraisal of the Kloof and surrounding area: Report 9350 (unpublished), 1–37.

11. CONCLUSIONS

Seismic data acquired between 1988 and 2003 covering the Wits West Line and West Rand goldfields have been re-processed, merged and interpreted using the latest processing and interpretation techniques.

The data have also been integrated with conventional methods, such as exploration boreholes and underground geological mapping, and modeled using advanced modeling techniques, boosting the efficiency of discovering new gold resources, mitigating hazards and risks associated with deep underground mining, unravelling the gross strato-structural architecture and tectonic evolution of the goldfields, and finally providing 3D seismic constraints on the long-standing controversy regarding the ore genetic models.

(1) The implementation of the Kirchhoff prestack time migration (KPSTM) technique in the processing workflow significantly improved the signal-to-noise ratio of the data, thus improving the imaging of steeply dipping stratigraphy and structures (faults and dikes), and horizon and fault intersections. This technique has also led to better imaging of the ore blocks in structurally complex faulted areas, thus leading to the discovery of new ore resources. Furthermore, the revised interpreted velocity field picked during re-processing has made clear that some structures (e.g., faults, synclines, anticlines) identified using inaccurate velocity models actually do not exist.

(2) Interpretation of the seismic stratigraphy of the gold-bearing reefs using careful analysis of data conditioning techniques (e.g., mean, median and bi-harmonic filtering operators) and horizon-based seismic attributes (e.g., dip, azimuth and edge detection) have enhanced the detection of subtle geologic features that offset thin gold-bearing reefs by throws as small as 10 m. In particular, the edge detection attribute has improved the lateral resolution of faults and is able to characterize complex structural architectures (such as fault continuity, connectivity, bifurcations and cross-cutting relationships) that are extremely difficult to interpret conventionally on seismic sections.

(3) The newly invented modeling technique (NURBS) enabled complex fault architectures to be factored into the ore body model (Rock Deformation Research, 2004). Additionally, the integration of 3D seismics, surface and underground borehole, geological mapping, fault statistics and VCR paleogeomorphological data has provided Gold Fields Limited with a world-class orebody model of the VCR ore body. The orebody model could be used as the basis for accurate mine design and future project scheduling.

(4) The subtle structural linkage and timing of fault activity between the Ventersdorp Contact Reef (VCR) and Black Reef (BLR), as mapped by edge detection attributes, showed which faults are most likely to intersect dolomitic aquifers above the Black Reef Formation.

Furthermore, plotting known intersections of water and methane data on the VCR edge detection map shows that water and methane tend to occur along faults that are sub-vertical or steeply dipping (> 60^0). Thus these structures are most likely to channel methane gas along with the fissure water to the VCR mining level. This information could therefore be used to mitigate the risks associated with inrushes of water and the ignition of methane ahead of mining.

(5) Detailed interpretation of the large merged high-resolution 3D seismic data cube has enabled the reconstruction of a new complex gross structural architecture and Neoarchaean tectonic evolution of the Witwatersrand Basin. In particular, the focus was on the analysis of the first-order to third-order scale structures, fault throw distribution, fault geometry, dike intrusion and timing of fault activity. The 3D seismic data were correlated with absolute and relative geochronology, underground mapping and exploration borehole datasets. Seismic sections and fault-throw distribution show that West Rand and Bank faults are first-order, north-northeast trending and steeply dipping (65°–70° to the west) listric faults. The West Rand and Bank faults have maximum throws within the survey area of 1.5 and 2.5 km, respectively, and maximum sinistral offsets of 600 and 800 m, respectively.

(6) The seismic interpretation and analysis of the absolute and relative geochronological data led to the formulation of a new Neoarchaean tectonic model for the Witwatersrand Basin. In the model, the goldfields experienced three deformation events: (1) the Asazi Event at ca. 2.90 Ga (titling and/or deformation of the basin), (2) the Umzawami Event at ca. 2.73 Ga (fold/thrust tectonics) and (3) the Hlukana-Platberg Event at 2.70–2.64 Ga (rift-like extension tectonics). In effect, the present day-geometry of the first-order scale rift like systems (e.g., West Rand and Bank Faults) and their second and third-order scale normal faults is attributed to the Hlukana-Platberg Event. The first-order scale Libanon Anticline, with a wavelength and amplitude of 8 km and 2 km, respectively, its parasitic folds, and the Tandeka and Jabulani thrusts which displace the West Rand Group, formed during the Umzawami Event.

3D reflection seismic is arguably the first tool in South African gold mines to directly image the subsurface structures in 3D. The remaining scientific potential of this data far exceeds the results achieved thus far. For example, the resolution of first-order scale structures has stimulated a reappraisal of the collar of the Vredefort Dome (see Appendix B), where seismically identified structural architectures in the goldfields, or their equivalents, can be mapped at surface. The understanding of Neoarchaean tectonics may thereby be greatly improved.

PSEUDOTACHYLITE IN THE SOUTH BOUNDARY FAULT AT THE COOKE SHAFT, WITWATERSRAND BASIN, SOUTH AFRICA

P.W. MAMBANE
Paul Mambane, Kusasalethu Shaft, Harmony Gold Ltd, Republic of South Africa
e-mail: paul.mambane@harmony.co.za

K.A.A. HEIN
Corresponding Author; School of Geosciences, University of the Witwatersrand Johannesburg, Private Bag 3, WITS, 2050, Republic of South Africa
e-mail: kim.ncube-hein@wits.ac.za

S.G. TWEMLOW
Rand Uranium (Pty) Ltd, Block B, Cooke Central Office, PO Box 2, Randfontein, 1760, Republic of South Africa
e-mail: Steve.Twemlow@randuranium.co.za

M.S.D. MANZI
School of Geosciences, University of the Witwatersrand Johannesburg, Private Bag 3, WITS, 2050, Republic of South Africa
e-mail: Musa.Manzi@students.wits.ac.za

© 2011 June Geological Society of South Africa

ABSTRACT

The steeply-dipping South Boundary Fault in the Cooke Section on the West Rand goldfield hosts a series of crosscutting pseudotachylite fault and injection veins, and pseudotachylitic breccias that formed progressively by abrasive wear in a brittle (elastico-plastic) regime. The crosscutting pseudotachylite veins and breccias are hosted by faulted supracrustal rocks of the Witwatersrand Basin that are exposed by underground workings and production-development borehole cores. Evidence of frictional melting is represented by quenched vein margins, corona texture, turbulent flow and glassy texture. Underground mapping and logging of boreholes has confirmed the existence of at least three generations of pseudotachylite, which were tectonically-induced.

The relative age of tectonically-induced pseudotachylite formation is constrained to pre-2.58 Ga, or before deposition of the lower Transvaal Basin sequences, because 3D seismic data show that pseudotachylite-bearing faults do not penetrate the base of the Transvaal Basin. The conclusions made in previous research that the Hekpoort Andesite Formation (2224 ± 21 Ma) of the Transvaal Supergroup provides a maximum age for all pseudotachylite in the West Rand goldfield may therefore need revision.

Introduction

The occurrence of pseudotachylite is evidence of earthquakes (Sibson, 1980; Di Toro et al., 2009), high confining pressure and high strain rate (Davis and Reynolds, 1996; Andersen et al., 2008), and melt temperature to 1550°C or higher (Andersen and Austrheim 2006; Di Toro et al., 2009). It is also considered a diagnostic feature of shock tectonics (metamorphism) associated with impact cratering (Schwarzman et al., 1983; Gibson et al., 1997; Spray, 1998; Eiko, 2004, Riller et al., 2010 and others), rapid ascent of magma (Nicolaysen and Ferguson, 1990) and formation of fault zones (Maddock, 1983; and others). Pseudotachylites also occur at the base of massive landslides (Legros et al., 2000) and can form during diamond drilling (Killick, 1990).

Shand (1916) first introduced the term pseudotachylite (also pseudotachylyte) for the breccia with a black matrix that occurs on the gneiss of the Achaean basement at the Vredefort Dome of the Witwatersrand basin in South Africa (Figure 1). Roering et al. (1989) and Fletcher and Reimold (1989) recorded pseudotachylite throughout the Witwatersrand gold mines in fault planes and on lithological contacts, and regular and continuous veins, irregular injection veins, and complex irregular and interconnected vein systems. Spray (1995) and Killick et al. (1980) recorded cataclastic flow textures, quenched margins to pseudotachylite veins, and thermally corroded rock fragments in pseudotachylite fragments in faults.

In the Vredefort Dome of the Witwatersrand basin, pseudotachylite breccias (e.g. Shand, 1916; Bisschoff, 1962; Reimold and Colliston, 1994; Reimold and Gibson, 2006), granophyres dykes (e.g. Hall and Molengraaff, 1925; Bisschoff, 1988, Reimold and Gibson, 2006) and shatter cones (e.g. Hargraves, 1961; Manton, 1962; Wieland et al., 2006) present compelling evidence for the catastrophic impact of an extraterrestrial body ca.

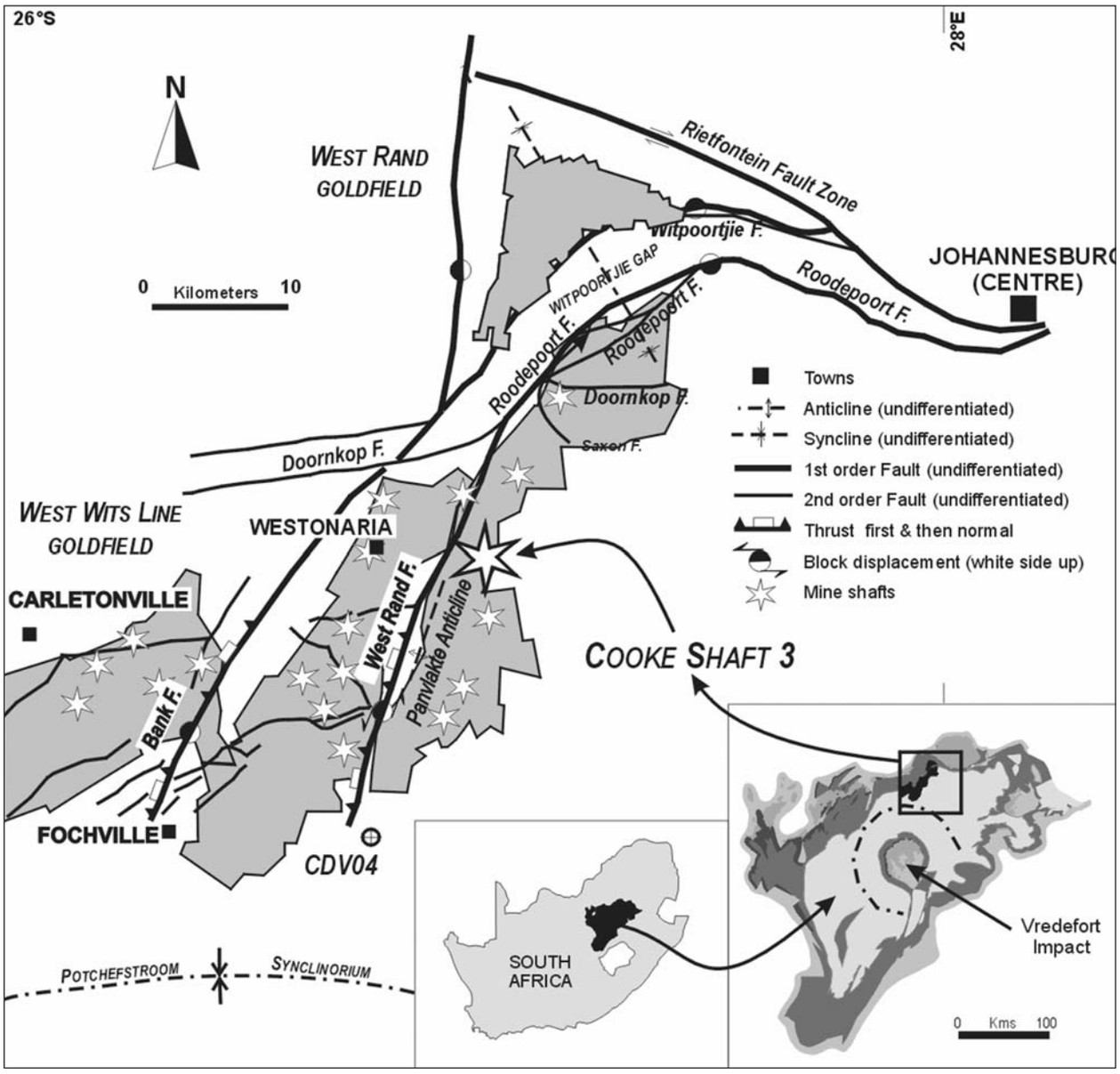


Figure 1. *Schematic geological map of the West Rand goldfield and position of Cooke Shaft 3, with Transvaal Basin sequences and Karoo Supergroup cover removed (modified after Dankert and Hein, 2010). Borehole CVD4, which was collared approximately 25 km south-southwest of Cooke Shaft 3 on the northern limb of the Potchefstroom Synclinorium, is also shown. Its approximate position is after Brink et al. (2000).*

2020 Ma (Kamo et al., 1996; Reimold and Gibson, 2006). With studies of pseudotachylite outside the Vredefort dome being largely limited to those in the West Wits Line and West Rand goldfields (c.f., Roering et al. 1989; Killick and Roering, 1995a; 1998) it has been tempting to conclude that all pseudotachylite in the goldfields (50 to 60 km to the north of the dome) formed during the impact event. However, several authors recognized more than one generation of pseudotachylite (c.f., Reimold et al., 1986; Killick and Reimold, 1990; Reimold and Gibson, 2006) indicating that more than one shock tectonic event took place in the goldfields. In the West Rand goldfield, crosscutting pseudotachylite veins and breccias are hosted by faulted metasedimentary rocks that are exposed by underground workings and production or development borehole cores.

At Cooke Shaft 3 (Figure 1), the South Boundary Fault (SBF) demarks the Cooke Shaft 3 mining lease (or Cooke Section) with the Ezulwini Mine lease to the south (Figure 2); the fault does not outcrop at surface. It is concave in form, strikes approximately east-west and dips 62 to 80° southeastward. The asymmetric fault damage zone is approximately 40 m wide and hosts numerous pseudotachylite veins and breccias in both the hanging- and footwall of the fault. It thereby provides an excellent natural laboratory to study the spatial and temporal relationships between pseudotachylite veins and breccia systems, and an

opportunity to constrain the relative chronology of crosscutting shock events.

Geological Setting

The Witwatersrand Basin (ca. 3.0 to 2.8 Ga, Kositcin and Krapež, 2004) in the Kaapvaal Craton consists of an 8 km succession of predominantly siliclastic metamorphosed sedimentary rocks (e.g. Robb and Robb, 1998) that unconformably or conformably overlies tholeiitic-andesitic lavas, quartzite and conglomerate units of the Dominion Group (c.f. Dankert and Hein, 2010), or unconformably overlies older Archaean basement (Stanistreet et al., 1986). In the goldfields, metamorphism was to lower greenschist facies with development of pyrophyllite-kyanite-(muscovite-quartz) mineral assemblages; peak metamorphism was about 350°C at a pressure of 2 to 3 Kbar (Phillips and Law, 1994) or 3 Kbar and 390°C (Coetzee et al., 1995).

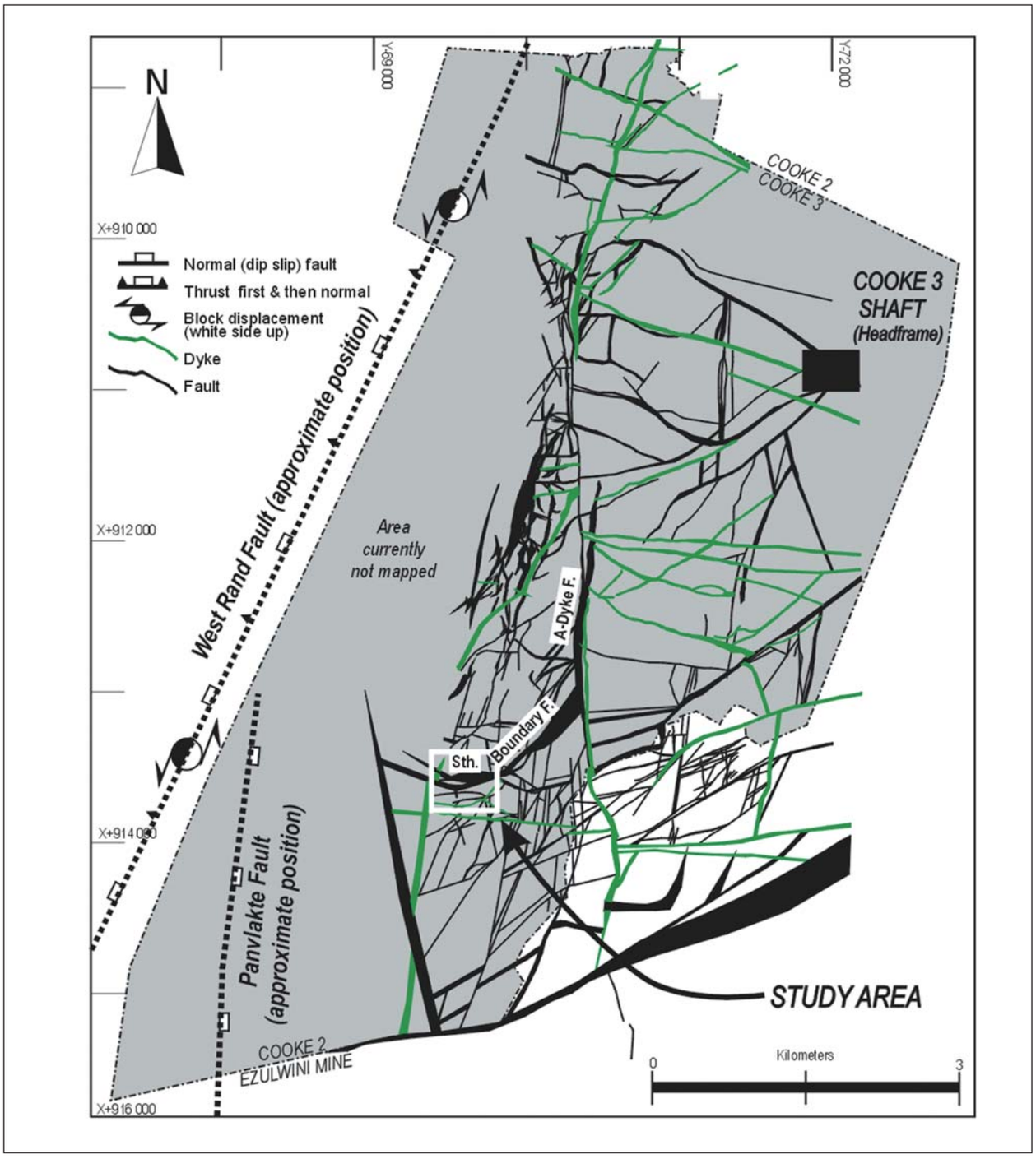


Figure 2. *Schematic geological map of faults and mafic dykes in the Cooke Section at the level of the Kimberley Reefs. This complex array of faults and dykes is located in the footwall (eastern block) of the West Rand Fault Zone and forms a macroscopic breccia.*

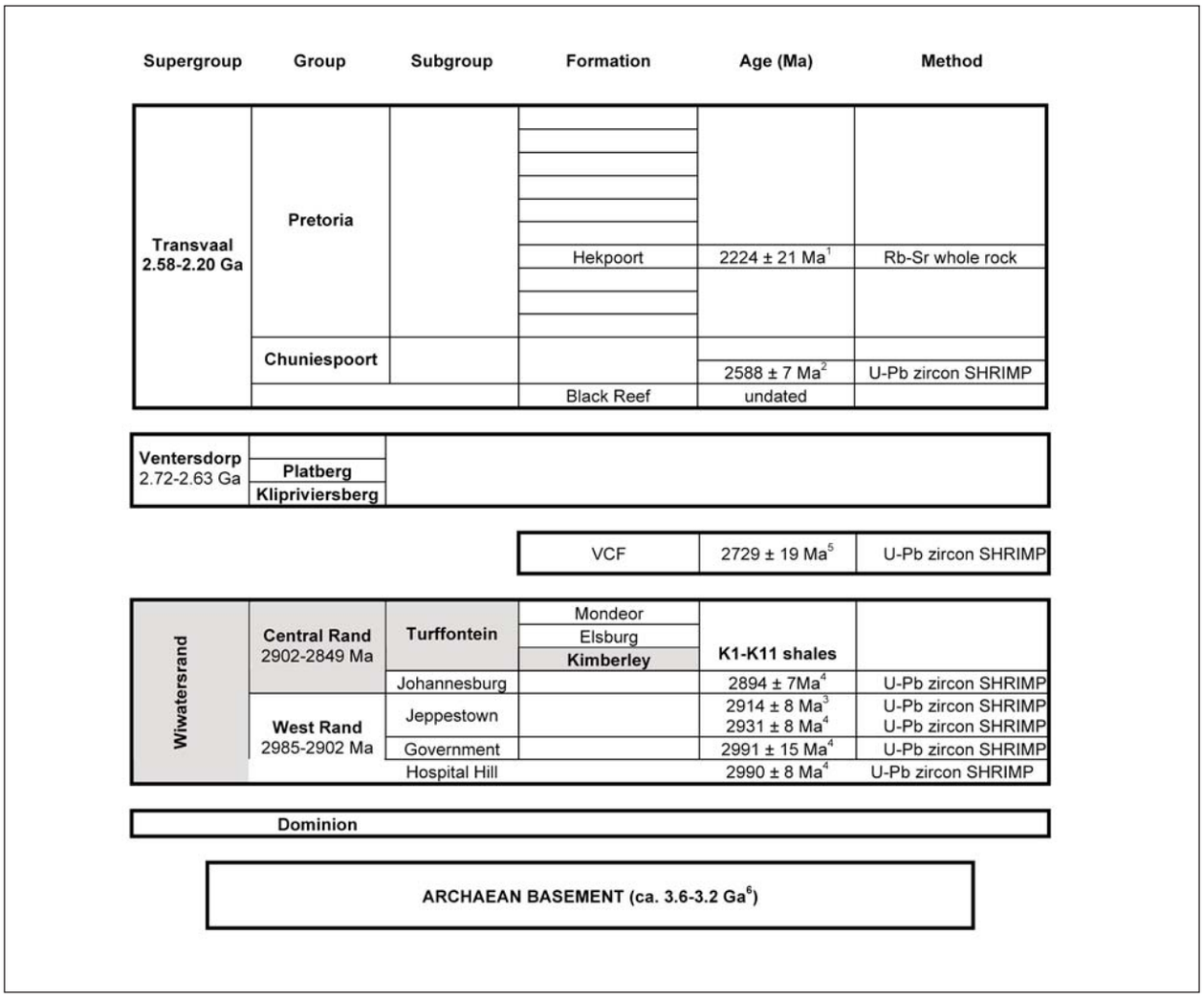


Figure 3. *Abridged lithostratigraphy (groups, subgroups and formations) of the Dominion Group, Witwatersrand, Ventersdorp supergroups and the Transvaal Basin sequences constrained to absolute geochronology. KEY: (**1**) Burger and Coertze (1973 to 1974; Rb-Sr whole rocks age); (**2**) Martin et al. (1998; single zircon U-Pb SHRIMP); (**3**) Armstrong et al. (1991; single zircon U-Pb SHRIMP); (**4**) Youngest concordant detrital zircon grain (Kositcin and Krapež, 2004); (**5**) Igneous-detrital xenotime/zircon aggregate Kositcin et al. (2003); (**6**) From Poujol et al. (2003). VCF = Ventersdorp Contact Formation*

The age of metamorphism remains problematic as summarised by Frimmel and Minter (2002).

The Witwatersrand (Supergroup) Basin is subdivided into the basal West Rand Group (ca. 3.0 to 2.9 Ga) and the overlying Central Rand Group (2.9 to 2.8 Ga; Kositcin and Krapež, 2004; U-Pb detrital zircon). The West Rand Group mainly consists of shale units, while the Central Rand Group mainly consists of conglomerate and quartzite units (McCarthy, 1997). The Ventersdorp Supergroup (ca. 2.72 to 2.63 Ga) and in turn, the Transvaal Basin sequences (ca. 2.58-2.20 Ga), unconformably overlie the Witwatersrand Supergroup in the West Rand goldfield.

The area of study, Cooke Shaft 3, is hosted by the Turffontein Subgroup (Figure 3) of the Central Rand Group (c.f., Dankert and Hein, 2010); the West Rand Group occurs at depth in the Cooke Section. The average dip of the Turffontein Subgroup is 10°E. The subgroup mainly consists of quartzite, metaconglomerate and shale units in the mine. It is overlain by the Ventersdorp Conglomerate Formation (ca. 2729 ± 19 Ma, igneous-detrital xenotime/zircon aggregate, Kositcin et al., 2003) both conformably and unconformably, and by the Ventersdorp Supergroup (ca. 2.72-2.63 Ga) unconformably. The Ventersdorp Supergroup comprises basalt-andesite lava flows, dykes and sills of the Klipriviersberg Group and the metasedimentary sequences of the Platberg Group.

In the West Rand and West Wits Line goldfields, studies by Fletcher and Reimold (1989) and Killick and Roering (1995b) have established that pseudotachylite crosscuts a considerable proportion of the stratigraphy, from the Jeppestown Subgroup (Figure 3 West Rand Group), which is dated at 2914 ± 8 Ma (Armstrong et al., 1991; single zircon U-Pb SHRIMP) and 2931 ± 8 Ma

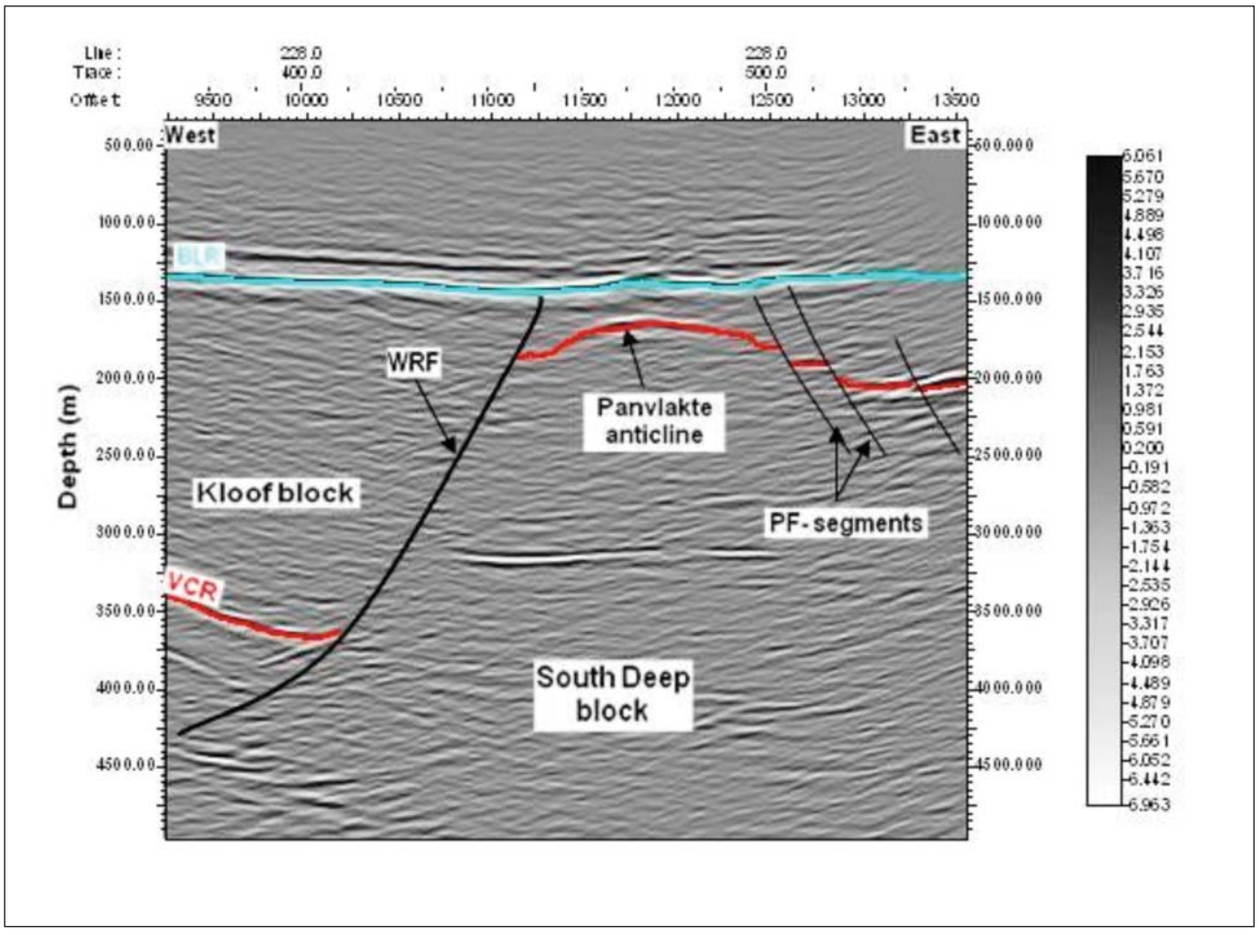


Figure 4. *An east-west seismic section (amplitude display) across the Panvlakte Anticline south of the Cooke Shaft permit. The section shows that the major West Rand Fault and minor fault segments do not breach the the base (unconformity) of the Transvaal Basin which is dated at 2.58-2.20 Ga (Kositcin and Krapež, 2004; U-Pb detrital zircon), i.e., Black Reef Formation. Displacement on the faults thus predates 2.58 Ga. Keys to Abbreviations, VCR: Ventersdorp Contact Reef; BLR: Black Reef Formation; PF: Panvlakte Fault.*

(youngest concordant detrital zircon grain, Kositcin and Krapež, 2004), to the base of the Transvaal basin, which is dated from the Chuniespoort Group at 2588 ± 7 Ma (Martin et al., 1998; single zircon U-Pb SHRIMP). Pseudotachylite veins also crosscut dykes and sills of the Ventersdorp Supergroup in the goldfields (Killick, 1992). Fletcher and Reimold (1989) and Killick and Roering (1995b) also described (but did not detail) an occurrence of pseudotachylite in borehole CDV04 in the Hekpoort Andesite Formation of the Pretoria Group of the Transvaal Supergroup: the Hekpoort Andesite Formation is dated at 2224 ± 21 Ma (Burger and Coertze, 1973 to 1974; Rb-Sr whole rocks age). Borehole CDV04 is located approximately 21.5 km south-southwest of the Cooke Shaft 3 and on the northern limb of the Potchefstroom Synclinorium that formed during the Vredefort Impact event ca. 2.02 Ga.

With respect to structural setting, Cooke Shaft 3 is located east and in the immediate footwall of the major north-northeasterly trending West Rand Fault Zone (Figure 1) and is hosted in the eastern limb of the Panvlakte Anticline (Figure 4). 3D geophysical studies by Campbell and Crotty (1988) and Gibson (2005) indicate that the West Rand Fault Zone is steeply west-dipping with an apparent sinistral offset of 600 m and a down-throw of 1.5 to 1.6 km of the hangingwall (i.e., sinistral-normal down throw of the western block); the fault was active as a reverse fault prior to deposition of the Ventersdorp Supergroup and subsequently as a listric fault prior to deposition of the Transvaal Basin. The Panvlakte anticline forms a drag (roll-over) fold in the footwall (east) of the West Rand Fault Zone. The anticline is crosscut by the subordinate Panvlakte fault (Killick, 1992), was excised, and subsequently overlain by the Klipriviersberg volcanic sequence, i.e., the West Rand Fault Zone and faults in the hangingwall or footwall, do not breach the base of the Transvaal basin and were thus not active during formation of the Transvaal Basin, i.e., after ca. 2.58 Ga.

Several steep-dipping faults in the Cooke Section host veins of pseudotachylite and bands of cataclasite, and occupy the Panvlakte and West Rand faults (Killick, 1992). Fault-related pseudotachylite formed either as fault veins, or planar injection veins that are irregular and terminate abruptly into the wallrock. The faults host pseudotachylite that has migrated as melt from the

generation site into structurally weak areas of the host rock (Killick and Roering, 1995b).

Methodology

Detailed structural mapping in the Cooke Section was undertaken in 128 Level West 15 in a haulage development drive southwest of the Cooke Shaft (location of the study area given in Figure 2). The development drive was extensively drilled; exploration diamond boreholes 128-G1478, 128-G1514 and 118-G3224 were made available for study. Boreholes 128-G1478 and 128-G1514 were drilled horizontally from the 128 Level and intersected numerous pseudotachylite veins. Borehole 118-G3224 was drilled from the 118 Level at +90° and intersected the South Boundary Fault. All boreholes were systematically logged. Fourteen samples of pseudotachylite were collected from borehole 128-G1514 for petrography of micro-structures and are consecutively numbered PT1-PT14.

Host rocks

The host rocks in the study area are quartzite, auriferous meta-conglomerate and shale units of the Kimberly Formation of the Turffontein Subgroup of the Central Rand Group (Figure 3). In the 128 Level West, 15 haulage, quartzite is the dominant rock type with subordinate thin meta-conglomerate bands and crosscutting meta-dolerite dykes that contact meta-morphosed the rock units. The meta-conglomerate bands (15 to 45 cm thick) contain clasts of vein quartz and black chert in a quartzite matrix. The black chert clasts are commonly replaced by pyrite. The K8 shale unit of the Kimberley Formation separates the upper and the lower Kimberly reefs; it is only exposed in drill-hole 128-G1478. The shale is laminated, with grey pyritic siltstone interbeds (~5 mm). It is cross-cut by multiple micro-faults (displacements of <2 mm) near the basal contact with the gritty quartzite. Pseudotachylite forms a sharp contact with quartzite; large quartzite fragments occur within the pseudotachylite fault veins where veins branch.

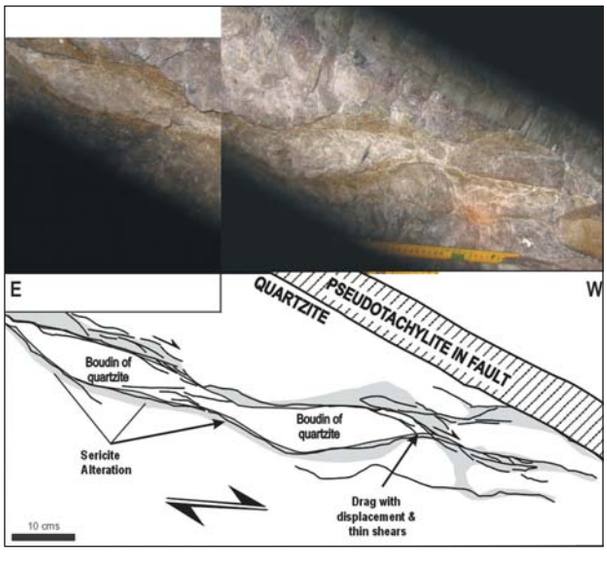


Figure 5. *The macroscopic sub-horizontal boudins in the 128 Level West 15 haulage. View is along the haulage to the south. Sericite alteration of the wall-rock quartzite around the boudins is marked by a distinct yellowish-brown colouration in thin shears. The overall sense of displacement is interpreted as normal with top block to the west. The boudins are crosscut by a pseudotachylite-bearing fault indicating they formed before the fault.*

Structure

The South Boundary Fault (SBF) presents evidence for three successive mine-scale tectonic events that are characterised by:

1. Formation of macroscopic sub-horizontal boudins;
2. Formation of faults (mean orientation of 093°/50°S) that host pseudotachylite fault and injection veins, *en echelon* quartz veins and pseudotachylite breccia;
3. Formation of sub-vertical barren faults that host *en echelon* quartz veins, and dip-slip and strike-slip quartz slickensides.

Macroscopic sub-horizontal boudins

The macroscopic sub-horizontal asymmetric boudins (Figure 5) are bounded by sheared and sericitized quartzite and have long curved lenticular shape. The boudins are typically composed of fractured and brecciated quartzite. A mineral lineation developed on the sheared margin of the boudins is parallel to the long axis of the boudins but could not be measured due to limited or unsafe access. The form of the boudins indicates that the hangingwall (top block of the boudins) was displaced normally and to the west. Sericite ± (pyrophyllite) alteration of the wall-rock quartzite around the boudins is marked by a distinct yellowish-brown colouration. The boudins are truncated and/or crosscut by pseudotachylite-bearing faults as shown in Figure 5.

Pseudotachylite fault veins, injection veins and breccia

In the study area, pseudotachylite-bearing faults are steeply to moderately south-dipping with a calculated mean strike and dip of 092°/50°S. They host a planar continuous infill of pseudotachylite (Figure 6a, b) that exhibits straight, undulating or contorted internal flow textures, and fragments of wall rock or older pseudotachylite. The faults are subtended by injection veins that branch from the generation site in the hangingwall of the fault to form irregular and/or discontinuous *en echelon* vein sets. The injection veins (~50 mm width) penetrate the host rock up to two meters. The *en echelon* arrangement of injection veins may suggest a reverse sense of displacement during vein formation (c.f., Roberts and Poulsen, 2001; Di Toro et al., 2009) with south block up. In addition, the pseudotachylite-bearing faults crosscut *en echelon* quartz veins (10 to 15 mm wide) in their footwall, indicating

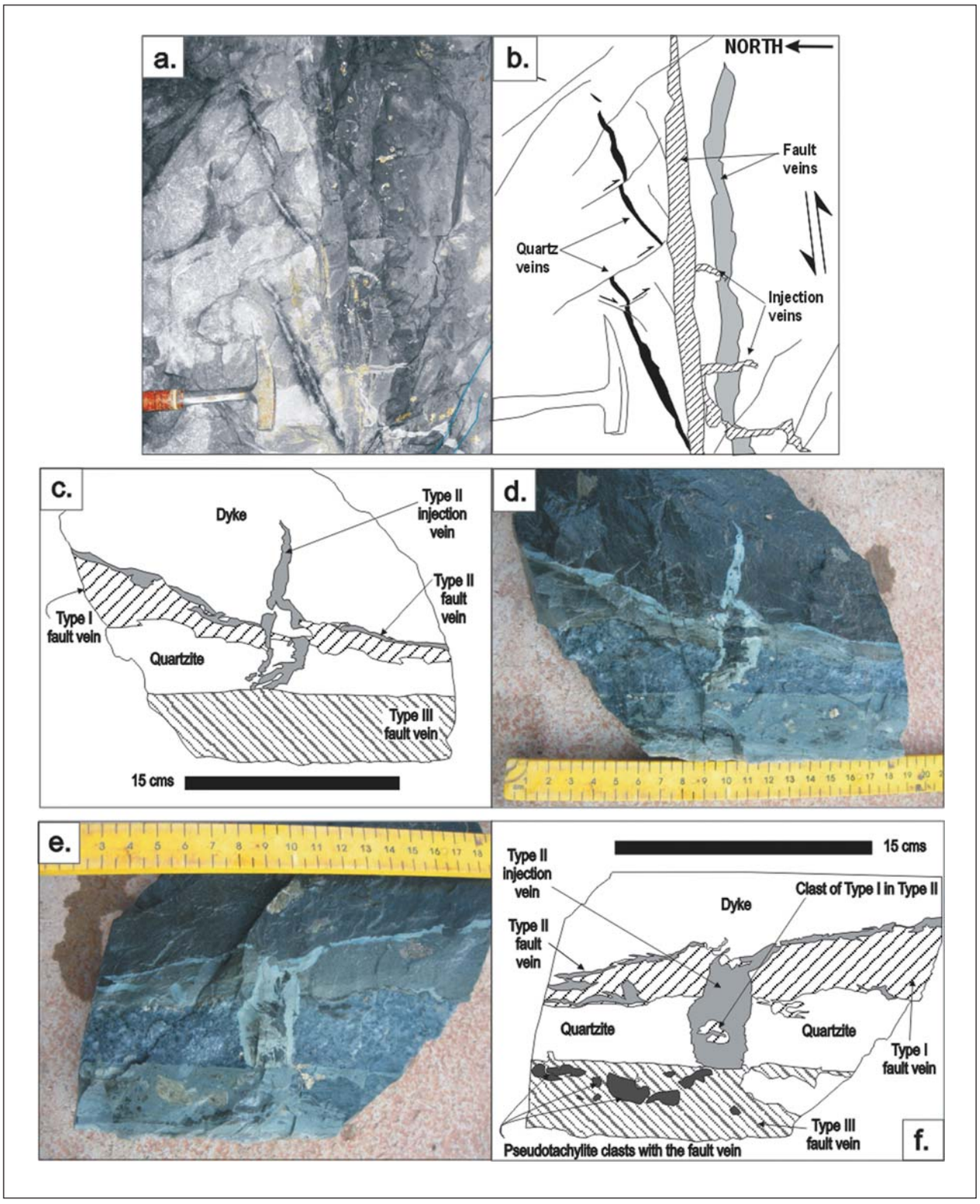


Figure 6. *(**a**, **b**) Photograph and sketch of eastern face of the 128 Level West 15 haulage. Psuedotachylite as fault and injection veins, crosscuts en echelon quartz veins but also pre-existing fault veins. Pseudotachylite-bearing faults are steep to moderate south-dipping with a calculated mean strike and dip of 092°/50°S. The overall displacement on the faults is reverse with south block up. (**c**, **d**) At least three generations of veins associated with pseudotachylite-bearing faults (Type-I, Type-II and Type-III) are exposed on the eastern wall of the 128 Level West 15 haulage. Type-II veins occur as fault veins and injection veins with a distinct pale-blue to light-green groundmass. Type-III veins crosscut Type II veins which crosscut Type 1 veins. (**d**, **e**) (back and front of the same sample): Type II fault veins frequently host clasts and slivers of younger pseudotachylite veins and indicate that several events of pseudotachylite formation have taken place. The dark mass that lies central to Type II injection veins is predominately glass.*

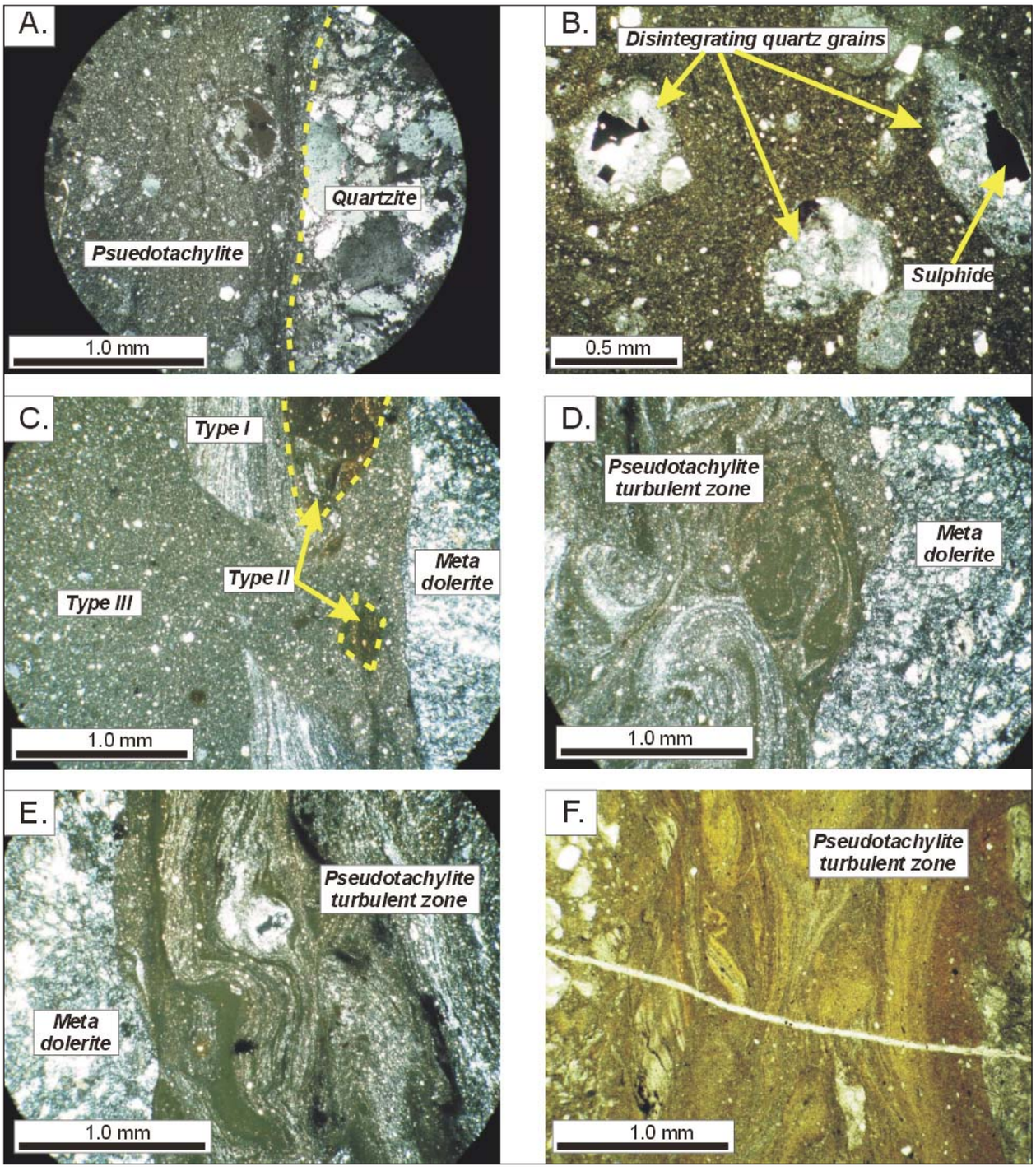


Figure 7. *(**a**) Photomicrograph of the contact between quartzite (wall rock) and pseudotachylite (sample P/T 4). The contact is sharp and darker in colour, which Barker (2005) described as chilled margin. The quartzite exhibits sub grain development and fragmentation. (**b**) Photomicrograph of disintegrating quartzite (wall rock) grains in a pseudotachylite Type III matrix (sample P/T 5). The grains have a rind of fine quartz rock flour (corona texture). Sulphides occur in the core of some grains. (**c**) Photomicrograph of three crosscutting pseudotachylite types adjacent to the contact of metadolerite (sample PT 10). The contact is sharp between dolerite and Type III pseudotachylite and between pseudotachylite Types I, II and III. (**d**, **e**, **f**) Photomicrograph of turbulence of Types I and II pseudotachylite adjacent to meta-dolerite, with micro-folding clearly evident (sample PT 10 and PT 35).*

their later formation. The calculated mean strike and dip of quartz veins is 060°/56°W. The *en echelon* arrangement of the quartz veins also indicates a reverse displacement during vein formation (Roberts and Poulsen, 2001; Di Toro et al., 2009), with south block up.

At least three generations of veins associated with pseudotachylite-bearing faults (Type-I, Type-II and Type-III) are exposed on the eastern wall of the 128 Level West 15 haulage (Figure 6c-e). Type-I and Type-III veins form sub-parallel fault veins that converge downwards. Type-I veins occur at the contact of meta-dolerite and quartzite (in the haulage) and range in observed thickness from 10 to 33 mm. Type-III veins occur at the contact between light-grey and dark-grey quartzite, and offset Type-I and Type-II veins. In contrast, Type-II veins occur as fault veins and injection veins with a distinct pale-blue to light-green groundmass. Type III veins host clasts of Type-I pseudotachylite veins. A yellowish brown pseudotachylite forms clasts within Type III veins (along with clasts of quartzite and mafic intrusive) and may represent a pseudotachylite phase intermediate to Type II and III. Type-III veins crosscut Type II veins which crosscut Type 1 veins.

In boreholes 128-G1478, 128-G1514 and 118-G3224 pseudotachylite fault and injection veins are hosted in all rock types (quartzite, meta-dolerite, meta-conglomerate and shale) on lithological contacts and within layers of the same rock type. Pseudotachylite in shale units is predominately hosted at shale-quartzite contacts, but also weakly crosscut shale units in thin veinlets. Rare pseudotachylite veins crosscut meta-conglomerate beds. Pseudotachylite fault veins in meta-dolerite typically host clasts of meta-dolerite.

Pseudotachylite veins form sharp contacts with their host rocks and are gradational with cataclasite (borehole 118-G3224). They may exhibit a dark quench or chill zone at the margin of the veins. Colour variations and internal banding reflect compositional variation as described by Killick (1992) and are marked by sharp contacts. However, colour variations and internal banding may also indicate different generations of formation. For example, a marginal light-grey pseudotachylite at the contact of the wall-rock may be subtended by medial dark-grey pseudotachylite that encloses clasts of gritty-quartzite. Alternatively, a clast-dominated mid-zone within a pseudotachylite vein can accompany a massive zone on one contact, and a finely-banded pseudotachylite zone on the other contact. Furthermore, clasts and slivers of older pseudotachylite that are hosted by younger pseudotachylite veins (Figures 6e and f) attest to multiple events of pseudotachylite formation (PT10) and support arguments for several events of cataclasis or pseudotachylite formation.

Petrographically, pseudotachylite veins are mainly composed of clasts of quartz in a very fine-grained (Figures 7a to c), or turbulent matrix (Figures 7d to f). The clasts of quartz are rounded to sub-rounded, commonly fragmented, and form corona texture (c.f., Reimold et al., 1999). The wall-rock quartzite to pseudotachylite fault veins is widely varied in grain size, typically exhibits undulose extinction and/or is composed of polycrystalline quartz. Chlorite occurs both within the pseudotachylite veins and the wall rock. Pyrophyllite occurs as rare interstitial laths in quartz grains (indicating that pseudotachylite vein formation and thus faulting occurred after peak metamorphism in the Witwatersrand Basin), whereas sericite commonly occurs as a fine-grained matrix surrounding quartz grains. Lithic fragments in pseudotachylite veins are dominantly composed of host rock fragments (i.e., quartzite, meta-dolerite and meta-conglomerate), with accessory chlorite, but also pseudotachylite clasts and pyritised pseudotachylite. Pseudotachylite veins are sometimes glassy.

The term 'pseudotachylitic breccia' was used by Reimold and Gibson (1996) for the Vredefort-related breccia that contains pseudotachylite matrix. In the SBFZ, pseudotachylitic breccia occurs as sub-rounded, fractured quartzite blocks (35 cm in length) in a fine-grained matrix of massive grey pseudotachylite. It occurs in an approximately 15 m wide zone that is bounded by sub-parallel pseudotachylite-bearing faults.

Sub-vertical barren faults

Sub-vertical faults have a calculated mean orientation of 091°/85°S. In the 128 Level West 15 haulage they cross-cut pseudotachylite-bearing faults and are characterised by thin discrete fault surfaces that host minor gouge, *en echelon* sigmoidal quartz veins in the footwall and quartz slickensides in the fault plane. They do not host pseudotachylite. The en echelon sigmoidal quartz veins have a calculated mean orientation of 110°/42°S. Several sub-vertical faults contain rare quartz slickensides that plunge 85° towards 168° (Set 1). The orientation of quartz veins, slickensides and sigmoidal form of the footwall quartz veins indicates a reverse sense of displacement with south block up. Set 2 slickensides crosscut and smear Set 1 and have a mean plunge of 10° towards 281°, i.e., the sub-vertical faults underwent sinistral normal (dip-slip) displacement subsequent to reverse displacement (south block up).

Discussion

This study of the South Boundary Fault (SBF) in the 128 Level West 15 haulage at the Cooke Section presents evidence for three successive tectonic events. Event 1 was associated with the formation of macroscopic boudins and bounding shears. The kinematics of boudinage formation warrant further investigation (subject to safe access) but the boudins resemble forward-vergent shear-band boudins of Goscombe and Passchier (2003) and Goscombe et al. (2004).

Event 2 marked a period of predominantly frictional melting and cataclasis on the SBFZ. The pseudotachylite fault veins exhibit complex internal flow textures, and glassy and corona texture. Turbulence-flow texture is

represented by curling. The texture is the result of viscous drag on the vein margins or, due to localized pressure gradients within the pseudotachylite fault vein (Magloughlin and Spray, 1992). Dark quench zones at the margin of the veins (Barker, 2005) and a glassy character attest to high temperature of pseudotachylite formation. In addition, fragmented quartz grains around larger quartz grains in fault veins indicate a degree of thermal corrosion (Magloughlin and Spray, 1992), which led to the formation of corona texture. Event 2 was progressive with formation of quartz veins being succeeded by at least three cross-cutting phases of pseudotachylite (Type 1 to III) in steep-dipping faults (south block up), which suggests that repeated rupturing and episodic melting took place on the SBFZ.

The pseudotachylites on the SBFZ are transitional with cataclasite as observed in borehole core of the SBFZ. Fragments of older pseudotachylite occur as clasts in younger pseudotachylite veins, together with wallrock rip-out clasts and glass. The extreme case of pseudotachylite-cataclasite formation is represented by pseudotachylite breccia trapped between sub-parallel pseudotachylite-bearing faults. These features are characteristic of cataclastic flow and brittle failure (Passchier and Trouw, 1998) concomitant with melt in a brittle deformation regime (Swanson, 1992). Pseudotachylite that is formed in the brittle (elastico-plastic) regime is associated with formation of cataclasite, as opposed to mylonite which is formed in the ductile (crystal-plastic) regime (Sibson, 1980).

Event 3 in the SBF was characterised by the formation of sub-vertical faults, *en echelon* sigmoidal quartz veins and quartz slickensides (on the fault plane) during reverse and finally, sinistral (normal) displacement subsequent to reverse displacement (south block up). The event marks a shift to strike-slip activity on the SBF.

The coexistence of pseudotachylite fault and injection veins, with cataclasite veins and breccia, and in cross-cutting relationship to quartz veins is suggestive of abrasive-wear processes as detailed by Swanson (1992) or, the formation of frictional melts as discussed by Magloughlin (1989). The agreement seems to be that these pseudotachylite melts are characteristic of a shallow (brittle) crustal regime and brittle fault systems. The arrangement and orientation of *en echelon* quartz veins, pseudotachylite fault and injection veins is similar throughout Event 2 and early in Event 3, which argues for progressive displacement (south block up) and repeated failure of the SBF. Thus, the suggestion of Killick and Roering (1995a) that all pseudotachylites in the West Rand goldfield formed during one event (i.e., the Vredefort impact) is problematic. The presence of multiple crosscutting pseudotachylite veins indicates that pseudotachylites in the SBF formed during several stages of fault reactivation. Indeed, we suggest they formed progressively by abrasive wear (Swanson, 1992) in a brittle (elastico-plastic) regime (Sibson, 1980; Swanson, 1992).

Therefore, we concur with Killick and Reimold (1990) that the majority of pseudotachylite veins in the West Rand goldfield are tectonically-induced (fault-induced) and formed before deposition of the lower Transvaal Basin sequences (i.e., after the Black Reef Formation but pre-2.58 Ga, c.f., Figure 3). This relative age is constrained by 3D geophysical data by Campbell and Crotty (1988), Gibson (2005) and Manzi (2010) and field data by Hilliard (1994), which concludes that very few faults penetrate the base of the Transvaal Basin, and for those that do, displacement are in the order of metres (Manzi, 2010). Furthermore, it is clear from 3D geophysical data for the West Wits Line and southern West Rand goldfields that the Panvlakte, West Rand and Bank faults, and their associated rollover anticlines, were exposed, eroded, and subsequently overlain by the Klipriviersberg volcanic sequence, reactivated as listric faults, excised again, and overlain by the Transvaal basin, i.e., the Panvlakte, West Rand and Bank faults do not breach the base of the Transvaal and were thus not active during formation of this basin.

It is therefore curious that attempts have been made to correlate pre-2.58 Ga tectonically-induced pseudotachylites from the goldfields with ca. 2.02 Ga impact-induced pseudotachylites in the Vredefort Dome (c.f., Reimold et al., 1999; Killick and Reimold, 1990; and others), especially because Fletcher and Reimold (1989), Killick (1992; 1994), Killick and Roering (1995a; 1995b; 1998) and Reimold et al. (1999) presented convincing evidence that tectonically-induced pseudotachylites were related to faulting. The need to correlate fault- and impact-induced pseudotachylites seems to lie with the recognition of pseudotachylites in the Hekpoort Andesite and "Jills Fault" in borehole CVD4, which were studied by Fletcher and Reimold (1989) and Killick and Roering (1995b). The borehole was collared approximately 25 km south-southwest of Cooke Shaft 3 on the northern limb of the Potchefstroom Synclinorium (Figure 1). The synclinorium arguably formed during the Vredefort Impact event ca 2.02 Ga (Brink et al., 1997; Wieland, 2006). The pseudotachylite occurrences in borehole CVD4 were not described by Fletcher and Reimold (1989) and Killick and Roering (1995b) and thus it has not possible to determine their structural relationships to the host rocks; we suggest that these pseudotachylites may actually be impact-induced because the borehole was collared on the northern limb of an impact-induced synclinorium. The relative age of pseudotachylite formation established by Killick and Roering (1995b; 1998), which suggests that the Hekpoort Andesite Formation provides a maximum age for all pseudotachylite formation in the West Rand goldfield, is not relevant for the tectonically-induced pseudotachylite hosted by the SBF.

Furthermore it is likely that both tectonically-induced and impact-induced pseudotachylites occur in the Witwatersrand basin, but those in the West Rand goldfield are mostly likely to be fault-related. These pseudotachylites may have a temporal and spatial

relationship to activity on the West Rand Fault Zone and its footwall which is the current focus of research in the West Rand goldfield.

Conclusion

The South Boundary Fault (SBF) in the 128 Level West 15 haulage at the Cooke Section presents evidence for three successive tectonic events:

- Event 1 was associated with the formation macroscopic boudins and bounding shears that resemble forward-vergent shear-band boudins. The boudins need further investigation.
- Event 2 marked a period of predominantly frictional melting and cataclasis on the SBFZ with formation of quartz veins being succeeded by at least three cross-cutting phases of pseudotachylite (Type 1 to III) in steep-dipping faults (south block up). The pseudotachylites on the SBFZ are transitional with cataclasite. The coexistence of pseudotachylite fault and injection veins suggests they formed progressively by abrasive wear (Swanson, 1992) in a brittle (elastico-plastic) regime (Sibson, 1980; Swanson, 1992).
- Event 3 in the SBF was characterised by the formation of sub-vertical faults and a shift to strike-slip activity on the SBF.

The majority of pseudotachylite veins in the West Rand goldfield are tectonically-induced (fault-induced) as stated by Killick and Reimold (1990). They formed before deposition of the lower Transvaal Basin sequences (i.e., after the Black Reef Formation but pre-2.58 Ga).

Pseudotachylite occurrences in the Hekpoort Andesite and Jills Fault in borehole CVD4 (c.f. Fletcher and Reimold, 1989; Killick and Roering, 1995b) are interpreted to be impact-induced because the borehole was collared on the northern limb of the impact-induced Potchefstroom Synclinorium. Thereby, the Hekpoort Andesite Formation does not provide a maximum age for all pseudotachylite formation in the West Rand goldfield or on the South Boundary Fault.

Acknowledgements

Part of this research was completed by P. Mambane in 2007 with logistic support from Harmony Gold Mining Ltd. Logistic support in 2010 was given by Rand Uranium. T Andersen and an anonymous referee are thanked for their useful reviews that greatly improved the quality of this work.

References

Andersen, T.B. and Austrheim, H., 2006. Fossil earthquakes recorded by pseudotachylytes in mantle peridotite from the Alpine subduction complex of Corsica. Earth and Planetary Science Letters, 242, 58–72.

Andersen, T.B., Mair, K., Austrheim, H., Podladchikov,Y.Y. and Vrijmoed, J.C., 2008. Stress-release in exhumed intermediate-deep earhquakes determined from ultramafic pseudotachylite. Geology, 36, 995–998.

Armstrong, R.A., Compston, W., Retief, E.A., Williams, I.S. and Welke, H.J., 1991. Zircon ion microprobe studies bearing on the age and evolution of the Witwatersrand triad. Precambrian Research, 53, 243–266.

Barker, S.L.L., 2005. Pseudotachylyte-generating faults in Central Otago, New Zealand. Tectonophysics 397, 211–223.Bisschoff, A.A., 1962. The pseudotachylite of the Vredefort Dome. Transactions of the Geological Society of South Africa, 65, 207–226.

Barker, S.L.L., 2005. Pseudotachylyte-generating faults in Central Otago, New Zealand. Tectonophysics, 397, 211–223.

Bisschoff, A.A., 1988. The history and origin of the Vredefort Dome. South African Journal of Science, 84, 413–417.

Brink, M.C., Waanders, F.B. and Bisschoff, A.A., 1997. Vredefort: a model for the anatomy of an astrobleme. Tectonophysics, 270, 83–114.

Brink, M.C., Waanders, F.B., Bisschoff, A.A. and Gay, N.C., 2000. The Foch Thrust-Potchefstroom Fault structural system, Vredefort, South Africa: a model for impact-related tectonic movement over a pre-existing barrier. Journal of African Earth Sciences, 30, 99–117.

Burger, A.J. and Coertze, F.J., 1973–1974. Age determinations - April 1972 to March 1974. Annals of the Geological Survey of South Africa, 10, 135–141.

Campell, G. and Crotty, J.H., 1988. Preliminary report on the results of a 3-D seismic reflection survey to map VCR structure over South Deep Prospect Area, West Rand goldfields on behalf of JCI Gold and Uranium Division. Unpublished report GA364 by JCI Geophysical Unit, 26pp.

Coetzee, D.S., van Reenen, D.D. and Roering, C., 1995, Quartz vein formation, metamorphism, and fluid inclusions associated with thrusting and bedding-parallel shear in Witwatersrand quartzites, South Africa. South African Journal of Geology, 98, 371–381.

Dankert, B.T. and Hein, K.A.A., 2010. Evaluating the structural character and tectonic history of the Witwatersrand Basin. Precambrian Research, 177, 1–22.

Davis, G.H. and Reynolds, S.J., 1996. Structural Geology of Rocks and Regions, 2nd Edition. Published by John Wiley & Sons, Inc., New York, USA, 284pp.

Di Toro, G., Pennacchioni, G. and Nielsen, S., 2009. Pseudotachylites and earthquake source mechanics. In: E. Fukuyama (Editor), Fault-Zone properties and earthquake rupture dynamics. Elsevier Academic Press, London, U.K., 87–133.

Eiko, H., 2004. Clast-size analysis of impact-generated pseudotachylite from Vredefort Dome, South Africa. Journal of Structural Geology, 26, 1419–1424.

Fletcher, P. and Reimold, W.U., 1989. Some notes and speculations on the pseudotachylites in the Witwatersrand Basin and Vredefort Dome, South Africa. South African Journal of Geology, 92, 223–234.

Frimmel, H.E. and Minter, W.E.L., 2002. Recent developments concerning the geological history and genesis of the Witwatersrand gold deposits, South Africa. Society of Economic Geology, Special Publications, 9, 17–45.

Gibson, M., 2005. Interpretation of the 2003 South Deep 3D seismic survey. Unpublished report to Gold Fields Mining by Geosciences Solutions, 64p.

Gibson, R.L., Reimold, W.U. and Wallmach, T., 1997. Origin of pseudotachylite in the lower Witwatersrand Supergroup, Vredefort Dome (South Africa): constraints from metamorphic studies. Tectonophysics, 283, 241–262.

Goscombe, B.D. and Passchier, C.W., 2003. Asymmetric boudins as shear sense indicators – an assessment from field data. Journal of Structural Geology, 25, 575–589.

Goscombe, B.D., Passchier, C.W. and Hand, M.,2004. Boudinage classification: end-member boudin types and modified boudin structures. Journal of Structural Geology, 26, 739–763.

Hall, A.L., Molengraaff, G.A.F., 1925. The Vredefort Mountain Land in southern Transvaal and northern Orange Free State. Verhandelingen der Koninklijke Akademie van Wetenschappen te Amsterdam, 24, 1–183.

Hargraves, R.B., 1961. Shatter cones in the rocks of the Vredefort ring. Transactions of the Geological Society of South Africa, 64, 147–161.

Hilliard, P., 1994. The structural evolution of the Johannesburg Dome, Kaapvaal Craton, South Africa. Unpublished MSc Thesis, University ofPretoria, South Africa, 2 microfiches, 2 Maps, 99pp.

Kamo, S.L., Reimold, W.U., Krogh, T.E. and Colliston, W.P., 1996. A 2.023 Ga age for the Vredefort impact event and a first report of shock metamorphosed zircons in pseudotachylitic breccias and Granophyre. Earth and Planetary Science Letters, 144, 369–387.

Killick, A.M., 1990. Pseudotachylite generated as a result of a drilling "burn-in". Tectonophysics, 171, 221–227.

Killick, A.M., 1992. Pseudotachylites of the West Rand Goldfield, Witwatersrand basin, South Africa. Unpublished PhD. Thesis, Rand Afrikaans University, Johannesburg, South Africa, 270pp.

Killick, A.M. and Reimold, W.U., 1990. Review of the pseudotachylites in and around the Vredefort 'Dome', South Africa. South African Journal of Geology, 93, 350–365.

Killick, A.M. and Roering, C., 1994. Bedding-parallel simple shear deformation at Randfontein Estates Gold Mine, Cooke section, Witwatersrand basin, South Africa. South African Journal of Geology, 97, 228–231.

Killick, A.M. and Roering, C., 1995a. Movement indicators for pseudotachylite-bearing faults. South African Journal of Geology, 98, 382–387.

Killick, A.M. and Roering, C., 1995b. The relative age of pseudotachylite formation in the West Rand region, Witwatersrand basin, South Africa, as deduced from sructural (sic) observations. South African Journal of Geology, 98, 78–81.

Killick, A.M. and Roering, C., 1998. An estimate of the physical conditions of pseudotachylite formation in the West Rand Goldfield, Witwatersrand Basin, South Africa. Tectonophysics, 284, 247–259.

Killick, A.M., Thwaites, A.M., Germs, G.J.B. and Schoch, A.E., 1980. Pseudotachylite associated with a bedding parallel fault zone between the Witwatersrand and Ventersdorp Supergroups, South Africa. Geologische Rundschau, 77, 329–344.

Kositcin, N. and Krapež, B., 2004. Relationship between detrital zircon age-spectra 1219 and the tectonic evolution of the Late Archaean Witwatersrand Basin, South Africa. Precambrian Research, 129, 141–168.

Kositcin, N., McNaughton, N.J., Griffin, B.J., Fletcher, I.R., Groves, D.I. and Rasmussen, B., 2003. Textural and geochemical discrimination between xenotime of different origin in the Archaean Witwatersrand Basin, South Africa. Geochimica et Cosmochimica Acta, 67, 709–731.

Legros, F., Cantagrel, J-M. and Devouard, B., 2000. Pseudotachylyte (Frictionite) at the Base of the Arequipa Volcanic Landslide Deposit (Peru): Implications for Emplacement Mechanisms. The Journal of Geology, 108, 601–611.

Maddock, R.H., 1983. Melt origin of fault-generated pseudotachylites demonstrated by textures. Geology, 11, 105–108.

Magloughlin, J.F., 1989. The nature and significance of pseudotachylite from the Nason terrane, North Cascade Mountains, Washington. Journal Structural Geology, 11, 907–917.

Magloughlin, J.F. and Spray, J.G., 1992. Frictional melting processes and products in geological material: introduction and discussion. Tectonophysics, 204, 197–204.

Manton, W.I., 1962. The orientation and implication of shatter cones in the Vredefort ring structure. Unpublished MSc Thesis, University of the Witwatersrand, Johannesburg, South Africa, 162pp.

Manzi., M.S.D., 2010. Interpretation preliminary results for Driefontein, Kloof - South Deep Merged 3-D Seismic Data. Confidential technical report to Gold Fields Mining Services, Kloof Mine, South Africa, 45pp.

Martin, D. McB., Clendenin, C.W., Krapež, B. and McNaughton, N.J., 1998. Tectonic and geochronological constraints on late Archaean and Palaeoproterozoic stratigraphic correlation within and between the Kaapvaal and Pilbara Cratons. Journal of the Geological Society, 155, 311–322.

McCarthy, T.S., 1997. Wits Supergroup. Geology Department, University of the Witwatersrand, Johannesburg, South Africa. 1–36.

Nicolaysen, L.O. and Ferguson, J., 1990. Cryptoexplosion structures, shock deformation and siderophile concentration related to explosive venting of fluids associated with alkaline ultramafic magmas. Tectonophysics, 171, 303-335.

Passchier, C.W. and Trouw, R.A.J., 1998. Microtectonics. Springer-Verlag Berlin Heidelberg, New York, U.S.A., 25–56.

Phillips, G.N. and Law, J.D.M., 1994. Metamorphism of the West Rand Goldfield. Ore Geology Reviews, 9, 1–31.

Reimold, W.U. and Colliston, W.P., 1994. Pseudotachylites of the Vredefort Dome and the surrounding Witwatersrand Basin, South Africa. In: B.O. Dressler, R.A.F. Grieve and V.L. Sharpton (Editors), Large Meteorite Impacts and Planetary Evolution. The Geological Society of America Special Paper, 293, 177–196.

Reimold, W.U., Fletcher, P., Snowden, P.A. and Wilson, J.D., 1986. Pseudotachylite – a general Witwatersrand phenomenon. Lunar and Planetary Science, 17, 701–702.

Reimold, W.U. and Gibson, R.L., 1996. Geology and evolution of the Vredefort impact structure, South Africa. Journal of African Earth Sciences, 23, 125–162.

Reimold, W.U. and Gibson, R.L., 2006. The melt rocks of the Vredefort impact structure – Vredefort granophyre and pseudotachylitic breccias: Implications for impact cratering and the evolution of the Witwatersrand basin. Chemie der Erde, 66, 1–35.

Reimold, W.U., Köberl, C., Fletcher, P., Killick, A.M. and Wilson, J.D., 1999. Pseudotachylitic breccias from fault zones in the Witwatersrand Basin, South Africa: evidence of autometasomatism and post-brecciation alteration processes. Mineralogy and Petrology, 66, 25–53.

Riller, U., Lieger, D., Gibson, R.L., Grieve, R.A.F. and Stöffler, D., 2010. Origin of large-volume pseudotachylite impact structures. Geology 38, 619–622.

Robb, L.J. and Robb, V.M., 1998. Gold in the Witwatersrand Basin. In: M.G.C. Wilson and C.R. Anhaeusser (editors), The Mineral Resources of South Africa. Handbook. Council for Geoscience, 294–349.

Roberts, F., Poulsen, H.K., 2001. Vein formation and deformation in greenstone gold deposits. In: J.P. Richards and R. M. Tosdal (Editors), Structural Controls on Ore Genesis. Reviews in Economic Geology, 14, 111–155.

Roering, C., Berlenbach, J. And Schweitzer., J.K., 1989. Guidelines for the classification of fault rocks. Department of Geology. Published by COMRO, Exploitation Technology, Auckland Park, Republic of South Africa, 22pp.

Schwarzman, E.C., Meyer, C.E. and Wilshire, H.G. 1983. Pseudotachylite from the Vredefort Ring, South Africa, and the origin of some lunar breccias. Bulletin of the Geological Society of America, 94, 926–935.

Shand, S.J., 1916. The pseudotachylyte of Parijs (Orange Free State) and its relation to 'trap-shotten gneiss' and 'flinty crush-rock'. Geological Society of London, 72, 198–221.

Sibson, R.H., 1980. Transient discontinuities in ductile shear zones. Journal of Structural Geology, 1, 165—171.

Spray, J.G., 1995. Pseudotachylite controversy: fact or fiction? Department of Geology, University of New Brunswick, Canada, 23, 1119–1122.

Spray, J.G., 1998. Localized shock- and friction-induced melting in response to hypervelocity impact. Journal of the Geological Society, London, Special Publication, 140, 195–204.

Stanistreet, I.G., McCarthy, T.S., Charlesworth, E.G., Myers, R.E. and Armstrong, R.A., 1986. Pre-Transvaal wrench tectonics along the northern margin of the Witwatersrand Basin. Tectonophysics, 131, 53–74.

Swanson, T., 1992. Fault structure, wear mechanisms and rupture processes in pseudotachylyte generation. Tectonophysics, 204, 223–242.

Wieland, F., 2006. Structural Analysis of Impact-Related Deformation in the Collar Rocks of the Vredefort Dome, South Africa. PhD Thesis, University of the Witwatersrand, Johannesburg, South Africa, 344pp.

Wieland, F., Reimold, W.U. and Gibson, R.L., 2006. New observations on shatter cones in the Vredefort impact structure, South Africa, and evaluation of current hypotheses for shatter cone formation. Meteoritics and Planetary Science, 41, 1737–1759.

Editorial handling: L. D. Ashwal

Geophysical Research Abstracts
Vol. 15, EGU2013-3923, 2013
EGU General Assembly 2013
© Author(s) 2013. CC Attribution 3.0 License.

Evidence for Neoarchaean extensional faults in the Vredefort Dome, South Africa.

sello mashabela
University of the Witwatersrand, Geosciences, South Africa (sello.mashabela@students.wits.ac.za)

EVIDENCE FOR NEOARCHAEAN EXTENSIONAL FAULTS IN THE VREDEFORT DOME, SOUTH AFRICA

Sello MASHABELA, Kim A.A HEIN, Roger L. GIBSON, Musa S. MANZI
School of Geosciences, University of the Witwatersrand, Private Bag 3, Wits 2050, South Africa.

The Vredefort Dome is an approximately 80-90 km wide impact structure, situated 120 km southwest of Johannesburg in South Africa. The dome is a preserved centrally uplifted region of an ancient 250-300 km wide multi-ringed crater that formed at 2.02 Ga. The ancient crater underwent 5-10 km of erosion to expose the Vredefort Dome, allowing for unique study of the deeper levels of the impact crater.
The Vredefort Dome is composed of a 40 km wide core, bounded by a 20-25 km wide collar. The core is wholly composed of Mesoarchaean basement gneiss (ca. 3.1 Ga), and the collar is made up of mid-amphibolite to lower greenschist facies supracrustal rocks (ca. 3.0-2.2 Ga).
Fault development in the collar has largely been attributed to the impact, except for two fault systems. The two exceptions have been described as pre-impact faults, with apparent strike-slip displacements up to 3 km. It is the focus of this study to distinguish pre-impact structures from impact-related structures.
Ortho-photographs, satellite images, and field mapping have shown that pre-impact faults were listric in character, and associated with second order accommodation faults. The main fault is associated with a 20 m wide zone of pseudotachylitic breccia. Most of the pseudotachylitic breccia in the dome has been attributed to the impact, so these faults were possibly associated with earlier pseudotachylite generation. Cleavage associated with the listric faults is displaced by impact-related faults, confirming the existence of two deformation events in the dome.
The geometry of the listric faults is similar to those observed in the West Wits Line and West Rand goldfields (55 km north of Vredefort Dome), which have been modelled by Manzi et al. (2012, a, b; submitted) using 3D seismic techniques. The authors attribute the development of listric faults (or a rift-like system of faults) to crustal extension that took place during deposition of Klipriviersberg Group lavas and Platberg Group (2709-2643 Ma) of the Ventersdorp Supergroup. The association potentially means that the Vredefort collar hosts rotated Ventersdorp-age extensional faults or a rift system of faults that predate impact-induced structures.

1. Manzi, M.S.D., Durrheim, R.J., Hein, K.A.A., King N., 2012. 3D edge detection seismic attributes used to map potential conduits for water and methane in deep gold mines in the Witwatersrand basin, South Africa. Geophysics 77 (5), 1-16.
2. Manzi, M., Gibson, M. A.S., Hein, K.A.A., King, N., Durrheim, R.J., 2012. Application of 3D Seismic techniques in evaluation of ore resources in the West Wits Line goldfield and portions of the West Rand Goldfield, South Africa. Geophysics 77, 1-9.
3. Manzi, M., Hein, K.A.A., King, N, Durrheim, R.J., submitted. NeoArchaean tectonic history of the Witwatersrand Basin and Ventersdorp Supergroup: New Constraints from high-resolution 3D seismic reflection data. Tectonophysics